Physiologically based kinetic (PBK) modeling as a tool to quantify the role of gut microbial metabolism in the in vivo effects of the foodborne estrogens daidzein and zearalenone

Qianrui Wang

Propositions

1. In vitro anaerobic fecal incubations enable definition of kinetic parameters for gut microbial metabolism of foodborne constituents.
   (this thesis)

2. Intestinal microbial metabolism can be included in physiologically based kinetic (PBK) models required for quantitative *in vitro* to *in vivo* extrapolations (QIVIVE) as a novel approach methodology (NAM) in toxicological risk assessment.
   (this thesis)

3. The developments of big data analysis and artificial intelligence in computer science boost multidisciplinary innovations in life sciences.

4. The approach from Chinese traditional medicine of treating the body as an "entirety" is underappreciated in current medical practice.

5. Education is a long-term investment in developing countries.

6. Be positive about negatives.

Propositions belonging to the thesis, entitled
Physiologically based kinetic (PBK) modeling as a tool to quantify the role of gut microbial metabolism in the in vivo effects of the foodborne estrogens daidzein and zearalenone

Qianrui Wang
Wageningen, 21 June 2022

Physiologically based kinetic (PBK) modeling as a tool to quantify the role of gut microbial metabolism in the in vivo effects of the foodborne estrogens daidzein and zearalenone

Qianrui Wang

Thesis committee

Promotor

Prof. Dr I.M.C.M. Rietjens
Professor of Toxicology
Wageningen University & Research

Co-promotor

Dr K. Beekmann
Scientist, Toxicology
Wageningen University & Research

Other members

Prof. Dr M. Kleerebezem, Wageningen University & Research
Dr M.J. Zeilmaker, National Institute of Public Health and Environment (RIVM), Bilthoven
Dr E.M. van Schothorst, Wageningen University & Research
Prof. Dr M. van Duursen, VU Amsterdam

This research was conducted under the auspices of the Graduate School VLAG (Advanced studies in Food Technology, Agrobiotechnology, Nutrition and Health Sciences)

Physiologically based kinetic (PBK) modeling as a tool to quantify the role of gut microbial metabolism in the in vivo effects of the foodborne estrogens daidzein and zearalenone

Qianrui Wang

Thesis

submitted in fulfilment of the requirements for the degree of doctor
at Wageningen University
by the authority of the Rector Magnificus
Prof. Dr A.P.J. Mol
in the presence of the
Thesis Committee appointed by the Academic Board
to be defended in public
on Tuesday 21 June 2022
at 1.30 p.m. in the Omnia Auditorium.

Qianrui Wang
Physiologically based kinetic (PBK) modeling as a tool to quantify the role of gut microbial metabolism in the in vivo effects of the foodborne estrogens daidzein and zearalenone,
244 pages

PhD thesis, Wageningen University, Wageningen, the Netherlands (2022)
With references, with summary in English

ISBN 978-94-6447-224-0
DOI https://doi.org/10.18174/569554

Table of contents

Chapter 1 ——— **7**

General introduction

Chapter 2 ——— **35**

Use of physiologically based kinetic modeling (PBK) to predict rat gut microbial metabolism of the isoflavone daidzein to S-equol and its consequences for ERα activation

Chapter 3 ——— **79**

Use of physiologically based kinetic (PBK) modeling to predict human gut microbial conversion of daidzein to S-equol

Chapter 4 ——— **117**

Physiologically based kinetic (PBK) model-based prediction of intestinal microbial and host metabolism of zearalenone and consequences for its estrogenicity

Chapter 5 ——— **163**

Integrating physiologically based kinetic (PBK) and Monte Carlo modeling to predict the interindividual human variability in metabolism of daidzein

Chapter 6 ——— **203**

General discussion

Chapter 7 ——— **231**

Summary

Appendix ——— **237**

Acknowledgements, About the author, List of publications

Overview of completed training activities

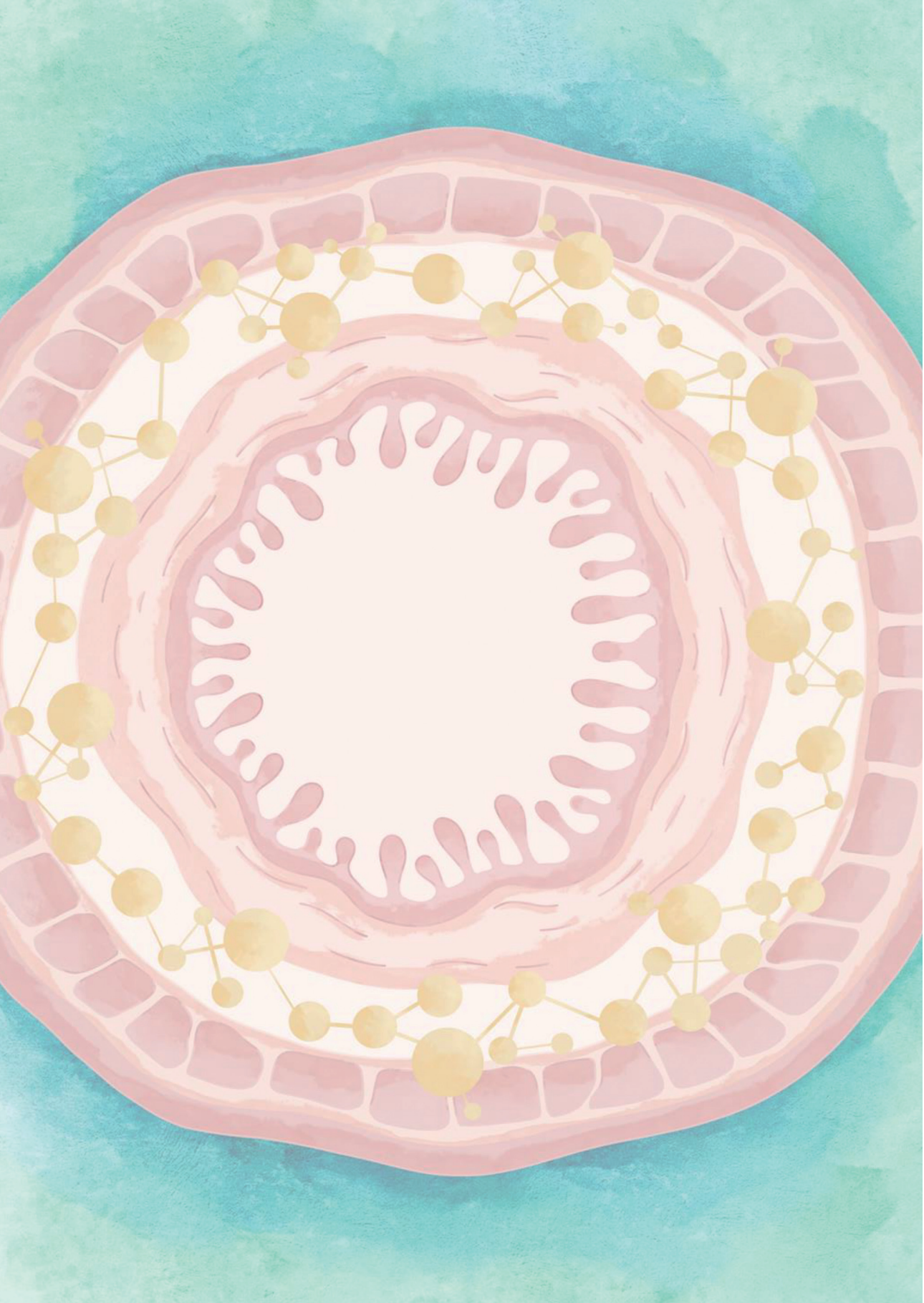

Chapter 1

General introduction

1. Background and aim of the study

The human gut microbiota is composed of trillions of bacterial cells, a number estimated to be in the same order as the number of human cells (Gill et al., 2006). With a collective genome of over 100 times that of the human genome, the gut microbiota encompasses a rich enzyme repository with metabolic potential (Zimmermann et al., 2019), enabling a wide range of biochemical and metabolic activities, mostly reduction and hydrolysis, as well as other transformations such as dehydroxylation, acetylation and deacetylation (Haiser and Turnbaugh, 2013; Sousa et al., 2008). The gut microbiota can modify substances, potentially increasing or decreasing their ultimate toxicity, and thereby consequently influencing the health of the hosts. The gut microbiota can thus influence both beneficial as well as adverse health effects of food ingredients, environmental contaminants, natural toxins and/or drugs (Klaassen and Cui, 2015).

The present thesis focusses on two food borne compounds whose toxicity may be influenced by the gut microbiota. These compounds are daidzein and zearalenone (ZEN), both known to exert estrogenic effects. The isoflavone daidzein represents an important bioactive food constituent in soy products which exerts estrogenicity due to structural similarity to the natural hormone 17β-estradiol (E2) (Niu et al., 2018). The mycotoxin zearalenone is a well-known example of a toxin produced by fungi growing on contaminated crops, showing potential estrogenicity (Drzymala et al., 2015). Both daidzein and ZEN can be metabolized by gut microbiota to metabolites with higher estrogenic potential than their parent compounds, being S-equol (Mayo et al., 2019) and α-zearalenol (α-ZEL) (Zinedine et al., 2007), respectively. Exposure to these microbial metabolites may add to the effects resulting from exposure to the respective parent compounds. The aim of the present thesis was to characterize the role of gut metabolism in the toxicity of daidzein and ZEN using novel approach methodologies (NAMs) for alternatives in animal testing, and to include the metabolism by gut microbiota in physiological based kinetic (PBK) models used in NAMs. The proofs-of-principle to be generated will show that the consequences of the metabolism by the gut microbiota for toxicity of foodborne chemicals in the host can be characterized without a need for in vivo studies in experimental animals or human intervention studies.

In the thesis a detailed insight into the microbial-mammalian co-metabolism will be generated for daidzein and ZEN using in vitro model systems, which will be combined with in silico PBK modeling to evaluate the role of gut microbial metabolism in the estrogenicity of these

substances. This in vitro-in silico approach aims to contribute to alternatives for animal testing for risk assessment and safety evaluation of foodborne chemicals, and will also provide insight in interindividual differences in metabolism and accompanying risks of the selected estrogenic model compounds daidzein and ZEN.

2. Gut microbiota

A huge variety of bacteria, yeasts, viruses and archaea inhabit the human body in for example the mouth, gut, skin and vagina (Human Microbiome Project, 2012). Especially in the gut, bacteria make up most of the microbes and their density and diversity increase from the proximal to the distal gut (Smith et al., 2007). As already indicated above, the human gut microbiota is reported to be composed of 10^{13} to 10^{14} microorganisms, whose collective genetic content is about 100 times larger than the human genome (Gill et al., 2006). The vast majority of the microbes present actively participates in the biosynthesis of essential amino acids, production of short-chain fatty acids and vitamins, utilization of otherwise indigestible food components, and the metabolism of xenobiotics (Laparra and Sanz, 2010; Le Chatelier et al., 2013; Rowland et al., 2018). Among these microorganisms, the *Firmicutes* and the *Bacteroidetes* are the most abundant gut microbiota at the taxonomic level, making up around 99% of the identified phylotypes (Sommer and Backhed, 2013). At the genus and species level, the composition of the gut microbiota have large interspecies and interindividual differences (Baumler and Sperandio, 2016).

2.1 Metabolic capacity of gut microbiota and related health effects

Due to the high bacterial genetic content and the abundance of related metabolic enzymes, the gut microbiota reveals tremendous metabolic potential and possible consequences for the field of toxicology. The metabolic capacity of gut microbiota is considered as extensive as that of liver (Sommer and Backhed, 2013), and is on the one hand producing a wide variety of metabolites relevant for the host, such as essential amino acids and short-chain fatty acids, and on the other hand metabolizing foodborne chemicals, drugs and industrial xenobiotics (Laparra and Sanz, 2010; Le Chatelier et al., 2013; Rowland et al., 2018). Through a wide range of biochemical and metabolic activities, including reduction, hydrolysis, dehydroxylation, acetylation, deacetylation, N-oxide cleavage, proteolysis, denitration and deconjugation (Haiser and Turnbaugh, 2013; Sousa et al., 2008), the gut microbiota can affect the ultimate toxicity of compounds, and consequently influence the health of the host. A well-

known example is melamine, which resulted in 54,000 children being hospitalized in China in 2008, caused by use of the illegal additive melamine in milk and infant formula. Through gut microbial conversion, melamine is transformed to cyanuric acid, facilitating formation of melamine–cyanurate complexes, that result in formation of kidney stones and cause renal toxicity (Dalal and Goldfarb, 2011). Metabolic activation to a more potent metabolite by the gut microbiota is also the case for the phytochemical daidzein and the mycotoxin ZEN, of which microbial conversion results in the formation of the more potently estrogenic metabolites S-equol (Mayo et al., 2019) and α-ZEL (Rogowska et al., 2019), respectively.

The gut microbiota is reported to be essential for the development of the intestinal epithelium, the immune system, bones, and the autonomic and central nervous system (Ochoa-Reparaz et al., 2011; Scheperjans et al., 2015; Sjogren et al., 2012). Dysbiosis of the gut microbiota, which refers to persistent imbalance of gut's microbial community, is reported to be associated with diseases, such as a non-alcoholic fatty liver disease, metabolic disorders, inflammatory bowel disease, and autism (Baumler and Sperandio, 2016; Khan et al., 2014; Scheperjans et al., 2015; Ussar et al., 2015). Interindividual variations in the composition and metabolic activity of gut microbiota may contribute to interindividual variation in the development of these health-related effects. This composition of the gut microbiota can be influenced by diverse factors such as diet, age, genetic background, lifestyle and the exposure to chemicals of the host (Flandroy et al., 2018; Gill et al., 2006; Jovel et al., 2016). Though metabolic contributions of the gut microbiota to the overall metabolism of foodborne chemicals in the host are observed, this metabolic compartment has so far not been taken into account when developing the PBK models used in NAMs. The aim of the present study includes to provide first proofs-of-principle for including intestinal metabolism by the gut microbiota in such PBK models.

2.2 Development of in vitro approaches in the study of gut microbial metabolism

Toxicity testing is currently undergoing a paradigm shift away from the use of experimental animals towards the use of in vitro experimentation and NAMs, in order to reduce the use of animal experimentation that induces ethical concerns and extrapolation uncertainties. Regarding the study of gut microbial metabolic activities, in vitro approaches using animal (e.g. rats) or human fecal samples have been developed to perform strain identification, isolation and incubations under anaerobic conditions (Franke et al., 2012; Hur et al., 2002; Matthies et al., 2009; Tamura et al., 2007). Fecal samples are considered to provide a

representative matrix in particular for the colonic microbiota, since fecal communities are reported to be highly comparable to colonic ones in composition and function (Behr et al., 2017; Lagkouvardos et al., 2017). Furthermore, while there are certain differences in the microbial composition along the intestinal tract, the colon is housing the vast majority of microbes and is considered to be the most important contributor to the metabolic activity of the gut microbiota (Meyer and Hostetter, 2012). Moreover, the fecal samples for in vitro anaerobic fecal incubations can be obtained non-invasively, which is also one of the advantages of using fecal samples. Subsequently, the kinetic parameters for gut microbial metabolism required for PBK modeling will be obtained in the present thesis using anaerobic fecal incubations in order to define the PBK models needed for PBK modeling-based reverse dosimetry, enabling extrapolation from in vitro to in vivo situations (Louisse et al., 2017).

3. Model compounds of the present thesis

3.1 Daidzein

3.1.1 Occurrence and consumption of daidzein

Daidzein (4',7-dihydroxyisoflavone) (**Figure 1**) is a naturally occurring isoflavone mainly present in soybean and soy products (Sun et al., 2016). Initially starting 4,000 to 5,000 years ago, Chinese have cultivated soybean as an important staple, as it was an affordable source of protein. Subsequently, use of soy based products rapidly spread to neighbouring countries such as Japan and Singapore throughout Asia, eventually resulting it in being popular as a dietary product all over the world at present times. Different from Asian counties that were using soybean for human consumption and animal feed already for a long time, soy firstly reached Europe and the Netherlands in the 18th century for biological taxonomic purpose (Kim et al., 2012).

As a representative legume, soybean contains a substantial amount of isoflavones, mainly consisting of daidzein, genistein and glycitein (Messina, 2010). These isoflavones can reach up to 0.1 to 0.3% of the total weight of soybean, and are mainly present in their corresponding glycoside form, daidzin, genistin and glycetin (Lee et al., 2018). Some commonly consumed soy products, such as soy milk, tofu, miso, tempeh and soy protein isolate, contain isoflavones in levels ranging from 0.5-3 mg/g dry weight and 0.1-2.5 mg/g fresh weight (D'Alessandro et al., 2005). Due to different cultural dietary habits, the daily dietary intake of isoflavones in the population differ largely throughout the world. In European countries and the United States,

the estimated daily intake of isoflavones is reported to be less than 2 mg/day/person, with for some countries such as Netherlands and United Kingdom, the intake being even lower than 1 mg/day/person (Eisenbrand and Senate Commission on Food Safety of the German Research, 2007; van Erp-Baart et al., 2003). Vegetarians from Western countries consume higher amounts of isoflavones, reaching up to 12 mg/day/person (Clarke et al., 2003), due to their intake of soy products as a source of protein. In some Asian countries, soybean and soy-based products are more commonly consumed, resulting in a daily dietary exposure to isoflavones that varies from 15 mg/day/person up to 61 mg/day/person (Arai et al., 2000; Kim and Kwon, 2001; Seow et al., 1998; Wakai et al., 1999). Since soy extracts are also marketed as supplements, individuals taking soy supplements usually have a relatively high intake of isoflavones, amounting to intakes between 20-150 mg/day/person (Anderson et al., 2007; Eisenbrand and Senate Commission on Food Safety of the German Research, 2007; Merz-Demlow et al., 2000; Steinberg et al., 2003).

3.1.2 Absorption, distribution, metabolism and excretion (ADME) of daidzein

Upon oral intake of dietary soy products, the isoflavone daidzein is present mainly in the form of a mixture of its aglycone and its glycoside daidzin. After reaching the small intestine, the glycoside daidzin is hydrolyzed to the aglycone daidzein by either intestinal bacterial β-glucosidases or the intestinal β-glucosidase lactose phlorizin hydrolase (LHP) located in the membrane at the brush border of the enterocytes (Day et al., 2000). Daidzein is partly taken up into the systemic circulation by passive diffusion in the small intestine, and also in the large intestine along bowel movement. In the large intestine, daidzein encounters gut microbiota which convert daidzein to dihydrodaidzein (DHD) by daidzein reductase. Subsequently, DHD is further converted by gut microbiota to either S-equol by DHD reductase or to O-desmethylangolensin (O-DMA) through C-ring cleavage (Gardana et al., 2009; Schwen et al., 2012) (**Figure 1**). In intestinal tissue and liver, daidzein further undergoes conjugation, predominantly glucuronidation mediated by uridine 5'-diphospho-glucuronosyltransferases (UGTs), and to a lesser extent sulfation mediated by sulfotransferases (SULTs) (Soukup et al., 2016). Daidzein glucuronidation and sulfation can both occur at the 7 and 4' hydroxyl moiety of daidzein, with a preference for the 7-position (Nakano et al., 2004). The conjugates formed are more hydrophilic than the parent compound daidzein, and are excreted mostly in urine and in feces after biliary excretion (Pritchett et al., 2008).

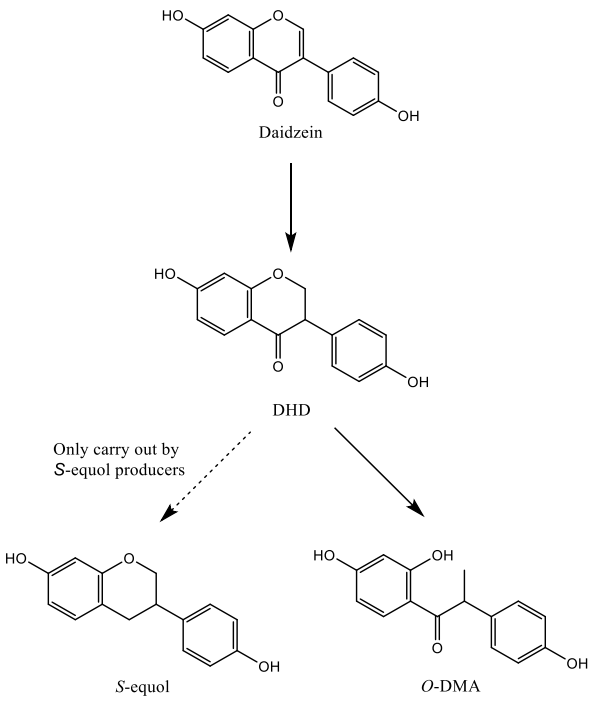

Figure 1. Gut microbial metabolism of daidzein.

3.1.3 Toxicity of daidzein

Daidzein is referred to as a phytoestrogen due to its weak estrogenicity. Moreover, its microbial metabolite, S-equol, is known to show higher estrogenicity, while DHD and O-DMA are less potent estrogens than the parent compound daidzein (Mayo et al., 2019). Both beneficial and adverse health effects have been reported upon exposure to daidzein (Andres et al., 2011). Positive relationships reported for soy consumption and health benefits include an association with lower risks for breast cancer and heart disease, less hot flushes and nocturnal sweating for post-menopausal women, improved bone density and cognitive health (Messina, 2010). Despite these beneficial effects for human health, potential adverse effects, as suggested in in vitro and in vivo experiments, raise concerns about the safety of high dosages of phytoestrogens. In vitro studies for example have shown that isoflavones stimulated the proliferation of estrogen-sensitive MCF-7 and T47D cells (Sotoca et al., 2008), and in vivo studies demonstrated that daidzein induced growth stimulation of estrogen-dependent mammary tumors in ovariectomized Sprague-Dawley rats (Allred et al., 2004). The mechanisms underlying these dualistic effects can be in part explained by the involvement of

the estrogen receptor (ER) α and ERβ, where activation of ERα stimulates cell proliferation while activation of ERβ promotes cell apoptosis and counteracts the ERα mediated cell proliferation (Rietjens et al., 2013). As a result, the cellular response towards different estrogens may differ with the levels and ratios of the ERα and ERβ within tissues, so that the ultimate effects may be tissue specific. For example, the main isoform in breast and uterus is ERα which activates cell proliferation (Bardin et al., 2004), sometimes accompanying a decrease in apolipoprotein levels, indicating an additional estrogenic stimulus (Hargreaves et al., 1999), while in prostate ERβ is dominant and able to counteract the ERα-mediated response (Enmark et al., 1997).

Due to the distinct higher amount of isoflavone intake via an Asian diet than a Western diet, as well as unregulated consumption of soy supplements by which the manufacturing claims to have beneficial health effects such as relieving menopausal-related symptoms, concerns arise for susceptible populations with high level of isoflavone exposures (Maskarinec, 2013). In a recent opinion, the European Food Safety Authority (EFSA) evaluated the possible association between the intake of isoflavones from food supplements and harmful effects on the mammary gland, uterus and thyroid, and concluded that the human data did not support the hypothesis of an increased risk but that it was not possible to derive a single health-based guidance value for the dietary intake of isoflavones (EFSA, 2015). Whether the current levels of intake of daidzein and other soy isoflavones result in plasma concentrations that cause estrogenic effects remains to be elucidated.

3.2 Zearalenone (ZEN)

3.2.1 Presence and consumption of ZEN

ZEN (**Figure 2**) is a phenolic resorcyclic acid lactone mycotoxin mainly found in contaminated crops, particularly in maize, and also in some other common cereal grains such as wheat, barley, rye and sorghum (Ropejko and Twaruzek, 2021). ZEN is a secondary metabolite produced by several *Fusarium* species, especially *F. graminearum*, with humid storage conditions stimulating the growth of the fungus and accompanying production of ZEN (Yazar and Omurtag, 2008). The presence of ZEN is observed to be 3- to 30-fold higher in raw cereal grains than in their cleaned and milled products, but ZEN is generally stable during food processing and cooking processes (EFSA, 2011).

The dietary consumption of grain-based products contributes most to the daily exposure to ZEN, with the contribution of different food categories varying from high to low in the order bread, corn flour and vegetable oils (Rogowska et al., 2019). Due to the estrogenic activity of ZEN and its metabolites, as well as widespread exposure through the diet, it is essential to establish health-based guidance values for ZEN. In the most sensitive animal species upon ZEN exposure (e.g. pig), a no-observed-effect-level (NOEL) of 10 µg/kg bw/ per day for ovary, uterus and vulva tissues was observed in female piglets. Consequently, the European Food Safety Authority (EFSA) established a tolerable daily intake (TDI) for ZEN of 0.25 µg/kg bw/day for human in all age groups, by dividing the NOEL with an uncertainty factor of 40, composed of a factor 10 for human interindividual differences and a factor of 4 for interspecies differences in toxicokinetics (EFSA, 2011). Given that the NOEL was derived from a species that was considered more sensitive than man, the default uncertainty factor of 2.5 for interspecies differences in toxicodynamics was not applied, reducing the uncertainty factor used from 100 to 40.

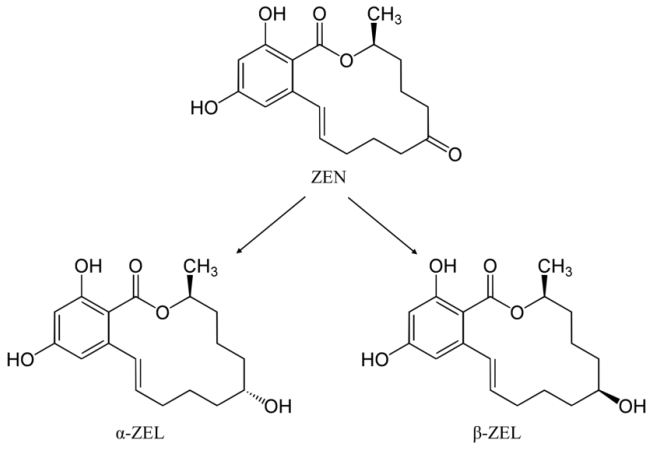

Figure 2. Liver and gut microbial reduction of ZEN.

3.2.2 Absorption, distribution, metabolism and excretion (ADME) of ZEN

Upon oral ingestion, ZEN enters the systemic circulation from the upper part of the intestine by passive diffusion in rats, rabbits, pigs, and human (Zinedine et al., 2007). The part not absorbed from the intestinal lumen reaches the large intestine. Here, ZEN encounters enterocytes and gut microbiota, both of which can enzymatically reduce the keto group of ZEN to α-ZEL and β-zearalenol (β-ZEL), in a reaction catalyzed by 3α- and 3β-

hydroxysteroid dehydrogenases (HSDs), respectively (Ropejko and Twaruzek, 2021)(**Figure 2**). For the reduction of ZEN, pigs are reported to preferentially produce α-ZEL over β-ZEL by 5-fold, while limited human data suggest that humans produce significant amounts for both metabolites, with a small preference for the α-isomer (Mirocha et al., 1981).

Being absorbed in the large intestine, ZEN and its reduced metabolites α-ZEL and β-ZEL undergo conjugation in the liver to form their respective glucuronides and sulfates, with the former one being dominant (Zinedine et al., 2007). The most active human UGTs for glucuronidation of ZEN, α-ZEL, and β-ZEL are UGT1A1, 1A3, and 1A8, with the 14-O-glucuronide being the major glucuronide for all of these substrates (Metzler et al., 2010). This efficient glucuronidation significantly reduces the amounts of unconjugated forms that reach the body circulation and facilitates the excretion through urine and feces (Mirocha et al., 1981).

3.2.3 Toxicity of ZEN

Originating from its structural similarity to the natural hormone E2, ZEN exerts estrogenicity and the exposure to ZEN is linked with endocrine, reproductive and developmental disturbance (Nikaido et al., 2004). ZEN is reported to stimulate the proliferation of human breast cancer MCF-7 cells in in vitro studies, and to have a higher affinity for ERα than ERβ (Yu et al., 2005).

Metabolism of ZEN modifies its ultimate estrogenic potency (Takemura et al., 2007). Through the pathway of enzymatic reduction of ZEN in liver and intestine, the formation of α-ZEL represents a bioactivation pathway since α-ZEL has been reported to be 60-times more potent than its parent compound, which implies that its estrogenic potency is only 10-fold lower than the estrogenicity of E2 (Everett et al., 1987). In contrast, reduction of ZEN to β-ZEL, provides a detoxification pathway with β-ZEL being 5-times less potent than ZEN (Everett et al., 1987). The overall estrogenic potency of E2, ZEN and its metabolites decreases in the order: E2> α-ZEL > ZEN > β-ZEL. The increased sensitivity of pigs towards ZEN might in part be related to their preferences for formation of α-ZEL over β-ZEL, while humans might generally be less susceptible than pigs and also show only a small preference for formation of α-ZEL (Zinedine et al., 2007). Except for the conversion of ZEN to its hepatic and microbial metabolites α-ZEL and β-ZEL, efficient glucuronidation occurring in the small intestine and liver significantly reduces the amounts of unconjugated ER-active

ZEN, α-ZEL and β-ZEL present in the systemic circulation (Drzymala et al., 2015). These conjugated metabolites are more hydrophilic and provide a way of detoxification and excretion in urine and feces (Ropejko and Twaruzek, 2021).

Compared with in vitro and animal studies, evidence in human is not yet substantive to directly link dietary ZEN exposure to the adverse outcomes of estrogenic effects. However, the production of ZEN by fungi growing on food due to poor storage conditions and its presence in foodstuffs may contribute to the occurrence of precocious puberty and breast cancer (Belhassen et al., 2015). Susceptible subgroups in the population such as fetuses and neonates are speculated to be more sensitive upon dietary exposure to ZEN due to metabolic and physiological immaturity (Belli et al., 2010).

4. Physiologically based kinetic (PBK) modeling

In order to assess the role of gut microbial metabolism of the foodborne chemicals daidzein and ZEN in their estrogenicity the present thesis applied a NAM including PBK modeling. In the present section PBK modeling is introduced in some more detail. PBK models are mechanism-based models that use mathematical equations to describe the ADME of chemicals in the body.

PBK modeling assumes that the whole body consists of different compartments corresponding to relevant tissues. As an example, **Figure 3** presents a basic structure of a PBK model. Separate compartments including liver, fat, gastrointestinal (GI) tract, rapidly perfused tissue (a lumped compartment comprising kidney, lung, brain and heart) and slowly perfused tissue (a lumped compartment comprising muscle, skin and bone) are connected by the circulating blood flow.

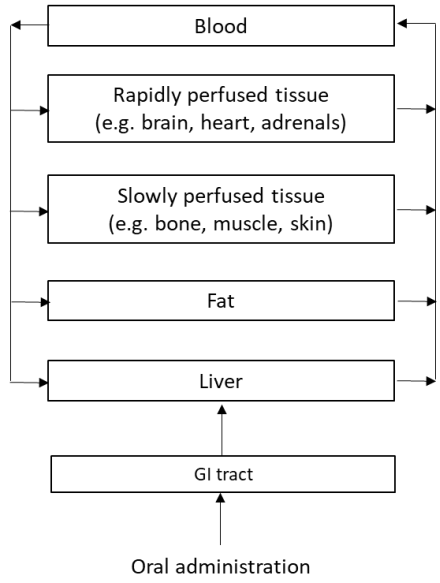

Figure 3. Schematic structure of a PBK model.

For each compartment in the PBK model a differential equation is defined to describe the change in the amount of the compound or metabolite of interest in that compartment over time. Three types of parameters are the basis to define these differential PBK equations, including: 1) physiological parameters which refer to for example cardiac output, tissue size/volumes and blood flows and are usually obtained from literature; 2) physico-chemical parameters, for example the chemical-specific tissue/blood coefficient which represents the ratio between the concentration of the compound of interest in the tissues and in blood, usually either calculated by in silico methods or obtained from in vivo studies; 3) kinetic parameters such as kinetic constants like maximum velocity (V_{max}) and the Michaelis–Menten constant (K_m) describing the rates of conversion and biotransformation, which can be obtained from literature or through analysis in in vitro experiments using incubations with relevant tissue fractions (Rietjens et al., 2011).

Once the schematic structure of the model is defined and the mathematical equations and relevant parameters are established, the PBK model is numerically integrated using Berkeley Madonna software (UC Berkeley, CA, USA). As a follow up, model validation is an important step to assess the performance of the developed PBK model. In model validation, a model predicted outcome (e.g. blood concentration or cumulative urinary excretion) is

compared to reported in vivo data, and with a less than 2-fold difference between the PBK model predicted and the observed value the PBK model is usually considered able to provide an accurate prediction (Sager et al., 2015).

The advancements in in-silico science and the knowledge explosion in biomedical sciences supported the development of PBK modeling, which provides an important method in the use of NAMs to replace conventional studies in experimental animals while at the same time providing also other advantages. First of all, PBK modeling facilitates interspecies extrapolation, since by replacing parameters from animals to those for humans, kinetics in human and experimental animals can be compared in a way that is more precise than using the default uncertainty factor for interspecies differences in kinetics of 4 for extrapolation from animals to human (WHO, 2005). PBK models also allow the extrapolation from high dose to realistic low dose dietary exposure, either upon single exposure or following multiple exposures over time, which may not be easily accessible by experiment, and thereby reduce the use of large numbers of animals. Moreover, with PBK modeling based reverse dosimetry (Section 6 below), in vitro concentration–response curves can be translated to in vivo dose–response curves that allow definition of PoDs that are required in risk assessment. Another application of PBK modeling is integration with Monte Carlo simulations (Section 5 below), thereby providing a useful tool to explore the consequences of interindividual differences within the human population caused by variance of influential parameters and interethnic differences in the ADME characteristics of a chemical, based on population-based frequency distributions. Overall, as part of the NAMs, the development and application of PBK modeling fulfills the principles of the 3Rs aiming at Replacement, Reduction and Refinement of animal studies and also contributes to risk assessment of drug and foodborne chemicals.

In the present thesis, PBK models are developed for daidzein and ZEN in rats and human, including submodels for their more potent metabolites S-equol and α-ZEL, respectively. As described in previous sections, gut microbiota plays an important role in the biotransformation of daidzein and ZEN. Previously established PBK models, however, did not yet include the gut microbiota. The PBK models developed in this thesis aimed to include gut microbiota metabolism, by introducing a separate intestinal lumen compartment containing the gut microbiota to describe the conversion of daidzein and ZEN in the large intestine. The inclusion of a separate compartment for the gut microbiota as well as submodels for the more bioactive metabolites in the PBK models enables predictions that provide an insight into the

overall outcomes of the ultimate estrogenicity of daidzein and ZEN while taking the role of the metabolites formed by the gut microbiota into account.

5. Integration of PBK modeling and Monte Carlo simulation

In human risk assessment and the subsequent risk management, interindividual variations and population-based distributions of metabolic outcomes are of interest, in order to protect most of the population and susceptible groups (e.g. at 95th or 99th percentile) when establishing health-based guidance values of chemicals. Monte Carlo simulation, which is able to generate large amounts of numerical results through repeated random sampling of values for influential parameters from distributions with a defined range (e.g. mean ± 3 SD), is widely used in mathematical in silico modeling to study interindividual differences in ADME characteristics (Ning et al., 2019; Shi et al., 2020; Strikwold et al., 2017). The integration of PBK modeling with Monte Carlo simulation has been used as a useful tool to predict human interindividual and interethnic differences in food borne chemical ADME characteristics and resulting toxicity within and between populations (Al-Subeihi et al., 2015; Li et al., 2017; Punt et al., 2016).

In the present study, a PBK model for human describing the ADME of daidzein and S-equol was first developed using average values of parameters as input so that output consisted of model predictions for the average population. In this initial approach, the uncertainty or variance of input parameters which may affect the output of the model predictions are not considered. To take this variation into account, the developed PBK model can be combined with Monte Carlo simulation to further assess the interindividual performance including the variance of influential parameters such as body weight, kinetic constants and chemical transit rates.

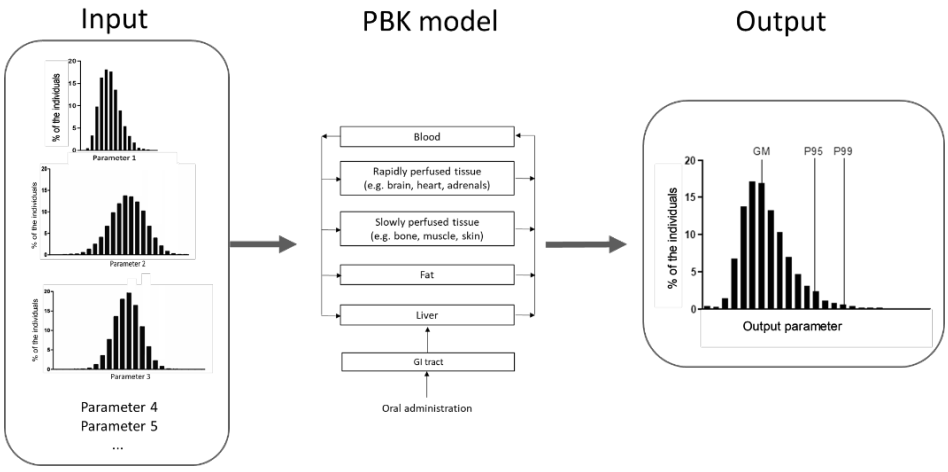

Figure 4. Schematic structure of PBK modeling integrated Monte Carlo simulation.

In the present thesis, the integration of PBK modeling with Monte Carlo simulation is performed for daidzein as the model compound in the following way: 1) Development of a PBK model for daidzein including a submodel for S-equol in human. 2) Validation of the developed PBK model. 3) Sensitivity analysis to assess the impact of parameters. The relative influence of each parameter is considered as: low, if the absolute value of the normalized sensitivity coefficient (NSC) is less than 0.2; medium, if the NSC is between 0.2 and 0.5; and high, if the NSC is above 0.5 (Li et al., 2017). Only parameters of medium and high influence were selected to be included in the Monte Carlo simulations. 4) Obtain the coefficient of variation (CV) of the selected parameters. CVs can be obtained from experimental data. If experimental data are not available, a default value of 30% can be used representing a moderate level of variation (Covington et al., 2007). 5) Description of normal distribution of selected parameters in the PBK model. This step is required when some chemical-specific parameters were in skewed distribution and assumed to follow log-normal distribution (Covington et al., 2007; Li et al., 2017). Since in Berkeley Madonna software only a "NORMAL" function is available, such parameters are first defined in log-normal distributions using equations (A) and (B), and then transformed to normal distribution by equation (C) to enable use of the Berkeley Madonna software (Li et al., 2017).

$$\mu_w = \ln\left(\mu_x/\sqrt{1 + CV_x^2}\right) \qquad \text{(A)}$$

$$\sigma_w^2 = \ln\left(1 + CV_x^2\right) \qquad \text{(B)}$$

$$Exp(NORMAL(\mu_w, \sigma_w)) = Lognormal(\mu_x, \sigma_x) \qquad \text{(C)}$$

In these equations μ_w and σ_w are the mean and CV of the parameter after the transformation to normal distribution, respectively; μ_w, CV_x and σ_w are the mean, CV and standard derivation of the parameter for log-normal distribution, respectively.

6) Repeated random sampling of selected influential parameters. The distributions for the parameter values are truncated within the range of ± 3 SD and used as input for the PBK model in the Monte Carlo simulation. The maximum iterations in one Monte Carlo run is 1,000 and can be repeated to reach thousands of runs. 6) Analyze the frequency distribution of the predicted outcome such as for example the Monte Carlo based predicted distribution for the maximum concentration (C_{max}) upon a defined oral dose, and derive geometrical mean (GM), 95th and 99th percentiles. 7) Calculation of chemical-specific adjustment factors (CSAFs) by dividing the 95th and 99th percentiles by the GM. The derived CSAFs can subsequently be compared with the default uncertainty factor of 3.16 for human interindividual differences in kinetics and can be considered as a replacement for this default uncertainty factor in risk assessment when establishing health-based guidance values for foodborne chemicals.

6. PBK modeling-based reverse dosimetry and benchmark dose (BMD) analysis

Another application of PBK modeling in risk assessment is so-called PBK modeling-based reverse dosimetry, which enables quantitative extrapolation of in vitro concentration-response curves to in vivo dose-response curves and the subsequent derivation of PoD values (Ning et al., 2019; Shi et al., 2020), such as a benchmark dose lower confidence limit (BMDL).

Figure 5 shows the schematic principle of the PBK modeling-based reverse dosimetry approach, that can be performed according to the following steps. Firstly, an in vitro concentration-response curve is obtained from an appropriate in vitro model. In vitro data can be obtained either by performing experiments using selected in vitro models or using data reported in literature. In the present thesis, the concentration-response curves used were those for ERα activation as quantified in the ERα-CALUX reporter gene assay (van der Burg et al., 2010). The next step consists of defining and validating a PBK model for the species of interest describing the ADME of the model compound of interest, so that the relevant internal exposure level (e.g. C_{max}) can be predicted upon an oral dose of the model compound. Thirdly, the in vitro concentration-response curve is translated to an in vivo dose-response curve,

assuming that the unbound free cell exposure concentration in the in vitro assay is equal to the internal unbound concentration in or at the target site (Ning et al., 2019). Since cell culture medium was prepared in albumin-free conditions, the in vitro concentrations were not corrected for protein binding (unbound fraction=1.0), assuming that the protein binding in the serum free medium was negligible, while in model predictions the plasma C_{max} was corrected to define the unbound C_{max} of the model compound to calculate the oral dose that would be needed to reach the respective free plasma concentration. At this dose the effect was considered comparable to the response observed at the respective concentration in the in vitro assay. By repeating this for each concentration the in vitro concentration-response curve is translated to an in vivo dose- response curve. Subsequently, BMD analysis of the predicted in vivo dose-response curve is performed, which enables the derivation of a PoD value such as a $BMDL_{10}$, which represents the 95% lower confidence limit of the dose level resulting in 10% extra response above background level. Finally, the previously obtained CSAFs can be applied to the predicted in vivo dose-response curve and/or to the PoD derived from the dose-response curve for the average population to define dose-response curves for the sensitive individuals at the 95th percentile or 99th percentile of the population or to establish health based guidance values. Altogether, the application of PBK modeling-based reverse dosimetry provides a useful tool for the safety evaluation of foodborne chemicals as part of the development of NAMs in toxicology.

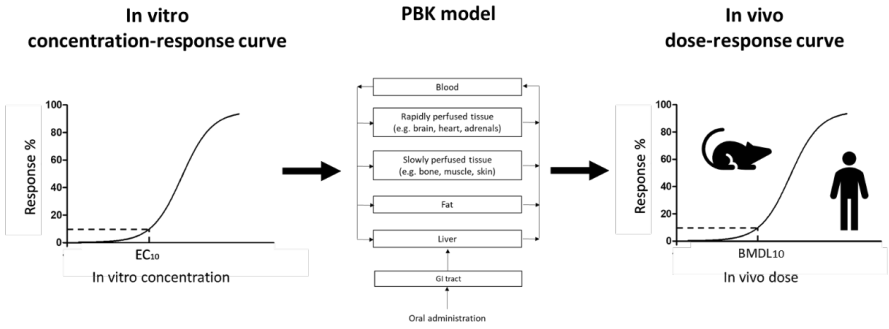

Figure 5. Schematic principle of the PBK modeling-based reverse dosimetry.

7. Outline of thesis

Chapter 1 gives an introduction to the thesis and defines the aim of the studies. It introduces gut microbiota and its metabolic capacity, which may affect the ultimate toxicity of a

foodborne compound. The two model compounds selected for the studies, the soy isoflavone daidzein and the mycotoxin ZEN, are introduced describing their ADME characteristics and toxicity. These compounds were selected because they can be converted by gut microbiota to more estrogenic metabolites. Some background information on PBK modeling and Monte Carlo simulations, used in the present thesis, are presented as well.

Chapter 2 defines a PBK model for daidzein in rats, consisting of a main model for daidzein and a submodel for S-equol. A separate compartment, the large intestinal lumen, was introduced allowing addition of the gut microbial metabolism of daidzein. Rat fecal samples were incubated anaerobically with daidzein to define the required kinetic parameters for the formation of its gut microbial metabolites DHD, S-equol and O-DMA. The obtained kinetics were used to include gut microbiota metabolism into the PBK model developed for rat, which enabled prediction of blood levels of daidzein and S-equol. The model was further evaluated by comparison of predictions made to in vivo data reported in literature. The PBK models obtained were also used to evaluate whether at defined dietary intake levels of daidzein mediated estrogenic effects are to be expected.

Chapter 3 describes the development of a PBK model for daidzein in human based on the model in rat described in **Chapter 2**. The PBK model-based predictions for the C_{max} of daidzein were compared to available literature data. The results, combined with those of **Chapter 2**, also allowed a comparison between human and rats to elucidate interspecies differences in daidzein kinetics.

In **Chapter 4**, ZEN and α-ZEL were chosen as model compounds to develop both rat and human PBK models, that included the intestinal microbial bioactivation and detoxification of ZEN. The developed PBK models enabled evaluation of the influence of intestinal metabolism on the C_{max} of ZEN and α -ZEL, and also interspecies comparisons. The PBK models obtained were also used to evaluate whether at defined dietary intakes levels of ZEN estrogenic effects are to be expected.

In Chapter 5, the developed PBK model for daidzein in human, described in **Chapter 3**, was integrated with Monte Carlo simulations to study the interindividual differences in the predicted C_{max} expressed in daidzein equivalents, taking the activity of its bioactive metabolite S-equol into account. Variations in gut microbial metabolism and liver glucuronidation of daidzein, as well as in 7 additional parameters shown to be of influence on

the PBK model predictions for C_{max}, were included in the Monte Carlo simulation. The results obtained allowed definition of CSAFs for daidzein and their comparison to the default uncertainty factor for interindividual differences in kinetics.

Chapter 6 summarizes and discusses the main findings of the thesis. It presents the innovations and limitations of the studies and methods applied and also provides future perspectives that can be addressed in the near future when studying the gut microbial metabolism of foodborne chemicals and its toxicological consequences.

References

Al-Subeihi, A. A., Alhusainy, W., Kiwamoto, R., Spenkelink, B., van Bladeren, P. J., Rietjens, I. M., and Punt, A. (2015). Evaluation of the interindividual human variation in bioactivation of methyleugenol using physiologically based kinetic modeling and Monte Carlo simulations. *Toxicol Appl Pharmacol* **283**, 117-26.

Allred, C. D., Allred, K. F., Ju, Y. H., Clausen, L. M., Doerge, D. R., Schantz, S. L., Korol, D. L., Wallig, M. A., and Helferich, W. G. (2004). Dietary genistein results in larger MNU-induced, estrogen-dependent mammary tumors following ovariectomy of Sprague-Dawley rats. *Carcinogenesis* **25**, 211-8.

Anderson, J. W., Fuller, J., Patterson, K., Blair, R., and Tabor, A. (2007). Soy compared to casein meal replacement shakes with energy-restricted diets for obese women: randomized controlled trial. *Metabolism* **56**, 280-288.

Andres, S., Abraham, K., Appel, K. E., and Lampen, A. (2011). Risks and benefits of dietary isoflavones for cancer. *Crit Rev Toxicol* **41**, 463-506.

Arai, Y., Watanabe, S., Kimira, M., Shimoi, K., Mochizuki, R., and Kinae, N. (2000). Dietary intakes of flavonols, flavones and isoflavones by Japanese women and the inverse correlation between quercetin intake and plasma LDL cholesterol concentration. *The Journal of nutrition* **130**, 2243-2250.

Bardin, A., Boulle, N., Lazennec, G., Vignon, F., and Pujol, P. (2004). Loss of ERbeta expression as a common step in estrogen-dependent tumor progression. *Endocr Relat Cancer* **11**, 537-51.

Baumler, A. J., and Sperandio, V. (2016). Interactions between the microbiota and pathogenic bacteria in the gut. *Nature* **535**, 85-93.

Behr, C., Kamp, H., Fabian, E., Krennrich, G., Mellert, W., Peter, E., Strauss, V., Walk, T., Rietjens, I., and van Ravenzwaay, B. (2017). Gut microbiome-related metabolic changes in plasma of antibiotic-treated rats. *Arch Toxicol* **91**, 3439-3454.

Belhassen, H., Jimenez-Diaz, I., Arrebola, J. P., Ghali, R., Ghorbel, H., Olea, N., and Hedili, A. (2015). Zearalenone and its metabolites in urine and breast cancer risk: a case-control study in Tunisia. *Chemosphere* **128**, 1-6.

Belli, P., Bellaton, C., Durand, J., Balleydier, S., Milhau, N., Mure, M., Mornex, J. F., Benahmed, M., and Le Jan, C. (2010). Fetal and neonatal exposure to the mycotoxin zearalenone induces phenotypic alterations in adult rat mammary gland. *Food Chem Toxicol* **48**, 2818-26.

Clarke, D. B., Barnes, K. A., Castle, L., Rose, M., Wilson, L. A., Baxter, M. J., Price, K. R., and DuPont, M. S. (2003). Levels of phytoestrogens, inorganic trace-elements, natural toxicants and nitrate in vegetarian duplicate diets. *Food Chemistry* **81**, 287-300.

Covington, T. R., Robinan Gentry, P., Van Landingham, C. B., Andersen, M. E., Kester, J. E., and Clewell, H. J. (2007). The use of Markov chain Monte Carlo uncertainty analysis to support a Public Health Goal for perchloroethylene. *Regul Toxicol Pharmacol* **47**, 1-18.

D'Alessandro, T. L., Boersma-Maland, B. J., Greg Peterson, T., Sfakianos, J., K. Prasain, J., Patel, R. P., Darley-Usmar, V. M., Botting, N. P., and Barnes, S. (2005). Metabolism of Phytoestrogen Conjugates. *In* "Phase II Conjugation Enzymes and Transport Systems", pp. 316-342.

Dalal, R. P., and Goldfarb, D. S. (2011). Melamine-related kidney stones and renal toxicity. *Nat Rev Nephrol* **7**, 267-74.

Day, A. J., Cañada, F. J., Díaz, J. C., Kroon, P. A., Mclauchlan, R., Faulds, C. B., Plumb, G. W., Morgan, M. R., and Williamson, G. (2000). Dietary flavonoid and isoflavone glycosides are hydrolysed by the lactase site of lactase phlorizin hydrolase. *FEBS letters* **468**, 166-170.

Drzymala, S. S., Binder, J., Brodehl, A., Penkert, M., Rosowski, M., Garbe, L. A., and Koch, M. (2015). Estrogenicity of novel phase I and phase II metabolites of zearalenone and cis-zearalenone. *Toxicon* **105**, 10-2.

EFSA (2011). Scientific Opinion on the risks for public health related to the presence of zearalenone in food. *EFSA Journal* **9**.

EFSA (2015). Risk assessment for peri- and post-menopausal women taking food supplements containing isolated isoflavones. *EFSA Journal* **13**.

Eisenbrand, G., and Senate Commission on Food Safety of the German Research, F. (2007). Isoflavones as phytoestrogens in food supplements and dietary foods for special medical purposes. Opinion of the Senate Commission on Food Safety (SKLM) of the German Research Foundation (DFG)-(shortened version). *Mol Nutr Food Res* **51**, 1305-12.

Enmark, E., Pelto-Huikko, M., Grandien, K., Lagercrantz, S., Lagercrantz, J., Fried, G., Nordenskjöld, M., and Gustafsson, J.-A. k. (1997). Human estrogen receptor β-gene structure, chromosomal localization, and expression pattern. *The Journal of Clinical Endocrinology & Metabolism* **82**, 4258-4265.

Everett, D., Perry, C., Scott, K., Martin, B., and Terry, M. (1987). Estrogenic potencies of resorcylic acid lactones and 17ß-estradiol in female rats. *Journal of Toxicology and Environmental Health, Part A Current Issues* **20**, 435-443.

Flandroy, L., Poutahidis, T., Berg, G., Clarke, G., Dao, M. C., Decaestecker, E., Furman, E., Haahtela, T., Massart, S., Plovier, H., Sanz, Y., and Rook, G. (2018). The impact of human activities and lifestyles on the interlinked microbiota and health of humans and of ecosystems. *Sci Total Environ* **627**, 1018-1038.

Franke, A. A., Lai, J. F., Pagano, I., Morimoto, Y., and Maskarinec, G. (2012). Equol production changes over time in pre-menopausal women. *Br J Nutr* **107**, 1201-6.

Gardana, C., Canzi, E., and Simonetti, P. (2009). The role of diet in the metabolism of daidzein by human faecal microbiota sampled from Italian volunteers. *J Nutr Biochem* **20**, 940-7.

Gill, S. R., Pop, M., DeBoy, R. T., Eckburg, P. B., Turnbaugh, P. J., Samuel, B. S., Gordon, J. I., Relman, D. A., Fraser-Liggett, C. M., and Nelson, K. E. (2006). Metagenomic analysis of the human distal gut microbiome. *science* **312**, 1355-1359.

Haiser, H. J., and Turnbaugh, P. J. (2013). Developing a metagenomic view of xenobiotic metabolism. *Pharmacol Res* **69**, 21-31.

Hargreaves, D. F., Potten, C. S., Harding, C., Shaw, L. E., Morton, M. S., Roberts, S. A., Howell, A., and Bundred, N. J. (1999). Two-week dietary soy supplementation has an estrogenic effect on normal premenopausal breast. *The Journal of Clinical Endocrinology & Metabolism* **84**, 4017-4024.

Human Microbiome Project, C. (2012). A framework for human microbiome research. *Nature* **486**, 215-21.

Hur, H. G., Beger, R. D., Heinze, T. M., Lay, J. O., Jr., Freeman, J. P., Dore, J., and Rafii, F. (2002). Isolation of an anaerobic intestinal bacterium capable of cleaving the C-ring of the isoflavonoid daidzein. *Arch Microbiol* **178**, 8-12.

Jovel, J., Patterson, J., Wang, W., Hotte, N., O'Keefe, S., Mitchel, T., Perry, T., Kao, D., Mason, A. L., Madsen, K. L., and Wong, G. K. (2016). Characterization of the Gut Microbiome Using 16S or Shotgun Metagenomics. *Front Microbiol* **7**, 459.

Khan, M. T., Nieuwdorp, M., and Backhed, F. (2014). Microbial modulation of insulin sensitivity. *Cell Metab* **20**, 753-760.

Kim, J.-S., and Kwon, C.-S. (2001). Estimated dietary isoflavone intake of Korean population based on National Nutrition Survey. *Nutrition Research* **21**, 947-953.

Kim, M. Y., Van, K., Kang, Y. J., Kim, K. H., and Lee, S. H. (2012). Tracing soybean domestication history: From nucleotide to genome. *Breed Sci* **61**, 445-52.

Klaassen, C. D., and Cui, J. Y. (2015). Review: Mechanisms of How the Intestinal Microbiota Alters the Effects of Drugs and Bile Acids. *Drug Metab Dispos* **43**, 1505-21.

Lagkouvardos, I., Overmann, J., and Clavel, T. (2017). Cultured microbes represent a substantial fraction of the human and mouse gut microbiota. *Gut Microbes* **8**, 493-503.

Laparra, J. M., and Sanz, Y. (2010). Interactions of gut microbiota with functional food components and nutraceuticals. *Pharmacol Res* **61**, 219-25.

Le Chatelier, E., Nielsen, T., Qin, J., Prifti, E., Hildebrand, F., Falony, G., Almeida, M., Arumugam, M., Batto, J. M., Kennedy, S., Leonard, P., Li, J., Burgdorf, K., Grarup, N., Jorgensen, T., Brandslund, I., Nielsen, H. B., Juncker, A. S., Bertalan, M., Levenez, F., Pons, N., Rasmussen, S., Sunagawa, S., Tap, J., Tims, S., Zoetendal, E. G., Brunak, S., Clement, K., Dore, J., Kleerebezem, M., Kristiansen, K., Renault, P., Sicheritz-Ponten, T., de Vos, W. M., Zucker, J. D., Raes, J., Hansen, T., Meta, H. I. T. c., Bork, P., Wang, J., Ehrlich, S. D., and Pedersen, O. (2013). Richness of human gut microbiome correlates with metabolic markers. *Nature* **500**, 541-6.

Lee, P. G., Lee, U. J., Song, H., Choi, K. Y., and Kim, B. G. (2018). Recent advances in the microbial hydroxylation and reduction of soy isoflavones. *FEMS Microbiol Lett* **365**.

Li, M., Gehring, R., Riviere, J. E., and Lin, Z. (2017). Development and application of a population physiologically based pharmacokinetic model for penicillin G in swine and cattle for food safety assessment. *Food Chem Toxicol* **107**, 74-87.

Louisse, J., Beekmann, K., and Rietjens, I. M. (2017). Use of Physiologically Based Kinetic Modeling-Based Reverse Dosimetry to Predict in Vivo Toxicity from in Vitro Data. *Chem Res Toxicol* **30**, 114-125.

Maskarinec, G. (2013). The human mammary gland as a target for isoflavones: how does the relation vary in individuals with different ethnicity? *Planta Med* **79**, 554-61.

Matthies, A., Blaut, M., and Braune, A. (2009). Isolation of a human intestinal bacterium capable of daidzein and genistein conversion. *Appl Environ Microbiol* **75**, 1740-4.

Mayo, B., Vazquez, L., and Florez, A. B. (2019). Equol: A Bacterial Metabolite from The Daidzein Isoflavone and Its Presumed Beneficial Health Effects. *Nutrients* **11**.

Merz-Demlow, B. E., Duncan, A. M., Wangen, K. E., Xu, X., Carr, T. P., Phipps, W. R., and Kurzer, M. S. (2000). Soy isoflavones improve plasma lipids in normocholesterolemic, premenopausal women. *The American journal of clinical nutrition* **71**, 1462-1469.

Messina, M. (2010). A brief historical overview of the past two decades of soy and isoflavone research. *J Nutr* **140**, 1350S-4S.

Metzler, M., Pfeiffer, E., and Hildebrand, A. (2010). Zearalenone and its metabolites as endocrine disrupting chemicals. *World Mycotoxin Journal* **3**, 385-401.

Meyer, T. W., and Hostetter, T. H. (2012). Uremic solutes from colon microbes. *Kidney Int* **81**, 949-954.

Mirocha, C., Pathre, S., and Robison, T. (1981). Comparative metabolism of zearalenone and transmission into bovine milk. *Food and Cosmetics Toxicology* **19**, 25-30.

Nakano, H., Ogura, K., Takahashi, E., Harada, T., Nishiyama, T., Muro, K., Hiratsuka, A., Kadota, S., and Watabe, T. (2004). Regioselective monosulfation and disulfation of the phytoestrogens daidzein and genistein by human liver sulfotransferases. *Drug metabolism and pharmacokinetics* **19**, 216-226.

Nikaido, Y., Yoshizawa, K., Danbara, N., Tsujita-Kyutoku, M., Yuri, T., Uehara, N., and Tsubura, A. (2004). Effects of maternal xenoestrogen exposure on development of the reproductive tract and mammary gland in female CD-1 mouse offspring. *Reprod Toxicol* **18**, 803-11.

Ning, J., Rietjens, I., and Strikwold, M. (2019). Integrating physiologically based kinetic (PBK) and Monte Carlo modeling to predict inter-individual and inter-ethnic variation in bioactivation and liver toxicity of lasiocarpine. *Arch Toxicol* **93**, 2943-2960.

Niu, Z.-R., Fang, L.-H., Qiang, G.-F., and Du, G.-H. (2018). Daidzein. *In* "Natural Small Molecule Drugs from Plants", pp. 31-35.

Ochoa-Reparaz, J., Mielcarz, D. W., Begum-Haque, S., and Kasper, L. H. (2011). Gut, bugs, and brain: role of commensal bacteria in the control of central nervous system disease. *Ann Neurol* **69**, 240-7.

Pritchett, L. E., Atherton, K. M., Mutch, E., and Ford, D. (2008). Glucuronidation of the soyabean isoflavones genistein and daidzein by human liver is related to levels of UGT1A1 and UGT1A9 activity and alters isoflavone response in the MCF-7 human breast cancer cell line. *J Nutr Biochem* **19**, 739-45.

Punt, A., Paini, A., Spenkelink, A., Scholz, G., Schilter, B., van Bladeren, P. J., and Rietjens, I. M. (2016). Evaluation of Interindividual Human Variation in Bioactivation and DNA Adduct Formation of Estragole in Liver Predicted by Physiologically Based Kinetic/Dynamic and Monte Carlo Modeling. *Chem Res Toxicol* **29**, 659-68.

Rietjens, I. M., Louisse, J., and Punt, A. (2011). Tutorial on physiologically based kinetic modeling in molecular nutrition and food research. *Mol Nutr Food Res* **55**, 941-56.

Rietjens, I. M., Sotoca, A. M., Vervoort, J., and Louisse, J. (2013). Mechanisms underlying the dualistic mode of action of major soy isoflavones in relation to cell proliferation and cancer risks. *Mol Nutr Food Res* **57**, 100-13.

Rogowska, A., Pomastowski, P., Sagandykova, G., and Buszewski, B. (2019). Zearalenone and its metabolites: Effect on human health, metabolism and neutralisation methods. *Toxicon* **162**, 46-56.

Ropejko, K., and Twaruzek, M. (2021). Zearalenone and Its Metabolites-General Overview, Occurrence, and Toxicity. *Toxins (Basel)* **13**.

Rowland, I., Gibson, G., Heinken, A., Scott, K., Swann, J., Thiele, I., and Tuohy, K. (2018). Gut microbiota functions: metabolism of nutrients and other food components. *Eur J Nutr* **57**, 1-24.

Sager, J. E., Yu, J., Ragueneau-Majlessi, I., and Isoherranen, N. (2015). Physiologically Based Pharmacokinetic (PBPK) Modeling and Simulation Approaches: A Systematic Review of Published Models, Applications, and Model Verification. *Drug Metab Dispos* **43**, 1823-37.

Scheperjans, F., Aho, V., Pereira, P. A., Koskinen, K., Paulin, L., Pekkonen, E., Haapaniemi, E., Kaakkola, S., Eerola-Rautio, J., Pohja, M., Kinnunen, E., Murros, K., and Auvinen, P. (2015). Gut microbiota are related to Parkinson's disease and clinical phenotype. *Mov Disord* **30**, 350-8.

Schwen, R. J., Nguyen, L., and Jackson, R. L. (2012). Elucidation of the metabolic pathway of S-equol in rat, monkey and man. *Food Chem Toxicol* **50**, 2074-83.

Seow, A., Shi, C.-Y., Franke, A. A., Hankin, J. H., Lee, H.-P., and Yu, M. C. (1998). Isoflavonoid levels in spot urine are associated with frequency of dietary soy intake in a population-based sample of middle-aged and older Chinese in Singapore. *Cancer Epidemiology and Prevention Biomarkers* **7**, 135-140.

Shi, M., Bouwmeester, H., Rietjens, I., and Strikwold, M. (2020). Integrating in vitro data and physiologically based kinetic modeling-facilitated reverse dosimetry to predict human cardiotoxicity of methadone. *Arch Toxicol* **94**, 2809-2827.

Sjogren, K., Engdahl, C., Henning, P., Lerner, U. H., Tremaroli, V., Lagerquist, M. K., Backhed, F., and Ohlsson, C. (2012). The gut microbiota regulates bone mass in mice. *J Bone Miner Res* **27**, 1357-67.

Smith, K., McCoy, K. D., and Macpherson, A. J. (2007). Use of axenic animals in studying the adaptation of mammals to their commensal intestinal microbiota. *Semin Immunol* **19**, 59-69.

Sommer, F., and Backhed, F. (2013). The gut microbiota--masters of host development and physiology. *Nat Rev Microbiol* **11**, 227-38.

Sotoca, A. M., Ratman, D., van der Saag, P., Strom, A., Gustafsson, J. A., Vervoort, J., Rietjens, I. M., and Murk, A. J. (2008). Phytoestrogen-mediated inhibition of proliferation of the human T47D breast cancer cells depends on the ERalpha/ERbeta ratio. *J Steroid Biochem Mol Biol* **112**, 171-8.

Soukup, S. T., Helppi, J., Muller, D. R., Zierau, O., Watzl, B., Vollmer, G., Diel, P., Bub, A., and Kulling, S. E. (2016). Phase II metabolism of the soy isoflavones genistein and daidzein in humans, rats and mice: a cross-species and sex comparison. *Arch Toxicol* **90**, 1335-47.

Sousa, T., Paterson, R., Moore, V., Carlsson, A., Abrahamsson, B., and Basit, A. W. (2008). The gastrointestinal microbiota as a site for the biotransformation of drugs. *Int J Pharm* **363**, 1-25.

Steinberg, F. M., Guthrie, N. L., Villablanca, A. C., Kumar, K., and Murray, M. J. (2003). Soy protein with isoflavones has favorable effects on endothelial function that are independent of lipid and antioxidant effects in healthy postmenopausal women. *The American journal of clinical nutrition* **78**, 123-130.

Strikwold, M., Spenkelink, B., Woutersen, R. A., Rietjens, I., and Punt, A. (2017). Development of a Combined In Vitro Physiologically Based Kinetic (PBK) and Monte Carlo Modeling Approach to Predict Interindividual Human Variation in Phenol-Induced Developmental Toxicity. *Toxicol Sci* **157**, 365-376.

Sun, M.-Y., Ye, Y., Xiao, L., Rahman, K., Xia, W., and Zhang, H. (2016). Daidzein: A review of pharmacological effects. *African Journal of Traditional, Complementary and Alternative Medicines* **13**.

Takemura, H., Shim, J. Y., Sayama, K., Tsubura, A., Zhu, B. T., and Shimoi, K. (2007). Characterization of the estrogenic activities of zearalenone and zeranol in vivo and in vitro. *J Steroid Biochem Mol Biol* **103**, 170-7.

Tamura, M., Tsushida, T., and Shinohara, K. (2007). Isolation of an isoflavone-metabolizing, Clostridium-like bacterium, strain TM-40, from human faeces. *Anaerobe* **13**, 32-5.

Ussar, S., Griffin, N. W., Bezy, O., Fujisaka, S., Vienberg, S., Softic, S., Deng, L., Bry, L., Gordon, J. I., and Kahn, C. R. (2015). Interactions between Gut Microbiota, Host Genetics and Diet Modulate the Predisposition to Obesity and Metabolic Syndrome. *Cell Metab* **22**, 516-530.

van der Burg, B., Winter, R., Weimer, M., Berckmans, P., Suzuki, G., Gijsbers, L., Jonas, A., van der Linden, S., Witters, H., Aarts, J., Legler, J., Kopp-Schneider, A., and Bremer, S. (2010). Optimization and prevalidation of the in vitro ERalpha CALUX method to test estrogenic and antiestrogenic activity of compounds. *Reprod Toxicol* **30**, 73-80.

van Erp-Baart, M.-A. J., Brants, H. A., Kiely, M., Mulligan, A., Turrini, A., Sermoneta, C., Kilkkinen, A., and Valsta, L. M. (2003). Isoflavone intake in four different European countries: the VENUS approach. *British Journal of Nutrition* **89**, S25-S30.

Wakai, K., Egami, I., Kato, K., Kawamura, T., Tamakoshi, A., Lin, Y., Nakayama, T., Wada, M., and Ohno, Y. (1999). Dietary intake and sources of isoflavones among Japanese. *Nutrition and cancer* **33**, 139-145.

WHO (2005). Chemical-specific adjustment factors for interspecies differences and human variability: guidance document for use of data in dose/concentration-response assessment. *Chemical-specific adjustment factors for interspecies differences and human variability: guidance document for use of data in dose/concentration-response assessment*, 96-96.

Yazar, S., and Omurtag, G. Z. (2008). Fumonisins, trichothecenes and zearalenone in cereals. *Int J Mol Sci* **9**, 2062-90.

Yu, Z., Zhang, L., Wu, D., and Liu, F. (2005). Anti-apoptotic action of zearalenone in MCF-7 cells. *Ecotoxicol Environ Saf* **62**, 441-6.

Zimmermann, M., Zimmermann-Kogadeeva, M., Wegmann, R., and Goodman, A. L. (2019). Mapping human microbiome drug metabolism by gut bacteria and their genes. *Nature* **570**, 462-467.

Zinedine, A., Soriano, J. M., Molto, J. C., and Manes, J. (2007). Review on the toxicity, occurrence, metabolism, detoxification, regulations and intake of zearalenone: an oestrogenic mycotoxin. *Food Chem Toxicol* **45**, 1-18.

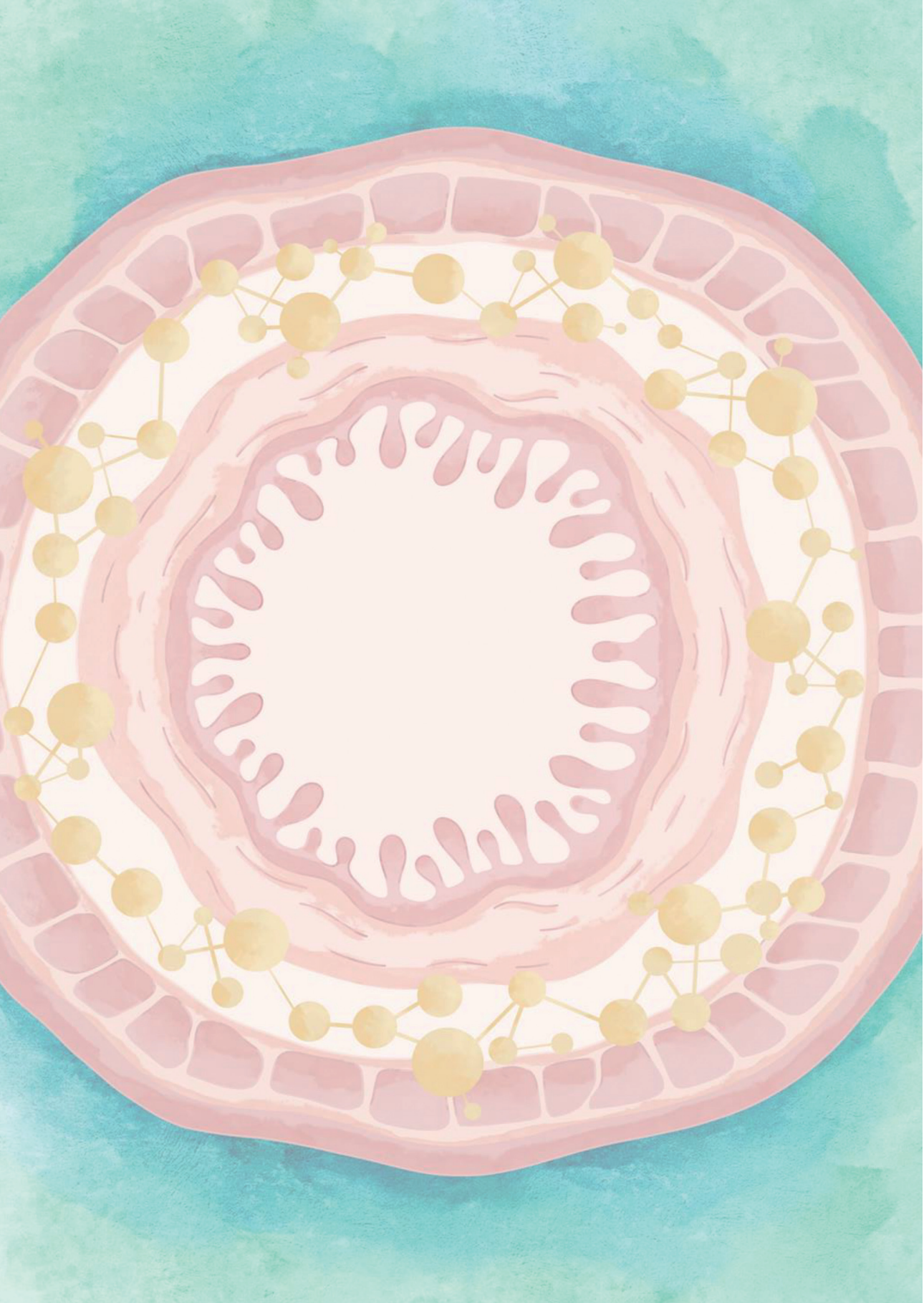

Chapter 2

Use of physiologically based kinetic modeling (PBK) to predict rat gut microbial metabolism of the isoflavone daidzein to S-equol and its consequences for ERα activation

Qianrui Wang, Bert Spenkelink, Rungnapa Boonpawa, Ivonne M.C.M. Rietjens and Karsten Beekmann

Published in Molecular Nutrition & Food Research. 2020; 64(6), 1900912

Abstract

To predict gut microbial metabolism of xenobiotics and the resulting plasma concentrations of metabolites formed, an in vitro-in silico based testing strategy was developed using the isoflavone daidzein and its gut microbial metabolite S-equol as model compounds. Anaerobic rat fecal incubations were optimized and performed to derive the apparent maximum velocities (V_{max}) and Michaelis-Menten constants (K_m) for gut microbial conversion of daidzein to dihydrodaidzein (DHD), S-equol and O-desmethylangolensin (O-DMA), which were used as input parameters for a physiologically based kinetic (PBK) model. The inclusion of gut microbiota in the PBK model allowed prediction of S-equol concentrations and slightly reduced predicted daidzein concentrations from 2.19 to 2.16 μM. The resulting predicted concentrations of daidzein and S-equol were comparable to in vivo levels reported. The optimized in vitro approach to quantify kinetics for conversions by gut microbiota and the newly developed PBK model in rats that includes gut microbial metabolism provide a unique tool to predict the in vivo consequences of daidzein microbial metabolism for systemic exposure of the host to daidzein and its metabolite S-equol. The predictions revealed a dominant role for daidzein in its ERα-mediated estrogenicity despite the higher estrogenic potency of its microbial metabolite S-equol.

1. Introduction

The human intestinal tract is host to a diverse microbial community consisting of bacteria, yeasts, viruses, archea, fungi and protozoa, of which anaerobic bacteria are dominating in number especially in the distal colon where the microbial density is the highest (Le Chatelier et al., 2013). The gut microbiota is known to play an important role in the health of the host, among others through metabolism of indigestible food components, formation of vitamins and protection of the host from pathogens (Maier et al., 2018; Smith et al., 2007). While there are significant interindividual differences in the composition of the microbiota, these do not necessarily translate to functional differences (Human Microbiome Project, 2012). Yet, dysbiosis of the gut microbiota is associated with various diseases, such as non-alcoholic fatty liver disease, metabolic disorders, inflammatory bowel disease, and autism(Greenblum et al., 2012; Karlsson et al., 2013; Larsen et al., 2010; Million et al., 2013; Qin et al., 2010). The gut microbiota can further affect the susceptibility of its host to adverse effects caused by foodborne chemicals and pharmaceuticals by modifying their toxicity through a broad range of reactions, such as reduction, hydrolysis, dehydroxylation, acetylation, deacetylation, and N-oxide cleavage (Haiser and Turnbaugh, 2013; Sousa et al., 2008).

To reduce the use of animal experimentation, toxicity testing is currently undergoing a paradigm shift away from the use of experimental animals towards the use of human-based in vitro experimentation combined with in silico modeling. At the heart of these testing strategies, physiologically based kinetic (PBK) models are used to describe the absorption, distribution, metabolism and excretion (ADME) to make sure kinetics are taken into account when using in vitro data to conclude on the in vivo situation (Louisse et al., 2017). With PBK model based reverse dosimetry in vitro concentration-response curves can be translated to in vivo dose-response curves that allow definition of points of departure that are required in risk assessment. In previous work we have shown proofs-of-principle for predicting, for example, liver toxicity of the pyrrolizidine alkaloids lasiocarpine and riddelliine in rat (Chen et al., 2018) and human (Ning et al., 2019), kidney toxicity of aristolochic acid (Abdullah et al., 2016) and developmental toxicity of glycol ethers (de Jong et al., 2009), phenols (Strikwold et al., 2017a; Strikwold et al., 2013), and all-trans-retinoic acid (Louisse et al., 2015). Currently established PBK models however, entirely ignore the gut microbiota, which may turn out an issue for compounds where metabolism by gut microbiota plays an important role in their ADME characteristics and/or toxicity. Currently established PBK models focus on the use of mammalian cell lines and tissue samples, yet entirely ignore the gut microbiota.

The isoflavone daidzein is an extensively studied example of a phytochemical that is affected by gut microbial metabolism. Daidzein is present in high levels in soybeans and soy products and is commonly consumed especially in Asian and vegetarian diets (Gardana and Simonetti, 2017). Microbial metabolism of daidzein yields dihydrodaidzein (DHD), which is subsequently further metabolized to S-equol and O-desmethylangolensin (O-DMA) by the gut microbiota (**Figure 1**) (Atkinson et al., 2005; Kobayashi et al., 2013). The metabolite S-equol is reported to have a higher bioavailability and slower clearance than daidzein (Setchell and Clerici, 2010), and to be a more potent inducer of estrogen receptors (ERs) than daidzein (Morito et al., 2001). S-equol is reported to preferentially bind to ERβ over ERα (Muthyala et al., 2004). Opposite to ERα activation, which is associated with adverse health effects through induction of cell proliferation, ERβ activation is associated with beneficial health effects through anti-proliferative activities (Kostelac et al., 2003). The microbial metabolite S-equol, however, is only produced by 20-35% of the Western adult population and 50-55% of the Asian adult population (Arai et al., 2000a; Atkinson et al., 2005; Setchell and Cole, 2006). Most animal species are reported to be capable of producing S-equol (Setchell et al., 2002), which indicates that studies in laboratory animals might overestimate the effect of isoflavone ingestion when compared to the general human population. Importantly, S-equol-producing individuals are reported to benefit more from isoflavone ingestion than non-producers (Crawford et al., 2013), Some previous studies isolated different bacterial species from rat, mice and human capable of converting daidzein to DHD and/or S-equol (Matthies et al., 2009; Matthies et al., 2008; Rafii et al., 2007; Wang et al., 2007), but these studies did not enable quantification of kinetic parameters required to include the gut microbial conversion of daidzein in PBK models.

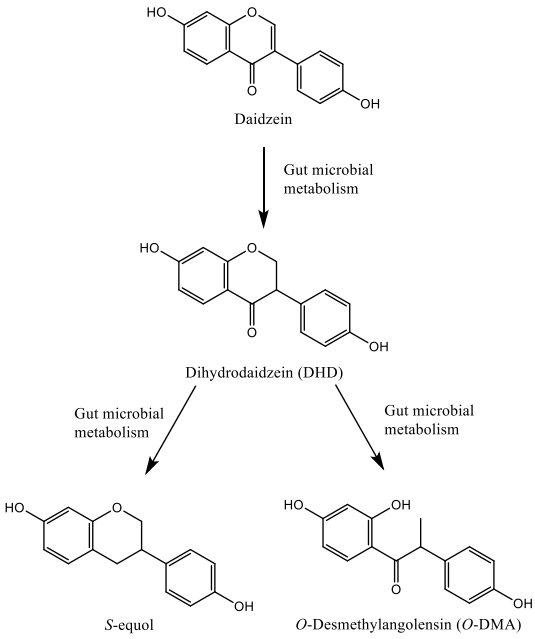

Figure 1. Schematic of daidzein metabolism by gut microbiota.

In the present study, the metabolic rates of gut microbial metabolism of the model compound daidzein in rat were derived using anaerobic fecal incubations. Based on the kinetic data obtained, a PBK model described previously (Boonpawa et al., 2017) was adapted to contain a gut microbial compartment, allowing to predict plasma concentrations not only of the isoflavone daidzein but also of its most important metabolite S-equol and relevant phase II metabolites. The predicted concentrations of these metabolites are compared to in vivo concentrations reported in literature.

2. Experimental Section

2.1 Materials and Standard Chemicals

Pooled Sprague Dawley (SD) male rat liver S9 was obtained from Corning (MA, USA). Daidzein, S-equol, O-DMA, 17β-estradiol (E_2), DMSO, glycerol, alamethicin, uridine 5′-diphosphoglucuronic acid (UDPGA), Tris, trans-1,2-diaminocyclohexane-N,N,N’,N’-tetracetic acid monohydrate (CDTA), tricine, $(MgCO_3)_4Mg(OH)_2 \cdot 5H_2O$, luciferine Na-salt, adenosine triphosphate (ATP) and 1,4-dithiothreitol (DTT) were purchased from Sigma–Aldrich (Zwijndrecht, The Netherlands) at the highest purity available. DHD was obtained

from Cayman Chemical (AA, USA) and O-DMA was purchased from Plantech (Reading, UK). Ethanol, trifluoroacetic acid (TFA), $MgCl_2$, $CuSO_4$, 37% HCl, $MgSO_4 \cdot 7H_2O$, NaOH, ethylenedinitrotetraacetic acid (EDTA·$2H_2O$; Titriplex III) and KCl were purchased from VWR International (Amsterdam, The Netherlands). Ultra-Performance Liquid Chromatography (UPLC) grade solvents ACN and methanol were obtained from Biosolve BV (Valkenswaard, The Netherlands). The human osteosarcoma U-2OS ERα cell line and the U-2OS Cytotox cell line were kindly provided by BioDetection Systems (Amsterdam, The Netherlands). Fetal calf serum (FCS) was obtained from Bodinco (Alkmaar, The Netherlands). PBS, fetal calf serum treated with dextran coated charcoal (DCC-FCS), DMEM/F-12 (catalogue number 31331-028) and DMEM/F-12 (catalogue number 21041-025) were supplied by Gibco (Paisley, UK). Non-essential amino acids (NEAA), trypsin (0.025%) and G418 disulfate salt (geneticin) were obtained from Invitrogen Life Technologies (Breda, The Netherlands). 96-well plates were purchased from Greiner Bio-One (Frickenhausen, Germany) and polystyrene cell culture flasks were purchased from Corning (Amsterdam, The Netherlands). 5 x 9 cm sterile medical gauze dressing was purchased from HEKApres (Venray, The Netherlands; catalogue number KO 0036).

2.2 Anaerobic incubation of rat feces

Fresh fecal samples from Wistar rats (20 males and 20 females) were kindly provided by BASF (Ludwigshafen, Germany). Feces were obtained by physical stimulation, weighed and immediately transferred into an anaerobic solution of 10% (v/v) glycerol in PBS and diluted to a final fecal concentration of 20% (w/v). Pooled samples were homogenized using a sterile glass wand, tubes flushed with N_2 gas and stored at -80 °C until further use. Subsequently, samples were filtered using sterile gauze under anaerobic conditions, and aliquoted samples of resulting fecal slurry were stored at -80 °C until use.

Conditions for anaerobic incubation of rat feces were optimized to achieve linear depletion of the substrate and linear formation of metabolites over time and concentration of feces. Incubation solutions of 100 µL were prepared in anaerobic PBS containing 0.3% to 8% feces (v/v), and 0.5% daidzein added from 200-times concentrated stock solutions in DMSO (final concentration 17.5 µM). Samples were prepared in an anaerobic chamber (Sheldon, Cornelius, USA) with an atmosphere of 85% N_2, 10% CO_2 and 5% H_2, and incubated in the same atmosphere at 37 °C. After incubation, 1 volume of ice-cold methanol was added to terminate the reaction. Subsequently, samples were put on ice for 10 min and centrifuged at 21,500 ×g

for 15 min at 4 °C to precipitate microorganisms, particles, and proteins. Quantification of the substrate and metabolites in supernatants was subsequently done using UPLC analysis performed as described below. For the kinetic incubations, 6% of feces (v/v) and an incubation duration of 35 min were chosen as optimal conditions.

To obtain the kinetics of rat microbial conversion of daidzein, incubations were carried out with a range of daidzein concentrations from 2.2 µM to 70 µM. Incubation solutions of 100 µL were prepared containing 6 % feces (v/v), 69.5% anaerobic PBS (v/v) and 0.5% daidzein (v/v) added from 200-times concentrated stock solutions in DMSO resulting in final concentrations as indicated. Solvent control and negative control samples were prepared either without daidzein (replaced by 0.5 % volume of DMSO) or without fecal slurries (replaced by 30% volume of PBS), respectively. These samples were prepared and processed in the same way as stated above. Incubations were repeated three times.

2.3 Glucuronidation of S-equol by rat liver S9

Incubations with pooled liver S9 fractions from male SD rats were performed as described previously (Islam et al., 2014) with some modifications. Incubation mixtures of 100 µL were prepared containing 10 mM UDPGA, 0.025 mg/mL alamethicin (added from a 200-time concentrated stock solution in methanol) and 0.5 mg protein/mL rat liver S9 fractions in 50 mM Tris-HCl (pH 7.4) with 10 mM of $MgCl_2$. After pre-incubation in a shaking water bath at 37 °C for 1 min, reactions were initiated by adding 0.5 µL of the substrate S-equol (from 200-times concentrated stock solutions in DMSO) resulting in final concentrations ranging from 1 µM to 200 µM. After incubation in a shaking water bath at 37 °C for 5 min, reactions were terminated by adding 25 µL of ice-cold ACN. Under these conditions, glucuronidation of S-equol was linear in time and with protein concentration (data not shown). Negative and blank controls were performed in the absence of either the substrate or UDPGA. Samples were subsequently centrifuged at 21,500 ×g for 15 min at 4 °C to precipitate proteins. Supernatants were stored at -80 °C until UPLC analysis. Incubations were repeated three times.

2.4 UPLC analysis

UPLC analysis was performed to quantify the concentrations of daidzein and its metabolites. The Waters ACQUITY UPLC system (Dublin, Ireland) was equipped with a guard column and a Waters Acquity UPLC BEH C18 (1.7 µm, 2.1 × 50 mm) column. 0.1% TFA in nanopure water (v/v) was used as solvent A and ACN as solvent B. The injection volume was

3.5 μL and wavelengths of 190-320 nm were recorded using a Waters photodiode array detector.

For analysis of gut microbial metabolites, a flow rate of 0.3 mL/min was applied, and elution was performed using the following gradient: 0% B in 0-1.00 min; 0-25% B in 1.00-1.30 min; 25-30% B in 1.30-2.70 min; 30-80% B in 2.70-3.70 min, 80-100% in 3.70-4.00 min, 100% B for 4.00-5.00, 100-0% B in 5.00-6.00 min and 0% B between 6.00-7.00 min. Identification and quantification of daidzein and its microbial metabolites, i.e. DHD, S-equol and O-DMA, were achieved using commercially available standards at a wavelength of 280 nm.

For the detection of rat liver S9 incubation products, a flow rate of 0.4 mL/min was applied, and elution was performed using the following gradient: 0-18% B in 0.20-0.40 min; 18% B for 0.20-3.00 min; 18-30% B in 3.00-3.50 min; 30-80% B in 3.50-5.00 min, 80-100% in 5.00-5.50 min, 100% B for 5.50-6.00, 100-0% B in 6.00-6.50 min and 0% B between 6.50-7.00 min. To verify the type of conjugation, non-terminated samples were also prepared to incubate them with beta-glucuronidase to carry out the deconjugation reaction. Standard S-equol was used as a reference to allow quantification at the wavelength of 280 nm.

2.5 Kinetic analysis

Kinetic constants, including the apparent maximum velocity (V_{max}) expressed in μmol/h/g feces and the apparent Michaelis-Menten constant (K_m) expressed in μM, were derived to describe the gut microbial conversion of daidzein and the glucuronidation of S-equol, using GraphPad Prism 5.04 (GraphPad Software, CA, USA). Data from rat fecal anaerobic incubations of daidzein and rat liver S9 incubations of S-equol were fitted to the standard Michaelis-Menten equation:

$$v = \frac{V_{max} \times [S]}{K_m + [S]}$$

where v is the conversion rate and [S] represents the substrate concentration.

2.6 PBK model development

The schematic structure of the PBK model for daidzein and S-equol is shown in **Figure 2**. This newly defined conceptual PBK model includes a main model for the parent compound daidzein, which involves separate compartments for blood, liver, fat, rapidly perfused tissue

(e.g. heart, lung and brain) and slowly perfused tissue (e.g. skin, muscle and bone). This model was based on the model previoulsy reported and validated for the related isoflavone genistein (Boonpawa et al., 2017). To simulate reactions in the intestine, the small intestinal lumen, intestinal tissue, and the large intestinal lumen are described as separate compartments, where the gut microbial metabolic activities are described in the large intestinal lumen. The conversion of daidzein by the gut microbiota results in the formation of three metabolites, DHD, S-equol and O-DMA. S-equol was modelled to directly enter the liver from the large intestinal lumen with the rate constant of 3.43/h, as the phase II metabolism of large intestinal tissue is considered negligible compared to that of the liver. To be able to predict the plasma concentrations of S-equol, being the most important metabolite due to its biological activity, a sub-model was prepared to describe its distribution and metabolism.

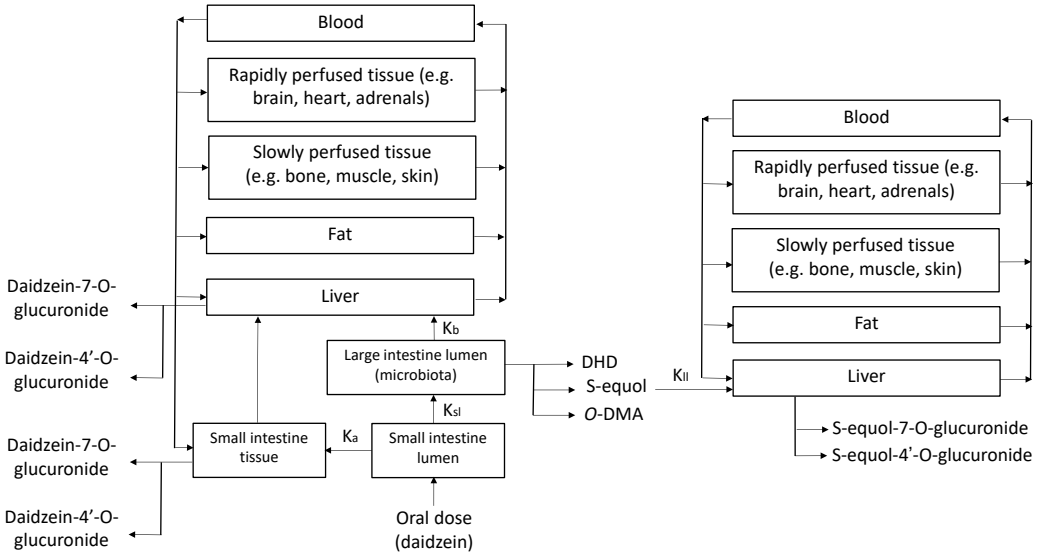

Figure 2. Schematic structure of the PBK model. The left part is the part that describes the metabolism of daidzein, which partly converts to S-equol in the large intestinal lumen by gut microbiota and is then imported in the right part of the model which describes the metabolism of S-equol. All compartments including blood, rapidly and slowly perfused tissues, fat and liver are identical in the two parts of the model.

In order to develop a PBK model, three types of parameters are needed: 1) physiological and anatomical descriptors, 2) physico-chemical parameters such as partition coefficients of the

compound and 3) kinetic parameters which describe the metabolic reactions (Rietjens et al., 2011). Values for the first two classes of parameters are presented in **Table 1**. Physiological parameter values such as tissue volumes and blood flows, were obtained from literature (Brown et al., 1997). Tissue/blood partition coefficients were calculated based on the method reported previously (DeJongh et al., 1997) using the octanol-water partition coefficient (Log P) of 2.51 and 3.20 for daidzein and S-equol (Rothwell et al., 2005), respectively.

Table 1. Parameters used for the PBK model of daidzein and S-equol in rats.

Physiological parameters (Brown et al., 1997)				Tissue: blood partition coefficients (DeJongh et al., 1997; Rothwell et al., 2005)			
Body weight (kg)	0.25	Cardiac output (L/h)	5.38	Daidzein		S-equol	
Percentage of body weight		Percentage of cardiac output		Intestine	1.62	Intestine	2.44
Small intestine	1.4	Intestine	15.1	Liver	1.62	Liver	2.44
Liver	3.4	Liver	9.9	Rapidly perfused tissue	1.62	Rapidly perfused tissue	2.44
Rapidly perfused tissue	6.8	Rapidly perfused tissue	51.0	Slowly perfused tissue	0.58	Slowly perfused tissue	0.72
Slowly perfused tissue	66.7	Slowly perfused tissue	17.0	Fat	44.75	Fat	96.29
Fat	7.0	Fat	7.0				
Blood	7.4						
Non-perfused tissue	5.7						
GI tract contents	5.0						

Kinetic parameters V_{max} and K_m defined in rat fecal anaerobic incubations as described above were used to describe gut microbial conversions from daidzein to DHD, S-equol and O-DMA, as was required for model development. To this end, rat fecal anaerobic incubations were carried out as described above. The obtained apparent V_{max} values expressed in µM/h/g feces were scaled to the whole body using a fecal fraction of body weight 0.0164 (Hoskins and Zamcheck, 1968).

Kinetic constants of daidzein glucuronidation by liver and small intestinal tissue samples were taken from published literature (Islam et al., 2014), whereas formation of sulfated metabolites was considered to be negligible, since previous studies showed the catalytic efficiencies

(V_{max}/K_m) for sulfation to be at least two orders of magnitude lower than glucuronidation (Islam et al., 2014). Kinetic constants for rat liver glucuronidation of S-equol were obtained by performing incubations with pooled SD male rat liver S9 fractions, carried out as described above.

V_{max} and catalytic efficiencies of intestinal glucuronidation were scaled to the small intestine, using an S9 protein yield of 38.6 mg/g small intestine. This value was obtained from the sum of cytosolic protein yield (18 mg/g small intestine) and microsomal protein yield (20.6 mg/g small intestine) (Cubitt et al., 2011). For example, the V_{max} for daidzein-7-glucoronide and daidzein-4'-glucoronide formation were scaled as follows:

$$VmaxSIDAI7G = (VmaxSIDAI7Gc/1000)*60*S9SI*SI*BW$$

$$VmaxSIDAI4iG = (VmaxSIDAI4iGc/1000)*60*S9SI*SI*BW$$

where VmaxSIDAI7G (µmol/h) and VmaxSIDAI7Gc (nmol/min/mg S9 protein) respectively stand for scaled and unscaled maximum formation rates of daidzein-7-glucoronide, VmaxSIDAI4iG (µmol/h) and VmaxSIDAI4iGc (nmol/min/mg S9 protein) respectively stand for scaled and unscaled maximum formation rates of daidzein-4'-glucoronide, S9SI (mg S9 protein/g small intestine) stands for small intestinal S9 protein yield, SI (g small intestine/kg bw) represents the fraction of the small intestine of total body weight and BW stands for body weight (kg). The factor 1/1000 is used to convert nmol to µmol and the factor *60 to convert the rate per minute to a rate per hour.

Similarly, for liver glucuronidation, V_{max} values were scaled to the liver by using an S9 protein yield of 143 mg/g liver. This value was obtained from the sum of cytosolic protein yield (108 mg/g liver) and microsomal protein yield (35 mg/g liver) (Medinsky et al., 1994). For example, the V_{max} for daidzein-7-glucoronide and daidzein-4'-glucoronide formation were scaled as:

$$VmaxLDAI7G = (VmaxLDAI7Gc/1000)*60* VLS9 *L*BW$$

$$VmaxLDAI4iG = (VmaxLDAI4iGc/1000)*60* VLS9 *L*BW$$

where VmaxLDAI7G (µmol/h) and VmaxLDAI7Gc (nmol/min/mg S9 protein) respectively stand for scaled and unscaled maximum formation rates of daidzein-7-glucoronide, VmaxLDAI4iG (µmol/h) and VmaxLDAI4iGc (nmol/min/mg S9 protein) respectively stand

for scaled and unscaled maximum formation rates of daidzein-4'-glucoronide, VLS9 (mg S9 protein/g liver) stands for liver S9 protein yield, L (g liver/kg bw) represents the fraction of liver of total body weight and BW stands for body weight (kg). The factor 1/1000 is used to convert nmol to µmol and the factor *60 to convert the rate per minute to a rate per hour.

The PBK model equations were coded and numerically integrated in Berkeley Madonna 8.3.18 (UC Berkeley, CA, USA) using Rosenbrock's algorithms for stiff systems. The model code is presented in **Supplementary Material 1**.

2.7 Sensitivity analysis

A sensitivity analysis was performed using a relatively simple linear method (Evans and Andersen, 2000) to assess which parameters of the PBK model have the largest impact on predicted maximum plasma concentrations (C_{max}) of daidzein and S-equol.Normalized sensitivity coefficients (SCs) were calculated according to the following equation (Evans and Andersen, 2000):

$$SC = \frac{(C' - C)}{(P' - P)} \times \frac{P}{C}$$

where C stands for the initial value of model output; C´ is the modified value of model output with a 5% increase of an input parameter; P is the initial parameter value and P' is the parameter value with an increase of 5%. For sensitivity analysis, only one parameter is changed each time, while other parameters are kept at their initial values. The lager the SC value is, the larger impact of this parameter on predicted plasma C_{max} of daidzein and S-equol.

The linear sensitivity analysis now performed is a simple first tier approach aiming to provide initial information about which parameters influence the predicted C_{max} values most, while a more extended analysis of variability in the thus identified most influential parameters, for example via example Monte Carlo modeling, might provide additional insight in intraspecies differences (Al-Subeihi et al., 2015; Punt et al., 2016; Strikwold et al., 2017b).

To further assess how gut microbial related kinetic parameters V_{max} and K_m affect plasma C_{max} of daidzein and S-equol, a sensitivity analysis was performed using K_m and V_{max} values amounting to their mean value plus or minus the standard deviation (P' in the formula equals P plus or P minus the respective standard deviation).

2.8 Estrogen receptor–mediated chemical-activated luciferase gene expression (ER-CALUX) assay of daidzein and S-equol

To assess the estrogenic potency of daidzein and S-equol, the reporter gene assay ERα-CALUX was performed, using the human osteosarcoma U-2OS ERα cell line which is stably expressing ERα in addition to a 3x estrogen response element (ERE) and TATA box binding protein combined with a luciferase gene as reporter (Sotoca et al., 2008).

Cells were cultured at 37°C in a humidified atmosphere and 5% CO_2. Cell culture medium used was DMEM/F-12 (with phenol red) supplemented with 10% FCS (v/v), 1% NEAA (v/v), and 1% penicillin streptomycin. Cultures were trypsinized and subcultured at a ratio of 1:6 to1:8 twice per week, when grown to 70-80% confluence. Two days before plating of the cells to perform the assay, cells were exposed to 0.2 mM geneticin in the cell culture medium to exert selection pressure.

To perform the assay, cells were trypsinized and plated in the inner 60 wells of 96-well plates with a density of 1×10^4 cells/well in 100 µL/well of assay medium. Assay medium used was DMEM/F-12 (without phenol red) supplemented with 10% FCS (v/v) and 1% NEAA (v/v). The outer 36 wells were filled only with 200 µl PBS. After 24 hours, the assay medium was carefully aspirated and replaced by 100 µL fresh assay medium/well. After another 24 hours of incubation, assay medium was aspirated and 100 µL exposure medium was added. Exposure medium consisted of test compounds in DMSO (0.5% final concentration) prepared from 200-times concentrated stocks in assay medium, and cells were exposed to 0.01-1,000 pM E_2, 0.1-100,000 nM daidzein or 0.1-100,000 nM S-equol, 1,000 pM of E_2 (positive control for ERα activation), 1 mM of $CuSO_4$ (positive control for cytotoxicity) and 0.5% DMSO as solvent control in each plate. Every condition was tested in 6 replicates per plate. Cells were incubated with test chemicals for 24 hours, after which cells were washed with 100 µL PBS, and 30 µL low salt buffer (LSB) were subsequently added to each well to lyse the cells. LSB contained 0.12% Tris, 0.03% DTT and 0.07% CDTA in nanopure water (w/w). Plates were placed on ice for 15 min and frozen at -80ºC overnight before measurement. Experiments were repeated three times.

For measurement, plates was thawed on a plate shaker at room temperature for 1 hour, and then, their luciferase activity was measured using flash mix in a GloMax Multi+ luminometer (Promega, CA, USA) at room temperature. Flash mix consisted of 20 mM tricine, 1.07 mM

$(MgCO_3)4Mg(OH)_2$, 2.67 mM $MgSO_4$, 0.1 mM EDTA, 2 mM DTT, 0.47 mM luciferine and 5 mM ATP in nanopure water (pH 7.8). The resulting relative light units (RLUs) were standardised by subtracting the background of the solvent control, and expressing results relative to the maximum luciferase response of E2 set at 100%.

Flavonoids are known to exert post-translational effects on luciferase (Beekmann et al., 2015; Sotoca et al., 2010). To be able to correct the results of the ERα-CALUX for these effects, the post-translational effects of daidzein and S-equol on luciferase were studied in U-2OS Cytotox cells constitutively expressing luciferase (van der Linden et al., 2014). In this assay, post-translational stabilization of luciferase leads to increased luciferase activity, and cytotoxicity leads to reduced luciferase activity. Cell culturing, plating and exposure conditions were identical to the ERα-CALUX assay described above. Experiments were also repeated three times.

The results of the ERα-CALUX assay were corrected for post-translational effects of the test chemicals on the reporter enzyme. To this end, chemical-induced changes to luciferase activity in the Cytotox assay relative to the solvent control were calculated, and the results of the ERα-CALUX were divided by the respective factors. A nonlinear regression was fitted to the data (three-parameter dose-response curve with a Hill slope of 1.0) to the corrected data to obtain the concentration-response curves for each compound, using GraphPad Prism 5.04.

3. Results

3.1 Clearance of daidzein in rat fecal anaerobic incubations

To assess gut microbial metabolism of daidzein, anaerobic incubations of daidzein with rat feces were performed. **Figure 3** shows the depletion of daidzein at different concentrations of feces. It can be seen that at low concentrations of feces (i.e. 0.3%, 0.6%, 0.9% and 1.2%), there is no or very low metabolism due to lag phases, while at high concentrations of feces (i.e. 4%, 6% and 8%), metabolism starts immediately. At high concentrations of feces, there are linear increases in the rate of daidzein depletion over fecal concentrations, and from that linear range 6% feces was selected for subsequent experiments. The rates of daidzein depletion were linear over time for at least 1 hour, and thus, the incubation time of 35 min was selected for subsequent experiments.

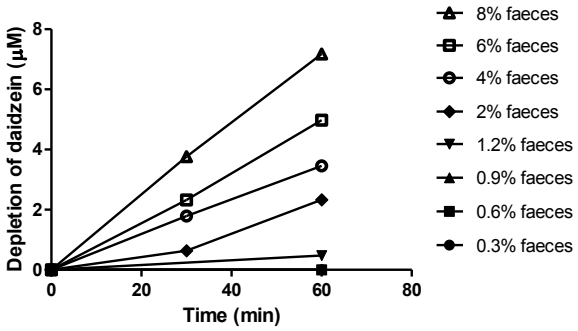

Figure 3. Depletion of daidzein (starting concentration 17.5 µM) in anaerobic incubations containing increasing concentrations of rat feces.

3.2 Kinetic constants of metabolite formation from daidzein in rat fecal incubations

Figure 4 presents the daidzein concentration dependent apparent formation rates of DHD, S-equol and O-DMA in rat fecal incubations. The metabolite formation followed Michaelis-Menten kinetics and allowed definition of apparent V_{max} and K_m values. Catalytic efficiencies (calculated as V_{max}/K_m) for the formation of DHD, S-equol and O-DMA derived from these kinetic parameters were calculated, and are shown in **Table 2**. Of the three microbial metabolites, S-equol is formed with the highest catalytic efficiency, which is 1.3- and 15.7-fold as high as that of DHD and O-DMA, respectively.

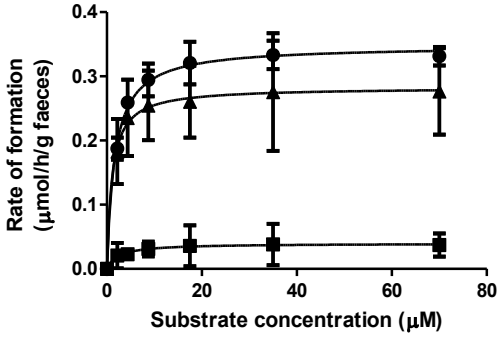

Figure 4. Concentration-dependent formation of DHD (circles), S-equol (triangles) and O-DMA (squares) in rat fecal incubations with daidzein under anaerobic conditions. Data are presented as mean ± SD of triplicate experiments.

Table 2. Kinetic parameters for formation of daidzein gut microbial metabolites.

	DHD	S-equol	O-DMA
V_{max} (μmol/h/g feces)	0.35	0.28	0.04
K_m (μM)	1.69	1.08	2.42
Catalytic efficiency (mL/h/g feces)	207.10	259.26	16.53

3.3 Enzymatic conjugation of S-equol in incubations with pooled rat liver S9 fractions

Kinetic parameters for liver phase II glucuronidation of S-equol were determined by in vitro incubations of pooled rat liver S9 fractions, as glucuronidation is the major pathway of host phase II conjugation of S-equol. Two glucuronides of S-equol were formed at similar rates in these incubations (**Figure 5**). Due to the molecular structure of S-equol, only having hydroxyl groups available for glucuronidation at the 4' and 7 positions, the formed metabolites are likely S-equol-4'-O-glucuronide and S-equol-7-O-glucuronide. The formation of the glucuronides followed Michaelis–Menten kinetics, resulting in V_{max} values of 11.0 and 10.6 nmol/min/mg S9 protein, and K_m values of 22.5 and 13.7 μM for formation of S-equol glucuronide-1 and glucuronide-2, respectively (**Table 3**). The catalytic efficiency for the formation of S-equol glucuronide-2 is 1.6-times higher than that for formation of glucuronide-1, especially because of a 1.6-fold lower K_m.

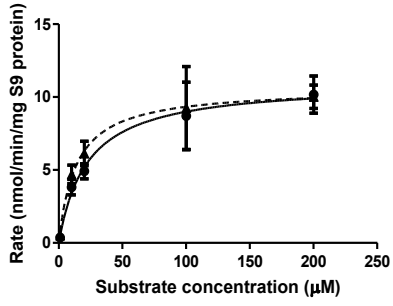

Figure 5. Concentration-dependent formation of S-equol glucuronide-1 (circles with solid line) and glucuronide-2 (triangles with dashed line) in incubations with pooled liver S9 fractions from male SD rats. Data are presented as mean ± SD of triplicate experiments.

Table 3. Kinetic parameters for formation of S-equol phase II metabolites by pooled rat liver S9 fractions.

	S-equol glucuronide-1	S-equol glucuronide-2
V_{max} (nmol/min/mg S9 protein)	11.0	10.6
K_m (μM)	22.5	13.7
Catalytic efficiency (mL/min/mg S9 protein)	0.49	0.77
Scaled V_{max} (nmol/min/g liver tissue)	1573	1515.8
Scaled catalytic efficiency (mL/min/g liver tissue)	70.1	110.1

3.4 PBK modeling

3.4.1 Influence of microbial metabolism on plasma concentrations of daidzein and S-equol

PBK modeling was used to predict the effect of gut microbial metabolism on the plasma concentrations of daidzein and its metabolite S-equol in the host.

The results obtained provide a first proof-of-concept for including the gut microbiota as a separate compartment in the PBK model structure, confirming that only in this way occurrence of S-equol in host plasma can be predicted. This is clearly shown in **Figure 6A** which presents the predicted time dependent plasma concentration of S-equol for both the PBK model without and with the gut microbiota included. It can be seen that upon oral dosing of 20 mg/kg bw daidzein, S-equol is not present in the circulation when microbial metabolism is not included in the PBK model, since its plasma concentration remains zero. Once microbial activity is introduced into the model, S-equol concentrations show a typical pharmacokinetic curve with a C_{max} of 0.007 μM. This is a proof-of-concept that the current developed PBK model including microbiota as a separate compartment works.

The metabolic activity of gut microbiota marginally affects the plasma levels of daidzein (**Figure 6B**), where plasma C_{max} of daidzein decreases from 2.19 to 2.16 μM, and the area under the concentration-time curve ($AUC_{0\text{-}4h}$) reduces from 0.018 to 0.016 μmol·h/L when microbial activity is introduced into the system.

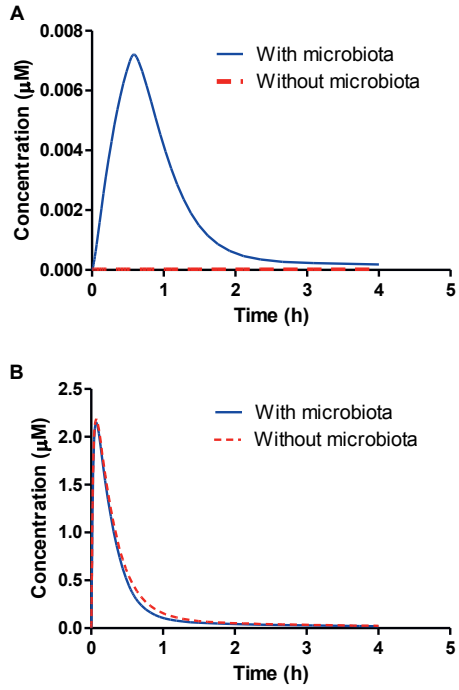

Figure 6. PBK model predicted plasma concentrations of: A) S-equol and B) daidzein upon oral dosing of 20 mg/kg bw daidzein. The red dashed line represents the predicted plasma concentrations without inclusion of the gut microbial compartment and the solid blue line represents the predicted plasma concentrations including the gut microbial compartment in PBK modeling.

3.4.2 Comparison of model predictions and in vivo data on daidzein and S-equol plasma concentrations

The plasma C_{max} of unconjugated daidzein and S-equol predicted by the model were compared with in vivo plasma concentrations upon oral administration of 1.14-30 mg/kg bw daidzein reported in literature (Bai et al., 2010; Chen et al., 2005; Islam et al., 2015; Janning et al., 2000; King, 1998; Mallis et al., 2003; Qiu et al., 2005; Sepehr et al., 2007; Shen et al., 2011; Zhang et al., 2014). For the literature data reporting the concentrations of daidzein and S-equol after hydrolysis, these data were corrected for the fractions of unconjugated daidzein and S-equol in the circulation (i.e. 8.1% and 1.1%, for daidzein and S-equol, respectively) (Setchell et al., 2011). **Figure 7** shows the ratio between the predicted plasma concentrations and the values reported in literature (details are presented in **Supplementary Material 2**).

There is considerable variation between the in vivo studies, and the predicted plasma C_{max} of daidzein is on average 1.22 times the reported in vivo plasma C_{max}. For S-equol, only two studies were found that could be included in this comparison, and based on these data the predicted plasma C_{max} of equol is on average 1.07 times the predicted in vivo plasma C_{max}.

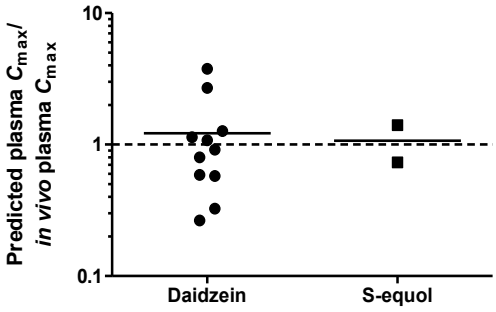

Figure 7. Ratio between the predicted plasma C_{max} and the in vivo C_{max} of unconjugated daidzein and S-equol upon oral dosing of 1.14-30 mg/kg bw daidzein (Bai et al., 2010; Chen et al., 2005; Islam et al., 2015; Janning et al., 2000; King, 1998; Mallis et al., 2003; Qiu et al., 2005; Sepehr et al., 2007; Shen et al., 2011; Zhang et al., 2014). Each data point represents a separate study reported in literature, if different doses were tested, each dose is represented by a data point.

3.5 Sensitivity analysis

To assess key parameters that influence the model output, in this case the plasma C_{max} of daidzein and S-equol, a sensitivity analysis was carried out. Parameters that appeared to have absolute normalized sensitivity coefficients (SCs) higher than 0.1 for at least one dose are presented in **Figure 8**, upon oral dosing of daidzein at 2 and 38 mg/kg bw which covers the doses that most in vivo studies used.

Results reveal that the normalized SCs for predicted plasma C_{max} of daidzein is predominantly influenced by the absorption rate of daidzein to small intestinal tissue (Ka), the fraction of liver tissue (VLc), the liver S9 protein yield (VLS9), the V_{max} for daidzein-7-O-glucuronide formation by the liver (VmaxLDAI7Gc) and the fraction of blood flow to rapidly perfused tissue (QRc).

Similarly, for S-equol, parameters including QRc, VLc and VLS9 affect its predicted plasma C_{max} to the largest extent. The parameters related to gut microbial activities have small effects on the plasma C_{max} of daidzein, but considerable influence on the C_{max} of S-equol. Especially the V_{max} for formation of S-equol in the large intestine (VmaxLIEQUc) and fraction of feces of body weight (VMB) are of influence on the C_{max} of S-equol.

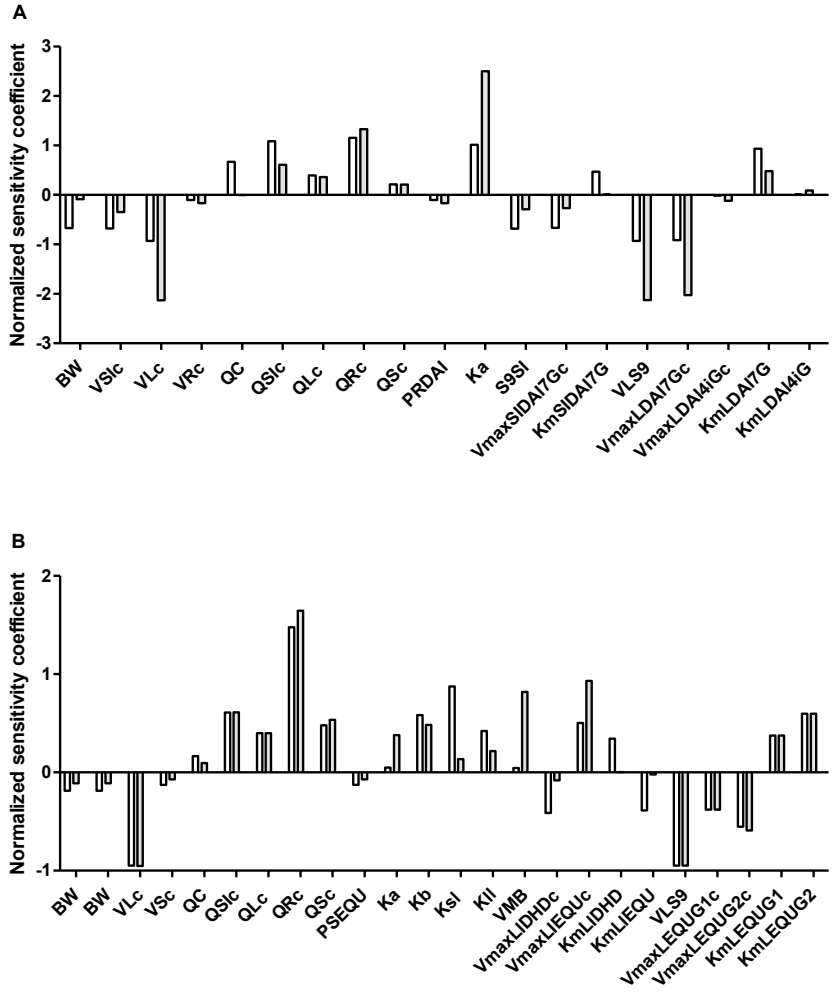

Figure 8. Sensitivity analysis of predicted plasma C_{max} of A) daidzein and B) S-equol upon oral dosing of daidzein at dose levels of 2 (white bars) and 38 (grey bars) mg/kg bw.

Parameters stand for: BW = body weight, VSIc = fraction of small intestine, VLc = fraction of liver, VRc = fraction of rapidly perfused tissue, QC = cardiac output, QSIc = fraction of blood

flow to small intestine, QLc = fraction of blood flow to liver, QRc = fraction of blood flow to rapidly perfused tissue, QSc = fraction of blood flow to slowly perfused tissue, PRDAI = rapidly perfused tissue/blood partition coefficient of daidzein, Ka= absorption rate of daidzein to intestinal tissue, S9SI= small intestinal S9 protein yield, VmaxSIDAI7Gc= V_{max} of daidzein-7-Oglucuronide by small intestine, KmSIDAI7G = K_m for formation of daidzein-7-Oglucuronide by small intestine, VLS9 = liver S9 protein yield, VmaxLDAI7Gc= V_{max} of daidzein-7-O-glucuronide by liver, VmaxLDAI4iGc= V_{max} of daidzein-4'-O-glucuronide by liver, KmLDAI7G = K_m for formation of daidzein-7-O-glucuronide by liver, KmLDAI4iG = K_m for formation of daidzein-4'-O-glucuronide by liver PSEQU = slowly perfused tissue/blood partition coefficient of S-equol, Kb = transfer rate of daidzein to feces Ksl = transfer rate of daidzein to feces, Kll = absorption rate of S-equol from intestine to liver, VMB= fraction of feces of body weight, VmaxLIDHDc = V_{max} of DHD by large intestine lumen, VmaxLIEQUc = V_{max} of S-equol by large intestine lumen, KmLIDHD = K_m for formation of DHD by large intestine lumen, KmLIEQU = K_m for formation of S-equol by large intestine lumen, VmaxLEQU1c = V_{max} of S-equol glucuronide-1 by liver, VmaxLEQU2c = V_{max} of S-equol glucuronide-2 by liver, KmLEQU1 = K_m for formation of S-equol glucuronide-1 by liver, KmLEQU2 = K_m for formation of S-equol glucuronide-2 by liver.

3.6 Estrogenicity of daidzein and S-equol

The ERα-CALUX assay was performed to assess the estrogenic potency of daidzein and S-equol. **Figure 9** shows the concentration-response curves of 17β-estradiol (E2), daidzein and S-equol. The respective effective concentrations to reach a 10% (EC_{10}) and 50% (EC_{50}) induction of ERα-mediated gene expression derived from these curves are listed in **Table 4**. The curves of daidzein and S-equol were corrected for post-translational effects on the luciferase enzyme quantified using the U-2OS Cytotox cells. The results obtained show that the gut microbial metabolite S-equol is a more potent estrogen than its parent compound daidzein, having a 6.3- and 12.7-fold higher potency when comparing EC_{10} and EC_{50} values, respectively.

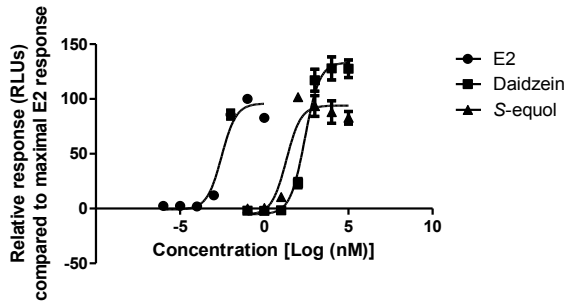

Figure 9. Concentration-response curves of E2, daidzein and S-equol in the ERα-CALUX assay.

Table 4. EC values of E2, daidzein and S-equol obtained in the ERα-CALUX assay.

	EC_{10} (nM)	EC_{50} (nM)
E2	0.001	0.003
Daidzein	62.5	261.6
S-equol	9.9	20.6

3.7 Comparison of in vitro EC_{10} and dietary resulting plasma concentrations

To obtain insight in the physiological relevance of the in vitro detected estrogenic activity of daidzein and S-equol the EC_{10} values for ERα activation derived from the ERα-CALUX assay were compared to predicted rat plasma C_{max} of daidzein and S-equol resulting from different dietary exposure scenarios. To this end, plasma C_{max} values of daidzein and S-equol as a result of a typical Western diet (daily isoflavone consumption <2 mg/day) (Csanady et al., 2002), a Western vegetarian diet (daily isoflavone consumption approximately 12 mg/day) (Clarke and Lloyd, 2004), an Asian diet (daily isoflavone consumption 15-61 mg/day) (de Kleijn et al., 2001; Horn-Ross et al., 2002; van Erp-Baart et al., 2003) and isoflavone supplement consumption (daily isoflavone consumption 80-120 mg/day) (Arai et al., 2000b; Franke et al., 1999; Kim and Kwon, 2001; Mei et al., 2001) were predicted using the developed PBK model. **Figure 10** shows that for daidzein, predicted plasma C_{max} values resulting from soy supplementary diet and Asian diet, were slightly lower EC_{10} value of daidzein for ERα activation, while that of Western and Western vegetarian diet were predicted to be evidently lower than the EC_{10} value of daidzein for ERα activation. Predicted plasma

C_{max} values of S-equol resulting from different dietary intakes were generally 1-2 orders of magnitude lower than the EC_{10} value of S-equol for ERα activation, indicating limited contribution of S-equol in the overall estrogenicity upon dietary exposure of daidzein.

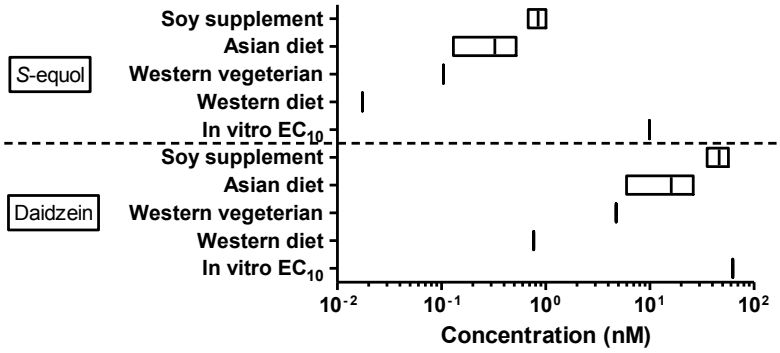

Figure 10. Comparison of in vitro derived EC_{10} values for induction of ERα mediated gene expression and predicted C_{max} plasma levels of S-equol (upper part) and daidzein (lower part) resulting from different dietary intake levels.

4. Discussion

The aim of the present study was to create an in vitro-in silico based testing strategy to predict gut microbial metabolism of xenobiotics and the resulting plasma concentrations of the metabolites formed, using the isoflavone daidzein and its gut microbial metabolite S-equol as model compounds. The anaerobic fecal incubations were optimized to establish a linear relationship of metabolites formed over fecal concentrations and time, to allow adequate kinetic experiments and definition of Michaelis-Menten parameters. To our knowledge, this is the first time that apparent V_{max} and K_m values are derived to describe the metabolism of a chemical by the gut microbiota, which are subsequently used for PBK modeling. Previous in vitro fecal incubations have reported microbial metabolism of daidzein and formation of S-equol (Matthies et al., 2009; Matthies et al., 2008; Schwen et al., 2012a; Wang et al., 2007; Yuan et al., 2007). However, from those studies no kinetic parameters could be derived, as the long incubation times in the reported studies lead to non-linear kinetics, which are in part due to microbial adaptation, usually resulting in exponential increases in metabolite degradation after a lag phase and/or depletion of the substrate at longer incubation times (Matthies et al., 2009; Matthies et al., 2008; Wang et al., 2007). In the present study it was shown that non-

linear kinetics could be avoided with use of diluted fecal slurries and only relatively short-incubation times. Fecal samples were used as a representative matrix for the colonic microbiota, since fecal communities are reported to be highly comparable to colonic ones in composition and function (Behr et al., 2017; Hillman et al., 2017; Hold et al., 2002). While there are certain differences in the microbial composition along the intestinal tract, the colon is housing the vast majority of microbes and is considered to be the most important contributor to the metabolic activity of the gut microbiota. A thorough review on the cultivation of bacteria from the intestine of mammals draw the conclusion that up to 65% of molecular species detected by sequencing have representative strains in culture (Lagkouvardos et al., 2017). Another study compared microbial-related metabolic changes in gut tissue, cecum content and feces of rats treated with antibiotics, and concluded that 'as a non-invasive sampling method, feces provide a suitable matrix for studies on metabolism by the gut microbiota'(Behr et al., 2018). Thus, using fecal incubations to describe intestinal microbial metabolism provides a reasonable first tier approach, which, based on the result of the present study appeared to result in an adequate PBK model.

Using the kinetic parameters derived for intestinal microbial conversion of daidzein to S-equol and for subsequent glucuronidation of S-equol in the liver, a PBK model able to predict plasma C_{max} of daidzein and S-equol in rat was developed. The PBK model was developed for rats because this enabled comparison of model based predictions to in vivo data available in the literature. Comparison of the PBK model based predictions to these in vivo data revealed that the predictions matched the available in vivo C_{max} data well, with the predicted plasma C_{max} being on average 1.22 and 1.07 times the in vivo plasma C_{max} of daidzein and S-equol, respectively.

The analysis also revealed that both the reported and predicted plasma levels of S-equol are substantially lower than those of daidzein. In line with this, inclusion of gut microbial metabolism in the PBK model appeared to have only a marginal effect on the daidzein C_{max} values, which leads to the suggestion that, in the case of isoflavones, models omitting the gut microbiota (Boonpawa et al., 2017; Zhang et al., 2018) can still adequately predict concentrations of the parent isoflavone. However, when metabolites with an increased toxicity or biological activity are formed, these potentially highly relevant and bioactive metabolites are overlooked. While animal studies are still the standard in toxicity testing, the described inclusion of microbial metabolism in in vitro-in silico methods can improve the predictions of QIVIVE and thereby contribute to their applicability and acceptance. The results of the

present study provide a proof-of-principle on how formation of metabolites by the intestinal microbiota can be included in PBK model predictions. The PBK model including microbial S-equol formation in the intestinal compartment adequately predicted plasma S-equol concentrations in the host. In line with literature, it was shown that S-equol is a more potent estrogen than daidzein (**Figure 9**), so that the formation of S-equol is generally considered to be relevant for health effects associated with daidzein ingestion in humans (Vergne et al., 2007; Yuan et al., 2007). However, the results of the present study, comparing predicted plasma concentrations of daidzein and S-equol with EC_{10} values for ERα activation obtained in the ERα-CALUX assay, indicate that in rats the ERα-mediated estrogenicity is likely to be dominated by daidzein in spite of its microbial metabolite S-equol being more potent.

It is important to note that the PBK model developed in the present study relates to rats. This was done because for rats there are data on dose-dependent C_{max} values of both daidzein and S-equol available, enabling evaluation of the model predictions. However, it should be kept in mind that although the model predictions appeared to be comparable to in vivo data from literature, the current developed PBK model still needs more validations and has some challenges. For example, the model describes body structures by dividing them into different independent compartments, but in reality, the living organism is far more complex with potential interactions between compartments. Also, the model refers to rats and not yet to humans. Furthermore, the model does not take interindividual differences in the many parameters used in the equations into account. This might be achieved by performing Monte Carlo modeling based on distributions describing the variability in either all model parameters, or, alternatively, especially the parameters that appear to be most influential on the predicted outcomes for C_{max} of daidzein and S-equol. This would also allow to take into account the fact that in contrast to rats, within the human population there are S-equol producers and non-producers. Thus, when interpreting the model results, these limitations should be kept in mind, while future research may consider addressing these aspects presently ignored. Based on this validated model a PBK model for humans can be developed using human fecal materials and human tissue fractions, although this remains a topic for further research.

In the current study, proof-of-principle for an in vitro-in silico based testing strategy to predict gut microbial metabolism of xenobiotics was developed, which could successfully be applied to predict the resulting plasma concentrations of an intestinal microbial metabolite in the host. This is a relevant addition to current QIVIVE strategies which are a key element of the 21st century toxicity testing strategies.

References

Abdullah, R., Alhusainy, W., Woutersen, J., Rietjens, I. M., and Punt, A. (2016). Predicting points of departure for risk assessment based on in vitro cytotoxicity data and physiologically based kinetic (PBK) modeling: The case of kidney toxicity induced by aristolochic acid I. *Food Chem Toxicol* **92**, 104-16.

Al-Subeihi, A. A., Alhusainy, W., Kiwamoto, R., Spenkelink, B., van Bladeren, P. J., Rietjens, I. M., and Punt, A. (2015). Evaluation of the interindividual human variation in bioactivation of methyleugenol using physiologically based kinetic modeling and Monte Carlo simulations. *Toxicol Appl Pharmacol* **283**, 117-26.

Arai, Y., Uehara, M., Sato, Y., Kimira, M., Eboshida, A., Adlercreutz, H., and Watanabe, S. (2000a). Comparison of isoflavones among dietary intake, plasma concentration and urinary excretion for accurate estimation of phytoestrogen intake. *Journal of Epidemiology* **10**, 127-135.

Arai, Y., Watanabe, S., Kimira, M., Shimoi, K., Mochizuki, R., and Kinae, N. (2000b). Dietary intakes of flavonols, flavones and isoflavones by Japanese women and the inverse correlation between quercetin intake and plasma LDL cholesterol concentration. *The Journal of nutrition* **130**, 2243-2250.

Atkinson, C., Frankenfeld, C. L., and Lampe, J. W. (2005). Gut bacterial metabolism of the soy isoflavone daidzein: exploring the relevance to human health. *Experimental biology and medicine* **230**, 155-170.

Bai, Y., Wen, H., Zhou, H., Qiu, Y., and Shan, C. (2010). Determination of daidzein and its pharmacokinetics in rat plasma by UPLC. *Chinese Pharmacological Bulletin* **26**, 1512-1515.

Beekmann, K., Rubio, L., de Haan, L. H., Actis-Goretta, L., van der Burg, B., van Bladeren, P. J., and Rietjens, I. M. (2015). The effect of quercetin and kaempferol aglycones and glucuronides on peroxisome proliferator-activated receptor-gamma (PPAR-gamma). *Food Funct* **6**, 1098-107.

Behr, C., Kamp, H., Fabian, E., Krennrich, G., Mellert, W., Peter, E., Strauss, V., Walk, T., Rietjens, I., and van Ravenzwaay, B. (2017). Gut microbiome-related metabolic changes in plasma of antibiotic-treated rats. *Arch Toxicol* **91**, 3439-3454.

Behr, C., Sperber, S., Jiang, X., Strauss, V., Kamp, H., Walk, T., Herold, M., Beekmann, K., Rietjens, I., and van Ravenzwaay, B. (2018). Microbiome-related metabolite changes in gut tissue, cecum content and feces of rats treated with antibiotics. *Toxicol Appl Pharmacol* **355**, 198-210.

Boonpawa, R., Spenkelink, A., Punt, A., and Rietjens, I. (2017). In vitro-in silico-based analysis of the dose-dependent in vivo oestrogenicity of the soy phytoestrogen genistein in humans. *Br J Pharmacol* **174**, 2739-2757.

Brown, R. P., Delp, M. D., Lindstedt, S. L., Rhomberg, L. R., and Beliles, R. P. (1997). Physiological parameter values for physiologically based pharmacokinetic models. *Toxicol Ind Health* **13**, 407-84.

Chen, L., Ning, J., Louisse, J., Wesseling, S., and Rietjens, I. (2018). Use of physiologically based kinetic modeling-facilitated reverse dosimetry to convert in vitro cytotoxicity data to predicted in vivo liver toxicity of lasiocarpine and riddelliine in rat. *Food Chem Toxicol* **116**, 216-226.

Chen, X., Feng, Q., Dafang, Z., Xiaotao, D., and Changxiao, L. (2005). Validated liquid chromatography-tandem mass spectrometric method for the quantitative determination of daidzein and its main metabolite daidzein glucuronide in rat plasma. *Die Pharmazie-An International Journal of Pharmaceutical Sciences* **60**, 334-338.

Clarke, D. B., and Lloyd, A. S. (2004). Dietary exposure estimates of isoflavones from the 1998 UK Total Diet Study. *Food Addit Contam* **21**, 305-16.

Crawford, S. L., Jackson, E. A., Churchill, L., Lampe, J. W., Leung, K., and Ockene, J. K. (2013). Impact of dose, frequency of administration, and equol production on efficacy of isoflavones for menopausal hot flashes: a pilot randomized trial. *Menopause* **20**, 936-45.

Csanady, G. A., Oberste-Frielinghaus, H. R., Semder, B., Baur, C., Schneider, K. T., and Filser, J. G. (2002). Distribution and unspecific protein binding of the xenoestrogens bisphenol A and daidzein. *Arch Toxicol* **76**, 299-305.

Cubitt, H. E., Houston, J. B., and Galetin, A. (2011). Prediction of human drug clearance by multiple metabolic pathways: integration of hepatic and intestinal microsomal and cytosolic data. *Drug Metab Dispos* **39**, 864-73.

de Jong, E., Louisse, J., Verwei, M., Blaauboer, B. J., van de Sandt, J. J., Woutersen, R. A., Rietjens, I. M., and Piersma, A. H. (2009). Relative developmental toxicity of glycol ether alkoxy acid metabolites in the embryonic stem cell test as compared with the in vivo potency of their parent compounds. *Toxicol Sci* **110**, 117-24.

de Kleijn, M. J., van der Schouw, Y. T., Wilson, P. W., Adlercreutz, H., Mazur, W., Grobbee, D. E., and Jacques, P. F. (2001). Intake of dietary phytoestrogens is low in postmenopausal women in the United States: the Framingham study. *The Journal of nutrition* **131**, 1826-1832.

DeJongh, J., Verhaar, H. J. M., and Hermens, J. L. M. (1997). A quantitative property-property relationship (QPPR) approach to estimate in vitro tissue-blood partition coeffcients of organic chemicals in rats and humans. *Arch Toxicol*, 72: 17-25.

Eisenbrand, G., and Senate Commission on Food Safety of the German Research, F. (2007). Isoflavones as phytoestrogens in food supplements and dietary foods for special medical purposes. Opinion of the Senate Commission on Food Safety (SKLM) of the German Research Foundation (DFG)-(shortened version). *Mol Nutr Food Res* **51**, 1305-12.

Evans, M. V., and Andersen, M. E. (2000). Sensitivity analysis of a physiological model for 2, 3, 7, 8-tetrachlorodibenzo-p-dioxin (TCDD): assessing the impact of specific model parameters on sequestration in liver and fat in the rat. *Toxicological sciences* **54**, 71-80.

Franke, A. A., Hankin, J. H., Yu, M. C., Maskarinec, G., Low, S.-H., and Custer, L. J. (1999). Isoflavone Levels in Soy Foods Consumed by Multiethnic Populations in Singapore and Hawaii. *Journal of Agricultural and Food Chemistry* **47**, 977-986.

Gardana, C., and Simonetti, P. (2017). Long-term kinetics of daidzein and its main metabolites in human equol-producers after soymilk intake: identification of equol-conjugates by UPLC-orbitrap-MS and influence of the number of transforming bacteria on plasma kinetics. *Int J Food Sci Nutr* **68**, 496-506.

Greenblum, S., Turnbaugh, P. J., and Borenstein, E. (2012). Metagenomic systems biology of the human gut microbiome reveals topological shifts associated with obesity and inflammatory bowel disease. *Proc Natl Acad Sci U S A* **109**, 594-9.

Haiser, H. J., and Turnbaugh, P. J. (2013). Developing a metagenomic view of xenobiotic metabolism. *Pharmacol Res* **69**, 21-31.

Hillman, E. T., Lu, H., Yao, T., and Nakatsu, C. H. (2017). Microbial Ecology along the Gastrointestinal Tract. *Microbes Environ* **32**, 300-313.

Hold, G. L., Pryde, S. E., Russell, V. J., Furrie, E., and Flint, H. J. (2002). Assessment of microbial diversity in human colonic samples by 16S rDNA sequence analysis. *FEMS microbiology ecology* **39**, 33-39.

Horn-Ross, P. L., Hoggatt, K. J., West, D. W., Krone, M. R., Stewart, S. L., Anton-Culver, H., Bernstein, L., Deapen, D., Peel, D., Pinder, R., and Reynolds, P. (2002). Recent diet and breast cancer risk: the California Teachers Study (USA). *Cancer Causes & Control* **13**, 407-415.

Hoskins, L. C., and Zamcheck, N. (1968). Bacterial degradation of gastrointestinal mucins: I. Comparison of mucus constituents in the stools of germ-free and conventional rats. *Gastroenterology* **54**, 210-217.

Human Microbiome Project, C. (2012). Structure, function and diversity of the healthy human microbiome. *Nature* **486**, 207-14.

Islam, M. A., Hooiveld, G., van den Berg, J. H. J., Boekschoten, M. V., van der Velpen, V., Murk, A. J., Rietjens, I., and van Leeuwen, F. X. R. (2015). Plasma bioavailability and changes in PBMC gene expression after treatment of ovariectomized rats with a commercial soy supplement. *Toxicol Rep* **2**, 308-321.

Islam, M. A., Punt, A., Spenkelink, B., Murk, A. J., Rolaf van Leeuwen, F. X., and Rietjens, I. M. (2014). Conversion of major soy isoflavone glucosides and aglycones in in vitro intestinal models. *Mol Nutr Food Res* **58**, 503-15.

Janning, P., Schuhmacher, U. S., Upmeier, A., Diel, P., Michna, H., Degen, G. H., and Bolt, H. M. (2000). Toxicokinetics of the phytoestrogen daidzein in female DA/Han rats. *Archives of Toxicology* **74**, 421-430.

Karlsson, F. H., Tremaroli, V., Nookaew, I., Bergstrom, G., Behre, C. J., Fagerberg, B., Nielsen, J., and Backhed, F. (2013). Gut metagenome in European women with normal, impaired and diabetic glucose control. *Nature* **498**, 99-103.

Kim, J. S., and Kwon, C. S. (2001). Estimated dietary isoflavone intake of Korean population based on National Nutrition Survey. *Nutrition Research* **21**, 947-953.

King, R. A. (1998). Daidzein conjugates are more bioavailable than genistein conjugates in rats. *The American journal of clinical nutrition* **68**, 1496S-1499S.

Kobayashi, S., Shinohara, M., Nagai, T., and Konishi, Y. (2013). Transport mechanisms for soy isoflavones and microbial metabolites dihydrogenistein and dihydrodaidzein across monolayers and membranes. *Biosci Biotechnol Biochem* **77**, 2210-7.

Kostelac, D., Rechkemmer, G., and Briviba, K. (2003). Phytoestrogens modulate binding response of estrogen receptors α and β to the estrogen response element. *Journal of agricultural and food chemistry* **51**, 7632-7635.

Lagkouvardos, I., Overmann, J., and Clavel, T. (2017). Cultured microbes represent a substantial fraction of the human and mouse gut microbiota. *Gut Microbes* **8**, 493-503.

Larsen, N., Vogensen, F. K., van den Berg, F. W., Nielsen, D. S., Andreasen, A. S., Pedersen, B. K., Al-Soud, W. A., Sorensen, S. J., Hansen, L. H., and Jakobsen, M. (2010). Gut microbiota in human adults with type 2 diabetes differs from non-diabetic adults. *PLoS One* **5**, e9085.

Le Chatelier, E., Nielsen, T., Qin, J., Prifti, E., Hildebrand, F., Falony, G., Almeida, M., Arumugam, M., Batto, J. M., Kennedy, S., Leonard, P., Li, J., Burgdorf, K., Grarup, N., Jorgensen, T., Brandslund, I., Nielsen, H. B., Juncker, A. S., Bertalan, M., Levenez, F., Pons, N., Rasmussen, S., Sunagawa, S., Tap, J., Tims, S., Zoetendal, E. G., Brunak, S., Clement, K., Dore, J., Kleerebezem, M., Kristiansen, K., Renault, P., Sicheritz-Ponten, T., de Vos, W. M., Zucker, J. D., Raes, J., Hansen, T., Meta, H. I. T. c., Bork, P., Wang, J., Ehrlich, S. D., and Pedersen, O. (2013). Richness of human gut microbiome correlates with metabolic markers. *Nature* **500**, 541-6.

Louisse, J., Beekmann, K., and Rietjens, I. M. (2017). Use of Physiologically Based Kinetic Modeling-Based Reverse Dosimetry to Predict in Vivo Toxicity from in Vitro Data. *Chem Res Toxicol* **30**, 114-125.

Louisse, J., Bosgra, S., Blaauboer, B. J., Rietjens, I. M., and Verwei, M. (2015). Prediction of in vivo developmental toxicity of all-trans-retinoic acid based on in vitro toxicity data and in silico physiologically based kinetic modeling. *Arch Toxicol* **89**, 1135-48.

Maier, L., Pruteanu, M., Kuhn, M., Zeller, G., Telzerow, A., Anderson, E. E., Brochado, A. R., Fernandez, K. C., Dose, H., Mori, H., Patil, K. R., Bork, P., and Typas, A. (2018). Extensive impact of non-antibiotic drugs on human gut bacteria. *Nature* **555**, 623-628.

Mallis, L., Sarkahian, A., Harris, H., Zhang, M., and McConnell, O. (2003). Determination of rat oral bioavailability of soy-derived phytoestrogens using an automated on-column extraction procedure and electrospray tandem mass spectrometry. *Journal of Chromatography B* **796**, 71-86.

Matthies, A., Blaut, M., and Braune, A. (2009). Isolation of a human intestinal bacterium capable of daidzein and genistein conversion. *Appl Environ Microbiol* **75**, 1740-4.

Matthies, A., Clavel, T., Gutschow, M., Engst, W., Haller, D., Blaut, M., and Braune, A. (2008). Conversion of daidzein and genistein by an anaerobic bacterium newly isolated from the mouse intestine. *Appl Environ Microbiol* **74**, 4847-52.

Medinsky, M. A., Leavens, T. L., Csanády, G. A., Gargas, M. L., and Bond, J. A. (1994). *In vivo* metabolism of butadiene by mice and rats a comparison of physiological model predictions and experimental data. *Carcinogenesis* **15**, 1329-1340.

Mei, J., Yeung, S. S., and Kung, A. W. (2001). High dietary phytoestrogen intake is associated with higher bone mineral density in postmenopausal but not premenopausal women. *The Journal of Clinical Endocrinology & Metabolism* **86**, 5217-5221.

Million, M., Lagier, J. C., Yahav, D., and Paul, M. (2013). Gut bacterial microbiota and obesity. *Clin Microbiol Infect* **19**, 305-13.

Morito, K., Hirose, T., Kinjo, J., HIRAKAWA, T., OKAWA, M., NOHARA, T., OGAWA, S., INOUE, S., MURAMATSU, M., and MASAMUNE, Y. (2001). Interaction of phytoestrogens with estrogen receptors α and β. *Biological and Pharmaceutical Bulletin* **24**, 351-356.

Muthyala, R. S., Ju, Y. H., Sheng, S., Williams, L. D., Doerge, D. R., Katzenellenbogen, B. S., Helferich, W. G., and Katzenellenbogen, J. A. (2004). Equol, a natural estrogenic metabolite from soy isoflavones: convenient preparation and resolution of R- and S-equols and their differing binding and biological activity through estrogen receptors alpha and beta. *Bioorg Med Chem* **12**, 1559-67.

Ning, J., Chen, L., Strikwold, M., Louisse, J., Wesseling, S., and Rietjens, I. (2019). Use of an in vitro-in silico testing strategy to predict inter-species and inter-ethnic human differences in liver toxicity of the pyrrolizidine alkaloids lasiocarpine and riddelliine. *Arch Toxicol* **93**, 801-818.

Punt, A., Paini, A., Spenkelink, A., Scholz, G., Schilter, B., van Bladeren, P. J., and Rietjens, I. M. (2016). Evaluation of Interindividual Human Variation in Bioactivation and DNA Adduct Formation of Estragole in Liver Predicted by Physiologically Based Kinetic/Dynamic and Monte Carlo Modeling. *Chem Res Toxicol* **29**, 659-68.

Qin, J., Li, R., Raes, J., Arumugam, M., Burgdorf, K. S., Manichanh, C., Nielsen, T., Pons, N., Levenez, F., Yamada, T., Mende, D. R., Li, J., Xu, J., Li, S., Li, D., Cao, J., Wang, B., Liang, H., Zheng, H., Xie, Y., Tap, J., Lepage, P., Bertalan, M., Batto, J. M., Hansen, T., Le Paslier, D., Linneberg, A., Nielsen, H. B., Pelletier, E., Renault, P., Sicheritz-Ponten, T., Turner, K., Zhu, H., Yu, C., Li, S., Jian, M., Zhou, Y., Li, Y., Zhang, X., Li, S., Qin, N., Yang, H., Wang, J., Brunak, S., Dore, J., Guarner, F., Kristiansen, K., Pedersen, O., Parkhill, J., Weissenbach, J., Meta, H. I. T. C., Bork, P., Ehrlich, S. D., and Wang, J. (2010). A human gut microbial gene catalogue established by metagenomic sequencing. *Nature* **464**, 59-65.

Qiu, F., Chen, X. Y., Song, B., Zhong, D. F., and Liu, C. X. (2005). Influence of dosage forms on pharmacokinetics of daidzein and its main metabolite daidzein-7-O-glucuronide in rats. *Acta Pharmacol Sin* **26**, 1145-52.

Rafii, F., Jackson, L. D., Ross, I., Heinze, T. M., Lewis, S. M., Aidoo, A., Lyn-Cook, L., and Manjanatha, M. (2007). Metabolism of Daidzein by Fecal Bacteria in Rats. *Comparative Medicine* **57**, 282-286.

Rietjens, I. M., Louisse, J., and Punt, A. (2011). Tutorial on physiologically based kinetic modeling in molecular nutrition and food research. *Mol Nutr Food Res* **55**, 941-56.

Rothwell, J. A., Day, A. J., and Morgan, M. R. (2005). Experimental determination of octanol− water partition coefficients of quercetin and related flavonoids. *Journal of agricultural and food chemistry* **53**, 4355-4360.

Schwen, R. J., Nguyen, L., and Jackson, R. L. (2012a). Elucidation of the metabolic pathway of S-equol in rat, monkey and man. *Food Chem Toxicol* **50**, 2074-83.

Schwen, R. J., Nguyen, L., Plomley, J. B., and Jackson, R. L. (2012b). Toxicokinetics and lack of uterotropic effect of orally administered S-equol. *Food Chem Toxicol* **50**, 1741-8.

Sepehr, E., Cooke, G., Robertson, P., and Gilani, G. S. (2007). Bioavailability of soy isoflavones in rats Part I: application of accurate methodology for studying the effects of gender and source of isoflavones. *Mol Nutr Food Res* **51**, 799-812.

Setchell, K. D., Brown, N. M., and Lydeking-Olsen, E. (2002). The clinical importance of the metabolite equol-a clue to the effectiveness of soy and its isoflavones. *The Journal of nutrition* **132**, 3577-3587.

Setchell, K. D., Brown, N. M., Zhao, X., Lindley, S. L., Heubi, J. E., King, E. C., and Messina, M. J. (2011). Soy isoflavone phase II metabolism differs between rodents and humans: implications for the effect on breast cancer risk. *Am J Clin Nutr* **94**, 1284-94.

Setchell, K. D., and Clerici, C. (2010). Equol: history, chemistry, and formation. *J Nutr* **140**, 1355S-62S.

Setchell, K. D., and Cole, S. J. (2006). Method of defining equol-producer status and its frequency among vegetarians. *Journal of nutrition* **136**, 2188-2193.

Shen, Q., Li, X., Li, W., and Zhao, X. (2011). Enhanced intestinal absorption of daidzein by borneol/menthol eutectic mixture and microemulsion. *AAPS PharmSciTech* **12**, 1044-9.

Smith, K., McCoy, K. D., and Macpherson, A. J. (2007). Use of axenic animals in studying the adaptation of mammals to their commensal intestinal microbiota. *Semin Immunol* **19**, 59-69.

Sotoca, A. M., Bovee, T. F., Brand, W., Velikova, N., Boeren, S., Murk, A. J., Vervoort, J., and Rietjens, I. M. (2010). Superinduction of estrogen receptor mediated gene expression in luciferase based reporter gene assays is mediated by a post-transcriptional mechanism. *J Steroid Biochem Mol Biol* **122**, 204-11.

Sotoca, A. M., Ratman, D., van der Saag, P., Strom, A., Gustafsson, J. A., Vervoort, J., Rietjens, I. M., and Murk, A. J. (2008). Phytoestrogen-mediated inhibition of

proliferation of the human T47D breast cancer cells depends on the ERalpha/ERbeta ratio. *J Steroid Biochem Mol Biol* **112**, 171-8.

Sousa, T., Paterson, R., Moore, V., Carlsson, A., Abrahamsson, B., and Basit, A. W. (2008). The gastrointestinal microbiota as a site for the biotransformation of drugs. *Int J Pharm* **363**, 1-25.

Strikwold, M., Spenkelink, B., de Haan, L. H. J., Woutersen, R. A., Punt, A., and Rietjens, I. (2017a). Integrating in vitro data and physiologically based kinetic (PBK) modeling to assess the in vivo potential developmental toxicity of a series of phenols. *Arch Toxicol* **91**, 2119-2133.

Strikwold, M., Spenkelink, B., Woutersen, R. A., Rietjens, I., and Punt, A. (2017b). Development of a Combined In Vitro Physiologically Based Kinetic (PBK) and Monte Carlo Modeling Approach to Predict Interindividual Human Variation in Phenol-Induced Developmental Toxicity. *Toxicol Sci* **157**, 365-376.

Strikwold, M., Spenkelink, B., Woutersen, R. A., Rietjens, I. M., and Punt, A. (2013). Combining in vitro embryotoxicity data with physiologically based kinetic (PBK) modeling to define in vivo dose-response curves for developmental toxicity of phenol in rat and human. *Arch Toxicol* **87**, 1709-23.

van der Linden, S. C., von Bergh, A. R., van Vught-Lussenburg, B. M., Jonker, L. R., Teunis, M., Krul, C. A., and van der Burg, B. (2014). Development of a panel of high-throughput reporter-gene assays to detect genotoxicity and oxidative stress. *Mutat Res Genet Toxicol Environ Mutagen* **760**, 23-32.

van Erp-Baart, M. A., Brants, H. A., Kiely, M., Mulligan, A., Turrini, A., Sermoneta, C., Kilkkinen, A., and Valsta, L. M. (2003). Isoflavone intake in four different European countries: the VENUS approach. *Br J Nutr* **89 Suppl 1**, S25-30.

Vergne, S., Titier, K., Bernard, V., Asselineau, J., Durand, M., Lamothe, V., Potier, M., Perez, P., Demotes-Mainard, J., Chantre, P., Moore, N., Bennetau-Pelissero, C., and Sauvant, P. (2007). Bioavailability and urinary excretion of isoflavones in humans: effects of soy-based supplements formulation and equol production. *J Pharm Biomed Anal* **43**, 1488-94.

Wang, X. L., Kim, H. J., Kang, S. I., Kim, S. I., and Hur, H. G. (2007). Production of phytoestrogen S-equol from daidzein in mixed culture of two anaerobic bacteria. *Arch Microbiol* **187**, 155-60.

Yuan, J. P., Wang, J. H., and Liu, X. (2007). Metabolism of dietary soy isoflavones to equol by human intestinal microflora--implications for health. *Mol Nutr Food Res* **51**, 765-81.

Zhang, M., van Ravenzwaay, B., Fabian, E., Rietjens, I., and Louisse, J. (2018). Towards a generic physiologically based kinetic model to predict in vivo uterotrophic responses in rats by reverse dosimetry of in vitro estrogenicity data. *Arch Toxicol* **92**, 1075-1088.

Zhang, Y., Yuan, J., Wang, Y., Wang, Y., An, R., and Wang, X. (2014). LC-MS/MS determination and pharmacokinetics study of puerarin and daidzein in rat plasma after oral administration of Gegenqinlian decoction and Radix Puerariae extract. *Pharmacogn Mag* **10**, 241-8.

Supplementary material 1. PBK model code

```
;==========================================================================
; Physiological parameters
;==========================================================================
; Tissue volumes (Brown et al., 1997)
BW = 0.250              {Kg}                ; body weight rat
VSIc = 0.014                                ; fraction of small intestine
VLc = 0.034                                 ; fraction of liver tissue
VRc = 0.068             ;0.082-VSIc-VLc     ; fraction of rapidly perfused tissue
VSc = 0.667             ;0.737-VFc          ; fraction of slowly perfused tissue
VFc = 0.070                                 ; fraction of fat tissue
VBc = 0.074                                 ; fraction of blood
VNc=0.057                                   ; fraction of non-perfused tissue
VGIc=0.050                                  ; fraction of GI tract contents

VSI = VSIc*BW           {L or Kg}           ; volume of small intestine tissue (calculated)
VL = VLc*BW             {L or Kg}           ; volume of liver tissue (calculated)
VR = VRc*BW             {L or Kg}           ; volume of rapidly perfused tissue (calculated)
VS = VSc*BW             {L or Kg}           ; volume of slowly perfused tissue (calculated)
VF = VFc*BW             {L or Kg}           ; volume of fat tissue (calculated)
VB = VBc*BW             {L or Kg}           ; volume of blood (calculated)

;-------------------------------------------------------------------------------------------------------------------
; Blood flow rates (Brown et al., 1997)
QC = 5.38               {L/h}               ; cardiac output:15*BW^0.74
QSIc = 0.151                                ; fraction of blood flow to small intestine
QLc = 0.099             ;0.25 - QSIc        ; fraction of blood flow to liver
QRc = 0.51              ;0.76 - QSIc - QLc  ; fraction of blood flow to rapidly perfused tissue
QSc = 0.17              ;0.24 - QFc         ; fraction of blood flow to slowly perfused tissue
QFc = 0.07                                  ; fraction of blood flow to fat


QSI = QSIc*QC           {L/h}               ; blood flow to small intestine tissue (calculated)
QL = QLc*QC             {L/h}               ; blood flow to liver tissue (calculated)
QR = QRc*QC             {L/h}               ; blood flow to rapidly perfused tissue (calculated)
QS = QSc*QC             {L/h}               ; blood flow to slowly perfused tissue (calculated)
QF = QFc*QC             {L/h}               ; blood flow to fat tissue (calculated)


;==========================================================================
; Physicochemical parameters
;==========================================================================
; partition coefficients, calculated using QPPR (DeJongh et al., 1997)

; Daizein in main model
PIDAI = 1.62                                ; intestine/blood partition coefficient
PLDAI = 1.62                                ; liver/blood partition coefficient
PRDAI = 1.62                                ; rapidly perfused tissue/blood partition coefficient
PSDAI = 0.58                                ; slowly perfused tissue/blood partition coefficient
PFDAI = 44.75                               ; fat/blood partition coefficient

; S-equol in sub-model
PIEQU = 2.44                                ; intestine/blood partition coefficient
PLEQU = 2.44                                ; liver/blood partition coefficient
PREQU = 2.44                                ; rapidly perfused tissue/blood partition coefficient
PSEQU = 0.72                                ; slowly perfused tissue/blood partition coefficient
PFEQU = 96.29                               ; fat/blood partition coefficient
```

```
;-----------------------------------------------------------------------------------------------------------------------;
; absorption/transfer rates

Ka =3.43                {/h}            ; absorption rate of daidzein to small intestinal tissue (Steensma et
al., 2004)
Kb=3.43                 {/h}            ; transfer rate of daidzein from large intestinal lumen to liver
(Steensma et al., 2004)
Ksl =0.464              {/h}            ; transfer rate of daidzein to faeces (Kimura and Higaki, 2002)
Kll =3.43               {/h}            ; transfer rate of S-equol from large intestinal lumen to liver
(Steensma et al., 2004)


;=========================================================================
; Kinetic parameters
;=========================================================================
; metabolism of small intestine tissue

; scaling factors
S9SI= 38.6      {mg S9 protein/gram intestine}      ; small intestinal S9 protein yield (Cubitt et al., 2011)
SI=VSIc*1000    {gram/kg BW}                        ; small intestine in body weight


; metabolites DAI-7G, DAI-4'G and DAI-7S, unscaled maximum rates of metabolism, {nmol/min/mg S9 protein}
(Islam et al., 2014)
VmaxSIDAI7Gc= 1.3
VmaxSIDAI4iGc= 0.15

; metabolites DAI-7G and DAI-4'G, scaled maximum rates of metabolism, {µmol/h}
VMaxSIDAI7G = VmaxSIDAI7Gc/1000*60* S9SI*SI*BW
VmaxSIDAI4iG= VmaxSIDAI4iGc/1000*60* S9SI*SI*BW


; metabolites DAI-7G and DAI-4'G, affinity constants, {µmol/L} (Islam et al., 2014)
KmSIDAI7G = 7.10
KmSIDAI4iG = 49.20

;-----------------------------------------------------------------------------------------------------------------
; metabolism of large intestine lumen (microbiota compartment)

; scaling factors
VMB = 0.0164                                        ; fraction of faeces of BW (Hoskins and Zamcheck, 1968)

; metabolites DHD, S-equol and O-DMA, unscaled maximum rates of metabolism, {µmol/h/g faeces}
VmaxLIDHDc=0.35                                     ; experimental data derived from anaerobic rat fecal
incubations
VmaxLIEQUc= 0.28                                    ; experimental data derived from anaerobic rat fecal
incubations
VmaxLIODMAc=0.04                                    ; experimental data derived from anaerobic rat fecal
incubations


; metabolites DHD, S-equol and O-DMA, scaled maximum rates of metabolism, {µmol/h}
VmaxLIDHD= VmaxLIDHDc*1000 *VMB*BW
VmaxLIEQU= VmaxLIEQUc*1000 *VMB*BW
VmaxLIODMA= VmaxLIODMAc*1000 *VMB*BW


; metabolites DHD, S-equol and O-DMA, affinity constants, {µmol/L}
KmLIDHD = 1.69                                      ; experimental data derived from anaerobic rat fecal
incubations
```

```
KmLIEQU = 1.08                          ; experimental data derived from anaerobic rat fecal
incubations
KmLIODMA = 2.42                         ; experimental data derived from anaerobic rat fecal
incubations

;-----------------------------------------------------------------------------------------------------------------------
; metabolism of liver

; scaling factors
VLS9 = 143      {mg S9 protein/gram liver}      ; liver S9 protein yield (Punt et al., 2008)
L=VLc*1000      {gram/kg BW}                    ; liver

; Part 1: Daidzein phase II metabolism-glucuronidation

; metabolites DAI-7G and DAI-4'G, unscaled maximum rates of metabolism, {nmol/min/mg S9 protein} (Islam
et al., 2014)
VmaxLDAI7Gc= 1.40
VmaxLDAI4iGc= 0.30


; metabolites DAI-7G and DAI-4'G, scaled maximum rates of metabolism, {µmol/h}
VmaxLDAI7G = VmaxLDAI7Gc/1000*60* VLS9 *L*BW
VmaxLDAI4iG= VmaxLDAI4iGc/1000*60* VLS9 *L*BW


; metabolites DAI-7G, DAI-4'G and DAI-7S, affinity constants, {µmol/L} (Islam et al., 2014)
KmLDAI7G = 5.60
KmLDAI4iG = 77.70

; Part 2: S-equol phase II metabolism: glucuronidation

; metabolites S-equol glucuronide-1 and glucuronide-2, unscaled maximum rates of metabolism, {nmol/min/mg
S9 protein}
VmaxLEQUG1c=11.02                       ; experimental data derived from rat liver S9 incubations
for S-equol
VmaxLEQUG2c=10.61                       ; experimental data derived from rat liver S9 incubations
for S-equol


; metabolites S-equol glucuronide-1 and glucuronide-2, scaled maximum rates of metabolism, {µmol/h}
VmaxLEQUG1 = VmaxLEQUG1c/1000*60* VLS9 *L*BW
VmaxLEQUG2= VmaxLEQUG2c/1000*60* VLS9 *L*BW


; metabolites S-equol glucuronide-1and glucuronide-2, affinity constants, {µmol/L}
KmLEQUG1 =22.48                         ; experimental data derived from rat liver S9 incubations
for S-equol
KmLEQUG2 =13.72                         ; experimental data derived from rat liver S9 incubations
for S-equol

;=====================================================================
; Run settings
;=====================================================================

; molecular weight
MWDAI = 254.23                          ; molecular weight DAI

;-----------------------------------------------------------------------------------------------------------------------
; oral dose
```

```
ODOSEmg =10                                  {mg/kg bw}          ; oral dose, variable

ODOSEumol= ODOSEmg*1000/MWDAI*BW             {µmol}              ; unit change to µmol

;-----------------------------------------------------------------------------------------------------------
; time
Starttime = 0                                {µmol}
Stoptime = 4                                 { µmol}             ; variable
;=========================================================================
; Main model calculations/dynamics: daidzein
;=========================================================================

; small intestine lumen compartment
; ASILuDAI: amount of daidzein remain in small intestinal lumen, {µmol}
ASILuDAI' = -Ka*ASILuDAI - Ksl*ASILuDAI
Init ASILuDAI = ODOSEumol

;-----------------------------------------------------------------------------------------------------------
; small intestine tissue compartment
; ASIDAI: amount of daidzein in small intestinal tissue, {µmol}
        ASIDAI' = ka* ASILuDAI + QSI*(CB- CVSIDAI) - ASIDAI7G' - ASIDAI4iG'
        Init ASIDAI=0
        CSIDAI = ASIDAI/VSI
        CVSIDAI = CSIDAI/PIDAI

; ASIDAI7G: amount of daidzein metabolized to metabolite DAI7G, {µmol}
        ASIDAI7G'= VmaxSIDAI7G*CVSIDAI/(KmSIDAI7G+ CVSIDAI)
        Init ASIDAI7G=0

; ASIDAI4iG= amount of daidzein metabolized to metabolite DAI4iG, {µmol}
        ASIDAI4iG'= VmaxSIDAI4iG *CVSIDAI/(KmSIDAI4iG+ CVSIDAI)
        Init ASIDAI4iG=0

;-----------------------------------------------------------------------------------------------------------
; large intestine lumen compartment: microbial activity
; ALIDAI: amount of daidzein in large intestine lumen, {µmol}
        ALIDAI' = Ksl*ASILuDAI - ALIDHD' - ALIEQU' - ALIODMA' - Kb*ALIDAI
        Init ALIDAI = 0
        CLIDAI = ALIDAI/ (VMB*BW)
        CVLIDAI = CLIDAI/PIDAI

; ALIDHD: amount of DHD formed due to gut microbial activity, {µmol}
        ALIDHD'= VmaxLIDHD*CVLIDAI/(KmLIDHD + CVLIDAI)
        Init ALIDHD=0

; ALIEQU: amount of S-equol formed due to gut microbial activity, {µmol}
        ALIEQU'= VmaxLIEQU * CVLIDAI/(KmLIEQU + CVLIDAI)
        Init ALIEQU=0

; ALIODMA: amount of O-DMA formed due to gut microbial activity, {µmol}
        ALIODMA'= VmaxLIODMA* CVLIDAI/(KmLIODMA + CVLIDAI)
        Init ALIODMA=0

;-----------------------------------------------------------------------------------------------------------
; liver compartment
; ALDAI: amount of daidzein in liver, {µmol}
        ALDAI' = QL*CB+QSI* CVSIDAI-(QL+QSI)*CVLDAI - ALDAI7G'-ALDAI4iG' +Kb* ALIDAI
        Init ALDAI=0
        CLDAI = ALDAI/VL
        CVLDAI = CLDAI/PLDAI
```

```
; ALDAI7G: amount of daidzein metabolized to metabolite DAI7G in liver, {µmol}
        ALDAI7G'= VmaxLDAI7G* CVLDAI/(KmLDAI7G+ CVLDAI)
        Init ALDAI7G=0

; ALDAI4iG: amount of daidzein metabolized to metabolite DAI4iG in liver, {µmol}
        ALDAI4iG'= VmaxLDAI4iG * CVLDAI/(KmLDAI4iG+ CVLDAI)
        Init ALDAI4iG=0

;-----------------------------------------------------------------------------------------------------------
; fat compartment
; AF = amount of daidzein in fat tissue, {µmol}
        AF' = QF*(CB-CVF)
        Init AF = 0
        CF = AF/VF
        CVF = CF/PFDAI

;-----------------------------------------------------------------------------------------------------------
; rapidly perfused tissue
; AR = amount of daidzein in rapidly perfused tissue, {µmol}
        AR' = QR*(CB-CVR)
        Init AR = 0
        CR = AR/VR
        CVR = CR/PRDAI

;-----------------------------------------------------------------------------------------------------------
; slowly perfused tissue
; AS = amount of daidzein in slowly perfused tissue, {µmol}
        AS' = QS*(CB-CVS)
        Init AS = 0
        CS = AS/VS
        CVS = CS/PSDAI

;-----------------------------------------------------------------------------------------------------------
; blood compartment
; AB: amount of daidzein in blood, {µmol}
        AB' = (QL+QSI)*CVLDAI+QF*CVF+QS*CVS+QR*CVR - QC*CB
        Init AB = 0
        CB = AB/VB
        AUC'=AB
        Init AUC=0

;==========================================================================
; Main model: mass balance calculation
;==========================================================================
Total = ODOSEumol
Calculated = ASILuDAI + ASIDAI +ASIDAI7G +ASIDAI4iG + ALIDAI+ ALIDHD+ALIEQU+ALIODMA +
ALDAI + ALDAI7G +ALDAI4iG + AF + AR + AS + AB

ERROR=((Total-Calculated)/Total+1E-30)*100
MASSBBAL=Total-Calculated + 1

;==============================================================================
; Sub-model calculations/dynamics: S-equol
;==============================================================================
; large intestine lumen compartment
; ARLIEQU = amount of S-equol in large intestine lumen, {µmol}
        ARLIEQU' = ALIEQU' - Kll*ARLIEQU
        init ARLIEQU = 0
```

```
;-----------------------------------------------------------------------------------------------------------
; liver compartment
; ALEQU: amount of S-equol in liver, {µmol}
        ALEQU' = Kll*ARLIEQU + (QL+QSI)*CBEQU - (QSI+QL)*CVLEQU - ALEQUG1' - ALEQUG2'
        Init ALEQU=0
        CLEQU = ALEQU/VL
        CVLEQU = CLEQU/PLEQU

; ALEQUG1: amount of S-equol glucuronide-1 in liver
        ALEQUG1'= VmaxLEQUG1* CVLEQU/(KmLEQUG1+ CVLEQU)
        Init ALEQUG1=0

; ALEQUG2: amount of S-equol glucuronide-2 in liver
        ALEQUG2'= VmaxLEQUG2* CVLEQU/(KmLEQUG2+ CVLEQU)
        Init ALEQUG2=0

;-----------------------------------------------------------------------------------------------------------
; fat compartment
; AFEQU: amount of S-equol in fat tissue, {µmol}
        AFEQU' = QF*(CBEQU-CVFEQU)
        Init AFEQU = 0
        CFEQU = AFEQU/VF
        CVFEQU = CFEQU/PFEQU

;-----------------------------------------------------------------------------------------------------------
; rapidly perfused tissue
; AREQU: amount of S-equol in rapidly perfused tissue, {µmol}
        AREQU' = QR*(CBEQU-CVREQU)
        Init AREQU = 0
        CREQU = AREQU/VR
        CVREQU = CREQU/PREQU

;-----------------------------------------------------------------------------------------------------------
; slowly perfused tissue
; ASEQU: amount of S-equol in slowly perfused tissue, {µmol}
        ASEQU' = QS*(CBEQU-CVSEQU)
        Init ASEQU = 0
        CSEQU = ASEQU/VS
        CVSEQU = CSEQU/PSEQU

;-----------------------------------------------------------------------------------------------------------
; blood compartment
; ABEQU: amount of S-equol in blood, {µmol}
        ABEQU' = (QL+QSI)*CVLEQU + QF*CVFEQU + QR*CVREQU + QS*CVSEQU - QC*CBEQU
        Init ABEQU= 0
        CBEQU = ABEQU/VB
        AUCEQU'=ABEQU
        Init AUCEQU=0
```

References

Brown, R. P., Delp, M. D., Lindstedt, S. L., Rhomberg, L. R., and Beliles, R. P. (1997). Physiological parameter values for physiologically based pharmacokinetic models. *Toxicol Ind Health* **13**, 407-84.

Cubitt, H. E., Houston, J. B., and Galetin, A. (2011). Prediction of human drug clearance by multiple metabolic pathways: integration of hepatic and intestinal microsomal and cytosolic data. *Drug Metab Dispos* **39**, 864-73.

DeJongh, J., Verhaar, H. J. M., and Hermens, J. L. M. (1997). A quantitative property-property relationship (QPPR) approach to estimate in vitro tissue-blood partition coeffcients of organic chemicals in rats and humans. *Arch Toxicol*, 72: 17-25.

Hoskins, L. C., and Zamcheck, N. (1968). Bacterial degradation of gastrointestinal mucins: I. Comparison of mucus constituents in the stools of germ-free and conventional rats. *Gastroenterology* **54**, 210-217.

Islam, M. A., Punt, A., Spenkelink, B., Murk, A. J., Rolaf van Leeuwen, F. X., and Rietjens, I. M. (2014). Conversion of major soy isoflavone glucosides and aglycones in in vitro intestinal models. *Mol Nutr Food Res* **58**, 503-15.

Kimura, T., and Higaki, K. (2002). Gastrointestinal transit and drug absorption. *Biological and Pharmaceutical Bulletin* **25**, 149-164.

Punt, A., Freidig, A. P., Delatour, T., Scholz, G., Boersma, M. G., Schilter, B., van Bladeren, P. J., and Rietjens, I. M. (2008). A physiologically based biokinetic (PBBK) model for estragole bioactivation and detoxification in rat. *Toxicol Appl Pharmacol* **231**, 248-59.
Steensma, A., Noteborn, H. P., and Kuiper, H. A. (2004). Comparison of Caco-2, IEC-18 and HCEC cell lines as a model for intestinal absorption of genistein, daidzein and their glycosides. *Environ Toxicol Pharmacol* **16**, 131-9.

Supplementary material 2.

Table S1. Predicted daidzein plasma C_{max} compared to in vivo C_{max} from literature upon oral dosing of daidzein.

Daidzein oral dose (mg/kg bw)	In vivo plasma C_{max} (µM)	Unconjugated in vivo plasma C_{max} (µM)[a]	Predicted plasma C_{max} (µM)	Predicted plasma C_{max} /in vivo plasma C_{max}	Reference
1.14	0.405	0.0328	0.0353	1.0762	(Islam et al., 2015)
3	0.195	No correction	0.1148	0.5887	(Mallis et al., 2003)
4.27	2.87	0.2325	0.1858	0.7991	(Zhang et al., 2014)
4.35	7.24	0.5864	0.1908	0.3253	(Zhang et al., 2014)
5.88	1.115	No correction	0.2949	0.2645	(Sepehr et al., 2007)
10	0.579	No correction	0.6600	1.1399	(Janning et al., 2000)
10	0.521	No correction	0.6600	1.2668	(Shen et al., 2011)
19.58	9.50	0.7695	2.0724	2.6932	(King, 1998)
20	3.74	No correction	2.1559	0.5764	(Chen et al., 2005)
20	2.36	No correction	2.1559	0.9135	(Qiu et al., 2005)
30	1.40	No correction	5.2775	3.7696	(Bai et al., 2010)
Average				1.2194	

[a] Plasma C_{max} is corrected by the fraction 8.1% (Setchell et al., 2011) of unconjugated daidzein, if the literature in vivo data processed hydrolysis of the plasma sample.

Table S2. Predicted S-equol plasma C_{max} compared to in vivo C_{max} from literature upon oral dosing of daidzein.

Daidzein oral dose (mg/kg bw)	In vivo plasma C_{max} (nM)	Unconjugated In vivo plasma C_{max} (nM)[a)]	Predicted plasma C_{max} (nM)	Predicted plasma C_{max} /in vivo plasma C_{max}	Reference

1.14	84.605	0.9307	0.6795	0.7301	(Islam et al., 2015)
11.4	342.206	3.7643	5.2958	1.4068	(Islam et al., 2015)
Average				1.0685	

[a)]Plasma C_{max} is corrected by the fraction 1.1% (Setchell et al., 2011) of unconjugated S-equol, if the literature in vivo data processed hydrolysis of the plasma sample.

References

Bai, Y., Wen, H., Zhou, H., Qiu, Y., and Shan, C. (2010). Determination of daidzein and its pharmacokinetics in rat plasma by UPLC. *Chinese Pharmacological Bulletin* **26**, 1512-1515.

Chen, X., Feng, Q., Dafang, Z., Xiaotao, D., and Changxiao, L. (2005). Validated liquid chromatography-tandem mass spectrometric method for the quantitative determination of daidzein and its main metabolite daidzein glucuronide in rat plasma. *Die Pharmazie-An International Journal of Pharmaceutical Sciences* **60**, 334-338.

Islam, M. A., Hooiveld, G., van den Berg, J. H. J., Boekschoten, M. V., van der Velpen, V., Murk, A. J., Rietjens, I., and van Leeuwen, F. X. R. (2015). Plasma bioavailability and changes in PBMC gene expression after treatment of ovariectomized rats with a commercial soy supplement. *Toxicol Rep* **2**, 308-321.

Janning, P., Schuhmacher, U. S., Upmeier, A., Diel, P., Michna, H., Degen, G. H., and Bolt, H. M. (2000). Toxicokinetics of the phytoestrogen daidzein in female DA/Han rats. *Archives of Toxicology* **74**, 421-430.

King, R. A. (1998). Daidzein conjugates are more bioavailable than genistein conjugates in rats. *The American journal of clinical nutrition* **68**, 1496S-1499S.

Mallis, L., Sarkahian, A., Harris, H., Zhang, M., and McConnell, O. (2003). Determination of rat oral bioavailability of soy-derived phytoestrogens using an automated on-column extraction procedure and electrospray tandem mass spectrometry. *Journal of Chromatography B* **796**, 71-86.

Qiu, F., Chen, X. Y., Song, B., Zhong, D. F., and Liu, C. X. (2005). Influence of dosage forms on pharmacokinetics of daidzein and its main metabolite daidzein-7-O-glucuronide in rats. *Acta Pharmacol Sin* **26**, 1145-52.

Sepehr, E., Cooke, G., Robertson, P., and Gilani, G. S. (2007). Bioavailability of soy isoflavones in rats Part I: application of accurate methodology for studying the effects of gender and source of isoflavones. *Mol Nutr Food Res* **51**, 799-812.

Setchell, K. D., Brown, N. M., Zhao, X., Lindley, S. L., Heubi, J. E., King, E. C., and Messina, M. J. (2011). Soy isoflavone phase II metabolism differs between rodents and humans: implications for the effect on breast cancer risk. *Am J Clin Nutr* **94**, 1284-94.

Shen, Q., Li, X., Li, W., and Zhao, X. (2011). Enhanced intestinal absorption of daidzein by borneol/menthol eutectic mixture and microemulsion. *AAPS PharmSciTech* **12**, 1044-9.

Zhang, Y., Yuan, J., Wang, Y., Wang, Y., An, R., and Wang, X. (2014). LC-MS/MS determination and pharmacokinetics study of puerarin and daidzein in rat plasma after oral administration of Gegenqinlian decoction and Radix Puerariae extract. *Pharmacogn Mag* **10**, 241-8.

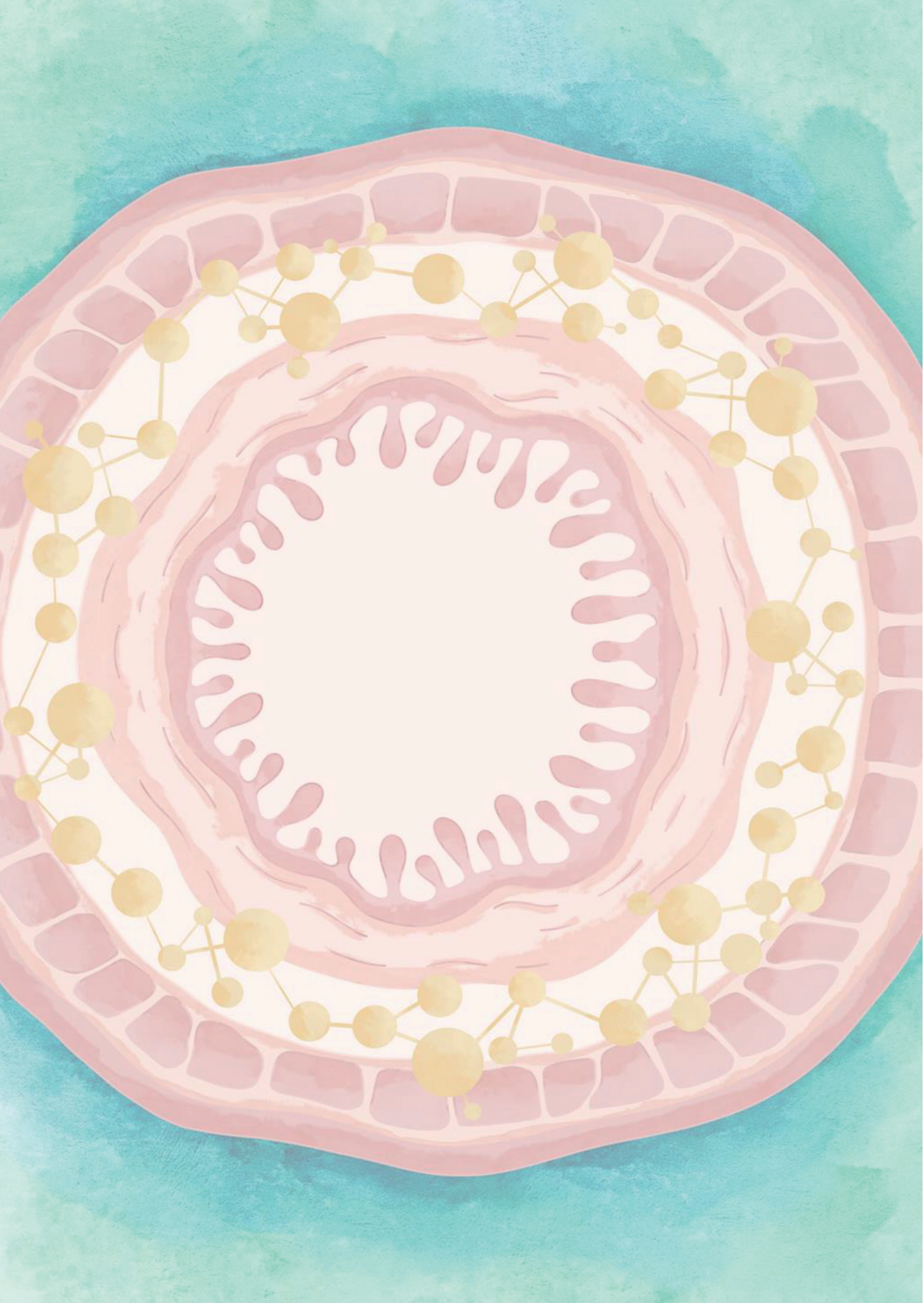

Chapter 3

Use of physiologically based kinetic (PBK) modeling to predict human gut microbial conversion of daidzein to S-equol

Qianrui Wang, Bert Spenkelink, Rungnapa Boonpawa and Ivonne M.C.M. Rietjens

Published in Journal of Agricultural and Food Chemistry. 2021; 70(1), 343-352

Abstract

A physiologically based kinetic (PBK) model was developed for daidzein and its metabolite S-equol. Anaerobic in vitro incubations of pooled fecal samples from S-equol producers and non-producers allowed definition of the kinetic constants. PBK model-based predictions for the maximum daidzein plasma concentration (C_{max}), were comparable to literature data. The predictions also revealed that the C_{max} of S-equol in producers was only up to 0.22% that of daidzein, indicating that despite of its higher estrogenicity, S-equol is likely to contribute to the overall estrogenicity upon human daidzein exposure to only a limited extent.

An interspecies comparison between human and rat revealed that the catalytic efficiency for S-equol formation in rats was 210-fold higher than that of human S-equol producers. The described in vitro-in silico strategy provides a proof-of-principle on how to include microbial metabolism in humans in PBK modeling as part of the development of new assessment methodologies (NAMs).

1. Introduction

The human body provides a habitat for vast microbial communities (Le Chatelier et al., 2013), the majority of which reside in the gastrointestinal tract, especially the distal gut (Zimmermann et al., 2019). Through a wide range of biochemical reactions (e.g. hydrolysis, reduction, dehydroxylation, acetylation and deacetylation), human gut microbiota may play a role in the toxicity of xenobiotics, changing their toxicokinetics and/or toxicodynamics (Petschow et al., 2013). Though microbial composition and abundance varies among individuals, these differences do not necessarily translate to functional differences since the overall metabolic pathways of the gut microbiota appear to remain stable (Human Microbiome Project, 2012). However, this is not necessarily the case for the metabolism of food-borne xenobiotics as the consequences of intestinal microbial conversion for their effects on the host often remain to be quantified. This also holds for the gut microbial metabolism of daidzein.

Daidzein is a dietary isoflavone present in soy and soybean products that is structurally similar to the naturally occurring hormone 17β-estradiol (E2), and thus referred to as a phytoestrogen. The consumption of isoflavones may have various health effects, such as increased bone-mineral density, reduction of post-menopausal hot flushes and anti-breast cancer potentials (Rietjens et al., 2017). Upon gut microbial metabolism, daidzein yields dihydrodaidzein (DHD) as the intermediate metabolite, which can be subsequently converted to O-desmethylangolensin (O-DMA) or S-equol. The formation of S-equol only applies to S-equol producers (**Figure 1**) (Vitale et al., 2013).

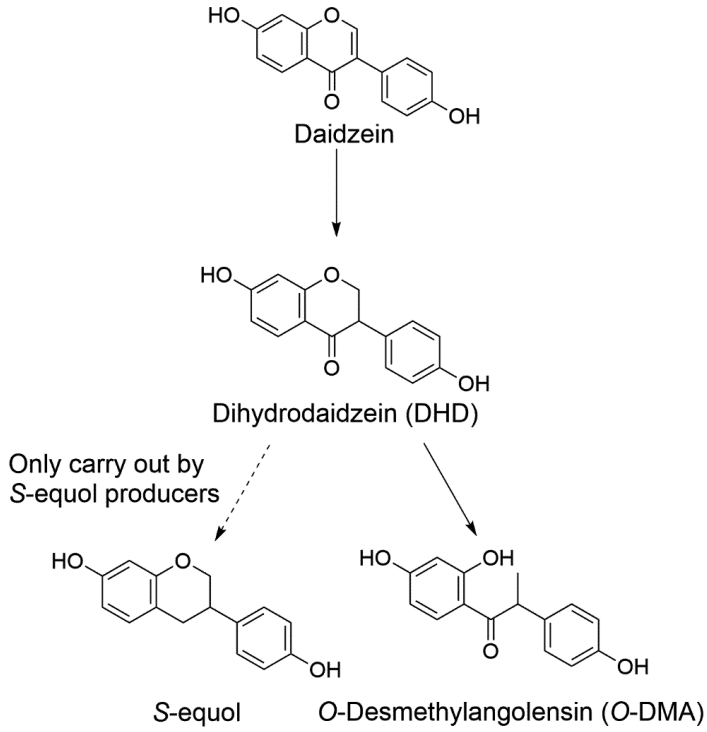

Figure 1. Metabolism of daidzein by gut microbiota in human. The plain arrows present the gut microbial conversion for both S-equol producers and non-producers, while the dashed arrow presents the reaction only carried out by S-equol producers.

S-equol is reported to be more potent as an estrogen receptor (ER) agonist than its precursor daidzein (Setchell and Clerici, 2010), providing a potential for an influence of metabolism by the microbiota on the ultimate consequences of dietary exposure to daidzein. Therefore it is also interesting to notice that there are interindividual differences in the potential for S-equol production, with around half of the Asian adult population and one-third of the Western adult population being S-equol producers (Arai et al., 2000; Atkinson et al., 2005). Diet, lifestyle and genotype of the host are reported to affect the capacity for S-equol production (Rietjens et al., 2013), with the individual status of being an S-equol producer or non-producers being relatively stable (Setchell and Cole, 2006). Given that S-equol producers make up a large part of the Asian population and the fact that their isoflavone daily intake is relatively high (Gardana and Simonetti, 2017), they may be more susceptible to the estrogenic effects caused by S-equol. In a previous study for rats (Wang et al., 2020), we used an in vitro-in silico approach including physiologically based kinetic (PBK) modeling to study the impact of

metabolism by the intestinal microbiota on the conversion of daidzein to S-equol and the resulting estrogenicity. This in vitro-in silico approach included quantification of the kinetics for microbial metabolite formation from daidzein and development of a rat PBK model that included gut microbial metabolism. The predictions revealed that daidzein is dominating the ERα-mediated estrogenicity even when taking the formation and estrogenicity of its more potent microbial metabolite S-equol into account. The in vitro-in silico approach presented a novel way of toxicity testing enabling a shift from laboratory animal models to a new approach methodologies (NAM) based on in vitro and in silico approaches, that could also be extended to human. In addition to ethical concerns, animal studies also may not adequately present the human situation given the potential kinetic and dynamic differences between animals and human, hampering extrapolation of data from experimental animals to the human situation (Soukup et al., 2016). These considerations motivate the development of NAMs that combine human-based in vitro models with PBK modeling to predict the human in vivo situation. The aim of the present study was to extend the PBK model based predictions for rats on the role of the gut microbiota in the in vivo effects of daidzein to human, in order to allow predictions for the human situation and elucidate potential species differences.

To this end, human fecal samples of S-equol producers and non-producers were used to derive kinetic parameters V_{max} and K_m, which described daidzein gut microbial conversion to its metabolites DHD, S-equol (only for producers) and O-DMA. This enabled inclusion of gut microbiota as an individual compartment in the PBK model, and facilitated the prediction of plasma concentrations of daidzein and S-equol in human.

2. Materials and methods

2.1 Materials and reagents

Daidzein, S-equol, DMSO, glycerol, alamethicin, uridine 5′-diphosphoglucuronic acid (UDPGA), 3’-phosphoadenosine-5’-phosphosulfate (PAPS) and Tromethamine (Tris) were obtained from Sigma–Aldrich (Zwijndrecht, The Netherlands). DHD and O-DMA were purchased from Cayman Chemical (AA, USA) and Plantech (Reading, UK), respectively. Trifluoroacetic acid (TFA), $MgCl_2$, 37% HCl and NaOH were obtained from VWR (Amsterdam, The Netherlands).

Acetonitrile (ACN) and methanol were obtained from Biosolve BV (Valkenswaard, The Netherlands). Phosphate Buffer Saline (PBS) was supplied by Gibco (Paisley, UK). Para-Pak

SpinCon™ Concentration System were bought from Meridian Bioscience (Schijndel, The Netherlands). Human pooled liver S9 fractions from 25 individuals (mixed gender) were supplied by Tebu-bio (Heerhugowaard, The Netherlands).

2.2 Anaerobic incubations with human feces

Human fecal samples were collected from 15 volunteers. They were asked to fill out a short questionnaire and sign a consent form (**Supplementary material 1**) to confirm the participation and make sure they did not fall into any excluded class (e.g. pregnancy, use of antibiotics in the past three months etc.). The participation was anonymous and researchers were not able to link the sample number with the participants. The design of the study was approved by The Medical Ethical Reviewing Committee of Wageningen University (METC-WU).

Each volunteer provided a one-time donation of around 5 grams of feces. Feces were collected and weighed immediately upon donating. They were subsequently brought into an anaerobic chamber (Sheldon, Cornelius, USA), containing 85% N_2, 10% CO_2 and 5% H_2, for further processing. The collected fecal samples were diluted 5 times (w/v) with an anaerobic solution consisting of 10% (v/v) glycerol in PBS Subsequently, they were filtered using filter tubes and centrifuged at 2500 × g for 5 min. The resulting fecal suspension was well mixed, aliquoted and stored at -80 °C until use.

A pre-test for feces from each participant was carried out to distinguish S-equol producers from non-producers. To this end, 100 µL incubation solutions were prepared containing (final concentrations) 60 mg/mL of feces in PBS and 17.5 µM daidzein that was added from a 200-times stock solutions in DMSO. Samples were prepared in the anaerobic chamber and incubated in the above mentioned anaerobic chamber at 37 °C for 8 hours. Subsequently, 100 µL ice-cold methanol was added to each sample to stop the reaction, followed by a 10 min cooling down on ice and a 15 min centrifuge at 21500 × g at 4 °C. Supernatants were transferred into vials for Liquid Chromatography Mass Spectrometry (LC-MS) analysis. Feces samples from S-equol producers and non-producers were mixed separately to get their respective pooled slurries.

The conditions for the anaerobic incubations with daidzein and human feces were adapted from those previously established for rat fecal incubations with some modifications.(Wang et al., 2020) Final incubation conditions were 100 µL prepared in anaerobic PBS containing 60

mg/mL pooled feces (v/v) (final concentration) from either S-equol producers or non-producers, and daidzein (final concentration range 2.5-60 μM) added from 200-times concentrated stock solutions in DMSO. Samples were prepared under the same anaerobic conditions as mentioned above. After incubating for 1 hour in the anaerobic chamber at 37 °C, the reaction was terminated by adding 100 μL ice-cold methanol. Following a 10 min ice cooling and 15 min centrifugation at 21500 × g at 4 °C, supernatants were transferred into vials for LC-MS analysis. Blank controls were prepared by replacing daidzein with DMSO and negative controls were prepared by replacing feces with PBS. Experiments were repeated three times.

2.3 Human liver S9 mediated conjugation of S-equol

Glucuronidation and sulfation of S-equol was carried out in incubations with pooled human liver S9 fractions performed as reported previously (Islam et al., 2014) with some adjustments. Glucuronidation was carried out in incubation mixtures of 100 μL, containing (final concentrations) 10 mM UDPGA, 0.025 mg/mL alamethicin, 10 mM $MgCl_2$, and 0.5 mg /mL human liver S9 protein in 50 mM Tris-HCl (pH 7.4) buffer.

After 1-min pre-incubation at 37 °C in a shaking water bath the reactions were started by the addition of 1-200 μM S-equol (added from 100-times concentrated stock solutions in DMSO). The incubations were carried out for 10 min until the addition of 25 μL ice-cold ACN to terminate the reactions. These conditions allowed linear formation of S-equol glucuronides over time and with the S9 protein concentration. Following a 15-min centrifuging at 21500 × g at 4 °C supernatants were kept on ice until immediate Ultra Performance Liquid Chromatography (UPLC) analysis. Blank incubations were performed in the absence of UDPGA and negative incubations were performed without the addition of S-equol. Incubations for S-equol glucuronidation were repeated three times.

Sulfation of S-equol by human liver S9 was carried out by preparing incubation mixtures of 100 μL containing 0.1 mM PAPS as cofactor, 5 mM $MgCl_2$ and 1 mg /mL human liver S9 protein in 50 mM potassium phosphate (pH 7.4). The incubations were carried out the same way as described above for the glucuronidation, except for the final concentrations of the substrate S-equol which ranged from 0.5-100 μM. Blank and negative incubations were performed in the absence of PAPS and S-equol, respectively. Incubations for S-equol sulfation were repeated three times.

2.4 Quantification of S-equol glucuronide and sulfate conjugates

A UPLC system (Waters Acquity) (Etten-Leur, The Netherlands) was used to quantify the concentration of S-equol and its glucuronide and sulfate conjugates in human liver S9 incubations. The system was equipped with a guard column and a BEH C18 column (1.7 µm, 2.1 × 50 mm, Waters), and UV detector recording wavelengths of 190-320 nm were used.

Nanopure water with 0.1% TFA (v/v, solvent A) and ACN (solvent B) at a flow rate of 0.4 mL/min were used with the following gradient: 0% B for 0-0.2 min, 0-18% B for 0.20-0.40 min; 18% B for 0.20-3.00 min; 18-30% B for 3.00-3.50 min; 30-80% B for 3.50-5.00 min, 80-100% for 5.00-5.50 min, 100% B for 5.50-6.00, 100-0% B for 6.00-6.50 min and 0% B between 6.50-7.00 min. The injection volume for each sample was 3.5 µL. Calibration curves were made for quantification of S-equol, its glucuronides and sulfates at the wavelength of 280 nm.

2.5 Quantification of daidzein and its microbial metabolites

A Shimadzu LC-MS/MS–8040 system (Etten-Leur, the Netherlands) was used to quantify the concentration of daidzein and its metabolites in human fecal anaerobic incubations. The electrospray ionization (ESI) source and a Kinetex XB-C18 100A analytical column (1.7µm, 100× 2.10 mm) were used for chemical ionization and compound separation, respectively. The mobile phase consisted of solvent A (0.1% TFA in nanopure water, v/v) and solvent B (0.1% TFA in ACN, v/v) at a flow rate of 0.3 mL/min, using the following mobile phase gradient program: 5% B for 0-1.00 min, 5-50% B for 1.00-1.50 min, 50-100% B for 1.50-4.50 min, 100% B for 6.50-6.60 min, 100-5% B for 6.60-10.50 min and 5% B for 10.50-11.00 min. The column temperature was set at 40 °C and the injection volume for each sample was 10 µL. The flow of the drying gas (N_2) was 15 L/min and that of the nebulizing gas (Ar) 2 L/min. The temperatures of desolvation line (DL) and heatblock were set at 250 °C and 400 °C, respectively. Data acquisition and processing were accomplished using Shimadzu LabSolutions LC/MS software (Kyoto, Japan).

2.6 Kinetic analysis of the in vitro fecal or liver S9 incubations

The apparent maximum velocity (V_{max}, expressed in µmol/h/g feces for fecal incubations or in µmol/h/mg S9 protein for liver S9 incubations) and the apparent Michaelis-Menten constant (K_m, expressed in µM), were obtained to describe the human gut microbial metabolite

formation from daidzein and the liver S9 catalysed formation of S-equol glucuronide and sulfate metabolites. Data on the concentration-dependent rate of metabolite formation in human fecal anaerobic incubations with daidzein and in human liver S9 incubations with S-equol were fitted using GraphPad Prism 5.04 (GraphPad Software, CA, USA) to the standard Michaelis-Menten equation:

$$v = \frac{V_{max} \times [S]}{K_m + [S]}$$

where v and [S] are the conversion rate (in µmol/h/g feces or nmol/min/mg S9 protein) and the substrate concentration (in µM), respectively. The V_{max} values thus obtained were scaled to the in vivo V_{max} values in the PBK model as described in the next section.

2.7 PBK model development

The human PBK model was adapted from a rat model for daidzein containing a submodel for S-equol reported previously (Wang et al., 2020). Shown in **Figure 2**, the developed PBK model includes separate compartments for blood, liver, fat, rapidly perfused tissue (e.g. heart, lung and brain), slowly perfused tissue (e.g. skin, muscle and bone), small intestine (lumen and tissue) and large intestine (lumen). The large intestine lumen compartment introduces the gut microbial activity in the model, allowing the description of microbial metabolite formation from daidzein. The model contains a sub-model for S-equol to enable definition of systemic S-equol concentrations in S-equol producers.

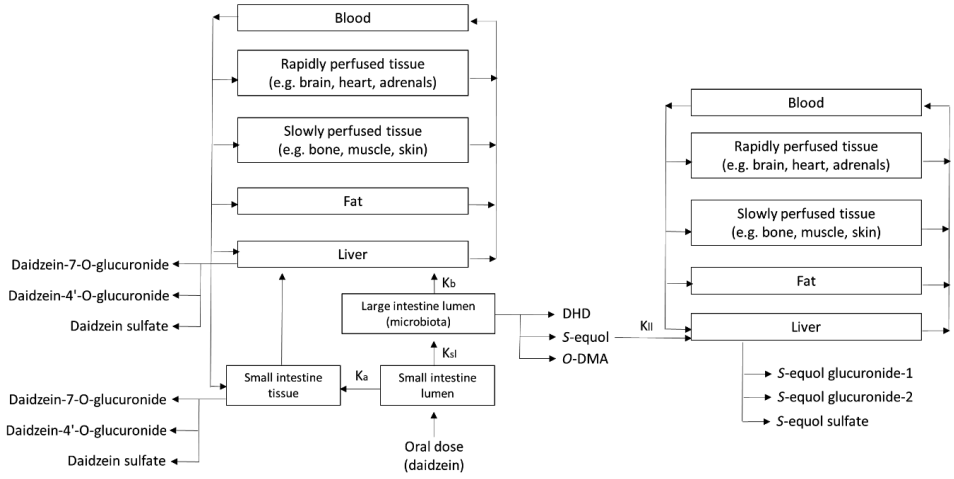

Figure 2. Structure of the PBK model for daidzein with a submodel for S-equol. For S-equol non-producers, only DHD and O-DMA are formed and the S-equol submodel is not applicable.

The gut microbial metabolism of daidzein results in formation of an intermediate metabolite DHD, and two further metabolites O-DMA and S-equol, the latter only for S-equol producers. For S-equol producers, S-equol was modelled to form in the large intestine lumen and enter the liver with a rate constant of 4.56/h (Steensma et al., 2004), while for S-equol non-producers, only the main model for daidzein applies, which includes the formation of DHD and O-DMA from daidzein microbial conversion (Brown et al., 1997).

Scaling of the kinetic V_{max} parameters obtained in vitro to the in vivo situation was included both for human fecal incubations and liver S9 incubations. For gut microbial conversions, the obtained apparent V_{max} values expressed in µmol/h/g feces were scaled to the whole body using a fecal fraction of human body weight 14 mL feces/kg bw (Brown et al., 1997). For liver and intestinal glucuronidation and sulfation of daidzein, kinetic constants were taken from published literature (Islam et al., 2014), and liver S9 incubations were performed for S-equol to define the kinetic constants for its conjugation. V_{max} values (nmol/min/mg protein) for S-equol glucuronidation and sulfation were scaled to in vivo V_{max} values, using an S9 protein yield of 143 mg S9 protein/g tissue for human liver. This value was obtained from the

sum of 108 mg/g tissue and 35 mg/g tissue of cytosolic protein yield and microsomal protein yield for human liver, respectively (Cubitt et al., 2011).

Coding and integration of differential equations of the PBK model was performed using Berkeley Madonna 8.3.18 (UC Berkeley, CA, USA) using Rosenbrock's algorithms for stiff systems. The full model code can be found in **Supplementary material 2**.

2.8 Sensitivity analysis

To assess key parameters that have the largest influence on the predicted C_{max} of daidzein and S-equol in S-equol producers a sensitivity analysis was performed. Normalized sensitivity coefficients (SCs) were calculated based on the following equation(Evans and Andersen, 2000):

$$SC = \frac{(C' - C)}{(P' - P)} \times \frac{P}{C}$$

in which P and P' are the initial and 5% increased parameter values, respectively; C represents the model output with input of the initial parameter value while C′ represents the model output upon a 5% increase in the initial parameter value. When performing the sensitivity analysis, each input parameter was changed individually, while other parameters were maintained at their initial values. The larger a SC value, the larger the impact of that model parameter on the predicted C_{max} of daidzein or S-equol.

3. Results

3.1 Daidzein metabolite formation in incubations with individual human fecal samples

Table 1 shows the concentration of S-equol detected after 8 hours anaerobic incubation of daidzein together with individual human fecal samples, as a pre-test to identify S-equol producers and non-producers. Among 15 participants, 6 appeared to be S-equol producers and 9 to be non-producers. For the S-equol producers, the gut microbial conversion of daidzein resulted in formation of S-equol upon 8 hour incubation at concentrations ranging from 0.268 to 3.611 μM.

Table 1. Human individual microbial formation of S-equol to after 8-hours anaerobic fecal incubation with daidzein (17.5 μM).

Participant No.	Production of S-equol	Concentration of S-equol (μM)
1	No	Not detected (N.D.)
2	Yes	1.75
3	No	N.D.
4	No	N.D.
5	No	N.D.
6	Yes	3.61
7	Yes	0.68
8	Yes	1.32
9	No	N.D.
10	Yes	0.27
11	No	N.D.
12	No	N.D.
13	Yes	1.35
14	No	N.D.
15	No	N.D.

3.2 Kinetic parameters for daidzein metabolite formation by pooled human fecal samples

Subsequently, fecal samples from the 6 S-equol producers were pooled and incubated as mentioned above to obtain the kinetic constants V_{max} and K_m for daidzein conversion to DHD, S-equol and O-DMA, while feces from the 9 S-equol non-producers were also pooled and incubated in the same way to obtain the kinetic constants V_{max} and K_m for daidzein conversions to DHD and O-DMA. The formation of DHD, S-equol (only for S-equol producers) and O-DMA followed Michaelis-Menten kinetics, which allowed definition of their respective apparent V_{max} ,K_m and catalytic efficiencies (calculated as V_{max}/K_m). These values are presented in **Table 2**. In fecal incubations with the sample from the S-equol producers, DHD was formed with the highest catalytic efficiency, which was 3.1- and 70- fold higher than that for S-equol and O-DMA formation, respectively. The catalytic efficiency for

formation of DHD and O-DMA for S-equol producers was 1.23 and 0.4 times that of obtained for the non-producers.

Table 2. Kinetic parameters for formation of daidzein gut microbial metabolites.

	S-equol producers			S-equol non-producers	
	DHD	S-equol	O-DMA	DHD	O-DMA
V_{max}[a] (μmol/h/g feces)	0.024 ± 0.004	0.009 ± 0.001	0.001 ± 0.0002	0.008 ± 0.001	0.0007 ± 0.0002
K_m[a] (μM)	6.24 ± 3.45	7.24 ± 3.24	18.07 ± 8.20	2.55 ± 1.95	5.12 ± 4.31
Catalytic efficiency[b] (mL/h/g feces)	3.85	1.24	0.06	3.13	0.14

[a] Average ± SD of three independent experiments

[b] Calculated as $V_{max}/K_m \times 1000$

3.3 Glucuronidation and sulfation of S-equol by pooled human liver S9 fractions

Kinetic parameters for the formation of S-equol glucuronides and sulfate were derived from in vitro incubations with pooled human liver S9 fractions. **Figure 3** presents the S-equol concentration-dependent rates of metabolite formation for glucuronidation (**Figure 3A**) and sulfation (**Figure 3B**), that appeared to follow Michaelis–Menten kinetics. In incubations with PAPS only formation of one S-equol sulfate metabolite was observed, for which substrate inhibition was observed at S-equol concentrations ≥ 25 μM, a phenomenon frequently reported for sulfation reactions (Al Zuhair et al., 2008; Schuur et al., 1998). For determination of the sulfation kinetic parameters only data points up to 25 μM S-equol were included. V_{max}, K_m and catalytic efficiencies thus derived from the data in **Figure 3** are presented in **Table 3.**

Formation of S-equol glucuronide-1 was observed with a scaled catalytic efficiency of 50.23 L/h/kg bw, which is 11-fold higher than that for S-equol glucuronide-2 formation, with a value of 4.58 L/h/kg bw. The formation of S-equol sulfate has a V_{max} of 9.24 nmol/min/mg S9 protein and a K_m of 6.50 μM, resulting in a scaled catalytic efficiency of 313.46 L/h/kg bw.

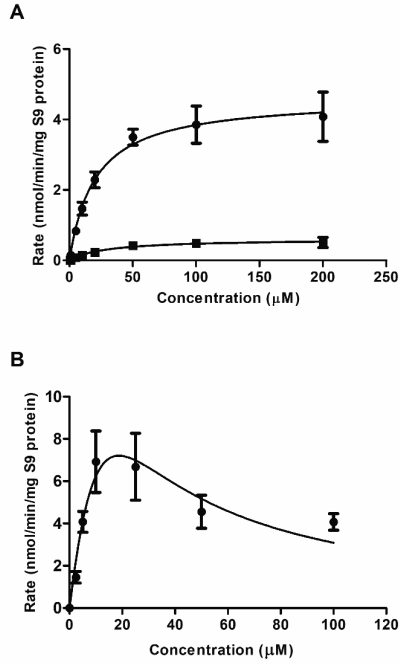

Figure 3. Concentration-dependent rate of formation of A) S-equol glucuronides and B) S-equol sulfate in incubations with pooled human liver S9 fractions. Data are presented as mean ± SD of three independent experiments.

Table 3. Kinetic parameters for human liver S9 mediated conjugation of S-equol

	S-equol glucuronide-1	S-equol glucuronide-2	S-equol sulfate
V_{max}[a] (nmol/min/mg S9 protein)	4.62 ± 0.19	0.61 ± 0.05	9.24 ± 1.51
K_m[a] (μM)	20.28 ± 2.85	29.39 ± 7.66	6.50 ± 2.77
Catalytic efficiency[b] (mL/min/mg S9 protein)	0.23	0.02	1.42
Scaled V_{max}[c] (μmol/h/kg bw)	1018.74	134.51	2037.48
Scaled catalytic efficiency[d] (L/h/kg bw)	50.23	4.58	313.46

[a] Average ± SD of three independent experiments

[b] Calculated as V_{max}/K_m

[c] Scaled V_{max} calculated from the in vitro V_{max} based on an S9 protein yield of 143 mg S9 protein/g tissue for human liver

[d] Calculated as scaled V_{max}/K_m

3.4 Model evaluation by comparison of predictions to literature data

The kinetic constants obtained were scaled to the in vivo situation and integrated in the PBK model to predict C_{max} values for unconjugated daidzein and S-equol. To evaluate model performance, the model predicted C_{max} of free daidzein was compared with human literature reporting C_{max} upon oral administration of daidzein-containing food (e.g. soy milk, soy based powder and etc.) upon oral doses in a range of 0.09- 3.34 mg/kg bw daidzein (Bloedon et al., 2002; Gardana et al., 2014; Izumi et al., 2000; King and Bursill, 1998; Manach et al., 2005; Rowland et al., 2003; Setchell et al., 2001; Setchell et al., 2003; Setchell et al., 2002; Tew et al., 1996; Watanabe et al., 1998; Xu, 1995; Xu et al., 1994; Zhang et al., 1999; Zubik and Meydani, 2003). Literature reported for the C_{max} of daidzein (conjugated plus free) were multiplied by a factor of 2.08% (Busby et al., 2002) to estimate the C_{max} for unconjugated daidzein in the circulation. Given that the blood-to-plasma ratio for neutral compounds is generally assumed to be 1 (Katyayan and Hui, 2019),no further correction between plasma and blood concentrations was applied. **Figure 4** presents the ratio between the model predicted C_{max} of unconjugated daidzein and the values derived from data reported in literature. From this overview it follows that there is a wide variability between data reported in literature. The model prediction is on average 1.62-times that of the reported in vivo plasma C_{max} for daidzein.

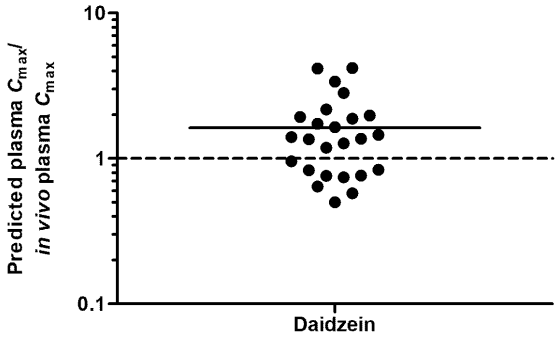

Figure 4. Ratio of predicted and in vivo observed C_{max} of unconjugated daidzein upon daidzein administration of 0.09-3.34 mg/kg bw.(Bloedon et al., 2002; Gardana et al., 2014; Izumi et al., 2000; King and Bursill, 1998; Manach et al., 2005; Rowland et al., 2003; Setchell et al., 2001; Setchell et al., 2003; Setchell et al., 2002; Tew et al., 1996; Watanabe et al., 1998;

Xu, 1995; Xu et al., 1994; Zhang et al., 1999; Zubik and Meydani, 2003) Each data point represents a separate ratio.

Table 4 compares the PBK model based prediction of the cumulative 24 hours urinary excretion of S-equol (mainly in the form of glucuronides and sulfates) with the in vivo S-equol urinary excretion as reported in studies with human volunteers orally exposed to daidzein (Karr et al., 1997; Lampe et al., 2001). The overall ratio of the predicted versus the reported in vivo cumulative urinary excretion amounts to 0.89, and reveals that the model adequately predicts the formation of S-equol and its conjugated metabolites.

Table 4. Ratio between cumulative urinary excretion of S-equol predicted by the PBK model and as reported in studies with human volunteers(Karr et al., 1997; Lampe et al., 2001) 24 hours upon oral doses of daidzein.

Dose daidzein (mg/kg bw)	Reported in vivo urinary excretion S-equol (mg)	Model predicted urinary excretion S-equol (mg)	Ratio predicted /in vivo urinary excretion
0.13	0.50	0.68	1.36
0.05	0.33	0.28	0.85
0.10	0.80	0.53	0.66
0.19	1.43	0.98	0.69
Average			0.89

3.5 PBK model based predictions of human plasma profiles of S-equol and daidzein in producers and non-producers

Subsequently, model based predictions for the time-dependent human blood levels of S-equol and daidzein upon different oral dose levels were calculated for both S-equol producers and non-producers (**Figure 5**). From these results, it follows that upon oral administration of 1 mg/kg bw daidzein in producers, S-equol was predicted to be present in plasma with a C_{max} of 0.18 nM and an $AUC_{(0\text{-}4h)}$ of 2.02 nmol h/L. For its parent compound daidzein, a C_{max} of 0.08 µM and an $AUC_{(0\text{-}4h)}$ of 0.60 µmol h/L was obtained, while in S-equol non-producers, the daidzein C_{max} and $AUC_{(0\text{-}4h)}$ were comparable, at 0.09 µM and 0.71 µmol h/L. These results reveal that introducing gut microbiota as a separate compartment in the PBK model provides a proof-of-concept for the effect of gut metabolism on systemic metabolite patterns in the host.

The results presented in **Figure 5** also reveal that the microbial intestinal daidzein conversion into S-equol appeared to be of only limited influence on the overall plasma daidzein kinetics, whereas S-equol levels are completely dependent on this reaction. The data also reveal that the S-equol C_{max} values in S-equol producers are predicted to amount to only 0.22 % of the plasma daidzein levels.

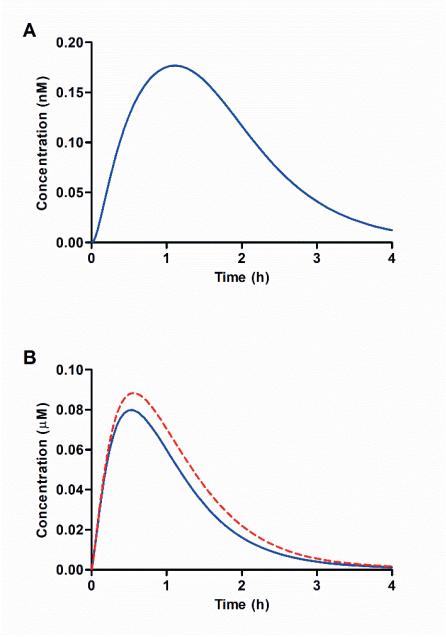

Figure 5. Model predictions for A) S-equol and B) daidzein plasma concentrations upon oral dosing of 1 mg/kg bw daidzein. The red dashed line is the model prediction of S-equol non-producers and the solid blue line is that of S-equol producers.

3.6 Sensitivity analysis

A sensitivity analysis was performed to assess the most influential parameters affecting the C_{max} of daidzein and S-equol. Oral doses of 1, 10 and 100 mg/kg bw daidzein were applied in the analysis. **Figure 6** shows the parameters having absolute normalized sensitivity coefficients (SCs) higher than 0.1, for at least one dose. From this it follows that the predicted C_{max} of daidzein is most sensitive to fraction of blood flow to rapidly perfused tissue (QRc), fraction of liver (VLc) and liver S9 protein yield (VLS9). The prediction of the C_{max} of S-equol is predominantly influenced by QRc, the maximum formation rate of S-equol by large intestine lumen (VmaxLIEQUc), and fraction of feces of body weight (VMB). Compared to

daidzein, the predicted C_{max} of S-equol is more sensitive to large intestine related parameters, which refer to gut microbial metabolism.

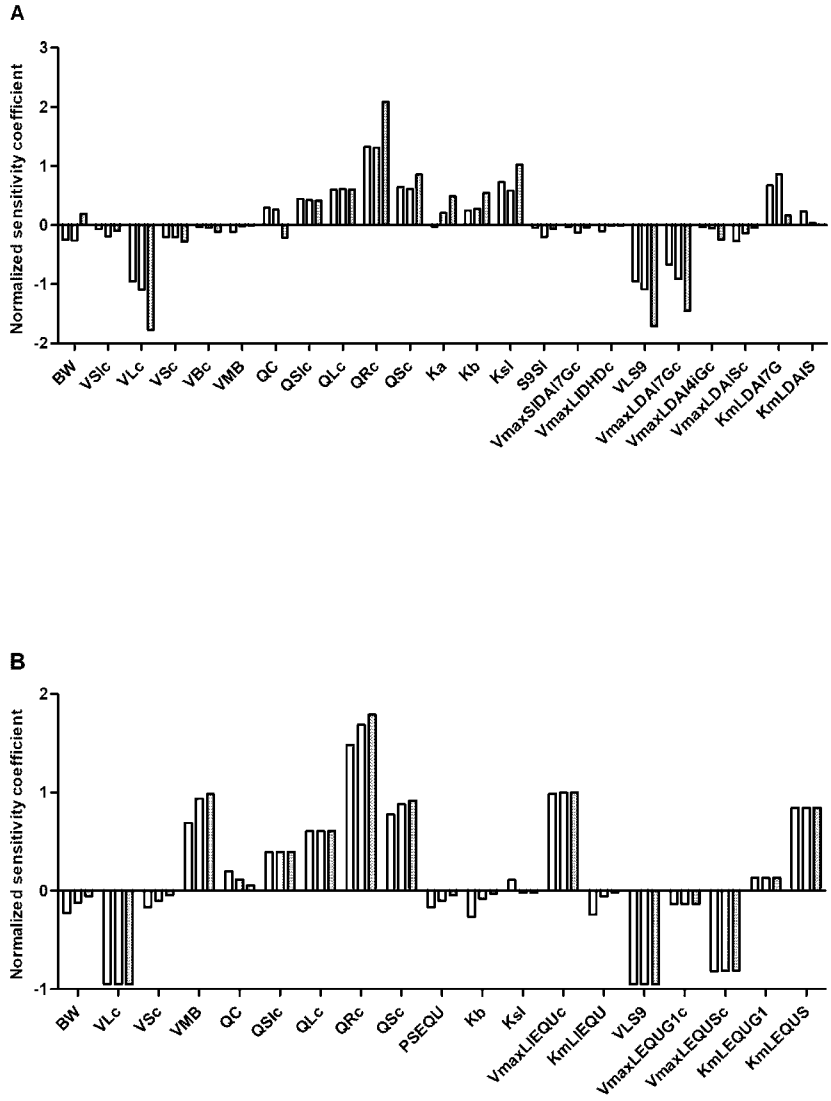

Figure 6. Sensitivity analysis for the predicted free C_{max} of A) daidzein and B) S-equol, at oral dose levels of 1 (white bars), 10 (light grey bars) and 100 (dark grey bars) mg/kg bw daidzein.

Parameters represent: BW = body weight, VSIc = fraction of small intestine, VLc = fraction of liver, VSc = fraction of slowly perfused tissue, VBc = fraction of blood, VMB = fraction of feces of body weight, QC = cardiac output, QSIc = fraction of blood flow to small intestine, QLc = fraction of blood flow to liver, QRc = fraction of blood flow to rapidly perfused tissue, QSc = fraction of blood flow to slowly perfused tissue, PSDAI = slowly perfused tissue/blood partition coefficient of daidzein, Ka = absorption rate of daidzein to intestinal tissue, Kb = transfer rate of daidzein from large intestinal lumen to liver, Ksl = transfer rate of daidzein to feces, S9SI = small intestinal S9 protein yield, VmaxSIDAI7Gc = V_{max} for formation of daidzein-7-O-glucuronide by small intestine, VmaxLIDHDc = V_{max} for formation of DHD by large intestine lumen, VmaxLDAI7Gc = V_{max} for formation of daidzein-7-O-glucuronide by liver, VmaxLDAI4iGc = V_{max} for formation of daidzein-4'-O-glucuronide by liver, VmaxLDAISc = V_{max} for formation of daidzein-sulfate by liver, KmLDAI7G = K_m for formation of daidzein-7-O-glucuronide by liver, KmLDAIS = K_m for formation of daidzein-sulfate by liver, PSEQU = slowly perfused tissue/blood partition coefficient of S-equol, VmaxLIEQUc = V_{max} for formation of S-equol by large intestine lumen, KmLIEQU = K_m for formation of S-equol by large intestine lumen, VmaxLEQUG1c = V_{max} for formation of S-equol glucuronide-1 by liver, VmaxLEQUSc = V_{max} for formation of S-equol sulfate by liver, KmLEQUG1 = K_m for formation of S-equol glucuronide-1 by liver, KmLEQUS = K_m for formation of S-equol sulfate by liver.

3.7 Comparison between human and rat microbial metabolic activities

To further characterize interspecies differences in daidzein metabolism by the gut microbiota, the metabolism of daidzein by the gut microbiota from human as quantified in the current study was compared to previous data obtained for rats (Wang et al., 2020). **Figure 7** shows the daidzein concentration-dependent rates of metabolite formation for the two species and kinetic parameters V_{max} and K_m values are shown in **Table 5**. For formation of S-equol, rat fecal samples showed a catalytic efficiency that was 209-fold higher than that obtained for human S-equol producers. For formation of DHD and O-DMA, rat fecal samples also showed much higher catalytic efficiencies than human fecal samples, the values being respectively 54- and 118-fold higher in S-equol producers. These differences were due to substantially higher values for the apparent V_{max} and somewhat lower K_m values.

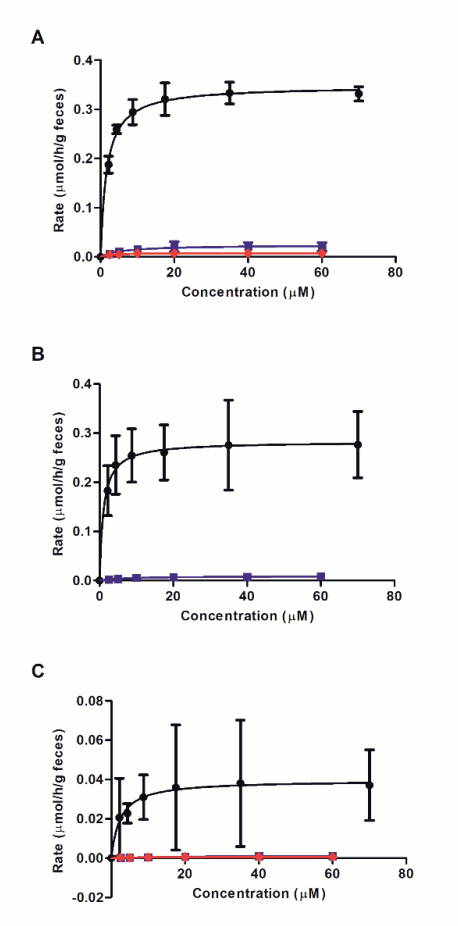

Figure 7. Comparison of microbial formation of A) DHD, B) S-equol and C) O-DMA in rats (black circles), human S-equol producers (blue squares) and non-producers (red rhombus) in fecal incubations with daidzein. Data are presented as mean ± SD of three independent experiments.

Table 5. Comparison of kinetic parameters between human and rat for formation of daidzein microbial metabolites.

	DHD			S-equol		O-DMA		
	Rats	Human S-equol producers	Human S-equol non-producers	Rats	Human S-equol producers	Rats	Human S-equol producers	Human S-equol non-producers
V_{max}[a] (μmol/h/g feces)	0.35 ± 0.01	0.024 ± 0.004	0.008 ± 0.001	0.28 ± 0.02	0.009 ± 0.001	0.04 ± 0.01	0.001 ± 0.0002	0.001 ± 0.0002
K_m[a] (μM)	1.69 ± 0.21	6.24 ± 3.45	2.55 ± 1.95	1.08 ± 0.55	7.24 ± 3.24	2.42 ± 2.31	5.12 ± 4.31	18.07 ± 8.20
Catalytic efficiency[b] (mL/h/g feces)	207.10	3.85	3.13	259.26	1.24	16.53	0.14	0.06

[a] Average ± SD of three independent experiments

[b] Calculated as V_{max}/K_m

4. Discussion

The aim of the present study was to extend the in vitro-in silico based NAMs for prediction of in vivo daidzein metabolism previously developed for rat to human. The results obtained also allowed an interspecies comparison between rat and human.

The results obtained describe the kinetic parameters for human fecal metabolic conversion of daidzein by the human gut microbiota. These parameters were subsequently used to define a human PBK model for daidzein that included metabolism by the intestinal microbiota. The formation of S-equol in some human individuals has been reported previously, and is known to result from microbial metabolism of daidzein (Jackson et al., 2011; Rodriguez-Morato et al., 2015; Setchell et al., 2009a), although in these earlier studies kinetic parameters were not obtained since most of these studies focused on isolation of bacterial strains capable of performing the conversions. Behr et al. reported that mammalian fecal materials are highly comparable to colonic ones in composition and function, and can be used as representative matrix to study the metabolic activity of the gut microbiota (Behr et al., 2018). In addition, the use of anaerobic fecal incubations to define PBK model kinetic constants for gut microbial metabolism of daidzein was previously shown to be valid for rats, for which PBK model based predictions made were in line with experimental data on C_{max} levels for both daidzein and S-equol (Wang et al., 2020). Thus, to quantify PBK model parameters for intestinal microbial metabolism the use of anaerobic human fecal incubations appears to provide an

adequate approach. This conclusion is corroborated by the present study because the PBK model based predictions for C_{max} values of daidzein were on average 1.62-fold different from values actually reported in the literature. It should be noted that the literature data show wide variability while the model predicts an average value based on in vitro incubations of respective pooled human feces, so the actual differences between predicted and reported values may be influenced by interindividual differences and variation between reported studies.

PBK model predictions were made for both S-equol producers and non-producers. When comparing S-equol producers and non-producers, S-equol producers show a slightly lower C_{max} for daidzein than non-producers, indicating that a small amount of daidzein undergoes the conversion to DHD and subsequently S-equol. However, since S-equol is known to be a more potent estrogen than its parent compound daidzein (Setchell et al., 2009b; Singh-Gupta et al., 2010; Zaheer and Humayoun Akhtar, 2017), it is of importance to study the estrogenic effects caused by S-equol taking its actual endogenous levels as compared to those of daidzein into account. As illustrated in **Figure 5,** the PBK model predicted that upon oral administration of daidzein at 1 mg/kg bw, the C_{max} of S-equol amounted to only 0.22 % of that of daidzein in human, and this value was predicted to be 0.30 % in rats(Wang et al., 2020). Considering the 12.7-times higher potency for S-equol than daidzein as derived from their EC50 values in the ER-CALUX assay (Wang et al., 2020), it can be estimated that upon daidzein exposure, S-equol will contribute 2.80% and 3.81% to the overall estrogenicity compared with daidzein in human and rats, respectively. Thus, given the relatively low systemic concentrations in both species, S-equol is not expected to make a substantial contribution to the overall estrogenicity compared with its parent compound daidzein.

Catalytic efficiencies for formation of DHD and O-DMA in S-equol producers were 1.23- and 0.4- fold that of those obtained for non-producers. This indicates that the conversion from daidzein to DHD appears comparable in the two populations, with the subsequent conversion of DHD to O-DMA being somewhat less effective in S-equol producers who also convert DHD to S-equol. The reason underlying the lack of S-equol production and its correlation with the composition and abundancy of microbiota remains to be elucidated (Minamida et al., 2006; Rafii, 2015). Further studies on the human individual microbiota density and composition between S-equol producers and non-producers may provide new clues for the observed differences.

The results of the present study also enabled a comparison of the gut microbial conversion of daidzein in human to that in rats. This revealed that for formation of S-equol, rat feces has a catalytic efficiency that is 209-fold higher than that of feces from pooled human S-equol producers. For formation of DHD and O-DMA, rat feces also shows substantially higher catalytic efficiencies being 54- and 118-fold higher than that of human. Taking into account that rat feces make up around 5% of the body weight while for human that value is only 1.4%,(Brown et al., 1997) the differences in per kg bw basis are even larger, adding an extra 3.57-fold interspecies difference to the differences between rat and human for the formation of each metabolite.

Contribution of S-equol to the overall estrogenicity in these two species can also be further compared. Rodents are reported to be S-equol producers (Liang et al., 2020; Tsuji et al., 2012), while in human only 20-55% of the population are S-equol producers (Arai et al., 2000; Atkinson et al., 2005). The results of the current work, however, reveal that in spite of this species difference rats may still reflect the human situation, because the results of the PBK modeling predict that S-equol contributes to the overall estrogenicity upon exposure to daidzein to an only limited extent in both species.

In the present study, an in vitro approach using human fecal material was developed to derive kinetics for a PBK model, which included microbiota as a separate compartment. The possibility of describing gut microbial conversions provides a unique tool to predict plasma concentrations of daidzein and S-equol for different target groups. Taken all together the described in vitro-in silico strategy provides a proof-of-principle on how to include metabolism by the gut microbiota in PBK model for human as part of the development of NAMs in safety testing.

References

Al Zuhair, S., El-Naas, M. H., and Al Hassani, H. (2008). Sulfate inhibition effect on sulfate reducing bacteria. *Journal of Biochemical Technology* **1**, 39-44.

Arai, Y., Uehara, M., Sato, Y., Kimira, M., Eboshida, A., Adlercreutz, H., and Watanabe, S. (2000). Comparison of isoflavones among dietary intake, plasma concentration and urinary excretion for accurate estimation of phytoestrogen intake. *Journal of Epidemiology* **10**, 127-135.

Atkinson, C., Frankenfeld, C. L., and Lampe, J. W. (2005). Gut bacterial metabolism of the soy isoflavone daidzein: exploring the relevance to human health. *Experimental biology and medicine* **230**, 155-170.

Behr, C., Sperber, S., Jiang, X., Strauss, V., Kamp, H., Walk, T., Herold, M., Beekmann, K., Rietjens, I., and van Ravenzwaay, B. (2018). Microbiome-related metabolite changes in gut tissue, cecum content and feces of rats treated with antibiotics. *Toxicol Appl Pharmacol* **355**, 198-210.

Bloedon, L. T., Jeffcoat, A. R., Lopaczynski, W., Schell, M. J., Black, T. M., Dix, K. J., Thomas, B. F., Albright, C., Busby, M. G., Crowell, J. A., and Zeisel, S. H. (2002). Safety and pharmacokinetics of purified soy isoflavones: single-dose administration to postmenopausal women. *The American journal of clinical nutrition* **76**, 1126-1137.

Brown, R. P., Delp, M. D., Lindstedt, S. L., Rhomberg, L. R., and Beliles, R. P. (1997). Physiological parameter values for physiologically based pharmacokinetic models. *Toxicol Ind Health* **13**, 407-84.

Busby, M. G., Jeffcoat, A. R., Bloedon, L. T., Koch, M. A., Black, T., Dix, K. J., Heizer, W. D., Thomas, B. F., Hill, J. M., Crowell, J. A., and Zeisel, S. H. (2002). Clinical characteristics and pharmacokinetics of purified soy isoflavones: single-dose administration to healthy men. *The American journal of clinical nutrition* **75**, 126-136.

Cubitt, H. E., Houston, J. B., and Galetin, A. (2011). Prediction of human drug clearance by multiple metabolic pathways: integration of hepatic and intestinal microsomal and cytosolic data. *Drug Metab Dispos* **39**, 864-73.

Eisenbrand, G., and Senate Commission on Food Safety of the German Research, F. (2007). Isoflavones as phytoestrogens in food supplements and dietary foods for special medical purposes. Opinion of the Senate Commission on Food Safety (SKLM) of the German Research Foundation (DFG)-(shortened version). *Mol Nutr Food Res* **51**, 1305-12.

Evans, M. V., and Andersen, M. E. (2000). Sensitivity analysis of a physiological model for 2, 3, 7, 8-tetrachlorodibenzo-p-dioxin (TCDD): assessing the impact of specific model parameters on sequestration in liver and fat in the rat. *Toxicological sciences* **54**, 71-80.

Gardana, C., Canzi, E., and Simonetti, P. (2014). R(-)-O-desmethylangolensin is the main enantiomeric form of daidzein metabolite produced by human in vitro and in vivo. *J Chromatogr B Analyt Technol Biomed Life Sci* **953-954**, 30-37.

Gardana, C., and Simonetti, P. (2017). Long-term kinetics of daidzein and its main metabolites in human equol-producers after soymilk intake: identification of equol-conjugates by UPLC-orbitrap-MS and influence of the number of transforming bacteria on plasma kinetics. *Int J Food Sci Nutr* **68**, 496-506.

Human Microbiome Project, C. (2012). A framework for human microbiome research. *Nature* **486**, 215-21.

Islam, M. A., Punt, A., Spenkelink, B., Murk, A. J., Rolaf van Leeuwen, F. X., and Rietjens, I. M. (2014). Conversion of major soy isoflavone glucosides and aglycones in in vitro intestinal models. *Mol Nutr Food Res* **58**, 503-15.

Izumi, T., Piskula, M. K., Osawa, S., Obata, A., Tobe, K., Saito, M., Kataoka, S., Kubota, Y., and Kikuchi, M. (2000). Soy isoflavone aglycones are absorbed faster and in higher amounts than their glucosides in humans. *The Journal of nutrition* **130**, 1695-1699.

Jackson, R. L., Greiwe, J. S., Desai, P. B., and Schwen, R. J. (2011). Single-dose and steady-state pharmacokinetic studies of S-equol, a potent nonhormonal, estrogen receptor β-agonist being developed for the treatment of menopausal symptoms. *Menopause* **18**, 185-193.

Karr, S. C., Lampe, J. W., Hutchins, A. M., and Slavin, J. L. (1997). Urinary isoflavonoid excretion in humans is dose dependent at low to moderate levels of soy-protein consumption. *The American journal of clinical nutrition* **66**, 46-51.

Katyayan, K. K., and Hui, Y. H. (2019). An evaluation of metabolite profiling of six drugs using dried blood spot. *Xenobiotica* **49**, 1458-1469.

King, R. A., and Bursill, D. B. (1998). Plasma and urinary kinetics of the isoflavones daidzein and genistein after a single soy meal in humans. *The American journal of clinical nutrition* **67**, 867-872.

Lampe, J. W., Skor, H. E., Li, S., Wähälä, K., Howald, W. N., and Chen, C. (2001). Wheat bran and soy protein feeding do not alter urinary excretion of the isoflavan equol in premenopausal women. *The Journal of nutrition* **131**, 740-744.

Le Chatelier, E., Nielsen, T., Qin, J., Prifti, E., Hildebrand, F., Falony, G., Almeida, M., Arumugam, M., Batto, J. M., Kennedy, S., Leonard, P., Li, J., Burgdorf, K., Grarup, N., Jorgensen, T., Brandslund, I., Nielsen, H. B., Juncker, A. S., Bertalan, M., Levenez, F., Pons, N., Rasmussen, S., Sunagawa, S., Tap, J., Tims, S., Zoetendal, E. G., Brunak, S., Clement, K., Dore, J., Kleerebezem, M., Kristiansen, K., Renault, P., Sicheritz-Ponten, T., de Vos, W. M., Zucker, J. D., Raes, J., Hansen, T., Meta, H. I. T. c., Bork, P., Wang, J., Ehrlich, S. D., and Pedersen, O. (2013). Richness of human gut microbiome correlates with metabolic markers. *Nature* **500**, 541-6.

Liang, W., Zhao, L., Zhang, J., Fang, X., Zhong, Q., Liao, Z., Wang, J., Guo, Y., Liang, H., and Wang, L. (2020). Colonization Potential to Reconstitute a Microbe Community in Pseudo Germ-Free Mice After Fecal Microbe Transplant From Equol Producer. *Frontiers in Microbiology* **11**.

Manach, C., Williamson, G., Morand, C., Scalbert, A., and Rémésy, C. (2005). Bioavailability and bioefficacy of polyphenols in humans. I. Review of 97 bioavailability studies. *The American journal of clinical nutrition* **81**, 230S-242S.

Minamida, K., Tanaka, M., Abe, A., Sone, T., Tomita, F., Hara, H., and Asano, K. (2006). Production of equol from daidzein by gram-positive rod-shaped bacterium isolated from rat intestine. *J Biosci Bioeng* **102**, 247-50.

Petschow, B., Dore, J., Hibberd, P., Dinan, T., Reid, G., Blaser, M., Cani, P. D., Degnan, F. H., Foster, J., Gibson, G., Hutton, J., Klaenhammer, T. R., Ley, R., Nieuwdorp, M., Pot, B., Relman, D., Serazin, A., and Sanders, M. E. (2013). Probiotics, prebiotics, and the host microbiome: the science of translation. *Ann N Y Acad Sci* **1306**, 1-17.

Rafii, F. (2015). The role of colonic bacteria in the metabolism of the natural isoflavone daidzin to equol. *Metabolites* **5**, 56-73.

Rietjens, I., Louisse, J., and Beekmann, K. (2017). The potential health effects of dietary phytoestrogens. *Br J Pharmacol* **174**, 1263-1280.

Rietjens, I. M., Sotoca, A. M., Vervoort, J., and Louisse, J. (2013). Mechanisms underlying the dualistic mode of action of major soy isoflavones in relation to cell proliferation and cancer risks. *Mol Nutr Food Res* **57**, 100-13.

Rodriguez-Morato, J., Farre, M., Perez-Mana, C., Papaseit, E., Martinez-Riera, R., de la Torre, R., and Pizarro, N. (2015). Pharmacokinetic Comparison of Soy Isoflavone Extracts in Human Plasma. *J Agric Food Chem* **63**, 6946-53.

Rowland, I., Faughnan, M., Hoey, L., Wahala, K., Williamson, G., and Cassidy, A. (2003). Bioavailability of phyto-oestrogens. *Br J Nutr* **89 Suppl 1**, S45-58.

Schuur, A. G., van Leeuwen-Bol, I., Jong, W. M., Bergman, Å., Coughtrie, M. W., Brouwer, A., and Visser, T. J. (1998). In vitro inhibition of thyroid hormone sulfation by polychlorobiphenylols: isozyme specificity and inhibition kinetics. *Toxicological sciences* **45**, 188-194.

Setchell, K. D., Brown, N. M., Desai, P., Zimmer-Nechemias, L., Wolfe, B. E., Brashear, W. T., Kirschner, A. S., Cassidy, A., and Heubi, J. E. (2001). Bioavailability of pure isoflavones in healthy humans and analysis of commercial soy isoflavone supplements. *The Journal of nutrition* **131**, 1362S-1375S.

Setchell, K. D., Brown, N. M., Desai, P. B., Zimmer-Nechimias, L., Wolfe, B., Jakate, A. S., Creutzinger, V., and Heubi, J. E. (2003). Bioavailability, disposition, and dose-response effects of soy isoflavones when consumed by healthy women at physiologically typical dietary intakes. *The Journal of nutrition* **133**, 1027-1035.

Setchell, K. D., Brown, N. M., Zimmer-Nechemias, L., Brashear, W. T., Wolfe, B. E., Kirschner, A. S., and Heubi, J. E. (2002). Evidence for lack of absorption of soy isoflavone glycosides in humans, supporting the crucial role of intestinal metabolism for bioavailability. *The American journal of clinical nutrition* **76**, 447-453.

Setchell, K. D., and Clerici, C. (2010). Equol: pharmacokinetics and biological actions. *J Nutr* **140**, 1363S-8S.

Setchell, K. D., and Cole, S. J. (2006). Method of defining equol-producer status and its frequency among vegetarians. *The Journal of nutrition* **136**, 2188-2193.

Setchell, K. D., Zhao, X., Jha, P., Heubi, J. E., and Brown, N. M. (2009a). The pharmacokinetic behavior of the soy isoflavone metabolite S-(-)equol and its diastereoisomer R-(+)equol in healthy adults determined by using stable-isotope-labeled tracers. *Am J Clin Nutr* **90**, 1029-37.

Setchell, K. D., Zhao, X., Shoaf, S. E., and Ragland, K. (2009b). The pharmacokinetics of S-(-)equol administered as SE5-OH tablets to healthy postmenopausal women. *J Nutr* **139**, 2037-43.

Singh-Gupta, V., Zhang, H., Yunker, C. K., Ahmad, Z., Zwier, D., Sarkar, F. H., and Hillman, G. G. (2010). Daidzein effect on hormone refractory prostate cancer in vitro and in vivo compared to genistein and soy extract: potentiation of radiotherapy. *Pharm Res* **27**, 1115-27.

Soukup, S. T., Helppi, J., Muller, D. R., Zierau, O., Watzl, B., Vollmer, G., Diel, P., Bub, A., and Kulling, S. E. (2016). Phase II metabolism of the soy isoflavones genistein and

daidzein in humans, rats and mice: a cross-species and sex comparison. *Arch Toxicol* **90**, 1335-47.

Steensma, A., Noteborn, H. P., and Kuiper, H. A. (2004). Comparison of Caco-2, IEC-18 and HCEC cell lines as a model for intestinal absorption of genistein, daidzein and their glycosides. *Environ Toxicol Pharmacol* **16**, 131-9.

Tew, B. Y., Xu, X., Wang, H. J., Murphy, P. A., and Hendrich, S. (1996). A diet high in wheat fiber decreases the bioavailability of soybean isoflavones in a single meal fed to women. *The Journal of nutrition* **126**, 871-877.

Tsuji, H., Moriyama, K., Nomoto, K., and Akaza, H. (2012). Identification of an enzyme system for daidzein-to-equol conversion in Slackia sp. strain NATTS. *Appl Environ Microbiol* **78**, 1228-36.

Vitale, D. C., Piazza, C., Melilli, B., Drago, F., and Salomone, S. (2013). Isoflavones: estrogenic activity, biological effect and bioavailability. *Eur J Drug Metab Pharmacokinet* **38**, 15-25.

Wang, Q., Spenkelink, B., Boonpawa, R., Rietjens, I., and Beekmann, K. (2020). Use of Physiologically Based Kinetic Modeling to Predict Rat Gut Microbial Metabolism of the Isoflavone Daidzein to S-Equol and Its Consequences for ERalpha Activation. *Mol Nutr Food Res* **64**, e1900912.

Watanabe, S., Yamaguchi, M., Sobue, T., Takahashi, T., Miura, T., Arai, Y., Mazur, W., Wähälä, K., and Adlercreutz, H. (1998). Pharmacokinetics of soybean isoflavones in plasma, urine and feces of men after ingestion of 60 g baked soybean powder (kinako). *The Journal of nutrition* **128**, 1710-1715.

Xu, X. (1995). Human bioavailability and health protective effects of soy isoflavones.

Xu, X., Wang, H.-J., Murphy, P. A., Cook, L., and Hendrich, S. (1994). Daidzein is a more bioavailable soymilk isoflavone than is genistein in adult women. *The Journal of nutrition* **124**, 825-832.

Zaheer, K., and Humayoun Akhtar, M. (2017). An updated review of dietary isoflavones: Nutrition, processing, bioavailability and impacts on human health. *Crit Rev Food Sci Nutr* **57**, 1280-1293.

Zhang, Y., Wang, G. J., Song, T. T., Murphy, P. A., and Hendrich, S. (1999). Urinary disposition of the soybean isoflavones daidzein, genistein and glycitein differs among humans with moderate fecal isoflavone degradation activity. *The Journal of nutrition* **129**, 957-962.

Zimmermann, M., Zimmermann-Kogadeeva, M., Wegmann, R., and Goodman, A. L. (2019). Mapping human microbiome drug metabolism by gut bacteria and their genes. *Nature* **570**, 462-467.

Zubik, L., and Meydani, M. (2003). Bioavailability of soybean isoflavones from aglycone and glucoside forms in American women. *The American journal of clinical nutrition* **77**, 1459-1465.

Supplementary material 1. Questionnaire and consent form for human fecal sample collection

Questionnaire YYYY

Registration number: _____

Dear participant,

Thank you for participating in our research. As part of our research, we would like to ask a couple of questions that would help us have a general view of some conditions. All the information recorded here will be treated confidentially.

1. Age: _____

2. Gender

☐ Male ☐ Female

3. Diet:

☐ Omnivorous ☐ Vegetarian ☐ Vegan

Consent form for participants TOX-FHM YYYY

Introduction to the research

We invite you to take part in our research to study the interactions of the bacteria present in our gut with chemicals we are exposed to in our daily lives. The main focus is the metabolism of these chemicals by the bacteria, and if the chemicals have an effect on the bacteria.

Participation

Your participation in this study is voluntary and anonymous to the researchers involved. This study will require three-time collection of ~ 5 grams of stool sample in different time points and answering a short questionnaire (one time).

The samples will not be used for any medical or diagnostic purposes.

You can decide to leave the study at any time by stopping donating for any reason without any consequences.

Storage of samples and information

The samples you provide will be stored with the code "YYYY-Sample #" at the Division of Toxicology for the length of the research (maximum of 5 years), after which the samples and any linking document will be destroyed.

The PI will check for the fulfilment of all the requirements. All information collected will be kept confidential. The documents will be kept under lock and will only be accessible to the PI.

In order to categorize the stool samples, the researchers involved with the study will be able to see the information provided in the questionnaire linked to the sample number but not to your name.

Statement of the participant

I have read the information related to my participation in the study and I have had the opportunity to ask questions about it. Therefore, I declare that:

- I am over the age of eighteen (18).
- I did not use antibiotics in the past three (3) months.
- I do not have an intestinal disease (e.g. Crohn's disease, ulcerative colitis, inflammatory bowel disease) and/or currently suffering from bowel complaints (e.g. diarrhea).
- I did not visit tropical countries in the past three (3) months.
- I am not pregnant or suspect to be pregnant.
- I understand the information related to the sample will be treated as confidential.
- I agree that the samples will be used only for research purposes.
- I agree that the results of the research using this sample can be used for publication in scientific journals.
- I consent voluntarily to participate as a participant in this research.

Signature of participant_____

Date _____

Supplementary material 2. PBK model code

```
;==========================================================================
; Physiological parameters
;==========================================================================
; Tissue volumes (Brown et al., 1997)
BW = 70                 {Kg}                ; body weight human
VSIc = 0.0091                               ; fraction of small intestine
VLc = 0.0257                                ; fraction of liver tissue
VRc = 0.0442                                ; fraction of rapidly perfused tissue
VSc = 0.5428                                ; fraction of slowly perfused tissue
VFc = 0.2142                                ; fraction of fat tissue
VBc = 0.0790                                ; fraction of blood
VNc=0.0710                                  ; fraction of non-perfused tissue(hair, nails, bone)
VMB=0.0140                                  ; Gastrointestinal tract contents

VSI = VSIc*BW           {L or Kg}           ; volume of small intestine tissue (calculated)
VL = VLc*BW             {L or Kg}           ; volume of liver tissue (calculated)
VR = VRc*BW             {L or Kg}           ; volume of rapidly perfused tissue (calculated)
VS = VSc*BW             {L or Kg}           ; volume of slowly perfused tissue (calculated)
VF = VFc*BW             {L or Kg}           ; volume of fat tissue (calculated)
VB = VBc*BW             {L or Kg}           ; volume of blood (calculated)

;-------------------------------------------------------------------------------------------------------------------
; Blood flow rates (Brown et al., 1997)
QC = 347.9              {L/h}               ; cardiac output:15*BW^0.74
QSIc = 0.09                                 ; fraction of blood flow to small intestine
QLc = 0.137             ;0.227 - QSIc       ; fraction of blood flow to liver
QRc = 0.473             ;0.7 - QSIc - QLc   ; fraction of blood flow to rapidly perfused tissue
QSc = 0.248             ;0.3 - QFc          ; fraction of blood flow to slowly perfused tissue
QFc = 0.052                                 ; fraction of blood flow to fat

QSI = QSIc*QC           {L/h}               ; blood flow to small intestine tissue (calculated)
QL = QLc*QC             {L/h}               ; blood flow to liver tissue (calculated)
QR = QRc*QC             {L/h}               ; blood flow to rapidly perfused tissue (calculated)
QS = QSc*QC             {L/h}               ; blood flow to slowly perfused tissue (calculated)
QF = QFc*QC             {L/h}               ; blood flow to fat tissue (calculated)

;==========================================================================
; Physicochemical parameters
;==========================================================================
; partition coefficients, calculated using QPPR (DeJongh et al., 1997)

; Daidzein in main model
PIDAI = 1.29                                ; intestine/blood partition coefficient
PLDAI = 1.29                                ; liver/blood partition coefficient
PRDAI = 1.29                                ; rapidly perfused tissue/blood partition coefficient
PSDAI = 0.56                                ; slowly perfused tissue/blood partition coefficient
PFDAI = 39.9                                ; fat/blood partition coefficient

; S-equol in sub-model
PIEQU = 1.83                                ; intestine/blood partition coefficient
PLEQU = 1.83                                ; liver/blood partition coefficient
PREQU = 1.83                                ; rapidly perfused tissue/blood partition coefficient
PSEQU = 0.65                                ; slowly perfused tissue/blood partition coefficient
PFEQU = 77.2                                ; fat/blood partition coefficient

;-------------------------------------------------------------------------------------------------------------------;
; absorption/transfer rates
```

```
Ka =4.56                {/h}            ; absorption rate of daidzein to small intestinal tissue (Steensma et
al., 2004)
Kb =4.56                {/h}            ; transfer rate of daidzein from large intestinal lumen to liver
(Steensma et al., 2004)
Ksl =0.46               {/h}            ; transfer rate of daidzein to feces (Kimura and Higaki, 2002)
Kll =4.56               {/h}            ; transfer rate of S-equol from large intestinal lumen to liver
(Steensma et al., 2004)

;=========================================================================
; Kinetic parameters
;=========================================================================
; metabolism of small intestine tissue

; scaling factors
S9SI= 38.6      {mg S9 protein/gram intestine}      ; small intestinal S9 protein yield (Cubitt et al., 2011)
SI=VSIc*1000    {gram/kg BW}                        ; small intestine in body weight

; metabolites DAI-7G, DAI-4'G and DAI-S, unscaled maximum rates of metabolism, {nmol/min/mg S9 protein}
(Islam et al., 2014)
VmaxSIDAI7Gc= 0.2
VmaxSIDAI4iGc= 0.1
VmaxSIDAISc= 0.02

; metabolites DAI-7G and DAI-4'G, scaled maximum rates of metabolism, {µmol/h}
VMaxSIDAI7G = VmaxSIDAI7Gc/1000*60* S9SI*SI*BW
VmaxSIDAI4iG= VmaxSIDAI4iGc/1000*60* S9SI*SI*BW
VmaxSIDAIS= VmaxSIDAISc/1000*60* S9SI*SI*BW

; metabolites DAI-7G and DAI-4'G, affinity constants, {µmol/L} (Islam et al., 2014)
KmSIDAI7G = 2.7
KmSIDAI4iG = 2.9
KmSIDAIS = 0.35

;-------------------------------------------------------------------------------------------------------------
; metabolism of large intestine lumen (microbiota compartment)

; metabolites DHD, S-equol and O-DMA, unscaled maximum rates of metabolism, {µmol/h/g feces}
VmaxLIDHDc=0.024                            ; experimental data derived from anaerobic human fecal
incubations
VmaxLIEQUc= 0.009                           ; experimental data derived from anaerobic human fecal
incubations
VmaxLIODMAc=0.001                           ; experimental data derived from anaerobic human fecal
incubations

; metabolites DHD, S-equol and O-DMA, scaled maximum rates of metabolism, {µmol/h}
VmaxLIDHD= VmaxLIDHDc*1000 *VMB*BW
VmaxLIEQU= VmaxLIEQUc*1000 *VMB*BW
VmaxLIODMA= VmaxLIODMAc*1000 *VMB*BW

; metabolites DHD, S-equol and O-DMA, affinity constants, {µmol/L}
KmLIDHD = 6.239                             ; experimental data derived from anaerobic human fecal
incubations
KmLIEQU = 7.243                             ; experimental data derived from anaerobic human fecal
incubations
KmLIODMA = 18.070                           ; experimental data derived from anaerobic human fecal
incubations

;-------------------------------------------------------------------------------------------------------------
; metabolism of liver
; scaling factors
```

```
VLS9 = 143        {mg S9 protein/gram liver}        ; liver S9 protein yield (Punt et al., 2008)
L=VLc*1000        {gram/kg BW}                      ; liver

; Part 1: Daidzein phase II metabolism-glucuronidation and sulfation (Islam et al., 2014)

; metabolites DAI-7G and DAI-4'G, unscaled maximum rates of metabolism, {nmol/min/mg S9 protein}
VmaxLDAI7Gc= 1.0
VmaxLDAI4iGc= 0.2
VmaxLDAISc= 0.02

; metabolites DAI-7G and DAI-4'G, scaled maximum rates of metabolism, {µmol/h}
VmaxLDAI7G = VmaxLDAI7Gc/1000*60* VLS9 *L*BW
VmaxLDAI4iG= VmaxLDAI4iGc/1000*60* VLS9 *L*BW
VmaxLDAIS= VmaxLDAISc/1000*60* VLS9 *L*BW

; metabolites DAI-7G, DAI-4'G and DAI-7S, affinity constants, {µmol/L}
KmLDAI7G = 18.9
KmLDAI4iG = 72.1
KmLDAIS = 0.82

; Part 2: S-equol phase II metabolism: glucuronidation and sulfation

; metabolites S-equol glucuronide-1, glucuronide-2 and sulfation, unscaled maximum rates of metabolism,
{nmol/min/mg S9 protein}
VmaxLEQUG1c=4.62                    ; experimental value derived from human liver S9 incubations for S-
equol
VmaxLEQUG2c=0.61                    ; experimental value derived from human liver S9 incubations for S-
equol
VmaxLEQUSc=9.24                     ; experimental value derived from human liver S9 incubations for S-
equol

; metabolites S-equol glucuronide-1, glucuronide-2 and sulfation, scaled maximum rates of metabolism, {µmol/h}
VmaxLEQUG1 = VmaxLEQUG1c/1000*60* VLS9 *L*BW
VmaxLEQUG2= VmaxLEQUG2c/1000*60* VLS9 *L*BW
VmaxLEQUS= VmaxLEQUSc/1000*60* VLS9 *L*BW

; metabolites S-equol glucuronide-1, glucuronide-2 and sulfation, affinity constants, {µmol/L}
KmLEQUG1 =20.28                     ; experimental value derived from human liver S9 incubations for S-
equol
KmLEQUG2 =29.39                     ; experimental value derived from human liver S9 incubations for S-
equol
KmLEQUS =6.50                       ; experimental value derived from human liver S9 incubations for S-
equol

;=====================================================================
; Run settings
;=====================================================================
; molecular weight
MWDAI = 254.23                      ; molecular weight DAI

;---------------------------------------------------------------------------------------------------
; oral dose
ODOSEmg =10                         {mg/kg bw}          ; oral dose, variable

ODOSEumol= ODOSEmg*1000/MWDAI*BW    {µmol}              ; unit change to µmol

;---------------------------------------------------------------------------------------------------
; time
Starttime = 0                       {µmol}
Stoptime = 6                        {µmol}              ; variable
```

```
;==========================================================================
; Main model calculations/dynamics: daidzein
;==========================================================================
; small intestine lumen compartment
; ASILuDAI: amount of daidzein remain in small intestinal lumen, {µmol}
ASILuDAI' = -Ka*ASILuDAI - Ksl*ASILuDAI
Init ASILuDAI = ODOSEumol
;-------------------------------------------------------------------------------------------------------------
; small intestine tissue compartment
; ASIDAI: amount of daidzein in small intestinal tissue, {µmol}
        ASIDAI' = ka* ASILuDAI + QSI*(CB- CVSIDAI) - ASIDAI7G' - ASIDAI4iG'- ASIDAIS'
        Init ASIDAI=0
        CSIDAI = ASIDAI/VSI
        CVSIDAI = CSIDAI/PIDAI

; ASIDAI7G: amount of daidzein metabolized to metabolite DAI7G, {µmol}
        ASIDAI7G'= VmaxSIDAI7G*CVSIDAI/(KmSIDAI7G+ CVSIDAI)
        Init ASIDAI7G=0

; ASIDAI4iG= amount of daidzein metabolized to metabolite DAI4iG, {µmol}
        ASIDAI4iG'= VmaxSIDAI4iG *CVSIDAI/(KmSIDAI4iG+ CVSIDAI)
        Init ASIDAI4iG=0

; ASIDAIS= amount of daidzein metabolized to metabolite DAIS, {µmol}
        ASIDAIS'= VmaxSIDAIS *CVSIDAI/(KmSIDAIS+ CVSIDAI)
        Init ASIDAIS=0
;-------------------------------------------------------------------------------------------------------------
; large intestine lumen compartment: microbial activity
; ALIDAI: amount of daidzein in large intestine lumen, {µmol}
        ALIDAI' = Ksl*ASILuDAI - ALIDHD' - ALIEQU' - ALIODMA' - Kb*ALIDAI
        Init ALIDAI = 0
        CLIDAI = ALIDAI/ (VMB*BW)

; ALIDHD: amount of DHD formed due to gut microbial activity, {µmol}
        ALIDHD'= VmaxLIDHD*CLIDAI/(KmLIDHD + CLIDAI)
        Init ALIDHD=0

; ALIEQU: amount of S-equol formed due to gut microbial activity, {µmol}
        ALIEQU'= VmaxLIEQU * CLIDAI/(KmLIEQU + CLIDAI)
        Init ALIEQU=0

; ALIODMA: amount of O-DMA formed due to gut microbial activity, {µmol}
        ALIODMA'= VmaxLIODMA* CLIDAI/(KmLIODMA + CLIDAI)
        Init ALIODMA=0
;-------------------------------------------------------------------------------------------------------------
; liver compartment
; ALDAI: amount of daidzein in liver, {µmol}
        ALDAI' = QL*CB+QSI* CVSIDAI-(QL+QSI)*CVLDAI - ALDAI7G'-ALDAI4iG'-ALDAIS' +Kb*
ALIDAI
        Init ALDAI=0
        CLDAI = ALDAI/VL
        CVLDAI = CLDAI/PLDAI

; ALDAI7G: amount of daidzein metabolized to metabolite DAI7G in liver, {µmol}
        ALDAI7G'= VmaxLDAI7G* CVLDAI/(KmLDAI7G+ CVLDAI)
        Init ALDAI7G=0

; ALDAI4iG: amount of daidzein metabolized to metabolite DAI4iG in liver, {µmol}
        ALDAI4iG'= VmaxLDAI4iG * CVLDAI/(KmLDAI4iG+ CVLDAI)
        Init ALDAI4iG=0
```

```
; ALDAIS: amount of daidzein metabolized to metabolite DAIS in liver, {µmol}
        ALDAIS'= VmaxLDAIS * CVLDAI/(KmLDAIS+ CVLDAI)
        Init ALDAIS=0
;-----------------------------------------------------------------------------------------------------------
; fat compartment
; AF = amount of daidzein in fat tissue, {µmol}
        AF' = QF*(CB-CVF)
        Init AF = 0
        CF = AF/VF
        CVF = CF/PFDAI
;-----------------------------------------------------------------------------------------------------------
; rapidly perfused tissue
; AR = amount of daidzein in rapidly perfused tissue, {µmol}
        AR' = QR*(CB-CVR)
        Init AR = 0
        CR = AR/VR
        CVR = CR/PRDAI
;-----------------------------------------------------------------------------------------------------------
; slowly perfused tissue
; AS = amount of daidzein in slowly perfused tissue, {µmol}
        AS' = QS*(CB-CVS)
        Init AS = 0
        CS = AS/VS
        CVS = CS/PSDAI
;-----------------------------------------------------------------------------------------------------------
; blood compartment
; AB: amount of daidzein in blood, {µmol}
        AB' = (QL+QSI)*CVLDAI+QF*CVF+QS*CVS+QR*CVR - QC*CB
        Init AB = 0
        CB = AB/VB
        AUC'=AB
        Init AUC=0
;=================================================================
; Main model: mass balance calculation
;=================================================================
Total = ODOSEumol
Calculated = ASILuDAI + ASIDAI +ASIDAI7G +ASIDAI4iG+ASIDAIS + ALIDAI+
ALIDHD+ALIEQU+ALIODMA + ALDAI + ALDAI7G +ALDAI4iG+ALDAIS + AF + AR + AS + AB

ERROR=((Total-Calculated)/Total+1E-30)*100
MASSBBAL=Total-Calculated + 1

;=================================================================
; Sub-model calculations/dynamics: equol
;=================================================================
; large intestine lumen compartment: microbial activity
; ARLIEQU = amount of S-equol in large intestine lumen, {µmol}
        ARLIEQU' = ALIEQU' - Kll*ARLIEQU
        init ARLIEQU = 0
;-----------------------------------------------------------------------------------------------------------
; liver compartment
; ALEQU: amount of S-equol in liver, {µmol}
        ALEQU' = Kll*ARLIEQU + (QL+QSI)*CBEQU - (QSI+QL)*CVLEQU - ALEQUG1' - ALEQUG2'-
ALEQUS'
        Init ALEQU=0
        CLEQU = ALEQU/VL
        CVLEQU = CLEQU/PLEQU

; ALEQUG1: amount of S-equol glucuronide-1 in liver
```

```
        ALEQUG1'= VmaxLEQUG1* CVLEQU/(KmLEQUG1+ CVLEQU)
        Init ALEQUG1=0

; ALEQUG2: amount of S-equol glucuronide-2 in liver
        ALEQUG2'= VmaxLEQUG2* CVLEQU/(KmLEQUG2+ CVLEQU)
        Init ALEQUG2=0

; ALEQUS: amount of S-equol glucuronide-1 in liver
        ALEQUS'= VmaxLEQUS* CVLEQU/(KmLEQUS+ CVLEQU)
        Init ALEQUS=0
;-----------------------------------------------------------------------------------------------------------
; fat compartment
; AFEQU: amount of S-equol in fat tissue, {µmol}
        AFEQU' = QF*(CBEQU-CVFEQU)
        Init AFEQU = 0
        CFEQU = AFEQU/VF
        CVFEQU = CFEQU/PFEQU
;-----------------------------------------------------------------------------------------------------------
; rapidly perfused tissue
; AREQU: amount of S-equol in rapidly perfused tissue, {µmol}
        AREQU' = QR*(CBEQU-CVREQU)
        Init AREQU = 0
        CREQU = AREQU/VR
        CVREQU = CREQU/PREQU
;-----------------------------------------------------------------------------------------------------------
; slowly perfused tissue
; ASEQU: amount of S-equol in slowly perfused tissue, {µmol}
        ASEQU' = QS*(CBEQU-CVSEQU)
        Init ASEQU = 0
        CSEQU = ASEQU/VS
        CVSEQU = CSEQU/PSEQU
;-----------------------------------------------------------------------------------------------------------
; blood compartment
; ABEQU: amount of S-equol in blood, {µmol}
        ABEQU' = (QL+QSI)*CVLEQU + QF*CVFEQU + QR*CVREQU + QS*CVSEQU - QC*CBEQU
        Init ABEQU= 0
        CBEQU = ABEQU/VB
        AUCEQU'=ABEQU
        Init AUCEQU=0
```

References

Brown, R. P., Delp, M. D., Lindstedt, S. L., Rhomberg, L. R., and Beliles, R. P. (1997). Physiological parameter values for physiologically based pharmacokinetic models. *Toxicol Ind Health* **13**, 407-84.

Cubitt, H. E., Houston, J. B., and Galetin, A. (2011). Prediction of human drug clearance by multiple metabolic pathways: integration of hepatic and intestinal microsomal and cytosolic data. *Drug Metab Dispos* **39**, 864-73.

DeJongh, J., Verhaar, H. J. M., and Hermens, J. L. M. (1997). A quantitative property-property relationship (QPPR) approach to estimate in vitro tissue-blood partition coeffcients of organic chemicals in rats and humans. *Arch Toxicol*, 72: 17-25.

Islam, M. A., Punt, A., Spenkelink, B., Murk, A. J., Rolaf van Leeuwen, F. X., and Rietjens, I. M. (2014). Conversion of major soy isoflavone glucosides and aglycones in in vitro intestinal models. *Mol Nutr Food Res* **58**, 503-15.

Kimura, T., and Higaki, K. (2002). Gastrointestinal transit and drug absorption. *Biological and Pharmaceutical Bulletin* **25**, 149-164.

Punt, A., Freidig, A. P., Delatour, T., Scholz, G., Boersma, M. G., Schilter, B., van Bladeren, P. J., and Rietjens, I. M. (2008). A physiologically based biokinetic (PBBK) model for estragole bioactivation and detoxification in rat. *Toxicol Appl Pharmacol* **231**, 248-59.

Steensma, A., Noteborn, H. P., and Kuiper, H. A. (2004). Comparison of Caco-2, IEC-18 and HCEC cell lines as a model for intestinal absorption of genistein, daidzein and their glycosides. *Environ Toxicol Pharmacol* **16**, 131-9.

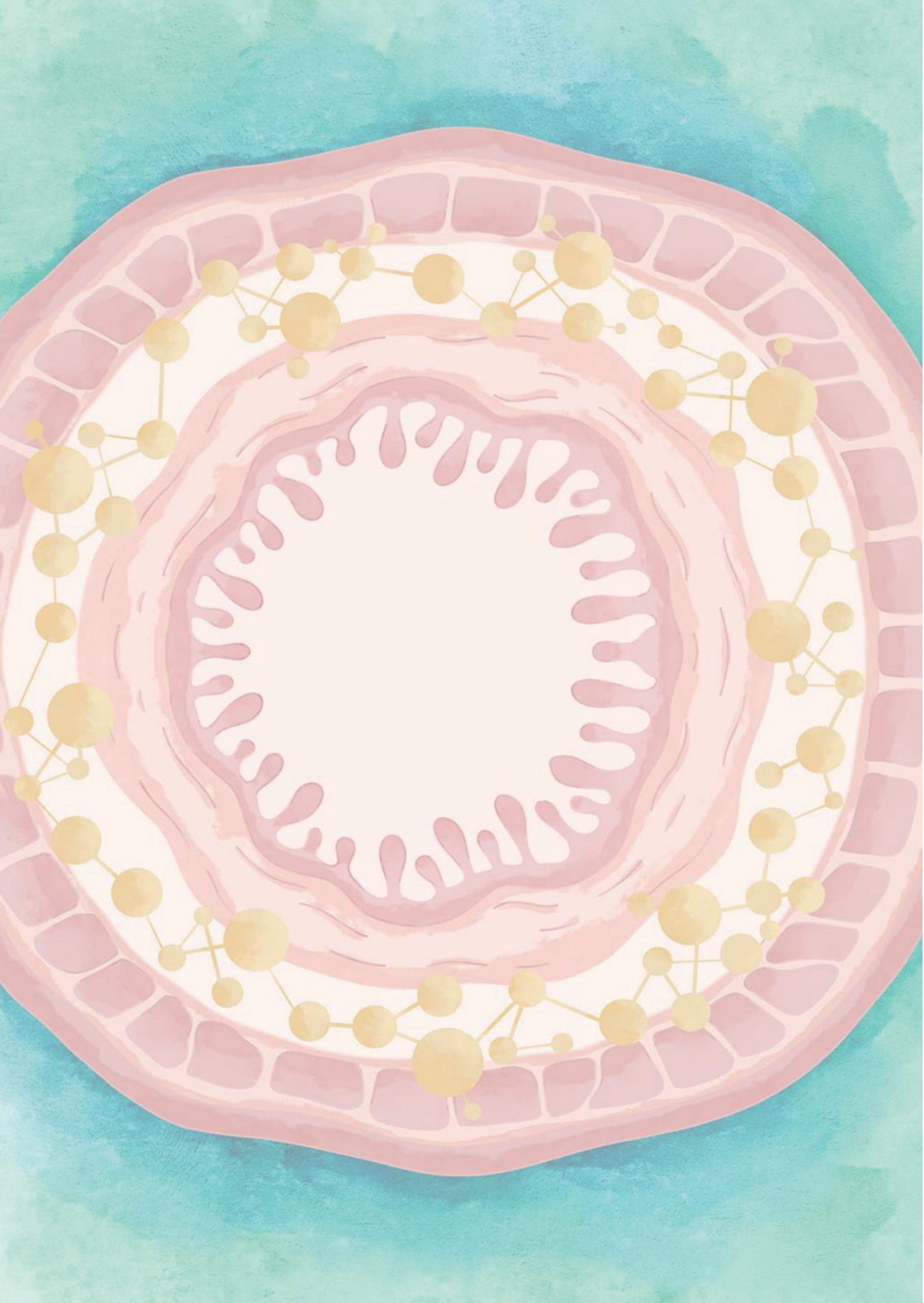

Chapter 4

Physiologically based kinetic (PBK) model-based prediction of intestinal microbial and host metabolism of zearalenone and consequences for its estrogenicity

Diana M. Mendez-Catala, Qianrui Wang and Ivonne M.C.M. Rietjens

Published in Molecular Nutrition & Food Research. 2021; 65(23), 2100443

Abstract

The aim of the present study was to develop physiologically based kinetic (PBK) models for rat and human that include intestinal microbial and hepatic metabolism of zearalenone (ZEN) in order to predict systemic concentrations of ZEN and to obtain insight in the contribution of metabolism by the intestinal microbiota to the overall metabolism of ZEN.

In vitro derived kinetic parameters, maximum velocities (V_{max}) and Michaelis-Menten constants (K_m), for liver and intestinal microbial metabolism of ZEN were included in the PBK models. The models include a sub-model for the metabolite, α-zearalenol (α-ZEL), a metabolite known to be 60-times more potent as an estrogen than ZEN. Integrating intestinal microbial ZEN metabolism into the PBK models revealed that hepatic metabolism drives the formation of α-ZEL. Furthermore, the models predicted that at the tolerable daily intake (TDI) of 0.25 μg/kg bw the internal concentration of ZEN and α-ZEL are 3-orders of magnitude below concentrations reported to induce estrogenicity in in vitro bioassays.

It is concluded that combining kinetic data on liver and intestinal microbial metabolism in a PBK model facilitates a holistic view on the role of the intestinal microbiota in the overall metabolism of the foodborne xenobiotic ZEN and its bioactivation to α-ZEL.

1. Introduction

Zearalenone (ZEN) is a nonsteroidal mycotoxin that is formed by *Fusarium spp*., primarily F. *graminearum*. The fungus is known to infect mainly crops of wheat and maize, and while in the field usually the concentrations of ZEN are still low, they show a tendency to increase under storage conditions with high moisture content (Gupta et al., 2018). In the European Union (EU), the presence of ZEN in food commodities is regulated with maximum permitted levels ranging from 20 to 400 µg/kg for cereals and cereal products (Borzekowski et al., 2018; EFSA, 2011).

The adverse health effects of ZEN have been related to its estrogenicity, originating from its structural similarity to the natural hormone 17β-estradiol (E2) and proceed through binding of ZEN to the estrogen receptors (ERs) (Metzler et al., 2010). Also, ZEN metabolites may play a role in this estrogenicity. ZEN is known to undergo reduction to form the metabolites α-zearalenol (α-ZEL) and β-zearalenol (β-ZEL) (Fitzpatrick et al., 1988), with α-ZEL showing a relative potency that is about 60-fold higher than that of ZEN reflecting bioactivation, while the formation of β-ZEL decreases the potency 5 times representing a detoxification (EFSA, 2016). ZEN as well as α-ZEL and β-ZEL can be further metabolized to glucuronide conjugates, before they are eliminated through urine and/or feces (Fitzpatrick et al., 1988; Mirocha et al., 1981b; Warth et al., 2013). ZEN and its metabolites are conjugated at a lower extent to sulfate conjugates as observed in vitro (Pfeiffer et al., 2010), but this not confirmed in vivo (Warth et al., 2013). This metabolism of ZEN may occur in the liver and intestinal tissue, while anaerobic in vitro fecal incubations have shown the intestinal microbiota to also play a role in the conversion of ZEN to α- and β-ZEL (Gratz et al., 2017; Mendez-Catala et al., 2020). In vitro studies with liver S9 fractions (Malekinejad et al., 2006a) and fecal slurries (Mendez-Catala et al., 2020) have shown interspecies differences in bioactivation and detoxification by both the liver and intestinal microbiota. Due to limited data available on the kinetics and toxicity of ZEN in humans, the risk assessment has been based on the observations in young gilts identified as the most sensitive species (Dänicke et al., 2005; Döll et al., 2003; EFSA, 2011). Based on a no observed effect level (NOEL) of 10.4 µg/kg bw for estrogenic effects of ZEN in young gilts (Döll et al., 2003) a tolerable daily intake (TDI) of 0.25 µg/kg bw/day was defined taking an uncertainty factor of only 40 to account for interspecies differences and human variability (EFSA, 2011).

Given the limited data on the role of the intestinal microbiota in the in vivo bioactivation and detoxification of ZEN, the aim of the present study was to develop a physiologically based kinetic (PBK) model in human that would enable an integrated description of the metabolism of ZEN, and provide insight in the overall role of the intestinal microbiota in the bioactivation and detoxification of ZEN in vivo. This model requires description of a separate compartment in the PBK model for intestinal microbial metabolism describing the formation of α- and β-ZEL by the microbiota. To enable evaluation of the model also a PBK model for rats was developed to allow comparison of model predictions to in vivo kinetic data, which for this species are available in literature (Shin et al., 2009). The PBK models obtained allowed evaluation of the role of metabolism of ZEN by the intestinal microbiota in the overall metabolism of ZEN and comparison of dose-dependent internal concentrations with in vitro concentrations for ZEN and α-ZEL able to induce estrogenicity.

2. Materials and methods

2.1 Materials

ZEN, α-ZEL and β-ZEL were purchased from Sigma-Aldrich (Schnelldorf, Germany). Test chemicals were prepared in dimethyl sulfoxide purchased from Merck (Darmstadt, Germany). Pooled rat and human liver S9 fractions were purchased from Corning (Woburn, MA, USA) and pooled rat and human intestinal S9 fractions were purchased from Xenotech (Kansas City, USA). Uridine 5-diphosphoglucuronide trisodium salt (UDPGA) was obtained from Carbosynth (Berkshire, United Kingdom). Trizma® base (Tris) and alamethicin were obtained from Sigma-Aldrich (Steinheim, Germany). Magnesium chloride hexahydrate ($MgCl_2 \cdot 6H_2O$) and formic acid (FA) were obtained from VWR International (Amsterdam, The Netherlands). Phosphate-buffered saline (PBS, pH 7.4), was obtained from Gibco (Paisley, UK). Methanol (MeOH) and acetonitrile (ACNwere purchased from Biosolve (Valkenswaard, The Netherlands).

2.2 In vitro incubations with ZEN and α-ZEL to derive kinetic parameters for the PBK model

The kinetic parameters (V_{max} and K_m) for the glucuronidation of ZEN and α-ZEL in liver tissue were obtained from in vitro incubations of ZEN and α-ZEL with rat and human liver S9 fractions. The incubation mixtures (final volume 100 µl) contained (final concentrations) 0.1 M Tris-HCl (pH 7.4), 5 mM $MgCl_2$, 0.025 mg/ml alamethicin, the substrate in concentrations

ranging from 0.3-150 µM (added from 100 times concentrated stock solutions in DMSO) and 0.2 mg/ml of pooled liver S9 fraction from rat or human. After 1 min preincubation in a shaking water bath at 37°C, the reaction was started by the addition of 3 mM (final concentration) UDPGA. Control incubations were performed without the addition of UDPGA. The incubations were carried out for 7 min. Intestinal S9 incubations for the glucuronidation of ZEN were performed in a similar way with only a few modifications. Final incubation mixtures contained 0.01 mg/ml alamethicin and 0.04 mg/ml intestinal S9 fractions. The incubations were carried out for 20 min. Under all these conditions the conversion was linear with time and S9 protein concentration (data not shown). All reactions were terminated by the addition of 20% (v/v) ice-cold ACN followed by centrifugation at 15,000 x g for 5 min and the supernatant was immediately analyzed by UPLC. The formation of glucuronides was confirmed by the incubation of non-terminated samples with β-glucuronidase.

2.3 UPLC analysis

An ultra-performance liquid chromatography (UPLC) system (Waters Acquity) was used for the quantification of ZEN, α-ZEL and their glucuronides. The UPLC system was equipped with an Acquity BEH C18 column 1.7 µm, 50 mm x 2.1 mm (Waters) set at 40 ºC and a UV diode array detection system recording wavelengths of 190-400 nm. Nanopure water (A) and ACN (B) were used as eluens at a flow rate of 0.3 ml/min with the following gradient profile: 0-40% B in 0 –1.3 min, 40-50% B in 1.3 - 5.7 min, 50-100% B in 5.7 - 6 min, 100 % B kept for 2 min and 100-0% B in 8 - 8.1 min for equilibration. Per run, 3.5 µl of sample were injected. ZEN, α-ZEL and β-ZEL were identified using commercially available standards. Chromatograms were analyzed at 235 nm and glucuronides quantified using calibration curves of the respective commercially available non-conjugated analogues. The glucuronides were identified by their conversion to the corresponding non-conjugated analogues upon incubation with β-glucuronidase.

2.4 Kinetic analysis

To derive the kinetic constants for the formation of ZEN-glucuronide and α-ZEL-glucuronide, the amount of metabolite formed expressed per mg of protein and per unit of time (rate of formation) was calculated and plotted against the substrate concentration. The curve for the concentration dependent metabolite formation was fitted in GraphPad Prism 5.04 (GraphPad software, San Diego California, U.S.A.) using a standard Michaelis-Menten equation

($V=V_{max}*[S]/(K_m+[S])$) to obtain the in vitro kinetic constants, V_{max} in pmol/min/mg S9 protein and K_m in μM.

2.5 Development of PBK models for rat and human

A schematic representation of the PBK model of ZEN, including a sub-model for α-ZEL, for rat and human is presented in **Figure 1**. The model is based on a model previously reported and evaluated by Wang et al. (2020) for the isoflavone daidzein. The PBK model describes the kinetics upon intravenous (i.v.) injection or oral exposure. The i.v. administration was included to allow comparison of the model predictions to available in vivo kinetic data in rats (Shin et al., 2009). The main model for the parent compound ZEN consisted of separate compartments for blood, fat, rapidly perfused tissue (heart, lung and brain), slowly perfused tissue (skin, muscle and bone), liver, intestine and stomach. The intestinal compartment consisted of three separate compartments including the small intestinal lumen, small intestinal tissue and the large intestinal lumen in order to enable description of both metabolism in small intestinal tissue and by the intestinal microbiota. The elimination of ZEN was modeled via its glucuronidation in intestinal and liver tissue assumed to be followed by efficient excretion.

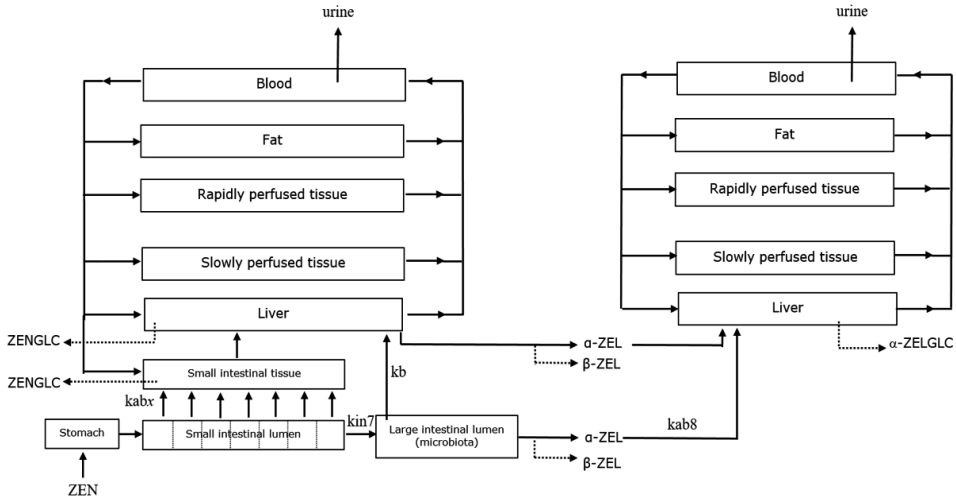

Figure 1. Schematic presentation of the main PBK model for ZEN including a sub-model for the bioactive metabolite α-ZEL.

In order to predict the blood concentrations of α-ZEL, a sub-model for α-ZEL was included. In this sub-model α-ZEL is formed in the liver from ZEN and also enters the liver upon its

formation by the intestinal microbiota. Glucuronidation of α-ZEL formed by the microbiota was assumed to occur in the liver following its transport from the large intestinal lumen to the liver.

The parameters required for the PBK model of ZEN are 1) physiological parameters, 2) physicochemical parameters and 3) kinetic parameters for metabolism and excretion. The values for the physiological parameters (e.g. tissue volumes and blood flows) were taken from literature (Brown et al., 1997) and are presented in **Table 1**. The physicochemical parameters (e.g.. tissue/blood partition coefficients) are presented in **Table 2** and were estimated as previously described (DeJongh et al., 1997) based on the octanol-water partition coefficients (Log P) of 3.32 and 3.16 for ZEN and α-ZEL, respectively, obtained from ChemDraw version 18 (Perkin Elmer & CambridgeSoft, USA).

Table 1. Physiological parameters used in the rat and human PBK model for ZEN based on Brown et al. (1997).

	Symbol	**Values**	
		Rat	**Human**
Physiological parameters			
Body weight (kg)	BW	0.25	70
Tissue volumes (fraction of body weight)			
Small intestine	VSIc	0.014	0.009
Liver	VLc	0.034	0.026
Rapidly perfused tissue	VRc	0.034	0.041
Slowly perfused tissue	VSc	0.667	0.596
Fat	VFc	0.07	0.214
Blood	VBc	0.074	0.074
Cardiac output (L/h)	Qc	5.38	347.9
Blood flow to tissue (fraction cardiac output)			
Intestine	QSIc	0.151	0.181
Liver	QLc	0.099	0.046
Rapidly perfused tissue	QRc	0.51	0.473
Slowly perfused tissue	QSc	0.17	0.248
Fat	QFc	0.07	0.052

Table 2. Physicochemical parameters used in the rat and human PBK model. Tissue: blood partition coefficients of ZEN and α-ZEL were calculated based on the method by DeJongh et al. (1997).

	Rat		**Human**	
	ZEN	**α-ZEL**	**ZEN**	**α-ZEL**
Intestine	2.64	2.38	6.56	6.11
Liver	2.64	2.38	6.56	6.11
Rapidly perfused tissues	2.64	2.38	6.56	6.11
Slowly perfused tissues	0.76	0.71	4.25	3.99
Fat	106.93	92.79	134.86	131.61

The apparent permeability coefficients (Papp) obtained from in vitro transport studies using Caco-2 cell layers were used to describe the intestinal absorption of ZEN and α-ZEL from the different sub-compartments in the model into the small intestinal tissue or from the large intestinal lumen directly to the liver. The $Papp_{,Caco\text{-}2}$ value reported for ZEN was 10.3×10^{-6} (Pfeiffer et al., 2011). The $Papp_{,Caco\text{-}2}$ value for ZEN was one of the most influential factors for the prediction of ZEN in blood (see result section), therefore this values was also optimized by curve fitting to the in vivo data from Shin et al. (2009) using the curve fit option present in Berkeley Madonna, yielding a value of 10.4×10^{-5} cm/s ($Papp_{,\ Caco\text{-}2\ fitted}$). The latter value was used for predictions and evaluation. Subsequently, in vivo Papp values ($Papp_{,\ in\ vivo}$) were estimated by the following correlation established by Sun et al. (2002): Log ($Papp_{,\ in\ vivo}$) = 0.6836 × Log ($Papp_{,\ Caco\text{-}2\ fitted}$) − 0.5579. It was assumed that the estimated $Papp_{,\ in\ vivo}$ was the same for both rats and humans. The parameter values for the intestinal absorption rates were derived from the $Papp_{,\ in\ vivo}$ by using the following equation (Gilbert-Sandoval et al., 2020; Li et al., 2017; Louisse et al., 2015; Verwei et al., 2006; Zhang et al., 2018): Absorption rate (μmol/h) = apparent permeability coefficient in vivo ($Papp_{,\ in\ vivo}$; cm/h) × surface area of the small intestine (cm^2) × luminal concentration of the compound (mM). The surface areas of the rat small and large intestine were calculated to be 94 [based on radius of 0.18 cm and small intestinal length of 83 cm (Tsutsumi et al., 2008)] and 157 cm^2 [based on radius of 1 cm and small intestinal length of 25 cm (Vdoviaková et al., 2016)]. For human the surface areas for small and large intestine were calculated to be 72 [based on radius of 2.5 cm (Kararli, 1995) and small intestine length of 460 cm (Hosseinpour and Behdad, 2008)] and 47 dm^2 [based on radius of 5 cm and large intestine length of 150 cm (Vdoviaková et al., 2016)]. The

luminal concentration of ZEN in the small intestine was calculated by dividing the amount of ZEN in the tissue by the small intestinal volume. The calculated volumes for rat and human small intestine were 8.4 mL (Tsutsumi et al., 2008) and 9 L (Hosseinpour and Behdad, 2008; Kararli, 1995), respectively, based on radius and small intestinal length. The transport of α-ZEL formed by intestinal microbiota was modeled to go directly from the large intestine to liver with the absorption calculated from $Papp_{caco-2}$ value of 5.4×10^{-6} cm/s, this value was kept as reported in literature (Pfeiffer et al., 2011), as no kinetic data for fitting is available for α-ZEL.

The kinetic constants (V_{max} and K_m) for the conversion of ZEN to α-ZEL and β-ZEL by the intestinal microbiota were obtained from anaerobic incubations with fecal samples performed as previously described (Mendez-Catala et al., 2020). The V_{max}, expressed in pmol/min/g feces, was scaled to the whole body by means of the fecal fraction of body weight of 0.0164 [based on a defecation volume per day of 4.1 g (Hoskins and Zamcheck, 1968)] for rats and 0.0018 for humans [based on a defecation volume per day of 128 g (Rose et al., 2015)]. The V_{max} values for the formation of α-ZEL and β-ZEL and the subsequent glucuronidation of α-ZEL, obtained from incubations with rat liver S9 (Malekinejad et al., 2006b) or human liver S9 (Mendez-Catala et al., 2020), were scaled to the whole tissue assuming an S9 protein concentration of 143 mg S9 protein/g liver for rats (Punt et al., 2008) and 120.7 mg protein/g liver (sum of 40 mg microsomal protein and 80.7 mg of cytosolic protein) for human (Cubitt et al., 2011). The intestinal V_{max} for glucuronidation of ZEN was scaled to whole tissue using an S9 protein yield of 37.1 and 35.2 mg S9 protein/g intestinal tissue for rat and human, respectively (Peters et al., 2016). The K_m values in vivo were assumed to be similar to those obtained in vitro.

Due to the absence of studies reporting dose related blood levels of ZEN in humans and because excretion through urine is presented as an adequate biomarker for ZEN biomonitoring (Lorenz et al., 2019), the urinary excretion of ZEN and α-ZEL were modeled to occur from the blood with excretion rates of 0.096 and 0.015/h, respectively, estimated before in Mukherjee et al. (2014). Additionally, the excretion of the ZEN glucuronide in humans was modeled taking under the assumption that with 90% of the glucuronides formed in the liver will be excreted through the urine (Teeguarden et al., 2005; Yang et al., 2013).

The PBK model equations were coded and integrated in Berkeley Madonna 8.0.1 (UC Berkeley, CA, USA) using the Rosenbrock's algorithm for stiff systems. The model code for rat and human are presented in **Supplementary material**.

2.6 PBK model evaluation

The performance of the model developed for rats was evaluated by comparison of 1) the predicted blood concentration time profile of ZEN to the time dependent blood concentrations reported in literature upon single i.v. doses of 1, 2, 4 and 8 mg/kg bw (Shin et al., 2009), and 2) the predicted maximum blood concentration (C_{max}) of ZEN to the C_{max} obtained in a rat study following a single oral dose of 8 mg/kg bw (Shin et al., 2009). The study from Mallis et al. (2003) was considered unsuitable for the evaluation due to differences in the experimental design, where ZEN was co-administered with 4 other isoflavones. As the PBK model developed predicts ZEN blood concentrations, the plasma concentrations of ZEN from in vivo studies in rats were converted to blood concentrations assuming that blood concentrations are 0.6 times the plasma concentration in rats (Probst et al., 2006; Walker et al., 1990; Yang et al., 2007).

As data on dose-dependent blood levels upon exposure to ZEN in humans suitable for model evaluation were not available, the evaluation of the human PBK model was done by comparison to the cumulative urinary concentration of ZEN and ZEN-glucuronide (total ZEN) reported by Mirocha et al. (1981a) and Warth et al. (2013) at oral doses of 1.43 mg/kg bw and 0.2 µg/kg bw, respectively.

To further evaluate the PBK models a sensitivity analysis was performed to identify the parameters having the largest impact on the model predictions. The sensitivity coefficients (SC) were determined following the equation (Evans and Andersen, 2000):

$$\mathrm{SC} = (\mathrm{C}' - \mathrm{C})/(\mathrm{P}' - \mathrm{P}) \times \mathrm{P}/\mathrm{C}$$

where C is the initial value of the model output (C_{max} of ZEN), C' the modified value of the model output resulting from a 5% increase in the parameter value, P is the initial parameter value and P' is the parameter value with a 5% increase. Each parameter change was analyzed individually, while others were kept at the initial values. The analysis was conducted with an oral dose of 8 mg/kg bw for rats and oral doses of 1.43 mg/kg bw and 0.2 µg/kg bw for human representing the dose levels from available in vivo studies used for model evaluation

(Mirocha et al., 1981a; Warth et al., 2013). Larger SC values represent a higher impact of the parameter on the predictions for the C_{max} of ZEN and α-ZEL.

3. Results

3.1 In vitro kinetic data for rats and humans

The in vitro kinetics for the formation of α-ZEL and β-ZEL in rat and human liver were obtained from literature (Malekinejad et al., 2006b; Mendez-Catala et al., 2020) and are presented in **Table 3** together with the scaled V_{max}, K_m and catalytic efficiency values for the formation of α-ZEL and β-ZEL. A substantial interspecies difference is observed in the catalytic efficiency for formation of α-ZEL and β-ZEL by rat and human liver. A comparison of the catalytic efficiency values shows humans to have a 563- and 2-fold higher catalytic efficiency for conversion of ZEN to respectively α-ZEL and β-ZEL than rat.

Table 3. In vitro and scaled in vivo kinetic parameters for the conversion of ZEN to α-ZEL and β-ZEL in rat and human liver, as derived from literature data using in vitro incubations of ZEN with rat and human liver S9 fractions.

Species Metabolite	V_{max}, in vitro (pmol/min/mg S9 protein)	K_m (μM)	Catalytic efficiency, in vitro (μl/min/mg S9 protein)	Scaled V_{max}, in vivo (μmol/h/kg bw)[a]	Scaled catalytic efficiency, in vivo (L/h/kg bw)
Rat [b]					
α-ZEL	32	592	0.05	9.34	0.02
β-ZEL	72	21	3.43	21	1.00
Human [c]					
α-ZEL	358.7	9	38.7	80.02	8.89
β-ZEL	209.3	23	9.02	46.7	2.03

[a] Calculated from [(V_{max}, in vitro) x (mg S9 protein/g liver) x (g liver) x (60 min/h)]/ (10^6 μmol/pmol)/ kg bw. For rat and human the mg S9 protein/g liver were 143 and 120.7, respectively.

[b] (Malekinejad et al., 2006a)

[c] (Mendez-Catala et al., 2020)

The kinetics for the formation of α-ZEL and β-ZEL from ZEN by the intestinal microbiota, obtained from anaerobic in vitro incubations of ZEN with pooled rat and human feces, were also obtained from literature (Mendez-Catala et al., 2020) and are presented in **Table 4** along with the scaled V_{max} and catalytic efficiency values for the formation of the metabolites based on the 24 h defecation volumes of 4.1 and 128 g for rats and humans, respectively. A comparison of the scaled catalytic efficiency values for formation of α-ZEL and β-ZEL by the intestinal microbiota shows that the values for rats are 4- and 14-fold higher than those obtained for humans. The ratio of α-ZEL/β-ZEL was shown to be higher in humans (e.g. 6/1) than in rats (e.g 2/1). Overall, humans showed a higher preference for the bioactivation of ZEN to α-ZEL in both liver and intestinal microbial metabolism.

Table 4. In vitro and scaled in vivo kinetic parameter for the conversion of ZEN to α-ZEL and β-ZEL by the intestinal microbiota as derived from anaerobic in vitro incubations of ZEN with rat and human fecal slurries (Mendez-Catala et al., 2020).

Species Metabolite	V_{max}, in vitro (pmol/min/mg feces)	K_m (µM)	Catalytic efficiency, in vitro (µl/min/mg feces) [a]	Scaled V_{max}, in vivo (µmol/h/kg bw)[b]	Scaled catalytic efficiency, in vivo (ml/h/kg bw)
Rat					
α-ZEL	0.23	66	3.5	0.23	2.60
β-ZEL	0.14	80	1.8	0.10	1.30
Human					
α-ZEL	0.90	135	6.6	0.10	0.73
β-ZEL	0.18	163	1.1	0.02	0.12

[a] (10^{-3}) µl/min/mg feces

[b] Calculated from [(V_{max}, in vitro) x (defecation volume in mg) x (60 min/h)]/ (10^6 µmol/pmol)/ (kg bw). Rat and human defecation volumes were 4.1 and 128 g, respectively

The extent of glucuronidation of ZEN and α-ZEL by rat and humans was quantified by UPLC analysis of formation of the respective glucuronides upon incubation of ZEN with liver (**Figure 2**) and intestinal (**Figure 3**) S9 fractions and of α-ZEL with liver S9 fractions (**Figure 2**). The results obtained show that the concentration dependent rate of glucuronidation followed Michaelis-Menten kinetics. The in vitro V_{max} and K_m values and the catalytic

efficiencies (catalytic efficiency calculated as V_{max}/K_m) for the glucuronidation of ZEN and α-ZEL derived from these data, as well as the scaled V_{max} and catalytic efficiency values are presented in **Table 5**. The in vivo catalytic efficiency for glucuronidation of ZEN by S9 liver fractions showed to be comparable for rats and humans. Larger interspecies differences were observed for the glucuronidation of ZEN by S9 intestinal tissue samples, with the in vivo catalytic efficiency for rats being 2.7-fold higher than for human.

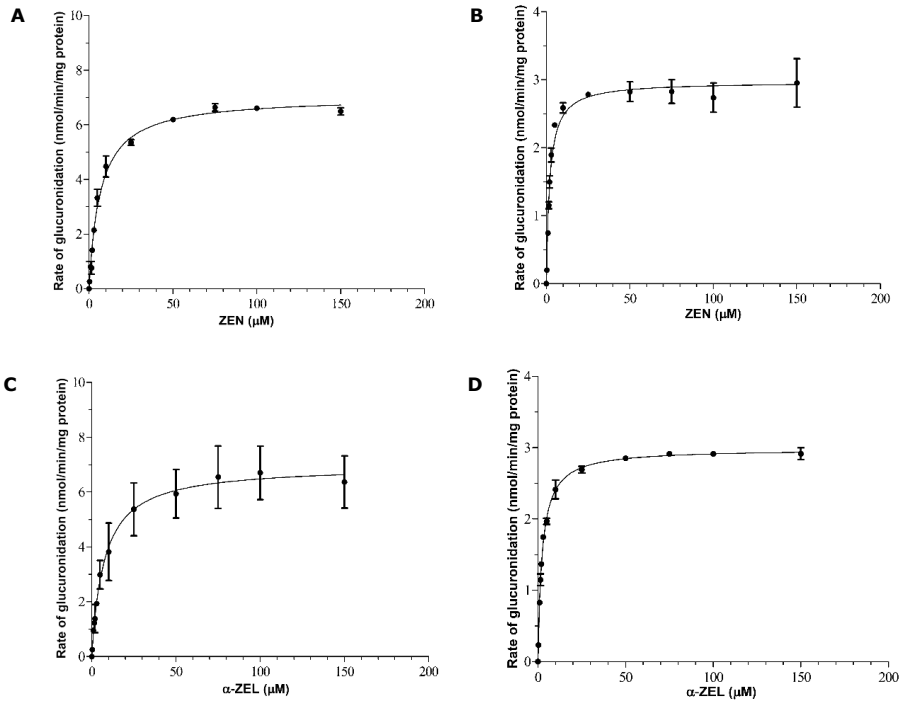

Figure 2. Concentration dependent formation of (A-B) ZEN glucuronide and (C-D) α-ZEL glucuronide in incubations with rat and human liver S9.

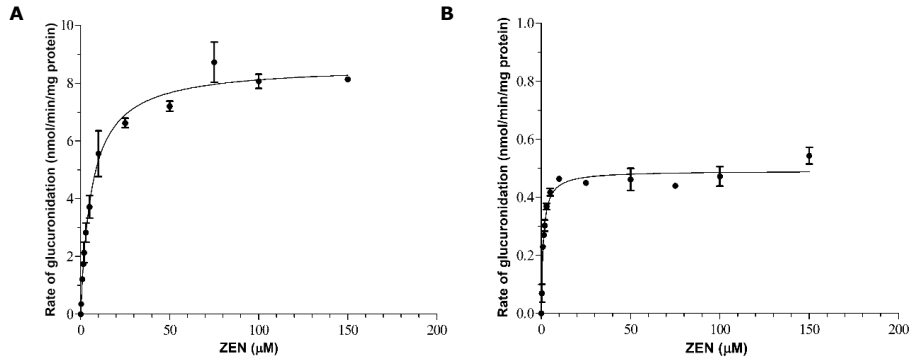

Figure 3. Concentration dependent formation of ZEN glucuronide in incubations with A) rat and B) human intestinal S9.

Table 5. In vitro and scaled in vivo kinetic parameters for the glucuronidation of ZEN and α-ZEL in incubations with rat or human liver S9 obtained from in vitro incubations of ZEN or α-ZEL with rat and human liver S9 fractions and UDPGA.

Compound Organ	V_{max}, in vitro (nmol/min/mg of protein)	K_m (µM)	Catalytic efficiency, in vitro (ml/min/mg protein)	Scaled V_{max}, in vivo (µmol/h/kg bw)[a]	Scaled catalytic efficiency, in vivo (L/h/kg bw)
Rat					
ZEN					
Liver	7.03	6.75	1.04	2050.50	303.64
Intestine	8.62	6.19	1.39	268.54	43.44
α-ZEL					
Liver	6.96	7.43	0.94	2031.25	273.53
Human					
ZEN					
Liver	2.97	2.04	1.45	559.23	273.73
Intestine	0.49	1.17	0.42	18.67	15.90
α-ZEL					
Liver	2.98	2.42	1.24	561.68	232.58

[a] Calculated from [(V_{max}, in vitro) x (mg S9/g liver) x (60 min/h)]/ (10^3 μmol/nmol)/ kg bw.

3.2 PBK model development and evaluation

The kinetic constants for the conversion of ZEN to α-ZEL and β-ZEL and for glucuronidation of ZEN and α-ZEL were integrated into the PBK models for rat and human. First, the performance of the model was evaluated based on the comparison of the concentration-time curves of ZEN predicted by the rat PBK model with available in vivo kinetic data upon i.v. administration of ZEN at various dose levels to rats (Shin et al., 2009) as shown in **Figure 4**. These results indicate that the model predicts the time dependent blood concentrations and clearance of ZEN well. In a next step literature data from an in vivo rat study with oral dosing were used for evaluation of the model. In **Figure 5** the C_{max} of unconjugated ZEN predicted upon oral dosing was compared to the C_{max} reported by Shin et al. (2009) upon oral dosing of rats with 8 mg/kg bw ZEN, with resulting values of 6.08 and 8.14 nM, respectively, showing an only 1.3-fold difference.

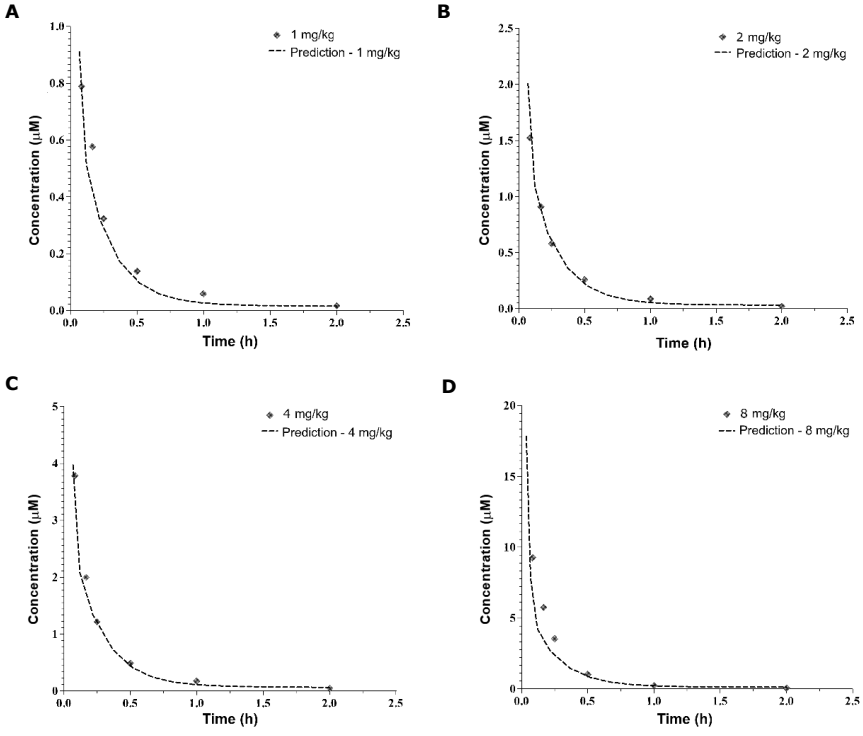

Figure 4. Comparison of predicted and reported (Shin et al., 2009) time dependent blood concentrations of ZEN in rats upon i.v. administration of doses of A) 1 mg/kg bw, B) 2 mg/kg bw, C) 4 mg/kg bw and D) 8 mg/kg bw.

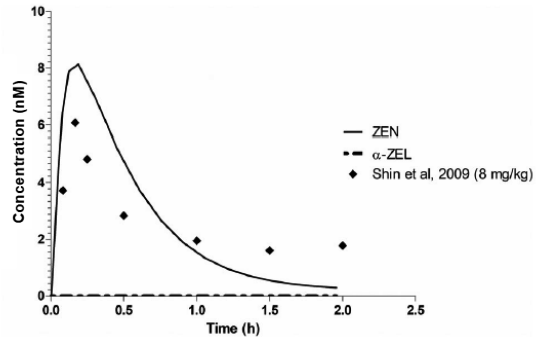

Figure 5. PBK model predicted time dependent blood concentration of ZEN and α-ZEL in rat upon an oral dose of 8 mg/kg bw.

It was also evaluated to what extent inclusion of the α-ZEL sub-model affected the prediction for the C_{max} of ZEN. The C_{max} of ZEN appeared to be minimally affected by the inclusion of its intestinal microbial metabolism to α-ZEL into the model, and the concentration of α-ZEL in blood was predicted to amount to less than 0.1% of the concentration of ZEN when ZEN is dosed at 8 mg/kg bw (**Figure 5**).

The predictions made by the human PBK model were evaluated based on urinary levels of ZEN and its metabolites reported in human studies (Mirocha et al., 1981a; Warth et al., 2013). The cumulative 24 hours urinary excretion data reported for humans by Mirocha et al. (1981a) and Warth et al. (2013) after an oral dose of ZEN were compared to the human PBK model predicted values in **Table 6**. The reported in vivo cumulative urinary concentrations were calculated based on a mean urinary volume for human of 2.42 L (Warth et al., 2013) to allow comparison with the PBK model based predicted amount of urinary excretion of ZEN metabolites.

Table 6. In vivo and predicted cumulative urinary excretion of total ZEN in humans 24 hours after oral dosing of ZEN.

Dose (mg)	In vivo urine amount (mg)[a]	Predicted urine amount (mg)	Predicted / in vivo	Reference

100	32.1	18.1	0.56	(Mirocha et al., 1981b)
0.01	0.73×10^{-3}	1.58×10^{-3}	2.08	(Warth et al., 2013)

[a] based on an average urine volume of 2.42 L per day (Warth et al., 2013)

The evaluation of the human model by comparison of the cumulative urinary amount (Table 6) resulted in an excretion of 15.1- 18.1% of the total oral dose, in line with the reported 7.2 - 32.1% of the dose recovered in urine. The comparison of the predicted excretion in urine with the reported data reveals that the model predicts the reported data reasonably well especially for the study of Mirocha et al. (1981a). The prediction of C_{max} of ZEN and α-ZEL showed the concentration of α-ZEL in blood to amount to about 3% of the concentration of ZEN when ZEN is dosed at 0.143 and 1.43 µg/kg bw (**Supplementary material Figure S1**). Finally, the contribution of intestinal microbiota to metabolism revealed that the formation of α-ZEL from ZEN was driven by hepatic metabolism (**Supplementary material Figure S2**)

The performance of the models was further evaluated through a sensitivity analysis to assess the parameters affecting the prediction of the concentration of ZEN in blood to the largest extent. **Figure 6** presents the results obtained. The sensitivity analysis was performed at an oral dose levels of 8 mg/kg bw in rats and 0.143 µg/kg bw and 1.43 mg/kg bw for humans, representing the dose levels used in the in vivo studies used for model evaluation (Mirocha et al., 1981a; Shin et al., 2009; Warth et al., 2013). Only the parameters resulting in a normalized sensitivity coefficient higher that 0.1 (absolute value) are shown in **Figure 6**. In all scenarios, the C_{max} values for ZEN were greatly affected by the kinetic parameters for glucuronidation of ZEN in the small intestine and liver tissue. Other parameters found to impact the C_{max} predictions for ZEN included physiological parameters such as body weight, tissue volume and blood flows, especially those of the small intestine and the liver. The parameters describing the absorption from the small intestinal lumen to the small intestinal tissue (Papp Caco-2, Vin, Ain) also appeared to have a substantial effect on the C_{max} prediction.

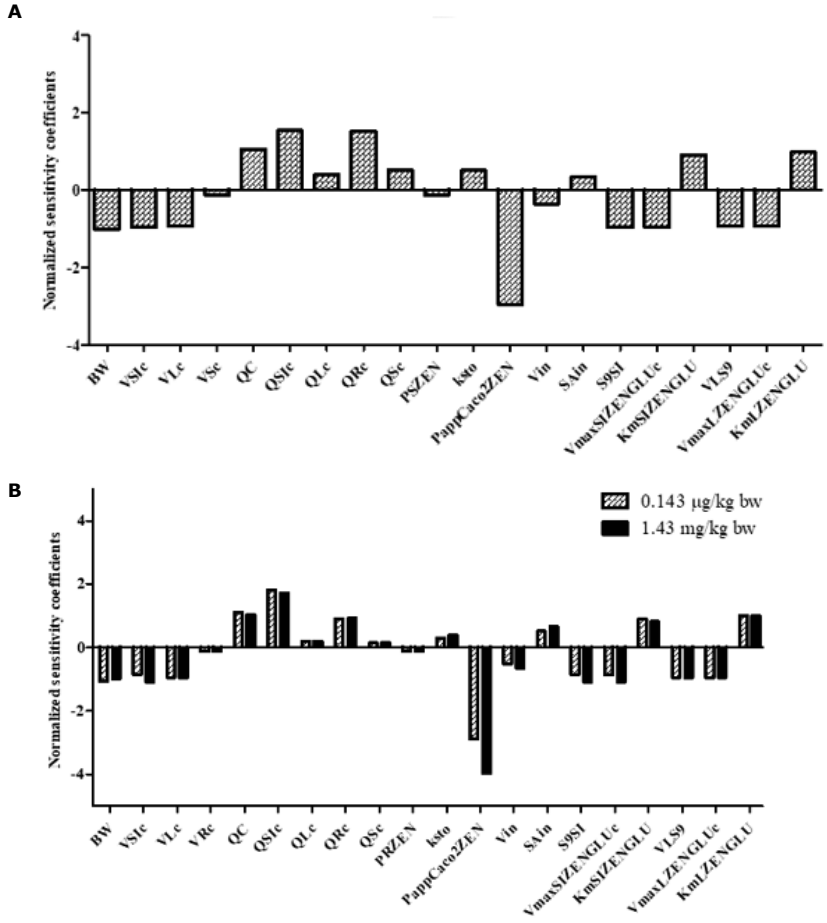

Figure 6. Sensitivity coefficients of the PBK model parameters for the predicted C_{max} of ZEN in A) rat at an oral dose of 8 mg/kg bw, and B) human at oral doses of 0.143 µg/kg bw and 1.43 mg/kg bw. The parameters stand for: BW = body weight, VTic = fraction of tissue volume (Ti = SI (small intestine), L (liver), R (rapidly perfused), S (slowly perfused)), Qc = cardiac output, QTic = fraction of blood flow to tissue (Ti = SI (small intestine), L (liver), R (rapidly perfused)), PRZEN = rapidly perfused tissue/blood partition coefficient, ksto = stomach emptying rate, PappCaco2ZEN = Papp valued derived from Caco-2 transport studies, Vin = volume for small intestinal sub-compartment, SAin = surface area for small intestinal subcompartment, S9SI = small intestinal S9 protein yield, VLS9 = liver S9 protein yield, V_{max} and K_m = maximum rate of formation and the Michaelis-Menten kinetic constant for the formation of ZEN glucuronide (ZENGLU) in SI (small intestine) and L (liver).

3.3 Comparison of EC_{10} values for estrogenicity with predicted C_{max} values derived from dietary exposure of an adult population

To obtain further insight in the potential of the PBK models, they were applied to evaluate whether at dose levels equal to the TDI of 0.25 µg/kg bw or equal to estimated dietary intakes of ZEN (2.4-29 ng/kg bw) (EFSA, 2011), the C_{max} values of ZEN and α-ZEL would reach levels that induce estrogenic responses. To this end predicted C_{max} values were compared to data from the ZEN or α-ZEL concentration-dependent responses in a selection of different in vitro model systems for estrogenicity. The predicted concentrations were corrected for the unbound fractions calculated to be 0.089 and 0.103 for ZEN and α-ZEL, respectively (WFSR, 2020). **Figure 7** reflects that different bioassays for estrogenicity result in somewhat different potencies for ZEN and α-ZEL. Nevertheless, the results presented in **Figure 7** also reveal that the C_{max} for both α-ZEL and ZEN predicted by the PBK models, both at levels of normal dietary intake and at the TDI are predicted to be below the EC_{10} values of all bioassays.

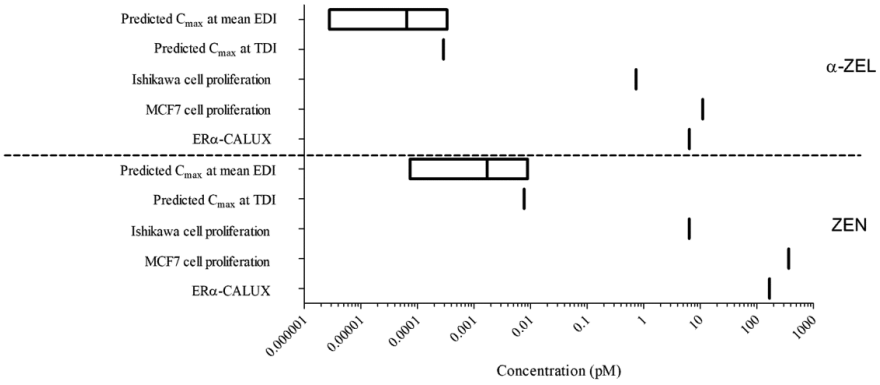

Figure 7. Comparison of EC_{10} values derived from estrogenic in vitro studies (Le Guevel and Pakdel, 2001; Mendez-Catala et al., 2020; Molina-Molina et al., 2014) to C_{max} values predicted by the human PBK model to occur at a mean estimated daily intake (EDI) of ZEN, ranging from 2.4-29 ng/ kg bw and at the TDI.

4. Discussion

In the present study, PBK models for ZEN in both rat and human were developed that include intestinal microbial metabolism of ZEN. The models include a sub-model for the metabolite, α-ZEL, known to be more active as an estrogen than ZEN itself (Fitzpatrick et al., 1989; Shier et al., 2001). By integrating microbial ZEN metabolism into the models they provide insight into the role of the intestinal microbiota in the metabolism of ZEN and its bioactivation to □-ZEL. The results obtained revealed that, in spite of the conversion of ZEN to α-ZEL by intestinal microbiota, the formation of α-ZEL from ZEN is mainly driven by hepatic metabolism. In the PBK models developed, the intestinal microbial metabolism of ZEN was integrated as a separate compartment by the inclusion of kinetic parameters obtained from in vitro anaerobic incubations of ZEN with fecal samples (Mendez-Catala et al., 2020). Previously Wang et al. (2020) showed a first proof-of-principle for the inclusion of microbial metabolism in a PBK model based on kinetic parameters obtained in such anaerobic fecal incubations. This earlier PBK study described the metabolism of the isoflavone daidzein including its microbial conversion to S-equol in addition to host-based metabolism. In this study it was shown that the inclusion of microbial metabolism allowed prediction of host blood levels of S-equol and its conjugates, and also revealed that in spite of the higher estrogenicity of S-equol its role compared to the contribution of daidzein itself was limited because of its substantially lower systemic concentrations (Wang et al., 2020). The results of the present study show a similar outcome for ZEN and α-ZEL. This followed from the fact that the C_{max} predicted for α-ZEL amounted to less than 0.1% or about 3% of the C_{max} for ZEN itself in rats and humans, respectively. This indicates that in despite of the 60-fold higher estrogenicity reported for α-ZEL its contribution to the in vivo estrogenicity upon exposure to ZEN may be limited, while in human it may be higher than in rats.

The PBK model for the metabolism of ZEN in rat allowed the comparison to available in vivo kinetic data in blood upon i.v. and oral dosing of ZEN. The model prediction of blood concentrations after 4 different i.v. doses of ZEN showed to be in line with the kinetics reported by (Shin et al., 2009). A study dosing ZEN at 8 mg/kg bw orally to rats (Shin et al., 2009) reported a C_{max} that was also adequately predicted by the model. The evaluation of the human model resulted in differences in the cumulative urinary amount possibly related to the exposure, while Mirocha et al. (1981a) exposed ZEN directly, Warth et al. (2013) did it from naturally contaminated products.

The PBK models developed showed that liver is the main site for the conversion of ZEN to α-ZEL (**Supplementary material Figure S2**), a conclusion that holds at dose levels as low as the dose representing daily dietary intake (2.4 ng/kg bw/day) (EFSA, 2011) to dose levels used in rodent bioassays of 8 mg/kg bw (Shin et al., 2009). The model predictions also revealed humans to have on average a 76-times higher concentration of α-ZEL in liver compared to rat. This is in line with previous reports on species differences in the metabolism of ZEN, indicating that humans (Bravin et al., 2009), similar to pigs, form relatively more α-ZEL than rats. The integration of the kinetic parameters for α-ZEL formation in the PBK model for human revealed the predicted blood concentration of α-ZEL to amount to about 3% of the total concentration of ZEN reaching the blood (**Supplementary material Figure S1**). The low concentration of α-ZEL reaching the circulation can be ascribed to an efficient glucuronidation of ZEN in the intestinal tissue and liver competing with formation of α-ZEL in these organs, in combination with efficient hepatic glucuronidation of α-ZEL. The glucuronidation of ZEN has previously been reported to represent the main conjugation pathway for ZEN (Kiessling and Pettersson, 1978; Malekinejad et al., 2006a; Mikula et al., 2012; Pfeiffer et al., 2010) and results in a decrease in the toxicity of ZEN due to the absence of estrogenic activity of ZEN glucuronide (Frizzell et al., 2015). The kinetic constants in Table 5 show rat and human liver to perform the glucuronidation of ZEN with comparable catalytic efficiencies, with rat being 1.1 times more efficient than humans. The glucuronidation of α-ZEL in liver was also comparable with rats again being 1.1 times more efficient than humans. These results are in line with those of Pfeiffer et al. (2010) reporting the percentage of glucuronidation of ZEN and α-ZEL by male rat liver fractions to be 1.6 and 1.5 and times higher than by human liver fractions, respectively. The somewhat higher catalytic efficiency observed for the glucuronidation by rat than human intestinal tissues in vitro is in line with results for glucuronidation of other UGT substrates such as flavonoids (Boonpawa et al., 2015; Brand et al., 2010). The glucuronidation of ZEN in human liver is reported to be catalyzed by UGTs, with UGT1A1, 1A3 and 1A8 being the major contributors (Pfeiffer et al., 2010). In the same study, intestinal glucuronidation of ZEN in humans was linked to UGT1A1 and 1A8. A higher mRNA expression of UGT1A1 and 1A3 in rat liver and intestine has been reported offering a possible explanation for the species differences in glucuronidation observed (Kutsukake et al., 2019). Based on studies in a rat everted model Ieko et al. (2020) reported the rapid glucuronidation of ZEN immediately after absorption and low transport of ZEN into the serosa portion. The amount of ZEN predicted by the PBK model to reach the liver in rats was lower than the amount reaching the small intestinal tissue,

in line with the notion from Ieko et al. (2020) that only low amounts of ZEN could reach the liver. The PBK model predicted the glucuronidation of ZEN to mainly occur in the small intestinal tissue (**Supplementary material Table S1**).

Furthermore, the outcomes of the human PBK model enabled prediction of the internal concentrations of ZEN and α-ZEL resulting from dietary intake of ZEN or from intake at the level of the TDI, with concentrations of ZEN and α-ZEL known to induce estrogenicity in in vitro bioassays. The predicted C_{max} values were on average 3 orders of magnitude lower than the EC_{10} for ZEN and α-ZEL in bioassays with different estrogenic endpoints, suggesting that at the current levels of dietary intake up to at least the TDI, the concentration of ZEN and α-ZEL in blood will not reach the concentrations known to cause estrogenic effects. This comparison illustrates the potential of the PBK model-based approach to conclude on in vivo effects without the need for studies in experimental animals or a human intervention study.

Nevertheless, it is of use to discuss some of the limitations of the current approach. First of all, it is important to note that the study is based on the average adult population and does not (yet) take interindividual differences or possible differences of different age groups in sensitivity to ZEN into account. To take such potential interindividual differences into account remains an interesting topic for further studies especially given a possible correlation between exposure to ZEN and early onset of puberty in young girls as suggested before (Bandera et al., 2011; Hannon et al., 1987; Massart and Saggese, 2010; Szuets et al., 1997). The human PBK model developed in the present study can form a basis to build individual PBK models and study such interindividual differences within the human population. Second, the potential of the use of fecal samples as a source of the intestinal microbiota for the study of intestinal microbial metabolism needs some further considerations. Although differences in the microbial composition along the intestinal tract are known, the colon harbors 70% of total bacteria in the intestinal tract, making it the main site for fermentation (Hillman et al., 2017). Furthermore, Behr et al. (2018) reported colon and fecal bacterial communities to be highly comparable, supporting the notion that fecal slurries can be used as a surrogate for intestinal microbiota. Furthermore, in a previous study the in vitro anaerobic incubations with fecal slurries were shown to adequately describe the kinetics of the formation of S-equol from daidzein, a metabolite formed only by intestinal microbiota, allowing description of S-equol kinetics by PBK modeling in both rat and human (Atkinson et al., 2004; Wang et al., 2020). Therefore, the in vitro anaerobic incubations with fecal slurries show a good first tier approach for the estimation of overall intestinal microbial metabolism in the host.

In conclusion, the PBK models developed in this study are able to quantify interspecies differences in metabolism of ZEN taking intestinal microbial metabolism into account. Results obtained reveal that in spite of the capacity of the microbial community in both rat and human to catalyze conversion of ZEN to α-ZEL, the contribution of this intestinal microbial metabolism to systemic concentrations of α-ZEL in the host are limited. Furthermore, it was shown that in spite of the higher estrogenic potency of α-ZEL its contribution to the estrogenic effects occurring upon exposure to ZEN are limited, and that at current levels of intake ZEN and also α-ZEL concentrations remain low enough to not raise a concern. The study also shows a proof of principle on how an in vitro- PBK model-based approach can be of use to conclude on in vivo effects of compounds studied without the need for studies in experimental animals or a human intervention study.

References

Atkinson, C., Berman, S., Humbert, O., and Lampe, J. W. (2004). In Vitro Incubation of Human Feces with Daidzein and Antibiotics Suggests Interindividual Differences in the Bacteria Responsible for Equol Production. *Nutr. J.* **134**, 596-599.

Bandera, E. V., Chandran, U., Buckley, B., Lin, Y., Isukapalli, S., Marshall, I., King, M., and Zarbl, H. (2011). Urinary mycoestrogens, body size and breast development in New Jersey girls. *Sci Total Environ* **409**, 5221-7.

Behr, C., Ramirez-Hincapie, S., Cameron, H. J., Strauss, V., Walk, T., Herold, M., Beekmann, K., Rietjens, I., and van Ravenzwaay, B. (2018). Impact of lincosamides antibiotics on the composition of the rat gut microbiota and the metabolite profile of plasma and feces. *Toxicol. Lett.* **296**, 139-151.

Boonpawa, R., Moradi, N., Spenkelink, A., Rietjens, I. M. C. M., and Punt, A. (2015). Use of physiologically based kinetic (PBK) modeling to study interindividual human variation and species differences in plasma concentrations of quercetin and its metabolites. *Biochemical Pharmacology* **98**, 690-702.

Borzekowski, A., Drewitz, T., Keller, J., Pfeifer, D., Kunte, H.-J., Koch, M., Rohn, S., and Maul, R. (2018). Biosynthesis and Characterization of Zearalenone-14-Sulfate, Zearalenone-14-Glucoside and Zearalenone-16-Glucoside Using Common Fungal Strains. *Toxins* **10**, 104.

Brand, W., Boersma, M. G., Bik, H., Hoek-van den Hil, E. F., Vervoort, J., Barron, D., Meinl, W., Glatt, H., Williamson, G., van Bladeren, P. J., and Rietjens, I. M. (2010). Phase II metabolism of hesperetin by individual UDP-glucuronosyltransferases and sulfotransferases and rat and human tissue samples. *Drug Metab Dispos* **38**, 617-25.

Bravin, F., Duca, R. C., Balaguer, P., and Delaforge, M. (2009). In vitro cytochrome p450 formation of a mono-hydroxylated metabolite of zearalenone exhibiting estrogenic activities: possible occurrence of this metabolite in vivo. *Int. J. Mol. Sci.* **10**, 1824-37.

Brown, R. P., Delp, M. D., Lindstedt, S. L., Rhomberg, L. R., and Beliles, R. P. (1997). Physiological parameter values for physiologically based pharmacokinetic models. *Toxicol. Ind. Health* **13**, 407-484.

Cubitt, H. E., Houston, J. B., and Galetin, A. (2011). Prediction of human drug clearance by multiple metabolic pathways: integration of hepatic and intestinal microsomal and cytosolic data. *Drug Metab Dispos* **39**, 864-73.

Dänicke, S., Swiech, E., Buraczewska, L., and Ueberschär, K. H. (2005). Kinetics and metabolism of zearalenone in young female pigs. *J. Anim. Physiol. Anim. Nutr.* **89**, 268-276.

Davies, B., and Morris, T. (1993). Physiological Parameters in Laboratory Animals and Humans. *Pharmaceutical Research* **10**, 1093-1095.

DeJongh, J., Verhaar, H. J., and Hermens, J. L. (1997). A quantitative property-property relationship (QPPR) approach to estimate in vitro tissue-blood partition coefficients of organic chemicals in rats and humans. *Arch Toxicol* **72**, 17-25.

Döll, S., Dänicke, S., Ueberschär, K. H., Valenta, H., Schnurrbusch, U., Ganter, M., Klobasa, F., and Flachowsky, G. (2003). Effects of graded levels of Fusarium toxin contaminated maize in diets for female weaned piglets. *Arch. Anim. Nutr.* **57**, 311-334.

EFSA (2011). Scientific Opinion on the risks for public health related to the presence of zearalenone in food. *EFSA J.* **9**, 2197.

EFSA (2016). Appropriateness to set a group health-based guidance value for zearalenone and its modified forms. *EFSA J.* **14**, e04425.

Evans, M. V., and Andersen, M. E. (2000). Sensitivity analysis of a physiological model for 2,3,7,8-tetrachlorodibenzo-p-dioxin (TCDD): assessing the impact of specific model parameters on sequestration in liver and fat in the rat. *Toxicol Sci* **54**, 71-80.

Fitzpatrick, D. W., Arbuckle, L. D., and Hassen, A. M. (1988). Zearalenone metabolism and excretion in the rat: effect of different doses. *J. Environ. Sci. Health B* **23**, 343-54.

Fitzpatrick, D. W., Picken, C. A., Murphy, L. C., and Buhr, M. M. (1989). Measurement of the relative binding affinity of zearalenone, α-zearalenol and β-zearalenol for uterine and oviduct estrogen receptors in swine, rats and chickens: An indicator of estrogenic potencies. *Comparative Biochemistry and Physiology Part C: Comparative Pharmacology* **94**, 691-694.

Frizzell, C., Uhlig, S., Miles, C. O., Verhaegen, S., Elliott, C. T., Eriksen, G. S., Sørlie, M., Ropstad, E., and Connolly, L. (2015). Biotransformation of zearalenone and zearalenols to their major glucuronide metabolites reduces estrogenic activity. *Toxicol. In Vitro* **29**, 575-581.

Gilbert-Sandoval, I., Wesseling, S., and Rietjens, I. M. C. M. (2020). Predicting the Acute Liver Toxicity of Aflatoxin B1 in Rats and Humans by an In Vitro–In Silico Testing Strategy. *Molecular Nutrition & Food Research* **64**, 2000063.

Gratz, S. W., Dinesh, R., Yoshinari, T., Holtrop, G., Richardson, A. J., Duncan, G., MacDonald, S., Lloyd, A., and Tarbin, J. (2017). Masked trichothecene and zearalenone mycotoxins withstand digestion and absorption in the upper GI tract but are efficiently hydrolyzed by human gut microbiota *in vitro*. *Mol. Nutr. Food Res.* **61**, E1600680.

Gupta, R. C., Mostrom, M. S., and Evans, T. J. (2018). Chapter 76 - Zearalenone. *In* "Veterinary Toxicology (Third Edition)" (R. C. Gupta, ed.), pp. 1055-1063. Academic Press.

Hannon, W. H., Hill, R. H., Bernert, J. T., Haddock, L., Lebron, G., and Cordero, J. F. (1987). Premature thelarche in Puerto Rico: A search for environmental estrogenic contamination. *Archives of Environmental Contamination and Toxicology* **16**, 255-262.

Hillman, E. T., Lu, H., Yao, T., and Nakatsu, C. H. (2017). Microbial Ecology along the Gastrointestinal Tract. *Microbes and environments* **32**, 300-313.

Hoskins, L. C., and Zamcheck, N. (1968). Bacterial Degradation of Gastrointestinal Mucins: I. Comparison of mucus constituents in the stools of germ-free and conventional rats. *Gastroenterology* **54**, 210-217.

Hosseinpour, M., and Behdad, A. (2008). Evaluation of small bowel measurement in alive patients. *Surg Radiol Anat* **30**, 653-5.

Ieko, T., Inoue, S., Inomata, Y., Inoue, H., Fujiki, J., and Iwano, H. (2020). Glucuronidation as a metabolic barrier against zearalenone in rat everted intestine. *The Journal of veterinary medical science* **82**, 153-161.

Kararli, T. T. (1995). Comparison of the gastrointestinal anatomy, physiology, and biochemistry of humans and commonly used laboratory animals. *Biopharm. Drug Dispos.* **16**, 351-80.

Kiessling, K.-H., and Pettersson, H. (1978). Metabolism of Zearalenone in Rat Liver. *Acta Pharmacologica et Toxicologica* **43**, 285-290.

Kutsukake, T., Furukawa, Y., Ondo, K., Gotoh, S., Fukami, T., and Nakajima, M. (2019). Quantitative Analysis of UDP-Glucuronosyltransferase Ugt1a and Ugt2b mRNA Expression in the Rat Liver and Small Intestine: Sex and Strain Differences. *Drug Metabolism and Disposition* **47**, 38-44.

Le Guevel, R., and Pakdel, F. (2001). Assessment of oestrogenic potency of chemicals used as growth promoter by in-vitro methods. *Hum. Reprod.* **16**, 1030-1036.

Li, H., Zhang, M., Vervoort, J., Rietjens, I. M., van Ravenzwaay, B., and Louisse, J. (2017). Use of physiologically based kinetic modeling-facilitated reverse dosimetry of in vitro toxicity data for prediction of in vivo developmental toxicity of tebuconazole in rats. *Toxicol Lett* **266**, 85-93.

Lorenz, N., Dänicke, S., Edler, L., Gottschalk, C., Lassek, E., Marko, D., Rychlik, M., and Mally, A. (2019). A critical evaluation of health risk assessment of modified mycotoxins with a special focus on zearalenone. *Mycotoxin Res.* **35**, 27-46.

Louisse, J., Bosgra, S., Blaauboer, B. J., Rietjens, I. M., and Verwei, M. (2015). Prediction of in vivo developmental toxicity of all-trans-retinoic acid based on in vitro toxicity data and in silico physiologically based kinetic modeling. *Arch Toxicol* **89**, 1135-48.

Malekinejad, H., Maas-Bakker, R., and Fink-Gremmels, J. (2006a). Species differences in the hepatic biotransformation of zearalenone. *Vet. J.* **172**, 96-102.

Malekinejad, H., Maas-Bakker, R., and Fink-Gremmels, J. (2006b). Species differences in the hepatic biotransformation of zearalenone. *Vet J* **172**, 96-102.

Mallis, L. M., Sarkahian, A. B., Harris, H. A., Zhang, M.-Y., and McConnell, O. J. (2003). Determination of rat oral bioavailability of soy-derived phytoestrogens using an automated on-column extraction procedure and electrospray tandem mass spectrometry. *Journal of Chromatography B* **796**, 71-86.

Massart, F., and Saggese, G. (2010). Oestrogenic mycotoxin exposures and precocious pubertal development. *Int J Androl* **33**, 369-76.

Mendez-Catala, D. M., Spenkelink, A., Rietjens, I. M. C. M., and Beekmann, K. (2020). An in vitro model to quantify interspecies differences in kinetics for intestinal microbial bioactivation and detoxification of zearalenone. *Toxicology Reports* **7**, 938-946.

Metzler, M., Pfeiffer, E., and Hildebrand, A. (2010). Zearalenone and its metabolites as endocrine disrupting chemicals. *World Mycotoxin J.* **3**, 385-401.

Mikula, H., Hametner, C., Berthiller, F., Warth, B., Krska, R., Adam, G., and Fröhlich, J. (2012). Fast and reproducible chemical synthesis of zearalenone-14-β,D-glucuronide. *World Mycotoxin Journal* **5**, 289-296.

Mirocha, C. J., Pathre, S. V., and Robison, T. S. (1981a). Comparative metabolism of zearalenone and transmission into bovine milk. *Food and Cosmetics Toxicology* **19**, 25-30.

Mirocha, C. J., Pathre, S. V., and Robison, T. S. (1981b). Comparative metabolism of zearalenone and transmission into bovine milk. *Food and Cosmet. Toxicol.* **19**, 25-30.

Molina-Molina, J.-M., Real, M., Jimenez-Diaz, I., Belhassen, H., Hedhili, A., Torné, P., Fernández, M. F., and Olea, N. (2014). Assessment of estrogenic and anti-androgenic activities of the mycotoxin zearalenone and its metabolites using in vitro receptor-specific bioassays. *Food Chem. Toxicol.* **74**, 233-239.

Mukherjee, D., Royce, S. G., Alexander, J. A., Buckley, B., Isukapalli, S. S., Bandera, E. V., Zarbl, H., and Georgopoulos, P. G. (2014). Physiologically-based toxicokinetic modeling of zearalenone and its metabolites: application to the Jersey girl study. *PLoS One* **9**, e113632.

Peters, S. A., Jones, C. R., Ungell, A.-L., and Hatley, O. J. D. (2016). Predicting Drug Extraction in the Human Gut Wall: Assessing Contributions from Drug Metabolizing Enzymes and Transporter Proteins using Preclinical Models. *Clinical Pharmacokinetics* **55**, 673-696.

Pfeiffer, E., Hildebrand, A., Mikula, H., and Metzler, M. (2010). Glucuronidation of zearalenone, zeranol and four metabolites in vitro: formation of glucuronides by various microsomes and human UDP-glucuronosyltransferase isoforms. *Mol Nutr Food Res* **54**, 1468-76.

Pfeiffer, E., Kommer, A., Dempe, J. S., Hildebrand, A. A., and Metzler, M. (2011). Absorption and metabolism of the mycotoxin zearalenone and the growth promotor zeranol in Caco-2 cells in vitro. *Mol. Nutr. Food Res.* **55**, 560-567.

Probst, R. J., Lim, J. M., Bird, D. N., Pole, G. L., Sato, A. K., and Claybaugh, J. R. (2006). Gender differences in the blood volume of conscious Sprague-Dawley rats. *J Am Assoc Lab Anim Sci* **45**, 49-52.

Punt, A., Freidig, A. P., Delatour, T., Scholz, G., Boersma, M. G., Schilter, B., van Bladeren, P. J., and Rietjens, I. M. C. M. (2008). A physiologically based biokinetic (PBBK) model for estragole bioactivation and detoxification in rat. *Toxicology and applied pharmacology* **231**, 248-259.

Reilly, J. A., Forst, C. F., Quigley, E. M. M., and Rikkers, L. F. (1990). Gastric emptying of liquids and solids in the portal hypertensive rat. *Digestive Diseases and Sciences* **35**, 781-786.

Rose, C., Parker, A., Jefferson, B., and Cartmell, E. (2015). The Characterization of Feces and Urine: A Review of the Literature to Inform Advanced Treatment Technology. *Crit. Rev. Environ. Sci. Technol.* **45**, 1827-1879.

Shier, W. T., Shier, A. C., Xie, W., and Mirocha, C. J. (2001). Structure-activity relationships for human estrogenic activity in zearalenone mycotoxins. *Toxicon* **39**, 1435-8.

Shin, B. S., Hong, S. H., Bulitta, J. B., Hwang, S. W., Kim, H. J., Lee, J. B., Yang, S. D., Kim, J. E., Yoon, H. S., Kim, D. J., and Yoo, S. D. (2009). Disposition, oral bioavailability, and tissue distribution of zearalenone in rats at various dose levels. *J Toxicol Environ Health A* **72**, 1406-11.

Sun, D., Lennernas, H., Welage, L. S., Barnett, J. L., Landowski, C. P., Foster, D., Fleisher, D., Lee, K. D., and Amidon, G. L. (2002). Comparison of human duodenum and Caco-2 gene expression profiles for 12,000 gene sequences tags and correlation with permeability of 26 drugs. *Pharm Res* **19**, 1400-16.

Sun, W. M., Houghton, L. A., Read, N. W., Grundy, D. G., and Johnson, A. G. (1988). Effect of meal temperature on gastric emptying of liquids in man. *Gut* **29**, 302-5.

Szuets, P., Mesterhazy, A., Falkay, G. Y., and Bartok, T. (1997). Early Telarche Symptoms in Children and their Relations to Zearalenon Contamination in Foodstuffs. *Cereal Research Communications* **25**, 429-436.

Teeguarden, J. G., Waechter, J. M., Jr., Clewell, H. J., III, Covington, T. R., and Barton, H. A. (2005). Evaluation of Oral and Intravenous Route Pharmacokinetics, Plasma Protein Binding, and Uterine Tissue Dose Metrics of Bisphenol A: A Physiologically Based Pharmacokinetic Approach. *Toxicological Sciences* **85**, 823-838.

Tsutsumi, K., Li, S. K., Hymas, R. V., Teng, C.-L., Tillman, L. G., Hardee, G. E., Higuchi, W. I., and Ho, N. F. H. (2008). Systematic studies on the paracellular permeation of model permeants and oligonucleotides in the rat small intestine with chenodeoxycholate as enhancer. *Journal of pharmaceutical sciences* **97**, 350-367.

Vdoviaková, K., Petrovová, E., Maloveská, M., Krešáková, L., Teleky, J., Elias, M. Z. J., and Petrášová, D. (2016). Surgical Anatomy of the Gastrointestinal Tract and Its Vasculature in the Laboratory Rat. *Gastroenterology Research and Practice* **2016**, 2632368.

Verwei, M., Freidig, A. P., Havenaar, R., and Groten, J. P. (2006). Predicted serum folate concentrations based on in vitro studies and kinetic modeling are consistent with measured folate concentrations in humans. *J Nutr* **136**, 3074-8.

Walker, H. K., Hall, W. D., and Hurst, J. W. (1990). "Clinical Methods: The History, Physical, and Laboratory Examinations," Butterworths Copyright ©, Boston.

Wang, Q., Spenkelink, B., Boonpawa, R., Rietjens, I., and Beekmann, K. (2020). Use of Physiologically Based Kinetic Modeling to Predict Rat Gut Microbial Metabolism of

the Isoflavone Daidzein to S-Equol and Its Consequences for ERα Activation. *Mol. Nutr, Food Res.* **64**, e1900912.

Warth, B., Sulyok, M., Berthiller, F., Schuhmacher, R., and Krska, R. (2013). New insights into the human metabolism of the Fusarium mycotoxins deoxynivalenol and zearalenone. *Toxicol Lett* **220**, 88-94.

WFSR (2020). QIVIVE tools V 1.0

Yang, J., Jamei, M., Yeo, K. R., Rostami-Hodjegan, A., and Tucker, G. T. (2007). Misuse of the Well-Stirred Model of Hepatic Drug Clearance. *Drug Metabolism and Disposition* **35**, 501-502.

Yang, X., Doerge, D. R., and Fisher, J. W. (2013). Prediction and evaluation of route dependent dosimetry of BPA in rats at different life stages using a physiologically based pharmacokinetic model. *Toxicology and Applied Pharmacology* **270**, 45-59.

Zhang, M., van Ravenzwaay, B., Fabian, E., Rietjens, I. M. C. M., and Louisse, J. (2018). Towards a generic physiologically based kinetic model to predict in vivo uterotrophic responses in rats by reverse dosimetry of in vitro estrogenicity data. *Archives of Toxicology* **92**, 1075-1088.

Supplementary material 1. PBK model code

```
Model Code for Rat
;=================================================================
;Physiological parameters
;=================================================================
;Tissue volumes (Brown et al., 1997)
BW= 0.250           {Kg}                ; body weight rat
VSIc = 0.014                            ;fraction of small intestine
VLc = 0.034                             ;fraction of liver tissue
VRc = 0.034         ;0.082-VSIc-VLc     ;fraction of rapidly perfused tissue
VSc = 0.667         ;0.737-VFc          ;fraction of slowly perfused tissue
VFc = 0.070                             ;fraction of fat tissue
VBc = 0.074                             ;fraction of blood

VSI = VSIc*BW       {L or Kg}           ;volume of small intestine tissue (calculated)
VL = VLc*BW         {L or Kg}           ;volume of liver tissue (calculated)
VR = VRc*BW         {L or Kg}           ;volume of rapidly perfused tissue (calculated)
VS = VSc*BW         {L or Kg}           ;volume of slowly perfused tissue (calculated)
VF = VFc*BW         {L or Kg}           ;volume of fat tissue (calculated)
VB = VBc*BW         {L or Kg}           ;volume of blood (calculated)
; ---------------------------------------------------------------------------------------------
;Blood flow rates (Brown et al., 1997)
QC = 5.38           {L/h}               ;cardiac output:15*BW^0.74
QSIc = 0.151                            ;fraction of blood flow to small intestine
QLc = 0.099         ;0.25 - QSIc        ;fraction of blood flow to liver
QRc = 0.51          ;0.76 - QSIc – QLc  ;fraction of blood flow to rapidly perfused tissue
QSc = 0.17          ;0.24 – QFc         ;fraction of blood flow to slowly perfused tissue
QFc = 0.07                              ;fraction of blood flow to fat

QSI = QSIc*QC       {L/h}               ;blood flow to small intestine tissue (calculated)
QL = QLc*QC         {L/h}               ;blood flow to liver tissue (calculated)
QR = QRc*QC         {L/h}               ;blood flow to rapidly perfused tissue (calculated)
QS = QSc*QC         {L/h}               ;blood flow to slowly perfused tissue (calculated)
QF = QFc*QC         {L/h}               ;blood flow to fat tissue (calculated)

;=================================================================
;Physicochemical parameters
;=================================================================
;partition coefficients, calculated based on QPPR of DeJongh et al. (1997) (DeJongh et al., 1997)

;ZEN in main model
PIZEN = 2.64        ;intestine/blood partition coefficient
PLZEN = 2.64        ;liver/blood partition coefficient
PRZEN = 2.64        ;rapidly perfused tissue/blood partition coefficient
PSZEN = 0.76        ;slowly perfused tissue/blood partition coefficient
PFZEN = 106.93      ;fat/blood partition coefficient

;α-ZEL in sub-model
PIaZEL = 2.38       ;intestine/blood partition coefficient
PLaZEL = 2.38       ;liver/blood partition coefficient
PRaZEL = 2.38       ;rapidly perfused tissue/blood partition coefficient
PSaZEL = 0.71       ;slowly perfused tissue/blood partition coefficient
PFaZEL = 92.79      ;fat/blood partition coefficient
; ---------------------------------------------------------------------------------------------
;absorption/transfer rates

;Stomach emptying rate
ksto = 2.8                  ;stomach emptying rate (/h) (Reilly et al., 1990)
```

```
;intestinal absorption and transfer rates of ZEN
PappCaco2ZEN=-3.9838            ;fitted Log Papp, Caco-2 (cm/h) (Pfeiffer et al., 2011)

;Log (Papp,in vivo) = 0.6836*Log(PappCaco2ZEN)-0.5579            ;(Sun et al., 2002)
PappZEN=10^(0.6836*PappCaco2ZEN-0.5579)*3600/10                  {dm/h}

Vin = 0.0012                    ;volume for each compartment of intestines (L)
SAin = 0.134                    ;surface area (dm2)
kin = 4.17                      ;transfer rate to next compartment within the intestines (/hr)
kabin1 = PappZEN*SAin           ;absorption rate constant (L/hr)

Vin1 = Vin                      ;volume of intestine compartment 1 (L)
SAin1 = SAin                    ;surface area of intestine compartment 1 (dm2)
kabin1 = PappZEN*SAin1          ;absorption rate constant of intestine compartment 1 (L/hr)
kin1 = kin                      ;transfer rate to intestine compartment 2 (/hr)

Vin2 = Vin                      ;volume of intestine compartment 2 (L)
SAin2 = SAin                    ;surface area of intestine compartment 2 (dm2)
kabin2 = PappZEN*SAin2          ;absorption rate constant of intestine compartment 2 (L/hr)
kin2 = kin                      ;transfer rate to intestine compartment 3 (/hr)

Vin3 = Vin                      ;volume of intestine compartment 3 (L)
SAin3= SAin                     ;surface area of intestine compartment 3 (dm2)
kabin3 = PappZEN*SAin3          ;absorption rate constant of intestine compartment 3 (L/hr)
kin3 = kin                      ;transfer rate to intestine compartment 4 (/hr)

Vin4 = Vin                      ;volume of intestine compartment 4 (L)
SAin4 = SAin                    ;surface area of intestine compartment 4 (dm2)
kabin4 = PappZEN*SAin4          ;absorption rate constant of intestine compartment 4 (L/hr)
kin4 = kin                      ;transfer rate to intestine compartment 5 (/hr)

Vin5 = Vin                      ;volume of intestine compartment 5 (L)
SAin5 = SAin                    ;surface area of intestine compartment 5 (dm2)
kabin5 = PappZEN*SAin5          ;absorption rate constant of intestine compartment 5 (L/hr)
kin5 = kin                      ;transfer rate to intestine compartment 6 (/hr)
Vin6 = Vin                      ;volume of intestine compartment 6 (L)
SAin6 = SAin                    ;surface area of intestine compartment 6 (dm2)
kabin6 = PappZEN*SAin6          ;absorption rate constant of intestine compartment 6 (L/hr)
kin6 = kin                      ;transfer rate to intestine compartment 7 (hr)

Vin7 = Vin                      ;volume of intestine compartment 7 (L)
SAin7 = SAin                    ;surface area of intestine compartment 7 (dm2)
kabin7 = PappZEN*SAin7          ;absorption rate constant of intestine compartment 7 (L/hr)
kin7 = 0.464        (/h)        ;transfer rate of ZEN from small intestine to large intestine (Kimura and
Higaki, 2002)

Vinb = 0.0338                   ;volume of large intestine (L) (Vdoviaková et al., 2016)
SAinb = 1.57                    ;surface area of large intestine (dm2) (Vdoviaková et al., 2016)
Kb = PappZEN*SAinb              ;absorption rate constant from the large intestine (L/hr)
Kb= PappZEN*SAinb               ;absorption rate constant from the large intestine (L/hr)


;α-ZEL
;PappCaco2aZEL=-5.2676          Log Papp, Caco-2 (cm/h) (Pfeiffer et al., 2011)

;Log (Papp,in vivo) = 0.6836*Log(PappCaco2aZEL)-0.5579   (Sun et al., 2002)
PappaZEL=10^(0.6836*PappCaco2aZEL-0.5579)*3600/10 (dm/h)

Vin8 = Vin                      ;volume of intestine compartment 7 (L)
SAin8 = SAinb                   ;surface area of intestine compartment 7 (dm2)
```

```
kabin8 = PappaZEL*SAin8          ;absorption rate constant of α-ZEL from LI to liver (L/hr)

excretion (/h) (Mukherjee et al., 2014)
KurZ = 0.096                     ;urinary excretion of ZEN
KfeZ = 0.69                      ;fecal excretion of ZEN

KuraZ = 0.012                    ;urinary excretion of α-ZEL
KfeaZ = 0.69                     ;fecal excretion of α-ZEL

;==================================================================
;Kinetic parameters
;==================================================================
;metabolism in small intestine tissue

;scaling factors
S9SI= 37.1        ;small intestinal S9 protein yield (mg S9 protein/gram intestine) (Peters et al., 2016)
SI=VSIc*1000      ;small intestine in body weight (gram/kg BW)


;metabolites ZENGLU, unscaled maximum rates of metabolism, (nmol/min/mg S9 protein)
VmaxSIZENGLUc= 8.617             ;in vitro, S9 incubations from this study

;metabolites ZENGLU, scaled maximum rates of metabolism, (µmol/h)
VMaxSIZENGLU = VmaxSIZENGLUc/1000*60*S9SI*SI*BW

;metabolites ZENGLU, affinity constants, (µmol/L)
KmSIZENGLU = 6.198               ;in vitro, S9 incubations from this study
; ------------------------------------------------------------------------------------------------------------
;metabolism in large intestine lumen (microbiota compartment)

;scaling factors
VMB = 0.0164                     ;fraction of feces of BW (Brown et al., 1997)

;metabolites α-ZEL and β-ZEL, unscaled maximum rates of metabolism, (pmol/h/g faeces) (Mendez-Catala et al.,
2020)
VmaxLIaZELc=0.0138
VmaxLIbZELc= 0.0084

;metabolites α-ZEL and β-ZEL, scaled maximum rates of metabolism, (µmol/h)
VmaxLIaZEL= VmaxLIaZELc/1000000*1000 *VMB*BW
VmaxLIbZEL= VmaxLIbZELc/1000000*1000 *VMB*BW

;metabolites α-ZEL and β-ZEL, affinity constants, (µmol/L) (Mendez-Catala et al., 2020)
KmLIaZEL = 66
KmLIbZEL = 80
; ------------------------------------------------------------------------------------------------------------
;metabolism in liver
;scaling factors
VLS9 = 143                ;liver S9 protein yield (mg S9 protein/gram liver) (Punt et al., 2008)
L=VLc*1000                {gram/kg BW}            ;liver

;Part 1: Zearalenone phase I metabolism α-ZEL and β-ZEL formation

;metabolites α-ZEL and β-ZEL, unscaled maximum rates of metabolism, (pmol/min/mg S9 protein)
(Malekinejad et al., 2006)
VmaxLaZELc= 32
VmaxLbZELc= 72

;metabolites α-ZEL and β-ZEL, scaled maximum rates of metabolism, (µmol/h)
VmaxLaZEL = VmaxLaZELc/1000000*60* VLS9 *L*BW
```

```
VmaxLbZEL= VmaxLbZELc/1000000*60* VLS9 *L*BW

;metabolites α-ZEL and β-ZEL, affinity constants, (µmol/L) (Malekinejad et al., 2006)
KmLaZEL = 592
KmLbZEL = 21

;Part 2: Zearalenone phase II metabolism-glucuronidation

;metabolites ZENGLU, unscaled maximum rates of metabolism, (nmol/min/mg S9 protein)
VmaxLZENGLUc=7.029              ;in vitro, S9 incubations from this study

;metabolites ZENGLU, scaled maximum rates of metabolism, (µmol/h)
VmaxLZENGLU = VmaxLZENGLUc /1000*60* VLS9 *L*BW

;metabolites ZENGLU, affinity constants, (µmol/L)
KmLZENGLU = 6.753               ;in vitro, S9 incubations from this study

;Part 3: α-ZEL phase II metabolism: glucuronidation
;metabolites α-ZELGLU, unscaled maximum rates of metabolism, (nmol/min/mg S9 protein)
VmaxLaZELGLUc= 6.963            ;in vitro, S9 incubations from this study

;metabolites α-ZEL GLU, scaled maximum rates of metabolism, (µmol/h)
VmaxLaZELGLU = VmaxLaZELGLUc/1000*60* VLS9 *L*BW

;metabolites α-ZELGLU, affinity constants, (µmol/L)
KmLaZELGLU =7.426               ;in vitro, S9 incubations from this study

;=====================================================================
;Run settings
;=====================================================================
;molecular weight
MWZEN = 318.37          ;molecular weight ZEN
; ---------------------------------------------------------------------------------------------------
;oral dose
ODOSEmg =0                      {mg/kg bw}              ;oral dose, variable
ODOSEumol= ODOSEmg*1000/MWZEN*BW        {µmol}  ;unit change to µmol
;
;IV dose
IVDOSEmg1 = 8 {mg/kg bw}                                ;IV dose, variable
IVDOSEumol=IVDOSEmg1*1000/MWZEN*BW                      ;unit change to µmol

;time
Starttime = 0                   {h}
Stoptime = 24                   {h}                     ;variable

DTMIN = 1e-6                    ;minimum integration time (DT)
DTMAX = 0.15                    ;maximum integration time (DT)
;=====================================================================
;Main model calculations/dynamics: zearalenone
;=====================================================================
;Stomach
;Ast = amount in stomach
Ast' = -ksto*Ast

Init Ast =ODOSEumol
; ---------------------------------------------------------------------------------------------------
;small intestine lumen compartment
;intestines, divided in 7 compartments
;Ain1 = Amount ZEN in intestine compartment 1 (µmol)
Cin1 = Ain1/Vin1
```

```
Ain1' = ksto*Ast - kin1*Ain1- kabin1*Cin1
Init Ain1 = 0

;Ain2 = Amount ZEN in intestine compartment 2 (µmol)
Cin2 = Ain2/Vin2
Ain2' = kin1*Ain1 - kin2*Ain2 - kabin2*Cin2
Init Ain2 = 0

;Ain3 = Amount ZEN in intestine compartment 3 (µmol)
Cin3 = Ain3/Vin3
Ain3' = kin2*Ain2 - kin3*Ain3 - kabin3*Cin3
Init Ain3 = 0

;Ain4 = Amount ZEN in intestine compartment 4 (µmol)
Cin4 = Ain4/Vin4
Ain4' = kin3*Ain3 - kin4*Ain4 - kabin4*Cin4
Init Ain4 = 0

;Ain5 = Amount ZEN in intestine compartment 5 (µmol)
Cin5 = Ain5/Vin5
Ain5' = kin4*Ain4 - kin5*Ain5 - kabin5*Cin5
Init Ain5 = 0

;Ain6= Amount ZEN in intestine compartment 6 (µmol)
Cin6 = Ain6/Vin6
Ain6' = kin5*Ain5 - kin6*Ain6 - kabin6*Cin6
Init Ain6 = 0

;Ain7= Amount ZEN in intestine compartment 7 (µmol)
Cin7 = Ain7/Vin7
Ain7' = kin6*Ain6 - kin7*Ain7 - kabin7*Cin7
Init Ain7 = 0
; ----------------------------------------------------------------------------------------------------------------
;small intestine tissue compartment
;ASIZEN: amount of ZEN in small intestinal tissue, (µmol)
ASIZEN' = kabin1*Cin1+ kabin2*Cin2+ kabin3*Cin3+ kabin4*Cin4+ kabin5*Cin5 + kabin6*Cin6 +
kabin7*Cin7+ QSI*(CB- CVSIZEN) - ASIZENGLU'
        Init ASIZEN=0
        CSIZEN = ASIZEN/VSI
        CVSIZEN = CSIZEN/PIZEN

;ASIZENGLU: amount of ZEN metabolized to metabolite ZENGLU, (µmol)
        ASIZENGLU'= VmaxSIZENGLU*CVSIZEN/(KmSIZENGLU+ CVSIZEN)
        Init ASIZENGLU=0
; ----------------------------------------------------------------------------------------------------------------
; large intestine lumen compartment: microbial activity
; ALIZEN: amount of ZEN in large intestine lumen, (µmol)
        ALIZEN' = kin7*Ain7 - ALIaZEL' - ALIbZEL' - Kb*CLIZEN - KfeZ*ALIZEN
        Init ALIZEN = 0
        CLIZEN = ALIZEN/ (VMB*BW)

; ALIaZEL: amount of α-ZEL formed due to gut microbial activity, (µmol)
        ALIaZEL'= VmaxLIaZEL*CLIZEN/(KmLIaZEL + CLIZEN)
        Init ALIaZEL=0

; ALIbZEL: amount of β-ZEL formed due to gut microbial activity, (µmol)
        ALIbZEL'= VmaxLIbZEL * CLIZEN/(KmLIbZEL + CLIZEN)
        Init ALIbZEL=0
; ----------------------------------------------------------------------------------------------------------------
; liver compartment
```

```
; ALZEN: amount of ZEN in liver, (µmol)
        ALZEN' = QL*CB+QSI*CVSIZEN-(QL+QSI)*CVLZEN - ALaZEL' - ALbZEL'- ALZENGLU' + Kb*

CLIZEN
        Init ALZEN=0 CLZEN = ALZEN/VL
        CVLZEN = CLZEN/PLZEN

; ALaZEL: amount of ZEN metabolized to metabolite α-ZEL in liver, (µmol)
        ALaZEL'= VmaxLaZEL* CVLZEN /(KmLaZEL+ CVLZEN)
        Init ALaZEL=0

; ALbZEL: amount of ZEN metabolized to metabolite β-ZEL in liver, (µmol)
        ALbZEL'= VmaxLbZEL* CVLZEN /(KmLbZEL+ CVLZEN)
        Init ALbZEL=0

; ALZENGLU: amount of ZEN metabolized to metabolite ZENGLU in liver, (µmol)
        ALZENGLU'= VmaxLZENGLU* CVLZEN/(KmLZENGLU+ CVLZEN)
        Init ALZENGLU=0
; ---------------------------------------------------------------------------------------------------------------------
; fat compartment
; AF = amount of ZEN in fat tissue, (µmol)
AF' = QF*(CB-CVF)
Init AF = 0
CF = AF/VF
CVF = CF/PFZEN
; ---------------------------------------------------------------------------------------------------------------------
;rapidly perfused tissue
;AR = amount of ZEN in rapidly perfused tissue, (µmol)
AR' = QR*(CB-CVR)
Init AR = 0
CR = AR/VR
CVR = CR/PRZEN
; ---------------------------------------------------------------------------------------------------------------------
;slowly perfused tissue
;AS = amount of ZEN in slowly perfused tissue, (µmol)
AS' = QS*(CB-CVS)
Init AS = 0
CS = AS/VS
CVS = CS/PSZEN
; ---------------------------------------------------------------------------------------------------------------------
; blood compartment
; AB: amount of ZEN in blood, (µmol)
AB' = (QL+QSI)*CVLZEN + QF*CVF + QS*CVS + QR*CVR - QC*CB - KurZ*AB
Init AB = IVDOSEumol
CB = AB/VB
AUC'=AB
Init AUC=0
; ---------------------------------------------------------------------------------------------------------------------
;urinary excretion
AZur' = KurZ*AB
Init AZur = 0

;=====================================================================
;Main model: mass balance calculation
;=====================================================================
Total = ODOSEumol + IVDOSEumol
Calculated = Ast+ Ain1 + Ain2 + Ain3 + Ain4 + Ain5 + Ain6 + Ain7+ ASIZEN +ASIZENGLU + ALIZEN+
ALIaZEL + ALIbZEL+ ALZEN + ALaZEL + ALbZEL+ALZENGLU + AF + AR + AS + AB + AZur + AZfe

ERROR=((Total-Calculated)/Total+1E-30)*100
```

```
MASSBBAL=Total-Calculated + 1

; ==================================================================
; Sub-model calculations/dynamics: α-ZEL
; ==================================================================
; large intestine lumen compartment
; ARLIaZEL = amount of α-ZEL in large intestine lumen, (µmol)
        ARLIaZEL' = ALIaZEL' - kabin8*(ARLIaZEL/VMB*BW) - KfeaZ*ARLIaZEL
        init ARLIaZEL = 0
; ---------------------------------------------------------------------------------------------------
;liver compartment
;ARLaZEL: amount of α-ZEL in liver, (µmol)
        ARLaZEL' = ALaZEL'+kabin8*(ARLIaZEL/VMB*BW) + (QL+QSI)*CBaZEL -
(QL+QSI)*CVLaZEL - ALaZELGLU'
        Init ARLaZEL= 0
        CLaZEL = ARLaZEL/VL
        CVLaZEL = CLaZEL/PLaZEL

;ALaZELGLU: amount of α-ZEL glucuronide in liver
        ALaZELGLU'= VmaxLaZELGLU* CVLaZEL/(KmLaZELGLU+ CVLaZEL)
        Init ALaZELGLU=0

ALaZELGLUmg' = ALaZELGLU*MWZEN/1000*BW
Init ALaZELGLUmg = 0
; ---------------------------------------------------------------------------------------------------
;fat compartment
;AFaZEL: amount of α-ZEL in fat tissue, (µmol)
AFaZEL' = QF*(CBaZEL-CVFaZEL)
Init AFaZEL = 0
CFaZEL = AFaZEL/VF
CVFaZEL = CFaZEL/PFaZEL
; ---------------------------------------------------------------------------------------------------
;rapidly perfused tissue
;ARaZEL: amount of α-ZEL in rapidly perfused tissue, (µmol)
ARaZEL' = QR*(CBaZEL-CVRaZEL)
Init ARaZEL = 0
CRaZEL = ARaZEL/VR
CVRaZEL = CRaZEL/PRaZEL
; ---------------------------------------------------------------------------------------------------
;slowly perfused tissue
;ASaZEL: amount of α-ZEL in slowly perfused tissue, (µmol)
ASaZEL' = QS*(CBaZEL-CVSaZEL)
Init ASaZEL = 0
CSaZEL = ASaZEL/VS
CVSaZEL = CSaZEL/PSaZEL
; ---------------------------------------------------------------------------------------------------
;blood compartment
;ABaZEL: amount of α-ZELin blood, (µmol)
ABaZEL' = (QL+QSI)*CVLaZEL + QF*CVFaZEL + QR*CVRaZEL + QS*CVSaZEL - QC*CBaZEL -
KuraZ*ABaZEL
Init ABaZEL=0
CBaZEL = ABaZEL/VB
AUCaZEL'=ABaZEL
Init AUCaZEL=0
; ---------------------------------------------------------------------------------------------------
;urinary excretion
AaZur' = KurZ*ABaZEL
Init AaZur = 0
```

4

Model Code for Human

```
;=================================================================
;Physiological parameters
;=================================================================
;Tissue volumes (Brown et al., 1997)
BW= 70                  {Kg}            ;body weight rat
VSIc = 0.009                            ;fraction of small intestine
VLc = 0.026                             ;fraction of liver tissue
VRc = 0.041                             ;0.076-VSIc-VLc;fraction of rapidly perfused tissue
VSc = 0.596             ;0.81-VFc       ;fraction of slowly perfused tissue
VFc = 0.214                             ;fraction of fat tissue
VBc = 0.074                             ;fraction of blood
VSI = VSIc*BW           {L or Kg}       ;volume of small intestine tissue (calculated)
VL = VLc*BW             {L or Kg}       ;volume of liver tissue (calculated)
VR = VRc*BW             {L or Kg}       ;volume of rapidly perfused tissue (calculated)
VS = VSc*BW             {L or Kg}       ;volume of slowly perfused tissue (calculated)
VF = VFc*BW             {L or Kg}       ;volume of fat tissue (calculated)
VB = VBc*BW             {L or Kg}       ;volume of blood (calculated)

; ---------------------------------------------------------------------------------------------------
;Blood flow rates (Brown et al., 1997)
QC = 347.9              {L/h}           ;cardiac output:15*BW^0.74
QSIc = 0.181                            ;fraction of blood flow to small intestine
QLc = 0.046             ;0.227 - QSIc   ;fraction of blood flow to liver
QRc = 0.473             ;0.7 - QSIc – QLc;fraction of blood flow to rapidly perfused tissue
QSc = 0.248             ;0.3 – QFc      ;fraction of blood flow to slowly perfused tissue
QFc = 0.052                             ;fraction of blood flow to fat

QSI = QSIc*QC   {L/h}   ;blood flow to small intestine tissue (calculated)
QL = QLc*QC             {L/h}   ;blood flow to liver tissue (calculated)
QR = QRc*QC     {L/h}   ;blood flow to rapidly perfused tissue (calculated)
QS = QSc*QC             {L/h}   ;blood flow to slowly perfused tissue (calculated)
QF = QFc*QC             {L/h}   ;blood flow to fat tissue (calculated)

;=================================================================
;Physicochemical parameters
;=================================================================
;partition coefficients, calculated based on QPPR (Brown et al., 1997)

;ZEN in main model
PIZEN = 6.56            ;intestine/blood partition coefficient
PLZEN = 6.56            ;liver/blood partition coefficient
PRZEN = 6.56            ;rapidly perfused tissue/blood partition coefficient
PSZEN = 4.25            ;slowly perfused tissue/blood partition coefficient
PFZEN = 134.86          ;fat/blood partition coefficient

α-ZEL in sub-model
PIaZEL = 6.11           ;intestine/blood partition coefficient
PLaZEL = 6.11           ;liver/blood partition coefficient
PRaZEL = 6.11           ;rapidly perfused tissue/blood partition coefficient
PSaZEL = 3.99           ;slowly perfused tissue/blood partition coefficient
PFaZEL = 131.62         ;fat/blood partition coefficient

; ---------------------------------------------------------------------------------------------------
absorption/transfer rates

Stomach emptying rate
ksto = 2.8              ;stomach emptying rate (/h) (Reilly et al., 1990)
```

```
;intestinal absorption and transfer rates of ZEN
;Papp, Caco-2 ZEN = 10.3 ( x10^-5 cm/sec)     fitted apparent in vitro, from Caco-2 (Pfeiffer et al., 2011)
PappCaco2ZEN=-4.9829              ;Log Papp, Caco-2

;Log (Papp,in vivo) = 0.6836*Log(PappCaco2ZEN)-0.5579     (Sun et al., 2002)
PappZEN=10^(0.6836*PappCaco2ZEN-0.5579)*3600/10 (dm/h)

Vin = 1.29                        ;volume for each compartment of intestines (L)
SAin = 10.3                       ;surface area (dm2)
kin = 2.19                        ;transfer rate to next compartment within the intestines (/hr)
kabin1 = PappZEN*Sain             ;absorption rate constant (L/hr)

Vin1 = Vin                        ;volume of intestine compartment 1 (L)
SAin1 = SAin                      ;surface area of intestine compartment 1 (dm2)
kabin1 = PappZEN*SAin1            ;absorption rate constant of intestine compartment 1 (L/hr)
kin1 = kin                        ;transfer rate to intestine compartment 2 (/hr)

Vin2 = Vin                        ;volume of intestine compartment 2 (L)
SAin2 = SAin                      ;surface area of intestine compartment 2 (dm2)
kabin2 = PappZEN*SAin2            ;absorption rate constant of intestine compartment 2 (L/hr)
 kin2 = kin                       ;transfer rate to intestine compartment 3 (/hr)

Vin3 = Vin                        ;volume of intestine compartment 3 (L)
SAin3= SAin                       ;surface area of intestine compartment 3 (dm2)
kabin3 = PappZEN*SAin3            ;absorption rate constant of intestine compartment 3 (L/hr)
kin3 = kin                        ;transfer rate to intestine compartment 4 (/hr)

Vin4 = Vin                        ;volume of intestine compartment 4 (L)
SAin4 = SAin                      ;surface area of intestine compartment 4 (dm2)
kabin4 = PappZEN*SAin4            ;absorption rate constant of intestine compartment 4 (L/hr)
kin4 = kin                        ;transfer rate to intestine compartment 5 (/hr)

Vin5 = Vin                        ;volume of intestine compartment 5 (L)
SAin5 = SAin                      ;surface area of intestine compartment 5 (dm2)
kabin5 = PappZEN*SAin5            ;absorption rate constant of intestine compartment 5 (L/hr)
kin5 = kin                        ;transfer rate to intestine compartment 6 (/hr)

Vin6 = Vin                        ;volume of intestine compartment 6 (L)
SAin6 = SAin                      ;surface area of intestine compartment 6 (dm2)
kabin6 = PappZEN*SAin6            ;absorption rate constant of intestine compartment 6 (L/hr)
kin6 = kin                        ;transfer rate to intestine compartment 7 (/hr)

Vin7 = Vin                        ;volume of intestine compartment 7 (L)
SAin7 = SAin                      ; surface area of intestine compartment 7 (dm2)
kabin7 = PappZEN*SAin7            ;absorption rate constant of intestine compartment 7 (L/hr)
kin7 = 0.464                      ;transfer rate of ZEN from small intestine to large intestine (/h) (Kimura and
Higaki, 2002)

SAinb = 47.12                     ;surface area of large intestine (dm2) (Vdoviaková et al., 2016)
Kb= PappZEN*SAinb                 ;absorption rate constant from the large intestine (L/hr)


;α-ZEL
;Papp, Caco-2 α-ZEL = 5.4         (x10^-6 cm/sec), apparent in vitro, from Caco-2 (Pfeiffer et al., 2011)
PappCaco2aZEL=-5.2676 ;Log Papp, Caco-2

; Log (Papp,in vivo) = 0.6836*Log(PappCaco2aZEL)-0.5579 (Sun et al., 2002)
PappaZEL=10^(0.6836*PappCaco2aZEL-0.5579)*3600/10 (dm/h)

SAin8 = SAinb                     ;surface area of intestine compartment 7 (dm2)
```

```
kabin8 = PappaZEL*SAin8          ;absorption rate constant of α-ZEL from LI to liver(L/hr)

;excretion (/h) (Mukherjee et al., 2014)
KurZ = 0.096                     ;urinary excretion of ZEN
KfeZ = 0.024                     ;fecal excretion of ZEN
KuraZ = 0.015                    ;urinary excretion of α-ZEL

KfeaZ = 0.024                    ;fecal excretion of α-ZEL
KurG = 59.4                      ;urinary excretion of α-ZEL


;=====================================================================
; Kinetic parameters
;=====================================================================
;metabolism of small intestine tissue

;scaling factors
S9SI= 35.2                       ;small intestinal S9 protein yield (mg S9 protein/gram intestine) (Peters et al., 2016)
SI=VSIc*1000                     ;small intestine in body weight (gram/kg BW)


;metabolites ZENGLU, unscaled maximum rates of metabolism, (nmol/min/mg S9 protein)
VmaxSIZENGLUc= 0.491             ;in vitro, S9 incubations from this study

;metabolites ZENGLU, scaled maximum rates of metabolism, (µmol/h)
VMaxSIZENGLU = VmaxSIZENGLUc/1000*60*S9SI*SI*BW

;metabolites ZENGLU, affinity constants, (µmol/L)
KmSIZENGLU = 1.174               ;in vitro, S9 incubations from this study
; ---------------------------------------------------------------------------------------------------------------
;metabolism of large intestine lumen (microbiota compartment)

;scaling factors
VMB = 0.0018                     ;fraction of faeces of BW (Rose et al., 2015)

; metabolites α-ZEL and β-ZEL, unscaled maximum rates of metabolism, (pmol/h/g faeces)
VmaxLIaZELc=0.054                ;in vitro, anaerobic rat fecal incubations
VmaxLIbZELc= 0.0108              ;in vitro, anaerobic rat fecal incubations

; metabolites α-ZEL and β-ZEL, scaled maximum rates of metabolism, (µmol/h)
VmaxLIaZEL= VmaxLIaZELc/1000000*1000 *VMB*BW
VmaxLIbZEL= VmaxLIbZELc/1000000*1000 *VMB*BW

; metabolites α-ZEL and β-ZEL, affinity constants, (µmol/L)
KmLIaZEL = 135                   ;in vitro, anaerobic rat fecal incubations
KmLIbZEL = 163                   ;in vitro, anaerobic rat fecal incubations

; ---------------------------------------------------------------------------------------------------------------
;metabolism of liver

;scaling factors

VLS9 = 120.7                     ; liver S9 protein yield, (mg S9 protein/gram liver) (Cubitt et al., 2011)
L=VLc*1000      {gram/kg BW}     ;liver

;Part 1: Zearalenone phase I metabolism α-ZEL and β-ZEL formation

;metabolites α-ZEL and β-ZEL, unscaled maximum rates of metabolism, (pmol/min/mg S9 protein)
(Malekinejad et al., 2006)
VmaxLaZELc= 358.7
```

```
VmaxLbZELc= 209.3

; metabolites α-ZEL and β-ZEL, scaled maximum rates of metabolism, (µmol/h)
VmaxLaZEL = VmaxLaZELc/1000000*60* VLS9 *L*BW
VmaxLbZEL= VmaxLbZELc/1000000*60* VLS9 *L*BW

; metabolites α-ZEL and β-ZEL, affinity constants, (µmol/L) (Mendez-Catala et al., 2020)
KmLaZEL = 9
KmLbZEL = 23

; Part 2: Zearalenone phase II metabolism-glucuronidation

; metabolites ZENGLU, unscaled maximum rates of metabolism, (nmol/min/mg S9 protein)
VmaxLZENGLUc=2.97    ;in vitro, S9 incubations from this study

; metabolites ZENGLU, scaled maximum rates of metabolism, (µmol/h)
VmaxLZENGLU = VmaxLZENGLUc /1000*60* VLS9 *L*BW

; metabolites ZENGLU, affinity constants, (µmol/L)
KmLZENGLU = 2.043                ;in vitro, S9 incubations from this study

; Part 3: α-ZEL phase II metabolism: glucuronidation

; metabolites α-ZELGLU, unscaled maximum rates of metabolism, (nmol/min/mg S9 protein)
VmaxLaZELGLUc= 2.983             ;in vitro, S9 incubations from this study

; metabolites α-ZELGLU, scaled maximum rates of metabolism, (µmol/h)
VmaxLaZELGLU = VmaxLaZELGLUc/1000*60* VLS9 *L*BW

; metabolites α-ZELGLU, affinity constants, (µmol/L)
KmLaZELGLU =2.415                ;in vitro, S9 incubations from this study

;==================================================================
; Run settings
;==================================================================
;molecular weight
MWZEN = 318.37           ;molecular weight ZEN
; ----------------------------------------------------------------------------------------------------
;oral dose ODOSEmg = 8                          {mg/kg bw}      ;oral dose, variable
ODOSEumol= ODOSEmg*1000/MWZEN*BW       {µmol}          ;unit change to µmol
; time
Starttime = 0      {h}
Stoptime = 24      {h}                                          ;variable

DTMIN = 1e-6    ;minimum integration time (DT)
DTMAX = 0.15   ;maximum integration time (DT)
;==================================================================
; Main model calculations/dynamics: zearalenone
;==================================================================
; ----------------------------------------------------------------------------------------------------
; Stomach
; Ast = amount in stomach
Ast' = -ksto*Ast

Init Ast = 0
; ----------------------------------------------------------------------------------------------------
; small intestine lumen compartment
; intestines, divided in 7 compartments
; Ain1 = Amount ZEN in intestine compartment 1 (µmol)
Cin1 = Ain1/Vin1
```

```
Ain1' = ksto*Ast - kin1*Ain1- kabin1*Cin1
Init Ain1 = 0

; Ain2 = Amount ZEN in intestine compartment 2 (µmol)
Cin2 = Ain2/Vin2
Ain2' = kin1*Ain1 - kin2*Ain2 - kabin2*Cin2
Init Ain2 = 0

; Ain3 = Amount ZEN in intestine compartment 3 (µmol)
Cin3 = Ain3/Vin3
Ain3' = kin2*Ain2 - kin3*Ain3 - kabin3*Cin3
Init Ain3 = 0

; Ain4 = Amount ZEN in intestine compartment 4 (µmol)
Cin4 = Ain4/Vin4
Ain4' = kin3*Ain3 - kin4*Ain4 - kabin4*Cin4
Init Ain4 = 0

; Ain5 = Amount ZEN in intestine compartment 5 (µmol)
Cin5 = Ain5/Vin5
Ain5' = kin4*Ain4 - kin5*Ain5 - kabin5*Cin5
Init Ain5 = 0

; Ain6= Amount ZEN in intestine compartment 6 (µmol)
Cin6 = Ain6/Vin6
Ain6' = kin5*Ain5 - kin6*Ain6 - kabin6*Cin6
Init Ain6 = 0

; Ain7= Amount ZEN in intestine compartment 7 (µmol)
Cin7 = Ain7/Vin7
Ain7' = kin6*Ain6 - kin7*Ain7 - kabin7*Cin7
Init Ain7 = 0
; ----------------------------------------------------------------------------------------------------------------
;small intestine tissue compartment
; ASIZEN: amount of ZEN in small intestinal tissue, (µmol)
ASIZEN' = kabin1*Cin1+ kabin2*Cin2+ kabin3*Cin3+ kabin4*Cin4+ kabin5*Cin5+ kabin6*Cin6+
kabin7*Cin7+ QSI*(CB- CVSIZEN) - ASIZENGLU'
        Init ASIZEN=0
        CSIZEN = ASIZEN/VSI
        CVSIZEN = CSIZEN/PIZEN

; ASIZENGLU: amount of ZEN metabolized to metabolite ZENGLU, (µmol)
        ASIZENGLU'= VmaxSIZENGLU*CVSIZEN/(KmSIZENGLU+ CVSIZEN)
        Init ASIZENGLU=0
; ----------------------------------------------------------------------------------------------------------------
; large intestine lumen compartment: microbial activity
; ALIZEN: amount of ZEN in large intestine lumen, (µmol)
        ALIZEN' = kin7*Ain7 - ALIaZEL' - ALIbZEL' - Kb*CLIZEN - KfeZ*ALIZEN
        Init ALIZEN = 0
        CLIZEN = ALIZEN/ (VMB*BW)
; ALIaZEL: amount of α-ZEL formed due to gut microbial activity, (µmol)
        ALIaZEL'= VmaxLIaZEL*CLIZEN/(KmLIaZEL + CLIZEN)
        Init ALIaZEL=0

; ALIbZEL: amount of β-ZEL formed due to gut microbial activity, (µmol)
        ALIbZEL'= VmaxLIbZEL * CLIZEN/(KmLIbZEL + CLIZEN)
        Init ALIbZEL=0
; ----------------------------------------------------------------------------------------------------------------
; liver compartment
; ALZEN: amount of ZEN in liver, (µmol)
```

```
        ALZEN' = QL*CB+QSI* CVSIZEN-(QL+QSI)*CVLZEN - ALaZEL' - ALbZEL'- ALZENGLU' +
Kb* CLIZEN
        Init ALZEN=0 CLZEN = ALZEN/VL
        CVLZEN = CLZEN/PLZEN

; ALaZEL: amount of ZEN metabolized to metabolite α-ZEL in liver, (µmol)
        ALaZEL'= VmaxLaZEL* CVLZEN /(KmLaZEL+ CVLZEN)
        Init ALaZEL=0
; ALbZEL: amount of ZEN metabolized to metabolite β-ZEL in liver, (µmol)
        ALbZEL'= VmaxLbZEL* CVLZEN /(KmLbZEL+ CVLZEN)
        Init ALbZEL=0

; ALZENGLU: amount of ZEN metabolized to metabolite ZENGLU in liver, (µmol)

        ALZENGLU'= VmaxLZENGLU* CVLZEN/(KmLZENGLU+ CVLZEN)
        Init ALZENGLU=0
; ---------------------------------------------------------------------------------------------------
;fat compartment
; AF = amount of ZEN in fat tissue, (µmol)
AF' = QF*(CB-CVF)
Init AF = 0
CF = AF/VF
CVF = CF/PFZEN
; ---------------------------------------------------------------------------------------------------
;rapidly perfused tissue
;AR = amount of ZEN in rapidly perfused tissue, (µmol)
AR' = QR*(CB-CVR)
Init AR = 0
CR = AR/VR
CVR = CR/PRZEN
; ---------------------------------------------------------------------------------------------------
;slowly perfused tissue
;AS = amount of ZEN in slowly perfused tissue, (µmol)
AS' = QS*(CB-CVS)
Init AS = 0
CS = AS/VS
CVS = CS/PSZEN
; ---------------------------------------------------------------------------------------------------
;blood compartment
;AB: amount of ZEN in blood, (µmol)
AB' = (QL+QSI)*CVLZEN + QF*CVF + QS*CVS + QR*CVR - QC*CB - KurZ*AB
Init AB = 0
CB = AB/VB AUC'=AB
Init AUC=0
; ---------------------------------------------------------------------------------------------------
; urinary excretion
AZur' = KurZ*AB
Init AZur = 0
;=================================================================
; Main model: mass balance calculation
;=================================================================
Total = ODOSEumol
Calculated = Ast+ Ain1 + Ain2 + Ain3 + Ain4 + Ain5 + Ain6 + Ain7+ ASIZEN +ASIZENGLU + ALIZEN+
ALIaZEL + ALIbZEL+ ALZEN + ALaZEL + ALbZEL+ALZENGLU + AF + AR + AS + AB + AZur + AZfe

ERROR=((Total-Calculated)/Total+1E-30)*100
MASSBBAL=Total-Calculated + 1
;=================================================================
; Sub-model calculations/dynamics: α-ZEL
;=================================================================
```

```
; large intestine lumen compartment
;ARLIaZEL = amount of α-ZEL in large intestine lumen, (μmol)
        ARLIaZEL' = ALIaZEL' - kabin8*(ARLIaZEL/VMB*BW) - KfeaZ*ARLIaZEL
        init ARLIaZEL = 0
; ---------------------------------------------------------------------------------------------------------
;liver compartment

;ARLaZEL: amount of α-ZEL in liver, (μmol)
ARLaZEL' = ALaZEL'+kabin8*(ARLIaZEL/VMB*BW) + (QL+QSI)*CBaZEL - (QL+QSI)*CVLaZEL -
ALaZELGLU'
        Init ARLaZEL= 0
        CLaZEL = ARLaZEL/VL
        CVLaZEL = CLaZEL/PLaZEL

;ALaZELGLU: amount of α-ZEL glucuronide in liver
        ALaZELGLU'= VmaxLaZELGLU* CVLaZEL/(KmLaZELGLU + CVLaZEL)
        Init ALaZELGLU=0

ALaZELGLUmg' = ALaZELGLU*MWZEN/1000*BW
Init ALaZELGLUmg = 0
; ---------------------------------------------------------------------------------------------------------
;fat compartment
;AFaZEL: amount of α-ZEL in fat tissue, (μmol)
        AFaZEL' = QF*(CBaZEL-CVFaZEL)
        Init AFaZEL = 0
        CFaZEL = AFaZEL/VF
        CVFaZEL = CFaZEL/PFaZEL
; ---------------------------------------------------------------------------------------------------------
;rapidly perfused tissue
;ARaZEL: amount of α-ZEL in rapidly perfused tissue, (μmol)
        ARaZEL' = QR*(CBaZEL-CVRaZEL)
        Init ARaZEL = 0
        CRaZEL = ARaZEL/VR
        CVRaZEL = CRaZEL/PRaZEL
; ---------------------------------------------------------------------------------------------------------
;slowly perfused tissue
;ASaZEL: amount of α-ZEL in slowly perfused tissue, (μmol)
        ASaZEL' = QS*(CBaZEL-CVSaZEL)
        Init ASaZEL = 0
        CSaZEL = ASaZEL/VS
        CVSaZEL = CSaZEL/PSaZEL
; ---------------------------------------------------------------------------------------------------------
;blood compartment
;ABaZEL: amount of α-ZELin blood, (μmol)
ABaZEL' = (QL+QSI)*CVLaZEL + QF*CVFaZEL + QR*CVRaZEL + QS*CVSaZEL - QC*CBaZEL -
KuraZ*ABaZEL
        Init ABaZEL= 0
        CBaZEL = ABaZEL/VB
        AUCaZEL'=ABaZEL
        Init AUCaZEL=0
; ---------------------------------------------------------------------------------------------------------
;urinary excretion
AaZur' = KurZ*ABaZEL
Init AaZur = 0
; ---------------------------------------------------------------------------------------------------------
;fecal excretion
AaZfe' = KfeaZ*ARLIaZEL
Init AaZfe = 0
;=========================================================================
;Sub-model calculations for ZENG excretion
```

;==========
;ZEN and α-ZEL-glucuronide available for recirculation and urinary excretion (Labib et al., 2013; Teeguarden et al., 2005)

;Calculations for urinary excretion of the glucuronides assuming 90% is available for excretion via urine ADG'= 0.9*ALZENGLU - KurG*ADG
Init ADG = 0

AZGur' = KurG*ADG' ;Amount of ZEN-glucuronide excreted in urine Init AZGur =0

References

Brown, R. P., Delp, M. D., Lindstedt, S. L., Rhomberg, L. R., and Beliles, R. P. (1997). Physiological parameter values for physiologically based pharmacokinetic models. *Toxicology and industrial health* **13**, 407-484.

Cubitt, H. E., Houston, J. B., and Galetin, A. (2011). Prediction of human drug clearance by multiple metabolic pathways: integration of hepatic and intestinal microsomal and cytosolic data. *Drug metabolism and disposition* **39**, 864-873.

DeJongh, J., Verhaar, H. J., and Hermens, J. L. (1997). A quantitative property-property relationship (QPPR) approach to estimate in vitro tissue-blood partition coefficients of organic chemicals in rats and humans. *Archives of Toxicology* **72**, 17-25.

Kimura, T., and Higaki, K. (2002). Gastrointestinal transit and drug absorption. *Biological and Pharmaceutical Bulletin* **25**, 149-164.

Labib, S., Guo, C. H., Williams, A., Yauk, C. L., White, P. A., and Halappanavar, S. (2013). Toxicogenomic outcomes predictive of forestomach carcinogenesis following exposure to benzo (a) pyrene: relevance to human cancer risk. *Toxicology and applied pharmacology* **273**, 269-280.

Malekinejad, H., Maas-Bakker, R., and Fink-Gremmels, J. (2006). Species differences in the hepatic biotransformation of zearalenone. *The Veterinary Journal* **172**, 96-102.

Mendez-Catala, D. M., Spenkelink, A., Rietjens, I. M., and Beekmann, K. (2020). An in vitromodel to quantify interspecies differences in kinetics for intestinal microbial bioactivation and detoxification of zearalenone. *Toxicology Reports* **7**, 938-946.

Mukherjee, D., Royce, S. G., Alexander, J. A., Buckley, B., Isukapalli, S. S., Bandera, E. V., Zarbl, H., and Georgopoulos, P. G. (2014). Physiologically-based toxicokinetic modeling of zearalenone and its metabolites: Application to the Jersey girl study. *PLoS One* **9**, e113632.

Peters, S. A., Jones, C. R., Ungell, A.-L., and Hatley, O. J. (2016). Predicting drug extraction in the human gut wall: assessing contributions from drug metabolizing enzymes and transporter proteins using preclinical models. *Clinical pharmacokinetics* **55**, 673-696.

Pfeiffer, E., Kommer, A., Dempe, J. S., Hildebrand, A. A., and Metzler, M. (2011). Absorption and metabolism of the mycotoxin zearalenone and the growth promotor zeranol in Caco-2 cells in vitro. *Molecular nutrition & food research* **55**, 560-567.

Punt, A., Freidig, A. P., Delatour, T., Scholz, G., Boersma, M. G., Schilter, B., van Bladeren, P. J., and Rietjens, I. M. (2008). A physiologically based biokinetic (PBBK) model for estragole bioactivation and detoxification in rat. *Toxicology and applied pharmacology* **231**, 248-259.

Reilly, J. A., Forst, C. F., Quigley, E. M., and Rikkers, L. F. (1990). Gastric emptying of liquids and solids in the portal hypertensive rat. *Digestive diseases and sciences* **35**, 781-786.

Rose, C., Parker, A., Jefferson, B., and Cartmell, E. (2015). The characterization of feces and urine: a review of the literature to inform advanced treatment technology. *Critical reviews in environmental science and technology* **45**, 1827-1879.

Sun, D., Lennernas, H., Welage, L. S., Barnett, J. L., Landowski, C. P., Foster, D., Fleisher, D., Lee, K.-D., and Amidon, G. L. (2002). Comparison of human duodenum and Caco-2 gene expression profiles for 12,000 gene sequences tags and correlation with permeability of 26 drugs. *Pharmaceutical research* **19**, 1400-1416.

Teeguarden, J. G., Waechter Jr, J. M., Clewell III, H. J., Covington, T. R., and Barton, H. A. (2005). Evaluation of oral and intravenous route pharmacokinetics, plasma protein binding, and uterine tissue dose metrics of bisphenol A: a physiologically based pharmacokinetic approach. *Toxicological Sciences* **85**, 823-838.

Vdoviaková, K., Petrovová, E., Maloveská, M., Krešáková, L., Teleky, J., Elias, M. Z. J., and Petrášová, D. (2016). Surgical anatomy of the gastrointestinal tract and its vasculature in the laboratory rat. *Gastroenterology research and practice* **2016**.

Supplementary material 2.

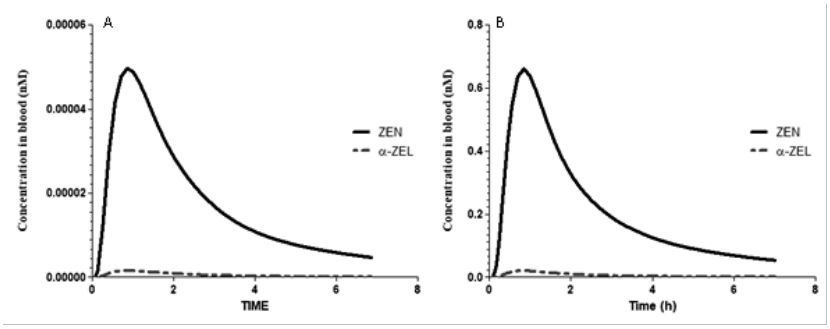

Figure S1. PBK model predicted time dependent blood concentration of ZEN and α-ZEL in human upon oral doses of 1.43×10^{-4} and 1.43 mg/kg bw.

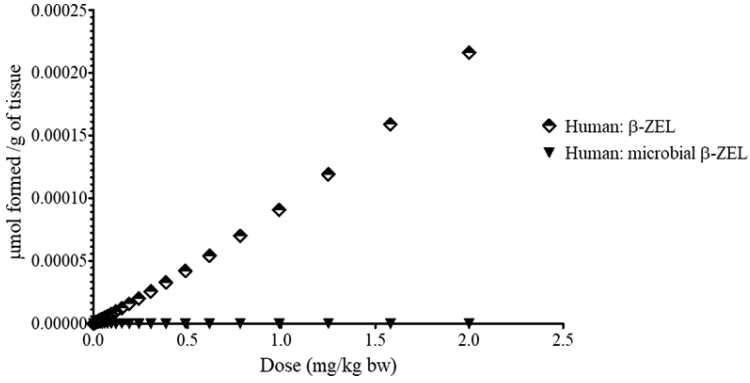

Figure S2. Predicted formation of α-ZEL in liver and from microbial metabolism at different dose levels in humans.

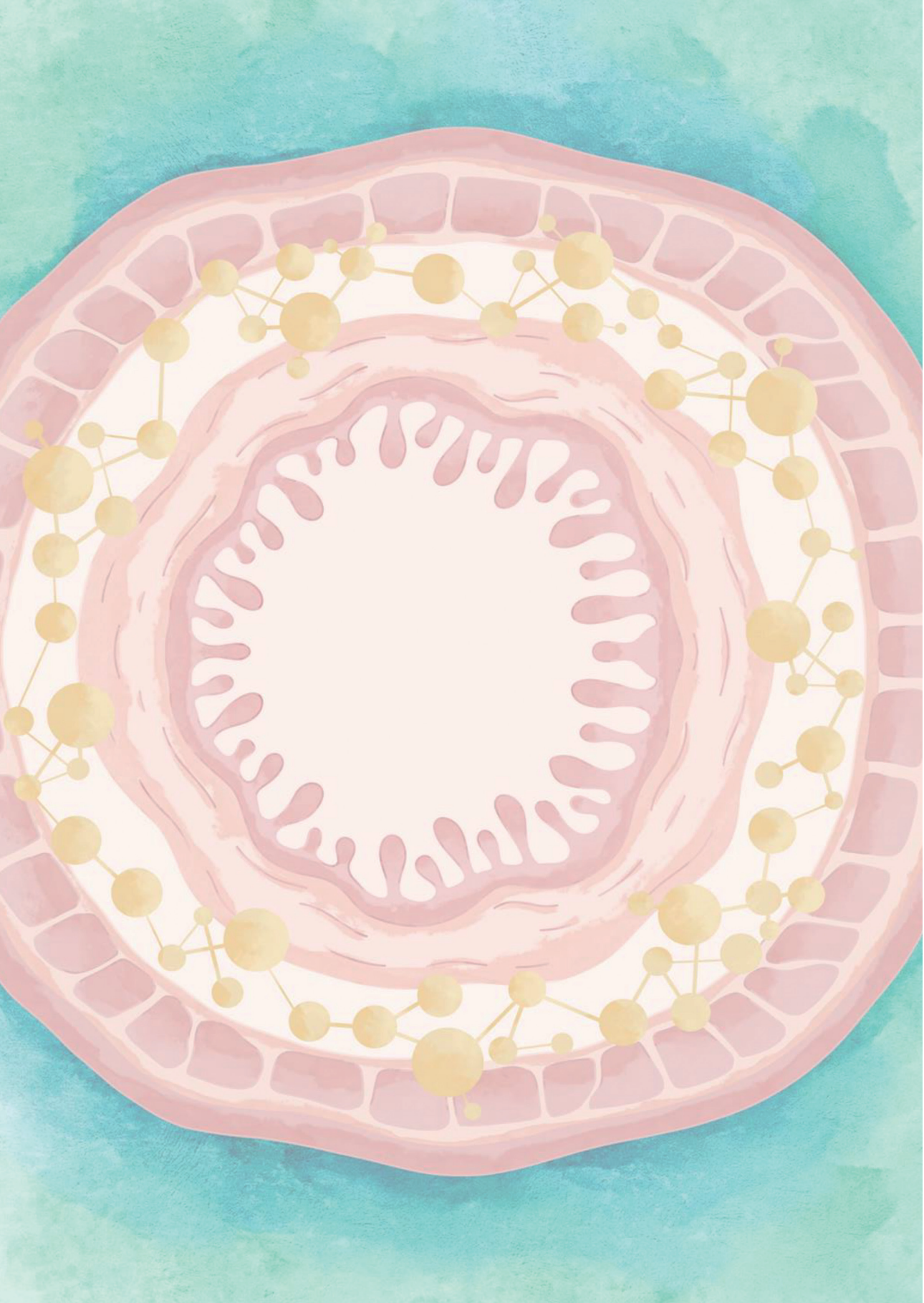

Chapter 5

Integrating physiologically based kinetic (PBK) and Monte Carlo modeling to predict the interindividual human variability in metabolism of daidzein

Qianrui Wang, Ivonne M.C.M. Rietjens, Bert Spenkelink, Sebastiaan Wesseling and Marije Strikwold

In preparation

Abstract

Daidzein is a dietary isoflavone abundantly present in soybean products and referred to as a phytoestrogen. Upon ingestion of daidzein, it enters the systemic circulation or is converted to dihydrodaidzein (DHD), and subsequently to S-equol, or O-desmethylangolensin (O-DMA) in the intestinal lumen by gut microbiota. To assess interindividual differences in the maximum blood concentration (C_{max}) of daidzein in humans, a previously developed physiologically based kinetic (PBK) model for daidzein in human was integrated with Monte Carlo simulations to obtain the population-based distribution of free C_{max} expressed in daidzein equivalents. Kinetic variations in gut microbial metabolism and liver glucuronidation of daidzein obtained from in vitro experiments, together with 7 other parameters shown to be influential in the PBK model were the variable parameters for the Monte Carlo simulation. Chemical-specific adjustment factors (CSAFs) subsequently derived at the 95th and 99th percentiles, being 1.97 and 2.54 respectively, indicated that the default uncertainty factor for interindividual differences in kinetics of 3.16 is protective for the healthy adult population. Additionally, comparing our predictions with dietary intake values indicate that the sensitive as well as the average humans following Asian diets and/or taking daidzein supplements according the manufacturers recommended dosage, may exceed the benchmark dose lower confidence limit that result in 10% estrogenic effect. Altogether, the application of PBK modeling integrated with Monte Carlo simulations appeared a promising new approach methodology (NAM) to assess interindividual human variability in kinetics and to refine the in vivo safety and/or effect levels of foodborne chemicals.

1. Introduction

The isoflavone daidzein belongs to the group of isoflavonoids and is abundantly present in soybean and soybean products (Atkinson et al., 2005). Due to the structural similarity with the naturally occurring hormone 17β-estradiol (E2), daidzein can exert estrogenic activity and is referred to as a phytoestrogen (Haron et al., 2009). Upon ingestion, daidzein enters the intestinal lumen where it is partly taken up into the systemic circulation via the enterocytes, while another part is further translocated to the large intestine where it is converted by gut microbiota to dihydrodaidzein (DHD), and subsequently to S-equol and/or O-desmethylangolensin (O-DMA) (Gardana et al., 2009; Schwen et al., 2012). The formation of S-equol is a bioactivation pathways since S-equol is reported to be a more potent estrogen than its parent compound daidzein, while the formation of O-DMA is a pathway of detoxification (Magee, 2011). Being absorbed into the systemic circulation, daidzein further undergoes conjugation in the liver, predominantly glucuronidation mediated by UDP-glucuronosyltransferases (UGTs), and to a lesser extent sulfation, the latter with a catalytic efficiency (CE) of less than half that of glucuronidation (Islam et al., 2014). The conjugates of daidzein are more hydrophilic than their parent compound, and not active as an estrogen, thus providing a detoxification route with respect to estrogenicity (Islam et al., 2015). The conjugates are excreted mostly in urine and in feces via biliary excretion (Pritchett et al., 2008; Qiu et al., 2005).

Interindividual differences have been widely observed both in gut microbial and hepatic metabolism of daidzein, which may potentially affect the ultimate estrogenicity of daidzein exposure. For microbial metabolism, differences in diet, age, gender and genetic influences of the host, as well as external factors such as environment and exposure to xenobiotics, may affect the composition and abundance of the gut microbiota thereby influencing the microbial conversion of daidzein (Catalkaya et al., 2020; Clarke et al., 2014; Karlsson et al., 2013). It is known that only a subset of the human population is capable to metabolise daidzein to S-equol in the gut (Arai et al., 2000; Atkinson et al., 2005), potentially leading to interindividual variations in the estrogenic related effects upon daidzein exposure. Except for intestinal metabolism, interindividual differences in the hepatic conjugation of daidzein, dominantly glucuronidation, may originate from variation in the activity of UGTs such as the isoforms UGT1A1 and UGT1A9 (Jiang & Hu, 2012; Pritchett et al., 2008), with the UGT1A9 reported to have a coefficient of variation (CV) of 36% among the human population for the glucuronidation of daidzein (Achour et al., 2017). All these variations potentially contribute to

interindividual differences in internal exposure levels of daidzein and its metabolites, and hence the ultimate estrogenicity, but this has not been quantified so far.

As a useful tool, physiological based kinetic (PBK) modeling integrated with Monte Carlo simulations has been applied to predict human interindividual and interethnic differences in the kinetics of (foodborne) compounds facilitating the prediction of differences in compound induced toxicity within and between populations (Ning et al., 2019; Punt et al., 2016; Strikwold et al., 2017). Within the risk assessment of compounds, interindividual differences are accounted for by the use of uncertainty factors when establishing health-based guidance values. By default, an interindividual uncertainty factor of 10 consisting of two times an uncertainty factor of 3.16, one for the kinetic and one for the dynamic interindividual differences, are applied to Point of Departure (PoD) values, such as a No Observed Adverse Effect Level (NOAEL) or a benchmark dose lower confidence limit (BMDL). For some compounds, though, these default uncertainty factors do not sufficiently capture the interindividual differences within the population (Ning et al., 2019) and as an alternative, chemical specific adjustment factors (CSAF) can be applied, introduced by the International Programme on Chemical Safety (IPCS) (WHO, 2005). The CSAF for interindividual differences in kinetics can be derived from population distribution data on the internal concentration (e.g. blood concentration) of the compound of interest and/or its active metabolite (WHO, 2005), which can be defined by PBK modeling integrated with Monte Carlo simulations.

In our previous study, a human PBK model with a separate microbiota compartment for the average human was developed and validated. The PBK model consisted of a main model for daidzein and a submodel for S-equol to allow prediction of their respective blood levels (Wang et al., 2021). Additionally, the PBK model facilitates the translation of in vitro derived estrogenic effect-concentrations of daidzein from the estrogen receptor (ER) α-CALUX assay, toward in vivo estrogenic dose-response data of daidzein by applying reverse dosimetry. To enable PBK model-facilitated reverse dosimetry to predict in vivo estrogenicity upon daidzein exposure, S-equol concentrations were taken into account by expressing its blood C_{max} levels in daidzein equivalents, thereby incorporating the S-equol concentration based on a relative potency for estrogenicity of 13 compared to daidzein (Wang et al., 2020). As outlined above, variation among individuals in terms of daidzein gut microbial conversion, hepatic metabolism and other influential parameters are present within the population. Therefore, the aim of the present study was to study the effect of variations in intestinal and hepatic

metabolism as well as in other parameters that appeared influential for the PBK model predictions on free C_{max} expressed in daidzein equivalents, and to derive CSAFs by applying PBK modeling integrating with Monte Carlo simulations, enabling the refinement of the risk assessment of daidzein.

2. Materials and methods

2.1 Chemicals and materials

Daidzein, S-equol, dimethylsulfoxide (DMSO), glycerol, tromethamine (Tris), alamethicin and trifluoroacetic acid (TFA) were purchased from Merck (Zwijndrecht, The Netherlands). DHD was obtained from Cayman Chemical (AA, USA) and O-DMA was obtained from Plantech (Reading, UK). Uridine 5′-diphosphoglucuronic acid (UDPGA) was purchased from Carbosynth (Berkshire, UK). Daidzein-7-O glucuronide and daidzein-4'-O glucuronide were purchased from Extrasynthese (Genay, France) and Toronto Research Chemicals (Toronto, Canada), respectively.

$MgCl_2$ and 37% HCl were supplied by VWR International BV (Amsterdam, The Netherlands). Acetonitrile (ACN) and methanol were purchased from Biosolve (Valkenswaard, The Netherlands) Phosphate Buffer Saline (PBS) was purchased from Gibco (Paisley, UK) and Para-Pak SpinCon™ stool concentration system was supplied by Meridian Bioscience (Amsterdam, The Netherlands). Human liver S9 proteins from 25 individuals were provided by Tebu-bio (Heerhugowaard, The Netherlands). The Hitmac CT 15RE centrifuge used was from VMR International BV (Leuven, Belgium) and the Bactron300 anaerobic chamber was from Sheldon Manufacturing Inc. (OR, USA).

2.2 General outline for PBK modeling and Monte Carlo simulation

The present study consists the following steps: 1) the metabolism of daidzein by gut microbiota was quantified using fecal samples from 24 individuals and the glucuronidation of daidzein in liver was characterised using liver S9 proteins from 25 individuals. From this, individual kinetic data and the CVs of the kinetics from respectively the 24 and the 25 individuals were obtained. 2) interindividual variation in the gut microbial metabolism, in the hepatic glucuronidation, and in 7 additional parameters shown to be influential in the sensitivity analysis (Wang et al., 2021) were included in the Monte Carlo simulation to predict interindividual variation in the free C_{max} expressed in daidzein equivalents. 3) CSAFs

were derived from the results of the Monte Carlo simulation, covering the 95th and 99th percentile of the population. 4) PBK modeling-based reverse dosimetry was carried out converting in vitro estrogenicity data obtained in the ERα-CALUX assay to in vivo dose-response curves for estrogenicity of daidzein in the average population and the sensitive populations (95th and 99th percentile).

2.3 Microbial metabolism of daidzein in incubations with fecal samples

In vitro fecal anaerobic incubations were performed for daidzein. First, human feces were collected from healthy adults, including both Asian and Western individuals, with some exclusion criteria (no pregnancy, no bowl complaints, no use of antibiotics for the last 3 months and no visit of tropical countries in the past 3 months) resulting in 24 eligible samples. Each donor provided a one-time donation of around 5 grams of feces. The collection of human feces was done anonymous so that samples could not be linked to a specific donor. Information on gender, and age was collected for the donors and they included 9 males and 15 females ranging from 19 to 65 years of age. Approval of the study design was obtained from the Medical Ethics Reviewing Committee of Wageningen University (METC-WU). Upon review of the research protocol the METC-WU concluded that this research does not fall within the remit of the Dutch 'Medical Research Involving Human Subjects Act'.

Immediately upon donation, fecal samples were weighed and transferred into an anaerobic chamber (85% N_2, 10% CO_2, and 5% H_2) for further processing. The collected fecal samples were diluted five times (w/v) with an anaerobic solution consisting of 10% (v/v) glycerol in PBS, and was manually mixed by a stirring rod to dissipate large particles. Subsequently, they were filtered using filter tubes (the Para-Pak SpinCon™ stool concentration system) and centrifuged at 2,500 × g for 5 min at 4°C. The resulting fecal suspension was collected, aliquoted, and stored at −80°C until use.

To obtain kinetic parameters describing gut microbial conversion of daidzein for each donor, the obtained fecal samples were incubated in an anaerobic chamber under the conditions reported previously (Wang et al., 2021) with some modifications. In short, each incubation mixture of 100 µL was prepared in anaerobic PBS containing 1-100 µM daidzein (added from a 200-times concentrated stock solution dissolved in DMSO) and 60 mg/mL feces (final concentration) from an individual donor. Blank and negative controls were without daidzein (replaced by DMSO) and without feces (replaced by PBS), respectively. After incubating for

1 hour at 37°C, 100 µL ice-cold methanol was added to each mixture to terminate the reaction. Subsequently, samples were put on ice for 10 min and centrifuged at 21,500 × g for 15 min at 4°C. Supernatants were transferred into LC-MS vials for immediate quantification. Experiments were independently repeated three times using the same batches of individual fecal materials. Previous studies already showed that under these conditions daidzein metabolite formation was linear in time and with the amount of fecal sample (Wang et al., 2021).

2.4 Liver S9 mediated glucuronidation of daidzein

Individual liver S9 incubations with daidzein were carried out for liver S9 samples from 25 individuals (detailed information of donors provided in **Supplementary material Table S1**) to obtain their daidzein glucuronidation kinetic parameters. Incubation conditions were adapted from a previously reported method (Islam et al., 2014) with some modifications. Incubation mixtures of 100 µL were prepared containing (final concentrations) 10 mM $MgCl_2$, 10 mM UDPGA, 0.025 mg/mL alamethicin (added from a 200-times concentrated stock solution in methanol) and 0.5 mg S9 protein/mL human liver S9 fraction in 50 mM Tris-HCl (pH 7.4). After a 5-min pre-incubation in a shaking water bath at 37°C, 1 µL of the substrate daidzein (final concentrations ranging from 1 µM to 200 µM, added from 100-times concentrated stock solutions in DMSO) was added to start the reaction. After 10-min incubation in a shaking water bath at 37°C, 25 µL ice-cold ACN was added to terminate the reaction. Negative and blank controls were performed in the absence of either the substrate daidzein (replaced by DMSO) or UDPGA (replaced by Tris-HCl). Samples were subsequently centrifuged at 21,500 × g for 15 min at 4°C to precipitate proteins. Supernatants were transferred into UPLC vials for immediate quantification. Experiments were independently repeated three times using the same batch of individual liver S9 materials. Previous studies already showed that under these conditions daidzein glucuronidation was linear in time and with the amount of S9 protein (Islam et al., 2015).

2.5 LC-MS quantification of the microbial metabolites DHD, S-equol and O-DMA

To quantify the concentrations of daidzein gut microbial metabolites DHD, S-equol and O-DMA, LC-MS analysis was performed using a Shimadzu LC-MS/MS–8040 system ('s-Hertogenbosch, The Netherlands). The system consisted of a high-performance liquid chromatography (LC) system and a triple quadrupole mass spectrometer (MS). The LC was

performed on a Kinetex XB-C18 100A analytical column (1.7 µm, 100×2.10 mm) and the MS contained an electrospray ionization (ESI) source which operated in positive mode. Data acquisition and processing were accomplished using Shimadzu LabSolutions LC/MS software (Kyoto, Japan).

Nanopure water with 0.1% TFA (v/v, mobile phase A) and ACN with 0.1% TFA (v/v, mobile phase B) were used to prepare the gradient using the following program: 5% B for 0-1.00 min, 5-50% B for 1.00-1.50 min, 50-100% B for 1.50-4.50 min, 100% B for 4.50-6.50 min, 100-5% B for 6.50-6.60 min and 5% B for 6.60-11.00 min. The LC column temperature was set at 40°C with a flow rate of 0.3 mL/min. The temperature was set at 250°C for desolvation line (DL) and at 400°C for heat block. The drying gas (N_2) and nebulizing gas (Ar) flows were 15 and 2 L/min, respectively.

The Multiple Reaction Monitoring positive (MRM+) mode was applied for the quantification of: DHD, with precursor (m/z) of 257.10 (MH^+) to products (m/z) 123.00 (collision energy (CE): -17 KV), 94.95 (CE: -28 KV) and 101.00 (CE: -11 KV); S-equol, with precursor (m/z) of 242.90 (MH^+) to products (m/z) 133.10 (CE: -17 KV), 123.00 (CE: -11 KV) and 105.20 (CE: -27 KV); O-DMA, with precursor (m/z) of 259.15 (MH^+) to products (m/z) 121.10 (CE: -25 KV), 149.10 (CE: -12 KV) and 80.95 (CE: -22 KV). Each injection was set at 10 µL. DHD, S-equol and O-DMA were quantified based on comparison of the respective peak areas to the peak areas of corresponding linear calibration curves prepared in PBS using commercially available standards.

2.6 UPLC quantification of daidzein and its glucuronides

To quantify the concentrations of daidzein and its liver S9 conjugated metabolites daidzein-7-O-glucuronide and daidzein-4'-O-glucuronide, UPLC analysis was performed using a Waters ACQUITY UPLC system (Etten-Leur, The Netherlands). The system was equipped with a Waters Acquity UPLC BEH C18 (1.7 µm, 2.1×50 mm) column and a photodiode array detector (PDA). Data acquisition and processing were accomplished using Waters EmPower software.

Nanopure water with 0.1% TFA (v/v, mobile phase A) and ACN (mobile phase B) were used for the gradient using the following program: 0% B for 0−0.2 min, 0-18% B for 0.20-0.40 min, 18% B for 0.40-3.00 min, 18-30% B for 3.00-3.50 min, 30-80% B for 3.50-5.00 min, 80-100% for 5.00-5.50 min, 100% B for 5.50-6.00, 100-0% B for 6.00-6.50 min and 0% B between

6.50-7.00 min. The column temperature was set at 40°C and the flow rate was 0.4 mL/min. Daidzein-7-O-glucuronide and daidzein-4'-O-glucuronide were quantified based on comparison of the respective peak areas to the peak areas of corresponding linear calibration curves prepared in Tris-HCl using commercial available standards, at a wavelength of 249 nm.

2.7 Determination of kinetic constants of the metabolites of daidzein

To obtain the kinetic constants, including the apparent maximum velocity (V_{max}) and the Michaelis-Menten constant (K_m), data on the substrate concentration-dependent rate of metabolite formation were fitted to the standard Michaelis-Menten equation:

$$v = \frac{V_{max} \times [S]}{K_m + [S]}$$

where v is the formation rate of the metabolite (expressed in nmol/h/g feces for fecal incubations or nmol/min/mg S9 protein for liver S9 incubations) and [S] represents the substrate concentration (expressed in μM). The kinetic analysis was performed using GraphPad Prism 5.04 (GraphPad Software, CA, USA).

For use in the PBK model, the obtained apparent V_{max} values (expressed in nmol/h/g feces) were scaled to the in vivo situation using a fecal fraction of 14 g feces/kg bw and an average body weight of 70 kg (Brown et al., 1997). V_{max} values (expressed in nmol/min/mg S9 protein) for daidzein glucuronidation were scaled to in vivo V_{max} values using an S9 protein yield of 143 mg S9 protein/g liver tissue for human (Cubitt et al., 2011).

2.8 Individual PBK models and Monte Carlo simulation

A previously developed PBK model for daidzein in human adult (Wang et al., 2021) was used in the present study to assess the interindividual differences upon exposure to daidzein. The model was designed with a main model for daidzein and a submodel for its gut microbial metabolite S-equol. Separate compartments for small intestine, large intestine, liver, fat, blood, rapidly and slowly perfused tissues, were included in the model, with the large intestine being the compartment enabling description of the microbial conversion of daidzein. Physiological, physiochemical and biochemical kinetic parameters previously defined were used in the PBK model to describe the fate of daidzein and S-equol within humans (Wang et al., 2021).

To assess interindividual variations in the predicted blood levels of daidzein and S-equol, two approaches were applied, using a single oral dose of 100 mg/day daidzein, representing an estimated daily intake of isoflavone supplements (Bresson et al., 2009). In the first approach, 24 individual models were defined using the individual kinetic parameters V_{max} and K_m for gut microbial conversion of daidzein obtained from individual fecal incubations (for the other parameters fixed values were used) and 25 individual models were defined using individual the kinetic parameters V_{max} and K_m for daidzein glucuronidation obtained from liver S9 incubations (for the other parameters fixed values were used). From the predicted C_{max} of daidzein and S-equol in blood, the total free C_{max} expressed in daidzein equivalents, was calculated for each model. Unbound fractions of 12.0% and 12.5% was used to correct the predicted C_{max} of daidzein and S-equol to their predicted free C_{max}, respectively (Csanady et al., 2002); a relative potency factor (RPF) of 1 was set for daidzein and 13 for S-equol for ERα activation, derived from the EC_{50} values obtained in the ERα-CALUX assay (Wang et al., 2020). Consequently, the free C_{max} expressed in daidzein equivalents was calculated by multiplying the C_{max} of daidzein and S-equol with their corresponding unbound fraction and RPF value and summarising.

In the second approach, a Monte Carlo simulation was performed connected with PBK modeling to simulate the population-based distribution of C_{max} in daidzein equivalents. Interindividual variations, including the kinetic variations in gut microbial conversion and liver glucuronidation of daidzein, as well as variations in 7 additional parameters were included in the Monte Carlo simulation. These 7 additional parameters were included because they were shown to be moderately or highly influential in the sensitivity analysis (Wang et al., 2021) with an absolute value of normalized sensitivity coefficient (NSC) over 0.2 (Li et al., 2017).

Table 1 presents the mean and CV of the 7 additional parameters. When a CV was not available, a default CV of 30% was applied representing a moderate level of variation (Covington et al., 2007). Variation of parameters in covariant with body weight, including fractions of organ/tissue or blood flow, were not included and considered to be represented by the variation in body weight. All parameters were regarded to be log-normally distributed. For the other parameters, fixed values were used.

Table 1. Mean and coefficients of variation (CV) of 7 additional variable parameters included in the PBK modeling integrated with Monte Carlo simulations. Parameters stand for: Ka,

absorption rate of daidzein taken up from lumen to small intestine; Kb, absorption rate of daidzein taken up from large intestine by liver; Ksl, transfer rate of daidzein from small intestine to large intestine; VmaxLDAISc, V_{max} for formation of daidzein sulfate by liver; VmaxLEQUSc, V_{max} for formation of S-equol sulfate by liver; KmLEQUS, K_m for formation of S-equol sulfate by liver.

Parameter	Mean	Reference	CV (%)	Reference
Body weight	70 (kg)	(Brown et al., 1997)	13.9	(Brown et al., 1997)
Ka	0.46 (/h)	(Steensma et al., 2004)	30	Default (Covington et al., 2007)
Kb	4.56 (/h)	(Steensma et al., 2004)	30	Default (Covington et al., 2007)
Ksl	1.16 (/h)	(Kimura & Higaki, 2002)	30	Default (Covington et al., 2007)
VmaxLDAISc	0.02 (nmol/min/mg S9 protein)	(Wang et al., 2020)	33.2	(Ronis et al., 2006)
VmaxLEQUSc	9.24 (nmol/min/mg S9 protein)	(Wang et al., 2021)	33.2	(Ronis et al., 2006)
KmLEQUS	6.5 (µmol/L)	(Wang et al., 2021)	7.1	(Adjei et al., 2008)

Given that Berkeley Madonna only offers the 'NORMAL' distribution function for sampling random numbers and not a lognormal function, the mean (μ_x) and standard deviations (σ_x) from the lognormally distributed parameters were transformed to parameters following a normal distribution using the following equation (Zhang et al., 2007):

$$\mu_w = \ln\left(\mu_x/\sqrt{1 + CV_x^2}\right)$$

and

$$\sigma_w^2 = \ln\left(1 + CV_x^2\right)$$

where μ_x is the mean for the respective input parameters in the Monte Carlo simulation, which in this study were the kinetic constants V_{max} or K_m obtained from either the fecal incubations

or the liver S9 incubations, or one of the 7 additional parameters described above; and CV_x is the CV of each parameter. Values were truncated within the range of mean ± 3 SD in the Monte Carlo simulation.

In total, 12,000 simulations were performed to obtain a population-based distribution of the free C_{max} expressed in daidzein equivalents, including 4,000 simulations for S-equol producers (accounting for 33% of the population) and 8,000 simulations for S-equol non-producers (accounting for 67% of the population), respectively. This frequency of S-equol producers, derived from the results of the fecal incubations (8 out of 24 individuals are S-equol producers, presented in the **Result 3.1**), was in line with the literature reporting that around 20%-50% of the whole population including Western as well as Asian individuals would be capable of producing S-equol, with the percentages being 20-30% for a Western population and 50% for an Asian population (Atkinson et al., 2005). Excluding 1.8% of the total 12,000 simulations with parameters beyond the range of mean ± 3 SD, the Monte Carlo simulation finally resulted in 11,789 valid individual free C_{max} values expressed in daidzein equivalents.

PBK modeling and Monte Carlo simulation were performed using Berkeley Madonna software version 10.2.8 (UC Berkeley, CA, USA). The output from the individual models and from Monte Carlo simulations was further analysed by Prism GraphPad 5.04 (GraphPad Software, CA, USA). The population-based distribution of free C_{max} expressed in daidzein equivalents resulting from Monte Carlo simulations allowed derivation of its geometric mean (GM), 95th and 99th percentile. CSAFs for interindividual differences in daidzein kinetics were subsequently obtained by dividing the 95th or 99th percentile of the predicted C_{max} of daidzein equivalents by the geometric mean (GM) (WHO, 2005).

2.9 PBK modeling-based reverse dosimetry and benchmark dose (BMD) analysis

PBK modeling-based reverse dosimetry was applied to extrapolate in vitro concentration response data to an in vivo dose-response curve for ERα activation by daidzein in human taking also the contribution of S-equol into account. To enable this, the in vitro concentration-response curve obtained from the ERα-CALUX assay (Wang et al., 2020) for daidzein was translated to an in vivo dose-response curve, using the developed human PBK model for daidzein (Wang et al., 2021) to calculate the oral dose of daidzein resulting in each effective concentration from the in vitro curve. This extrapolation from in vitro induced ERα activation

to in vivo estrogenicity was based on the free in vitro concentration which was set equal to the PBK model predicted free C_{max} expressed in daidzein equivalents. Since cell culture medium was prepared in albumin-free conditions, the in vitro concentrations were not corrected for protein binding (fub=1.0), assuming that the protein binding in the serum free medium was negligible, while the the free C_{max} expressed in daidzein equivalents was calculated from the C_{max} for daidzein and for S-equol taking their respective fub and RPF values into account as described above. Moreover, the in vivo dose-response curves for daidzein were defined for the average population, the 95th percentile and the 99th percentile of the population. The latter two curves were obtained by applying the respective CSAFs to the dose-response curve of the average population.

Subsequently, BMD analysis was performed for all three predicted in vivo dose-response curves regarding the estrogenicity of daidzein, to derive BMD values that give 10% response compared to the background. The lower and upper 95% confidence interval confidence of the BMD were defined as $BMDL_{10}$ and $BMDU_{10}$, respectively. The BMD analysis was performed in the web-tool provided by European Food Safety Authority (EFSA), using the R-package PROAST (version 66.20) available at https://shiny-efsa.openanalytics.eu/app/bmd. In short, four models, namely the Exponential, Hill, Inverse Exponential, and the Log-Normal Family models were fitted to the in vivo dose-response curves. These models were used for model averaging, where a lower Akaike's Information Criterion (AIC) value gives a larger weight to the respective model, and subsequently to its contribution to the derivation of a weighted average model. In total, 200 bootstrap runs were performed for calculating model-averaged BMD_{10} confidence intervals.

3. Results

3.1 Formation of daidzein microbial metabolites by incubations with individual fecal samples

Table 2 summarizes the kinetic constants V_{max} and K_m, and catalytic efficiency for the formation of the gut microbial metabolites DHD, S-equol and O-DMA in the anaerobic incubations of daidzein with 24 individual human fecal samples (individual kinetic curves are provided in **Supplementary material Figure S1**). Among these 24 individual fecal samples, 8 were capable of producing S-equol classifying the donors as S-equol producers, accounting

for 33% of the donors, while the other 16 donors, accounting for 67% of the donors, were classified as non-producers.

DHD was found to be the major metabolite among the three (or two for non S-equol producers) microbial metabolites of daidzein formed in the anaerobic fecal incubations. DHD was formed with an average catalytic efficiency (n=24) of 6.4 mL/h/g feces, calculated from a V_{max} of 29.1 nmol/h/g feces and a K_m of 6.3 µM, with a CV of 107%. In the incubations with fecal samples of S-equol producers (n=8), S-equol was formed with a V_{max} of 9.6 nmol/h/g feces and a K_m of 9.3 µM, resulting in a mean catalytic efficiency being 1.3 mL/h/g feces with a CV of 82.9%, which was 4.9-fold lower than the mean catalytic efficiency for formation of DHD. Formation of O-DMA was observed with a mean catalytic efficiency (n=24) of only 0.4 mL/h/g feces, being 16- and 3.3-fold lower than that of DHD and S-equol, respectively. The CV for the catalytic efficiency for O-DMA formation was relatively high, amounting to 157.6%, which was 1.5- and 1.9-fold higher than the CV for the catalytic efficiency for formation of DHD and S-equol, respectively. **Table 2** also presents the mean and CV values for the V_{max} and K_m as derived from the anaerobic fecal incubations, and these parameters were used as input for the subsequent individual PBK models and the Monte Carlo simulation.

Table 2. Kinetic parameters V_{max}, K_m and catalytic efficiency for the formation of DHD, S-equol and O-DMA by 24 individual human fecal samples.

Individual	DHD			S-equol			O-DMA		
	V_{max}[a]	K_m[b]	Catalytic efficiency[c]	V_{max}[a]	K_m[b]	Catalytic efficiency[c]	V_{max}[a]	K_m[b]	Catalytic efficiency[c]
1	23.3 ± 3.5	2.9 ± 2.7	8.1	3.4 ± 0.3	10.0 ± 3.4	0.34	0.5 ± 0.1	2.1 ± 1.7	0.2
2	37.5 ± 5.7	2.6 ± 2.6	14.5	-	-	n.a.[i]	2.4 ± 0.3	1.8 ± 1.8	1.3
3	1.4 ± 0.2	7.3 ± 6.0	0.2	-	-	n.a.	0.4 ± 0.05	11.7 ± 5.6	0.03
4	43.2 ± 5.5	18.8 ± 7.3	2.3	-	-	n.a.	9.0 ± 1.3	6.6 ± 4.3	1.4
5	15.0 ± 1.3	0.5 ± 0.4	28.5	-	-	n.a.	1.9 ± 0.3	10.0 ± 6.7	0.2
6	9.4 ± 1.2	14.0 ± 5.9	0.7	-	-	n.a.	0.2 ± 0.04	6.8 ± 6.3	0.03
7	18.0 ± 1.6	1.7 ± 1.1	10.4	-	-	n.a.	1.3 ± 0.1	2.6 ± 1.8	0.5

8	14.3 ± 2.3	8.6 ± 5.9	1.7	-	-	n.a.	0.4 ± 0.05	2.0 ± 1.8	0.2
9	9.3 ± 1.5	3.3 ± 3.2	2.8	15.2 ± 2.1	5.3 ± 3.7	2.9	1.4 ± 0.3	15.1 ± 11.0	0.09
10	27.6 ± 3.4	11.5 ± 5.3	2.4	-	-	n.a.	0.6 ± 0.1	10.2 ± 7.1	0.06
11	2.0 ± 0.3	1.8 ± 1.7	1.1	-	-	n.a.	0.3 ± 0.05	9.6 ± 7.2	0.03
12	4.6 ± 0.4	1.6± 0.9	2.9	3.1 ± 0.3	15.3 ± 4.2	0.20	0.3 ± 0.05	8.4 ± 6.1	0.03
13	14.5 ± 3.6	14.5 ± 12.2	1.0	-	-	n.a.	0.5 ± 0.1	19.7 ± 10.4	0.03
14	43.5 ± 4.1	2.9 ± 1.7	15.1	-	-	n.a.	11.7 ± 1.0	9.2 ± 3.3	1.3
15	2.3 ± 0.4	9.6 ± 7.6	0.2	-	-	n.a.	2.3 ± 0.8	36.0 ± 28.5	0.06
16	28.4 ± 2.1	5.4 ± 2.0	5.2	-	-	n.a.	1.0 ± 0.2	8.4 ± 6.3	0.1
17	3.9 ± 0.4	1.7 ± 1.2	2.3	-	-	n.a.	0.9 ± 0.2	13.4 ± 12.9	0.06
18	4.8 ± 0.3	1.5 ± 0.6	3.1	-	-	n.a.	1.3 ± 0.1	10.6 ± 4.2	0.1
19	140.0 ± 28.7	17.5 ± 11.3	8.0	20.8 ± 1.8	14.2 ± 4.3	1.46	0.3 ± 0.05	9.4 ± 6.6	0.03
20	14.6 ± 2.3	2.5 ± 2.5	5.9	12.9 ± 1.7	7.7 ± 4.4	1.7	2.3 ± 0.5	10.3 ± 8.7	0.2
21	158.3 ± 15.2	8.8 ± 3.5	18.0	11.0 ± 1.0	4.2 ± 2.1	2.6	7.6 ± 0.7	3.7 ± 2.0	2.1
22	66.8 ± 11.1	8.3 ± 5.8	8.1	8.1 ± 1.1	11.2 ± 5.9	0.71	0.5 ± 0.1	6.8 ± 5.8	0.08
23	10.7 ± 1.0	1.5 ± 1.0	7.1	2.0 ± 0.2	6.2 ± 2.5	0.32	1.5 ± 0.2	7.0 ± 4.8	0.2
24	4.8 ± 0.6	1.3 ± 1.1	3.6	-	-	n.a.	0.4 ± 0.04	5.4 ± 2.8	0.08
Mean (μ_x)[d]	29.1	6.3	6.4	9.6	9.3	1.3	2.0	9.5	0.4
SD[e]	40.5	5.6	6.8	6.6	4.1	1.1	3.0	7.1	0.6
CV_x %[f]	139.1	88.9	107.0	69.6	44.6	82.9	147.4	75.2	157.6
μ_w[g]	2.8	1.5	n.a.	2.1	2.1	n.a.	0.1	2.0	n.a.
σ_w[h]	1.0	0.76	n.a.	0.6	0.4	n.a.	1.1	0.7	n.a.

5

[a] nmol/h/g feces

[b] μM

[c] mL/h/g feces, calculated as V_{max}/K_m

[d] Mean of the kinetic parameters for the formation of DHD, S-equol

[e] Standard deviation (SD) of the kinetic parameters for the formation of DHD, S-equol

[f] Coefficient variation % = SD/Mean (μ_x) × 100%

[g] The mean transformed to a normal distribution via $\mu_w = \ln [\mu_x / \text{sqrt} (1+CV_x^2)]$

[h] The SD transformed to a normal distribution via $\sigma_w = \text{sqrt} [\ln (1+CV_x^2)]$

[i] Not available

3.2 Formation of daidzein glucuronides in incubations with individual liver S9 samples

Table 3 presents the kinetic constants V_{max} and K_m, and catalytic efficiency for the formation of daidzein-7-O-glucuronide and daidzein-4'-O-glucuronide in incubations of daidzein with 25 individual liver S9 samples (individual kinetic curves are provided in **Supplementary material Figure S2**).

Formation of daidzein-7-O-glucuronide was observed with an average catalytic efficiency of 57.0 μL/min/mg S9 protein, calculated from a C_{max} of 1.1 nmol/min/mg S9 protein and a K_m of 21.7 μM, with a CV of 60.9%. For the formation of daidzein-4'-O-glucuronide, the average catalytic efficiency amounted only to 1.7 μL/min/mg S9 protein, which was 33.5-fold lower than that for formation of daidzein-7-O-glucuronide. The CV for the catalytic efficiency for daidzein-4'-O-glucuronide formation was 45.1%, which was 1.4-fold lower than that for formation of daidzein-7-O-glucuronide. The present results indicate an overall preference for formation of daidzein-7-O-glucuronide over formation of daidzein-4'-O-glucuronide by human liver S9 metabolism. **Table 3** also presents the mean and CV values for the V_{max} and K_m as derived from the liver S9 incubations, and these parameters were used as input for the subsequent individual PBK models and the Monte Carlo simulation.

Table 3. Kinetic parameters V_{max}, K_m and catalytic efficiencies for the formation of daidzein-7-O-glucuronide and daidzein-4'-O-glucuronide by 25 individual liver S9 samples.

Individual	Daidzein-7-O-glucuronide			Daidzein-4'-O-glucuronide		
	V_{max}[a]	K_m[b]	Catalytic efficiency[c]	V_{max}[a]	K_m[b]	Catalytic efficiency[c]
1	2.0 ± 0.08	13.2 ± 2.2	154.4	0.50 ± 0.07	135.9 ±	3.7

					34.3	
2	1.0 ± 0.08	19.7 ± 5.6	51.2	0.19 ± 0.04	235.6 ± 74.3	0.8
3	1.1 ± 0.07	17.9 ± 4.3	60.9	0.32 ± 0.09	173.2 ± 82.6	1.8
4	1.3 ± 0.2	29.3 ± 12.9	43.5	0.16 ± 0.04	117.6 ± 54.2	1.4
5	1.3 ± 0.2	23.0 ± 12.1	54.5	0.22 ± 0.08	175.4 ± 112.8	1.3
6	0.6 ± 0.07	24.7 ± 9.0	26.2	0.14 ± 0.05	165.9 ± 106.1	0.8
7	1.0 ± 0.2	28.0 ± 13.2	37.1	0.28 ± 0.09	122.4 ± 77.4	2.3
8	0.7 ± 0.06	25.8 ± 6.7	28.3	0.23 ± 0.06	175.3 ± 76.9	1.3
9	1.0 ± 0.1	21.5 ± 11.5	45.3	0.17 ± 0.05	112.0 ± 62.5	1.5
10	0.6 ± 0.05	17.5 ± 5.7	34.7	0.09 ± 0.02	74.6 ± 33.6	1.1
11	0.8 ± 0.06	24.1 ± 6.0	34.7	0.16 ± 0.03	139.9 ± 48.2	1.1
12	0.9 ± 0.09	36.1 ± 11.0	24.6	0.14 ± 0.04	120.3 ± 65.8	1.2
13	1.0 ± 0.07	22.4 ± 5.4	46.2	0.19 ± 0.04	191.8 ± 77.2	1.0
14	0.8 ± 0.09	21.6 ± 8.9	37.6	0.09 ± 0.02	69.3 ± 32.9	1.3
15	0.7 ± 0.05	26.8 ± 6.2	25.9	0.16 ± 0.06	172.7 ± 117.8	1.0
16	0.7 ± 0.09	25.5 ± 11.2	27.8	0.29 ± 0.04	166.3 ± 41.3	1.7
17	1.3 ± 0.07	8.1 ± 2.2	157.7	0.19 ± 0.02	82.8 ± 23.7	2.3
18	1.5 ± 0.1	21.5 ± 5.9	69.4	0.47 ± 0.10	305.7 ± 100.0	1.5
19	0.5 ± 0.05	15.9 ± 6.1	31.3	0.10 ± 0.02	159.9 ±	0.6

					57.7	
20	1.5 ± 0.1	23.0 ± 5.7	66.1	0.27 ± 0.03	161.4 ± 36.2	1.7
21	1.0 ± 0.08	14.9 ± 4.6	66.0	0.26 ± 0.08	96.5 ± 67.9	2.7
22	1.5 ± 0.1	19.7 ± 6.2	75.6	0.31 ± 0.05	116.2 ± 34.3	2.7
23	1.6 ± 0.07	20.7 ± 3.1	76.9	0.23 ± 0.04	88.9 ± 30.8	2.6
24	1.0 ± 0.05	13.3 ± 2.8	75.8	0.24 ± 0.04	89.6 ± 31.7	2.6
25	2.0 ± 0.3	27.6 ± 13.7	72.4	0.29 ± 0.03	143.0 ± 24.0	2.0
Mean (μ_x)[d]	1.1	21.7	57.0	0.2	143.7	1.7
SD[e]	0.4	6.0	34.7	0.1	53.2	0.8
CV_x %[f]	37.2	27.7	60.9	45.5	37.0	45.1
μ_w[g]	0.03	3.0	-	-1.6	4.9	-
σ_w[h]	0.4	0.3	-	0.4	0.4	-

[a] nmol/min/mg S9 protein

[b] μM

[c] μL/min/mg S9 protein, calculated as $V_{max}/K_m \times 1000$

[d] Mean of the kinetic parameters for the formation of daidzein-7-O-glucuronide and daidzein-4'-O-glucuronide derived from 25 individuals

[e] Standard deviation (SD) of the kinetic parameters for the formation of daidzein 7-O-glucuronide and daidzein-4'-O-glucuronide derived from 25 individuals

[f] Coefficient variation, % = SD/Mean (μ_x) × 100%

[g] The mean transformed to a normal distribution via $\mu_w = \ln [\mu_x / \text{sqrt} (1+CV_x^2)]$

[h] The SD transformed to a normal distribution via $\sigma_w = \text{sqrt} [\ln (1+CV_x^2)]$

3.3. Prediction of interindividual variations characterized by individual PBK models and PBK modeling integrated with Monte Carlo simulations

Figure 1 presents the distribution of the predicted C_{max} expressed in daidzein equivalents as obtained using the individual PBK models and when performing PBK modeling integrated with Monte Carlo simulations. **Table 4** shows the GM, GM CV and fold variation derived by these approaches.

When using individual models for either 24 fecal kinetic data sets or 25 liver S9 kinetic data sets, the GMs of the predicted free C_{max} values expressed in daidzein equivalents were quite comparable, being 15.46 and 16.24 nM, respectively, while the GM derived from the Monte Carlo simulation was 1.1-fold lower than what was obtained by both series of individual models, amounting to 14.25 nM. Monte Carlo simulation resulted in a GM CV of 41.3%, which was 3.9- and 1.2-fold higher than the GM CV values derived from the individual models obtained using the 24 fecal kinetic data sets (33.1%) and the 25 liver S9 kinetic data sets (10.6%), respectively. This indicates that the approaches based on the individual models could adequately predict the GM, while the Monte Carlo approach simulation seemed more appropriate to identify sensitive individuals in the population due to its larger GM CV values and wider distribution than the individual PBK modeling approaches.

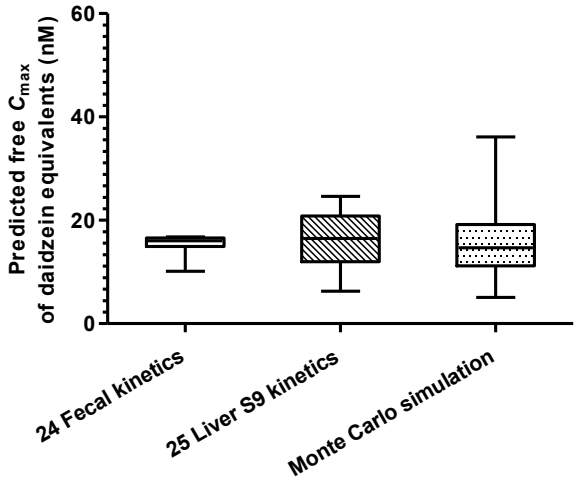

Figure 1. Distribution of the predicted free C_{max} expressed in daidzein equivalents upon a single oral dose of 100 mg/day daidzein, obtained using 24 individual fecal kinetic data sets (clear box), 25 individual liver S9 kinetic data sets (box with lines), and PBK modeling integrated with Monte Carlo simulations including variations in daidzein gut microbial conversions, liver S9 mediated glucuronidation and 7 additional parameters (box with dots representing individuals). The whiskers for the individual models represent the highest and lowest predicted free C_{max} expressed in daidzein equivalents; the whiskers for the Monte

Carlo simulation represent the 1st and 99th percentile of the predicted free C_{max} expressed in daidzein equivalents.

Table 4. Prediction of geometric mean (GM), GM CV and fold difference for the free C_{max} expressed in daidzein equivalents upon a single oral dosing of 100 mg /day daidzein, by individual PBK models using 24 individual fecal kinetic data sets and 25 individual liver S9 kinetic data sets, and by PBK modeling integrated with Monte Carlo simulations.

	Using 24 individual fecal kinetic data sets	Using 25 individual liver S9 kinetic data sets	PBK model integrated with Monte Carlo simulations
GM (nM)	15.46	16.24	14.25
GM CV (%)	10.6	33.1	41.3
Fold-variation	1.66[a]	3.92[a]	3.79[b] 7.14[c]

[a] fold variation of the predicted maximum/minimum free C_{max} expressed in daidzein equivalents by individual models

[b] fold variation of the predicted 95th/5th percentile free C_{max} expressed in daidzein equivalents by Monte Carlo simulation

[c] fold variation of the predicted 99th/1st percentile free C_{max} expressed in daidzein equivalents by Monte Carlo simulation

Figure 2 presents the frequency distribution of the predicted free C_{max} expressed in daidzein equivalents obtained from the PBK modeling integrated with Monte Carlo simulations. It can be seen that the distribution of the predicted free C_{max} expressed in daidzein equivalents is considerably wide, with the lowest prediction below 2 nM and the highest prediction over 58 nM. The GM of free C_{max} expressed in daidzein equivalents for the whole population amounted to 14.25 nM, with the 95th and 99th percentiles amounting to 28.13 nM and 36.14 nM, respectively. Subsequently, the CSAF at the 95th percentile and the CSAF at 99th percentile were calculated by dividing the 95th and 99th percentile by the GM, resulting in CSAF values for the interindividual differences in daidzein kinetics of 1.97 and 2.54, respectively, which are both smaller than the default uncertainty factor of 3.16.

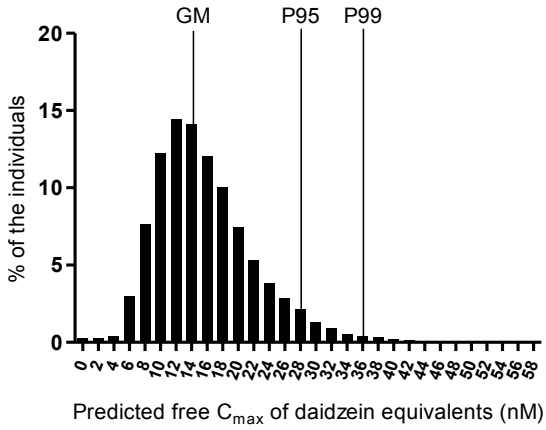

Figure 2. Frequency distribution for the predicted free C_{max} expressed in daidzein equivalents (representing 11789 individuals) upon a single oral dose of 100 mg/day daidzein obtained from PBK modeling integrated with Monte Carlo simulations, including variations in daidzein microbial conversions, liver S9 mediated glucuronidation and 7 additional parameters. The GM represents the geometric mean, and P95 and P99 represent the 95th and 99th percentile of the distribution, respectively. The bar refers to the predicted C_{max} interval between 2 ticks on the x-axis, for example, the bar at 0 refer to the interval of 0-2 nM, and so on.

3.4. PBK modeling-based reverse dosimetry and BMD analysis

Figure 3 shows the predicted in vivo dose-response curve for the average population obtained by PBK modeling-based reverse dosimetry of the in vitro concentration-response curve for estrogenicity of daidzein previously quantified in the ERα-CALUX assay (Wang et al., 2020). **Figure 3** also presents the dose-response curves for the 95th and 99th percentile sensitive individuals which were obtained by dividing the dose levels of the curve for the average population by the respective CSAF values. **Table 5** lists the predicted $BMDL_{10}$ values for the predicted estrogenicity of daidzein derived from these curves, which are the benchmark dose lower confidence limits resulting in 10% response with 95% confidence interval. The $BMDL_{10}$ for the average population was 9.38 mg/day, which was 1.97- and 2.54-fold higher than the corresponding values for the 95th the 99th percentile of the sensitive populations, being 4.76 mg/day and 3.69 mg/day, respectively. Predicted curves of dose-free C_{max} expressed in daidzein equivalents can be found in **Supplementary material Figure S3** and

detailed results of the BMD analysis can be found in **Supplementary material Table 2-Table 4**.

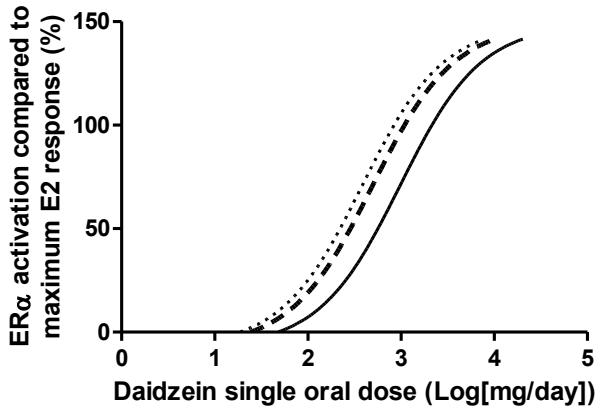

Figure 3. Predicted in vivo dose-response curve for the average (solid line), the 95th percentile (dashed line) and the 99th percentile (dotted line) of the population.

Table 5. The predicted $BMDL_{10}$ for the average, the 95th percentile and the 99th percentile of the population.

Point of departure (PoD)	The average population	Sensitive population	
		95th percentile	99th percentile
$BMDL_{10}$ (mg/day)	9.38	4.76	3.69

The obtained $BMDL_{10}$ values for the average, the 95th and 99th percentile of the population, were compared with daidzein intake from different diets in **Figure 4**. It can be seen that for a Western diet, the dietary daidzein intake, which is less than 2 mg/day (Eisenbrand & Senate Commission on Food Safety of the German Research, 2007), is substantially lower than the $BMDL_{10}$ values. For Asian diets, the intake varies from 15-61 mg/day (Kim & Kwon, 2001; Seow et al., 1998; Wakai et al., 1999), which exceeds the $BMDL_{10}$ values. Upon use of soy supplements, for which the recommended dosage by manufactures can reach up to 80-120 mg/day (Anderson et al., 2007; Merz-Demlow et al., 2000; Steinberg et al., 2003), the daily intake is notably higher than all the $BMDL_{10}$ values.

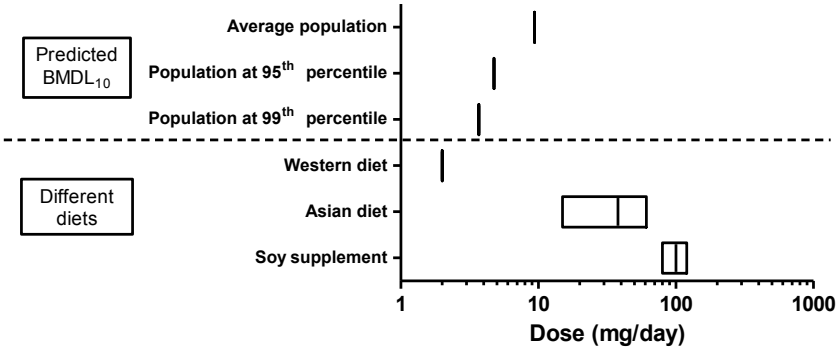

Figure 4. Comparison of predicted $BMDL_{10}$ for the average, the 95th and 99th percentile of the population with daidzein intake from different diets. The dose of daidzein in Western diet is less than 2 mg/day (Eisenbrand & Senate Commission on Food Safety of the German Research, 2007); in Asian diet is 15-61 mg/day (Kim & Kwon, 2001; Seow et al., 1998; Wakai et al., 1999); and in soy supplement diet is 80-120 mg/day (Anderson et al., 2007; Merz-Demlow et al., 2000; Steinberg et al., 2003).

5

4. Discussion

The aim of the present study was to investigate the interindividual differences in the human population in the predicted free C_{max} expressed in daidzein equivalents upon dosing daidzein, taking into account the kinetic variation in daidzein gut microbial metabolism and liver glucuronidation, and also the variation in 7 additional influential PBK model parameters. To achieve this, the developed PBK model was integrated with Monte Carlo simulations to make predictions of population-based distributions of daidzein equivalents, which ultimately allowed definition of CSAFs for interindividual differences in daidzein kinetics. The obtained CSAFs were further used to extrapolate a predicted in vivo dose-response curve for daidzein induced estrogenicity in the average population to the most sensitive population (at 95th and 99th percentile). The results obtained illustrate the potential for use of this in vitro-in silico strategy, as part of new approach methodologies (NAMs), in the safety and risk assessment of food-born chemicals.

In the present study, PBK modeling integrated with Monte Carlo simulations included interindividual variations in kinetics for fecal metabolism and liver glucuronidation of daidzein, and variation in 7 additional parameters. When looking at the individual anaerobic

fecal incubations of daidzein, substantial interindividual differences were observed in kinetic parameters, for formation of DHD, S-equol and O-DMA. These variations in daidzein conversion are mainly caused by human gut microbiota produced redox enzymes, where daidzein reductase is responsible for the conversion from daidzein to DHD, and DHD is converted to either S-equol by dihydrodaidzein reductase or to O-DMA through C-ring cleavage dioxygenases (Lee et al., 2018). Some studies reported on isolation of gut bacteria and identification of enzymes from human responsible for the daidzein conversion (Guo et al., 2021; Karlsson et al., 2013; Monti et al., 2011; Shimada et al., 2010). For example the family *Eggerthellaceae* as well as the narrowly related family *Coriobacteriaceae* were able to convert daidzein to S-equol, with a potential that varies between individuals (Soukup et al., 2021),. These interindividual variations in composition and abundance of gut microbiota were reported to be affected by factors including diet, age, genetic background, lifestyle and the exposure to chemicals of the host (Flandroy et al., 2018; Gill et al., 2006; Jovel et al., 2016).

Evident interindividual variations were also observed in liver glucuronidation of daidzein. UGTs are responsible for mediating daidzein glucuronidation in the liver, with UGT1A9 and UGT1A1 reported to be the main isoforms (Pritchett et al., 2008), of which the presence was shown to be dominantly genetically determined (Girard et al., 2004). The variability in the mRNA level of UGT1A9 was reported to vary over 400 fold from 0.3-132.4 $\times 10^4$ copy/μg RNA, leading to a 17-fold variation in expression levels of UGT1A9 protein in human liver microsomes (Izukawa et al., 2009). Within the human population, several structural polymorphisms were found in the coding region of the gene of UGT1A9, leading to complete or partial inactivation of glucuronidation activity for various substrates (Girard et al., 2004), but in what way these polymorphisms affect the glucuronidation of daidzein remains to be elucidated.

The CSAF values obtained using the 95th and 99th percentile of the free C_{max} expressed in daidzein equivalents as derived from the Monte Carlo simulation, amounted to 1.97 and 2.54 respectively (**Figure 2**), and were thus both smaller than the default uncertainty factor for interindividual differences in kinetics of 3.16 (WHO, 2005), indicating that the current default uncertainty factor is protective for healthy adults. The obtained CSAF values were further applied to PBK modeling-based reverse dosimetry to extrapolate an in vitro concentration-response curve to an in vivo dose-response curve for the 95th percentile and the 99th percentile of the population. In risk assessment, the 95th percentile is generally considered to protect sensitive individuals in a population (EFSA, 2014), Given that daily daidzein intake via a

Western diet is considerably lower than the derived 95th percentile $BMDL_{10}$ for ERα activation, the Western population is unlikely to display estrogenic effects upon daidzein consumption, while populations on an Asian diet and individuals taking soy supplements are predicted to potentially experience estrogenic effects induced by their dietary daidzein exposure (**Figure 4**). This could raise a concern given that ERa-mediated estrogenic effects have been related to cell proliferation and cancer risks (Allred et al., 2004; Hsieh et al., 1998; Rietjens et al., 2017; Zava & Duwe, 1997). However, it should be noted that the conversion of the curve for the average population was translated to the sensitive sub populations assuming that the CSAFs would be dose-independent but it remains to be investigated whether the CSAFs stay the same with increasing dose level. Simultaneously, dietary phytoestrogens including isoflavones also have been linked with beneficial effects such as reduction of cardiovascular disease, maintenance of bone mineral density and reduction of vasomotor symptoms associated with menopause (de Cremoux et al., 2010; Gomez-Zorita et al., 2020; Mayo et al., 2019; Rietjens et al., 2017). The mechanisms underlying the possible dualistic mode of action may in part be explained by the role of ERα and ERβ, where ERα activation is associated with cell proliferation while ERβ activation is associated with beneficial health effects through apoptosis in various estrogen-sensitive tissues and/or epigenetic effects (Rietjens et al., 2017; Rietjens et al., 2013). Since the levels and the ratio of ERα and ERβ varies from tissues to tissue, for example in the uterus ERα dominates over ERβ while in the prostate ERβ is the major isoform, the ultimate effects upon intake of isoflavones may be tissue-specific (Enmark et al., 1997; Pearce & Jordan, 2004). Thus the dietary intake of isoflavones through consumption of soybean products and supplements may lead to both adverse and beneficial effects, and they may be present simultaneously at similar dose levels (Rietjens et al., 2013). The $BMDL_{10}$ values derived by BMD analysis of the predicted dose-response curves for ERa-mediated estrogenicity induced by daidzein exposure presented in this study provide useful information on the levels of daidzein which may induce estrogenic activity especially also in subgroups of the population for which kinetics of daidzein metabolism make them more sensitive. These predictions may need further confirmation in future studies, including also evaluation of the interindividual differences in the toxicodynamics of daidzein induced estrogenic effects in potentially sensitive subgroups of the population such as children, post-menopausal women and individuals at high risk of developing estrogen sensitive breast cancers.

Overall, the PBK modeling integrated with Monte Carlo simulations in this study can be a powerful tool to illustrate the interindividual variations in the free C_{max} expressed in daidzein equivalents resulting from the interindividual variations in the kinetics of daidzein gut microbial conversions and of liver glucuronidation and in 7 additional influential PBK model parameters. The CSAFs obtained in this study for the 95th and 99th percentile of the population were used to translate a predicted dose-response curve for estrogenicity of daidzein in vivo, to dose-response curves for the sensitive individuals in the population. Altogether, the data presented provide another proof-of-principle for the use of an in vitro-in silico strategy integrating PBK modeling with Monte Carlo simulations to evaluate in vivo safety and or effect levels of food-born chemicals as part of the development of NAMs in toxicology.

References

Achour, B., Dantonio, A., Niosi, M., Novak, J. J., Fallon, J. K., Barber, J., . . . Goosen, T. C. (2017). Quantitative Characterization of Major Hepatic UDP-Glucuronosyltransferase Enzymes in Human Liver Microsomes: Comparison of Two Proteomic Methods and Correlation with Catalytic Activity. *Drug Metab Dispos, 45*(10), 1102-1112. https://doi.org/10.1124/dmd.117.076703.

Adjei, A. A., Gaedigk, A., Simon, S. D., Weinshilboum, R. M., & Leeder, J. S. (2008). Interindividual variability in acetaminophen sulfation by human fetal liver: implications for pharmacogenetic investigations of drug-induced birth defects. *Birth Defects Res A Clin Mol Teratol, 82*(3), 155-165. https://doi.org/10.1002/bdra.20535.

Allred, C. D., Allred, K. F., Ju, Y. H., Clausen, L. M., Doerge, D. R., Schantz, S. L., . . . Helferich, W. G. (2004). Dietary genistein results in larger MNU-induced, estrogen-dependent mammary tumors following ovariectomy of Sprague–Dawley rats. *Carcinogenesis, 25*(2), 211-218.

Arai, Y., Uehara, M., Sato, Y., Kimira, M., Eboshida, A., Adlercreutz, H., & Watanabe, S. (2000). Comparison of isoflavones among dietary intake, plasma concentration and urinary excretion for accurate estimation of phytoestrogen intake. *Journal of Epidemiology, 10*(2), 127-135.

Atkinson, C., Frankenfeld, C. L., & Lampe, J. W. (2005). Gut bacterial metabolism of the soy isoflavone daidzein: exploring the relevance to human health. *Experimental biology and medicine, 230*(3), 155-170.

Brown, R. P., Delp, M. D., Lindstedt, S. L., Rhomberg, L. R., & Beliles, R. P. (1997). Physiological parameter values for physiologically based pharmacokinetic models. *Toxicology and industrial health, 13*(4), 407-484.

Catalkaya, G., Venema, K., Lucini, L., Rocchetti, G., Delmas, D., Daglia, M., . . . Capanoglu, E. (2020). Interaction of dietary polyphenols and gut microbiota: Microbial metabolism of polyphenols, influence on the gut microbiota, and implications on host health. *Food Frontiers, 1*(2), 109-133. https://doi.org/10.1002/fft2.25.

Clarke, S. F., Murphy, E. F., O'Sullivan, O., Lucey, A. J., Humphreys, M., Hogan, A., . . . Cotter, P. D. (2014). Exercise and associated dietary extremes impact on gut microbial diversity. *Gut, 63*(12), 1913-1920. https://doi.org/10.1136/gutjnl-2013-306541.

Covington, T. R., Robinan Gentry, P., Van Landingham, C. B., Andersen, M. E., Kester, J. E., & Clewell, H. J. (2007). The use of Markov chain Monte Carlo uncertainty analysis to

support a Public Health Goal for perchloroethylene. *Regul Toxicol Pharmacol, 47*(1), 1-18. https://doi.org/10.1016/j.yrtph.2006.06.008.

Cubitt, H. E., Houston, J. B., & Galetin, A. (2011). Prediction of human drug clearance by multiple metabolic pathways: integration of hepatic and intestinal microsomal and cytosolic data. *Drug Metab Dispos, 39*(5), 864-873. https://doi.org/10.1124/dmd.110.036566.

de Cremoux, P., This, P., Leclercq, G., & Jacquot, Y. (2010). Controversies concerning the use of phytoestrogens in menopause management: bioavailability and metabolism. *Maturitas, 65*(4), 334-339. https://doi.org/10.1016/j.maturitas.2009.12.019.

EFSA. (2014). Guidance on the assessment of exposure of operators, workers, residents and bystanders in risk assessment for plant protection products. *EFSA Journal, 12*(10), 3874.

Enmark, E., Pelto-Huikko, M., Grandien, K., Lagercrantz, S., Lagercrantz, J., Fried, G., . . . Gustafsson, J.-A. k. (1997). Human estrogen receptor β-gene structure, chromosomal localization, and expression pattern. *The Journal of Clinical Endocrinology & Metabolism, 82*(12), 4258-4265.

Gardana, C., Canzi, E., & Simonetti, P. (2009). The role of diet in the metabolism of daidzein by human faecal microbiota sampled from Italian volunteers. *J Nutr Biochem, 20*(12), 940-947. https://doi.org/10.1016/j.jnutbio.2008.08.006.

Girard, H., Court, M. H., Bernard, O., Fortier, L. C., Villeneuve, L., Hao, Q., . . . Guillemette, C. (2004). Identification of common polymorphisms in the promoter of the UGT1A9 gene: evidence that UGT1A9 protein and activity levels are strongly genetically controlled in the liver. *Pharmacogenetics, 14*(8), 501-515. https://doi.org/10.1097/01.fpc.0000114754.08559.27.

Gomez-Zorita, S., Gonzalez-Arceo, M., Fernandez-Quintela, A., Eseberri, I., Trepiana, J., & Portillo, M. P. (2020). Scientific Evidence Supporting the Beneficial Effects of Isoflavones on Human Health. *Nutrients, 12*(12). https://doi.org/10.3390/nu12123853.

Guo, Y., Zhao, L., Fang, X., Zhong, Q., Liang, H., Liang, W., & Wang, L. (2021). Isolation and identification of a human intestinal bacterium capable of daidzein conversion. *FEMS Microbiol Lett, 368*(8). https://doi.org/10.1093/femsle/fnab046.

Haron, H., Ismail, A., Azlan, A., Shahar, S., & Peng, L. S. (2009). Daidzein and genestein contents in tempeh and selected soy products. *Food Chemistry, 115*(4), 1350-1356. https://doi.org/10.1016/j.foodchem.2009.01.053.

Hsieh, C.-Y., Santell, R. C., Haslam, S. Z., & Helferich, W. G. (1998). Estrogenic effects of genistein on the growth of estrogen receptor-positive human breast cancer (MCF-7) cells in vitro and in vivo. *Cancer research, 58*(17), 3833-3838.

Islam, M. A., Bekele, R., Vanden Berg, J. H., Kuswanti, Y., Thapa, O., Soltani, S., . . . Murk, A. J. (2015). Deconjugation of soy isoflavone glucuronides needed for estrogenic activity. *Toxicol In Vitro, 29*(4), 706-715. https://doi.org/10.1016/j.tiv.2015.01.013.

Islam, M. A., Punt, A., Spenkelink, B., Murk, A. J., Rolaf van Leeuwen, F. X., & Rietjens, I. M. (2014). Conversion of major soy isoflavone glucosides and aglycones in in vitro intestinal models. *Mol Nutr Food Res, 58*(3), 503-515. https://doi.org/10.1002/mnfr.201300390.

Izukawa, T., Nakajima, M., Fujiwara, R., Yamanaka, H., Fukami, T., Takamiya, M., . . . Yokoi, T. (2009). Quantitative analysis of UDP-glucuronosyltransferase (UGT) 1A and UGT2B expression levels in human livers. *Drug Metab Dispos, 37*(8), 1759-1768. https://doi.org/10.1124/dmd.109.027227.

Jiang, W., & Hu, M. (2012). Mutual interactions between flavonoids and enzymatic and transporter elements responsible for flavonoid disposition via phase II metabolic pathways. *RSC Adv, 2*(21), 7948-7963. https://doi.org/10.1039/C2RA01369J.

Karlsson, F. H., Tremaroli, V., Nookaew, I., Bergstrom, G., Behre, C. J., Fagerberg, B., . . . Backhed, F. (2013). Gut metagenome in European women with normal, impaired and diabetic glucose control. *Nature, 498*(7452), 99-103. https://doi.org/10.1038/nature12198.

Kimura, T., & Higaki, K. (2002). Gastrointestinal transit and drug absorption. *Biological and Pharmaceutical Bulletin, 25*(2), 149-164.

Lee, P. G., Lee, U. J., Song, H., Choi, K. Y., & Kim, B. G. (2018). Recent advances in the microbial hydroxylation and reduction of soy isoflavones. *FEMS Microbiol Lett, 365*(19). https://doi.org/10.1093/femsle/fny195.

Li, M., Gehring, R., Riviere, J. E., & Lin, Z. (2017). Development and application of a population physiologically based pharmacokinetic model for penicillin G in swine and cattle for food safety assessment. *Food Chem Toxicol, 107*(Pt A), 74-87. https://doi.org/10.1016/j.fct.2017.06.023.

Magee, P. J. (2011). Is equol production beneficial to health? *Proc Nutr Soc, 70*(1), 10-18. https://doi.org/10.1017/S0029665110003940.

Mayo, B., Vazquez, L., & Florez, A. B. (2019). Equol: A Bacterial Metabolite from The Daidzein Isoflavone and Its Presumed Beneficial Health Effects. *Nutrients, 11*(9). https://doi.org/10.3390/nu11092231.

Monti, D., Ottolina, G., Carrea, G., & Riva, S. (2011). Redox reactions catalyzed by isolated enzymes. *Chem Rev, 111*(7), 4111-4140. https://doi.org/10.1021/cr100334x.

Ning, J., Rietjens, I., & Strikwold, M. (2019). Integrating physiologically based kinetic (PBK) and Monte Carlo modeling to predict inter-individual and inter-ethnic variation in bioactivation and liver toxicity of lasiocarpine. *Arch Toxicol, 93*(10), 2943-2960. https://doi.org/10.1007/s00204-019-02563-x.

Pearce, S. T., & Jordan, V. C. (2004). The biological role of estrogen receptors α and β in cancer. *Critical reviews in oncology/hematology, 50*(1), 3-22.

Pritchett, L. E., Atherton, K. M., Mutch, E., & Ford, D. (2008). Glucuronidation of the soyabean isoflavones genistein and daidzein by human liver is related to levels of UGT1A1 and UGT1A9 activity and alters isoflavone response in the MCF-7 human breast cancer cell line. *J Nutr Biochem, 19*(11), 739-745. https://doi.org/10.1016/j.jnutbio.2007.10.002.

Punt, A., Paini, A., Spenkelink, A., Scholz, G., Schilter, B., van Bladeren, P. J., & Rietjens, I. M. (2016). Evaluation of Interindividual Human Variation in Bioactivation and DNA Adduct Formation of Estragole in Liver Predicted by Physiologically Based Kinetic/Dynamic and Monte Carlo Modeling. *Chem Res Toxicol, 29*(4), 659-668. https://doi.org/10.1021/acs.chemrestox.5b00493.

Qiu, F., Chen, X. Y., Song, B., Zhong, D. F., & Liu, C. X. (2005). Influence of dosage forms on pharmacokinetics of daidzein and its main metabolite daidzein-7-O-glucuronide in rats. *Acta Pharmacol Sin, 26*(9), 1145-1152. https://doi.org/10.1111/j.1745-7254.2005.00187.x.

Rietjens, I. M., Louisse, J., & Beekmann, K. (2017). The potential health effects of dietary phytoestrogens. *Br J Pharmacol, 174*(11), 1263-1280. https://doi.org/10.1111/bph.13622.

Rietjens, I. M., Sotoca, A. M., Vervoort, J., & Louisse, J. (2013). Mechanisms underlying the dualistic mode of action of major soy isoflavones in relation to cell proliferation and cancer risks. *Mol Nutr Food Res, 57*(1), 100-113. https://doi.org/10.1002/mnfr.201200439.

Ronis, M. J., Little, J. M., Barone, G. W., Chen, G., Radominska-Pandya, A., & Badger, T. M. (2006). Sulfation of the isoflavones genistein and daidzein in human and rat liver and gastrointestinal tract. *Journal of medicinal food, 9*(3), 348-355.

Schwen, R. J., Nguyen, L., & Jackson, R. L. (2012). Elucidation of the metabolic pathway of S-equol in rat, monkey and man. *Food Chem Toxicol, 50*(6), 2074-2083. https://doi.org/10.1016/j.fct.2012.03.048.

Shimada, Y., Yasuda, S., Takahashi, M., Hayashi, T., Miyazawa, N., Sato, I., . . . Hishigaki, H. (2010). Cloning and expression of a novel NADP(H)-dependent daidzein reductase, an enzyme involved in the metabolism of daidzein, from equol-producing Lactococcus strain 20-92. *Appl Environ Microbiol, 76*(17), 5892-5901. https://doi.org/10.1128/AEM.01101-10.

Soukup, S. T., Stoll, D. A., Danylec, N., Schoepf, A., Kulling, S. E., & Huch, M. (2021). Metabolism of Daidzein and Genistein by Gut Bacteria of the Class Coriobacteriia. *Foods, 10*(11). https://doi.org/10.3390/foods10112741.

Steensma, A., Noteborn, H. P., & Kuiper, H. A. (2004). Comparison of Caco-2, IEC-18 and HCEC cell lines as a model for intestinal absorption of genistein, daidzein and their glycosides. *Environ Toxicol Pharmacol, 16*(3), 131-139. https://doi.org/10.1016/j.etap.2003.11.008.

Strikwold, M., Spenkelink, B., Woutersen, R. A., Rietjens, I., & Punt, A. (2017). Development of a Combined In Vitro Physiologically Based Kinetic (PBK) and Monte Carlo Modeling Approach to Predict Interindividual Human Variation in Phenol-Induced Developmental Toxicity. *Toxicol Sci, 157*(2), 365-376. https://doi.org/10.1093/toxsci/kfx054.

Wang, Q., Spenkelink, B., Boonpawa, R., & Rietjens, I. (2021). Use of Physiologically Based Pharmacokinetic Modeling to Predict Human Gut Microbial Conversion of Daidzein to S-Equol. *J Agric Food Chem*. https://doi.org/10.1021/acs.jafc.1c03950.

Wang, Q., Spenkelink, B., Boonpawa, R., Rietjens, I., & Beekmann, K. (2020). Use of Physiologically Based Kinetic Modeling to Predict Rat Gut Microbial Metabolism of the Isoflavone Daidzein to S-Equol and Its Consequences for ERalpha Activation. *Mol Nutr Food Res, 64*(6), e1900912. https://doi.org/10.1002/mnfr.201900912.

WHO. (2005). Chemical-specific adjustment factors for interspecies differences and human variability: guidance document for use of data in dose/concentration-response assessment. In *Chemical-specific adjustment factors for interspecies differences and*

human variability: guidance document for use of data in dose/concentration-response assessment (pp. 96-96).

Zava, D. T., & Duwe, G. (1997). Estrogenic and antiproliferative properties of genistein and other flavonoids in human breast cancer cells in vitro.

Zhang, X., Tsang, A. M., Okino, M. S., Power, F. W., Knaak, J. B., Harrison, L. S., & Dary, C. C. (2007). A physiologically based pharmacokinetic/pharmacodynamic model for carbofuran in Sprague-Dawley rats using the exposure-related dose estimating model. *Toxicol Sci, 100*(2), 345-359. https://doi.org/10.1093/toxsci/kfm232.

Supplementary material.

Table S1. Information of the human liver S9 donors.

Individual	Sample code[a]	Gender	Age (years)	Weight (kg)	Height (inches)
1	H0025	Female (F)	30	99	63
2	H0026	Male (M)	22	65	70
3	H0033	M	44	84	70
4	H0041	M	33	75	71
5	H0057	F	2	16	36
6	H0062	F	72	68	66
7	H0068	M	58	57	67
8	H0164	M	30	104	74
9	H0177	F	45	107	65
10	H0208	F	78	61	66
11	H0217	F	66	114	64
12	H0220	F	33	60	60
13	H0236	M	17	34	48
14	H0246	F	40	120	64
15	H0291	F	18	59	64
16	H0311	M	21	86	92
17	H0397	M	60	79	73
18	H0420	M	42	105	74
19	H0428	F	57	114	66
20	H0430	M	59	70	68
21	H0447	F	54	138	63
22	H0463	F	58	52	80
23	H0487	M	48	113	70
24	H0533	M	28	108	66
25	H0751	M	29	104	79

[a] Sample code from supplier Tebu-bio (Heerhugowaard, The Netherlands).

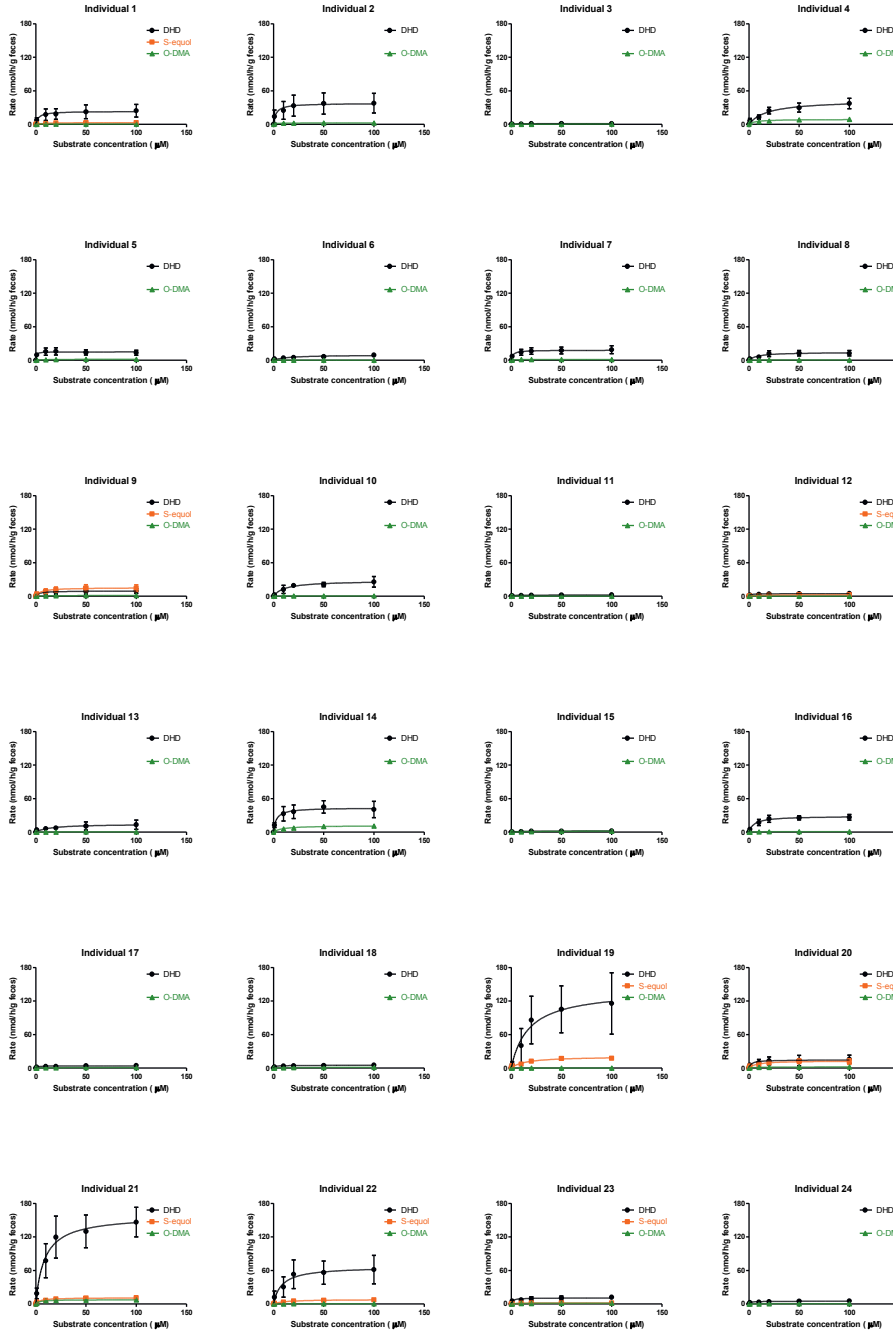

Figure S1. Concentration-dependent formation of DHD, S-equol and O-DMA in human individual fecal incubations with daidzein under anaerobic conditions. Data are presented as mean ± SD of triplicate experiments.

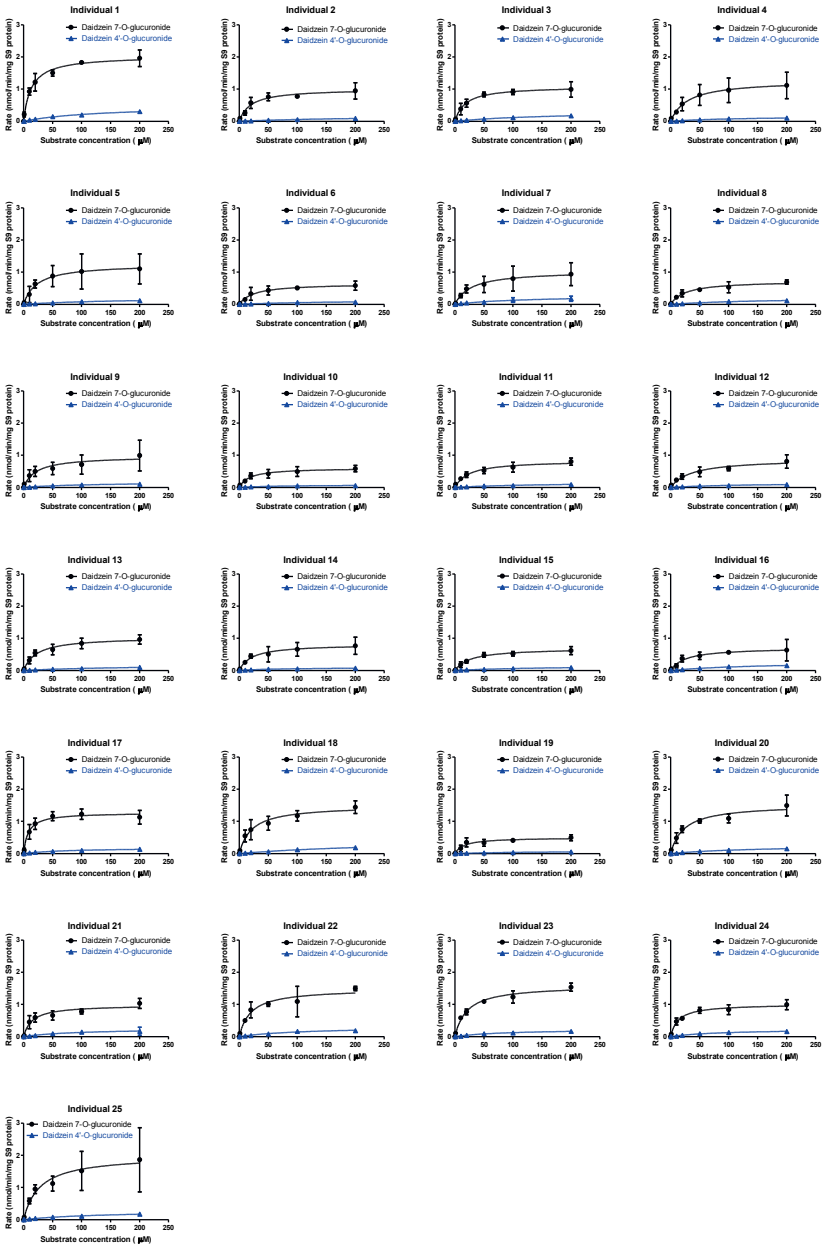

Figure S2. Concentration-dependent formation of daidzein-7-O-glucuronide and daidzein-4'-O-glucuronide in human individual liver S9 fractions incubations with daidzein. Data are presented as mean ± SD of triplicate experiments.

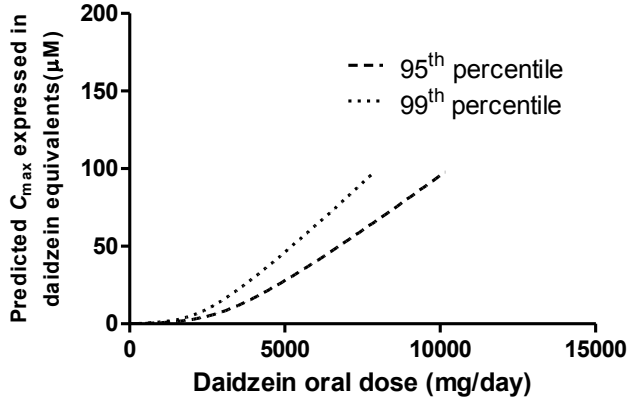

Figure S3. Predicted curves of dose-C_{max} expressed in daidzein equivalents in the 95th percentile (dashed line) and the 99th percentile (dotted line) of the population. The curves for 95th and 99th of the population were obtained by applying the respective CSAFs to the average population.

Table S2. Results of the BMD analysis (for the average population) of the predicted dose-response curve for ERα activation compared to the maximum E2 response, using dose-response data obtained from PBK modelling-based reverse dosimetry of the ERα-CALUX assay data. The table and figures present the characteristics of fitted models, the weights for model averaging and the final benchmark dose for 10% response with the 95% intervals.

model	converged	loglik	npar	AIC	weights	BMD values from averaging		
						$BMDL_{10}$ (mg/day)	BMD_{10} (mg/day)	$BMDU_{10}$ (mg/day)
full model	yes	4.27	7	5.46	-	9.38	34.83	64
null model	yes	-37.91	2	79.82	-			
Expon. m3-	yes	-22.24	4	52.48	-			
Expon. m5-	yes	4.08	5	1.84	0.3196			
Hill m3-	yes	-21.22	4	50.44	-			
Hill m5-	yes	4.07	5	1.86	0.3164			
Inv.Expon. m3-	yes	-17.85	4	43.7	-			
Inv.Expon. m5-	yes	-8.05	5	26.1	0			
LN m3-	yes	-19.31	4	46.62	-			
LN m5-	yes	4.21	5	1.58	0.364			

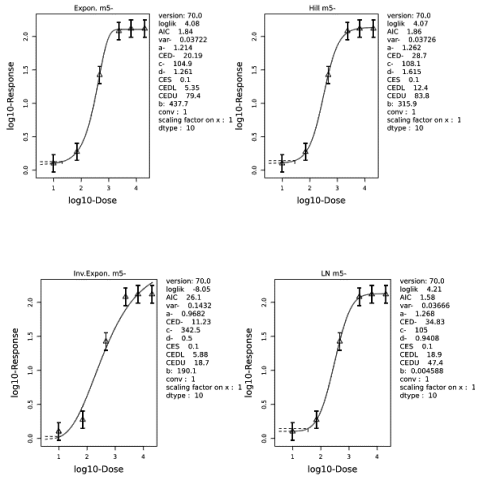

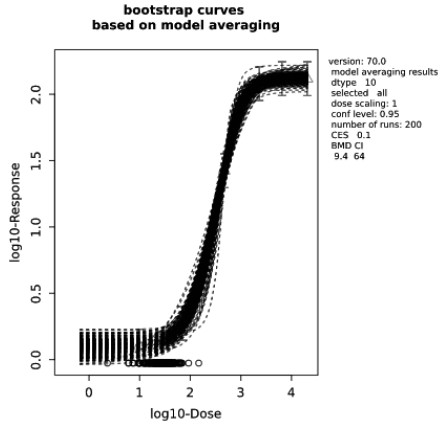

5

Table S3. Results of the BMD analysis (for the 95th percentile of the population) of the predicted dose-response curve for ERα activation compared to the maximum E2 response, using dose-response data obtained from PBK modelling-based reverse dosimetry of the ERα-CALUX assay data. The table and figures present the characteristics of fitted models, the weights for model averaging and the final benchmark dose for 10% response with the 95% intervals.

model	converged	loglik	npar	AIC	weights	BMD values from averaging		
						$BMDL_{10}$ (mg/day)	BMD_{10} (mg/day)	$BMDU_{10}$ (mg/day)
full model	yes	4.27	7	5.46	-	4.76	17.68	32.5
null model	yes	-37.91	2	79.82	-			
Expon. m3-	yes	-22.24	4	52.48	-			
Expon. m5-	yes	4.08	5	1.84	0.3196			
Hill m3-	yes	-21.39	4	50.78	-			
Hill m5-	yes	4.07	5	1.86	0.3164			
Inv.Expon. m3-	yes	-17.93	4	43.86	-			
Inv.Expon. m5-	yes	-8.05	5	26.1	0			
LN m3-	yes	-19.44	4	46.88	-			
LN m5-	yes	4.21	5	1.58	0.364			

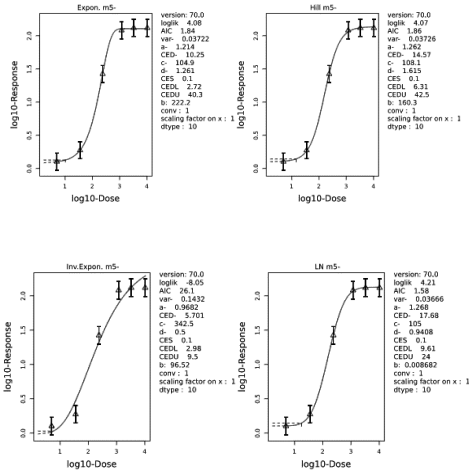

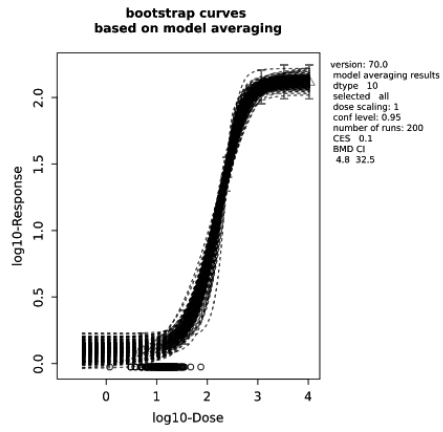

Table S4. Results of the BMD analysis (for the 99th percentile of the population) of the predicted dose-response curve for ERα activation compared to the maximum E2 response, using dose-response data obtained from PBK modelling-based reverse dosimetry of the ERα-CALUX assay data. The table and figures present the characteristics of fitted models, the weights for model averaging and the final benchmark dose for 10% response with the 95% intervals.

model	converged	loglik	npar	AIC	weights	BMD values from averaging		
						$BMDL_{10}$ (mg/day)	BMD_{10} (mg/day)	$BMDU_{10}$ (mg/day)
full model	yes	4.27	7	5.46	-	3.69	13.71	25.2
null model	yes	-37.91	2	79.82	-			
Expon. m3-	yes	-22.24	4	52.48	-			
Expon. m5-	yes	4.08	5	1.84	0.3196			
Hill m3-	yes	-21.45	4	50.9	-			
Hill m5-	yes	4.07	5	1.86	0.3164			
Inv.Expon. m3-	yes	-17.97	4	43.94	-			
Inv.Expon. m5-	yes	-8.05	5	26.1	0			
LN m3-	yes	-19.48	4	46.96	-			
LN m5-	yes	4.21	5	1.58	0.364			

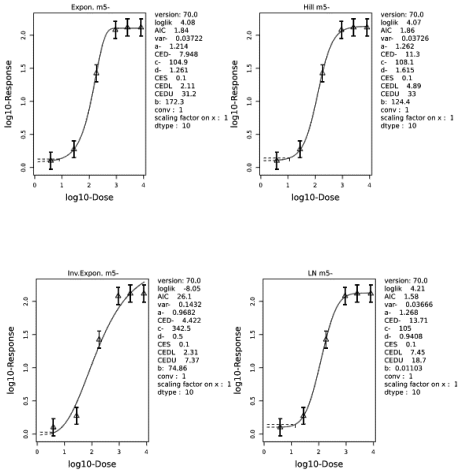

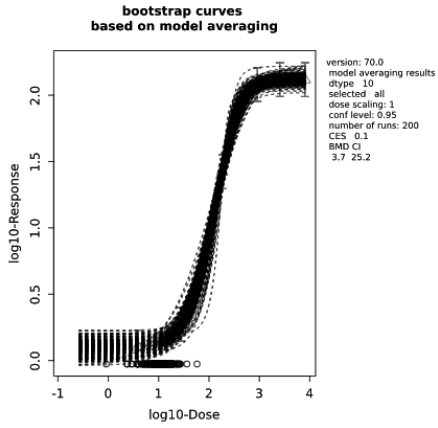

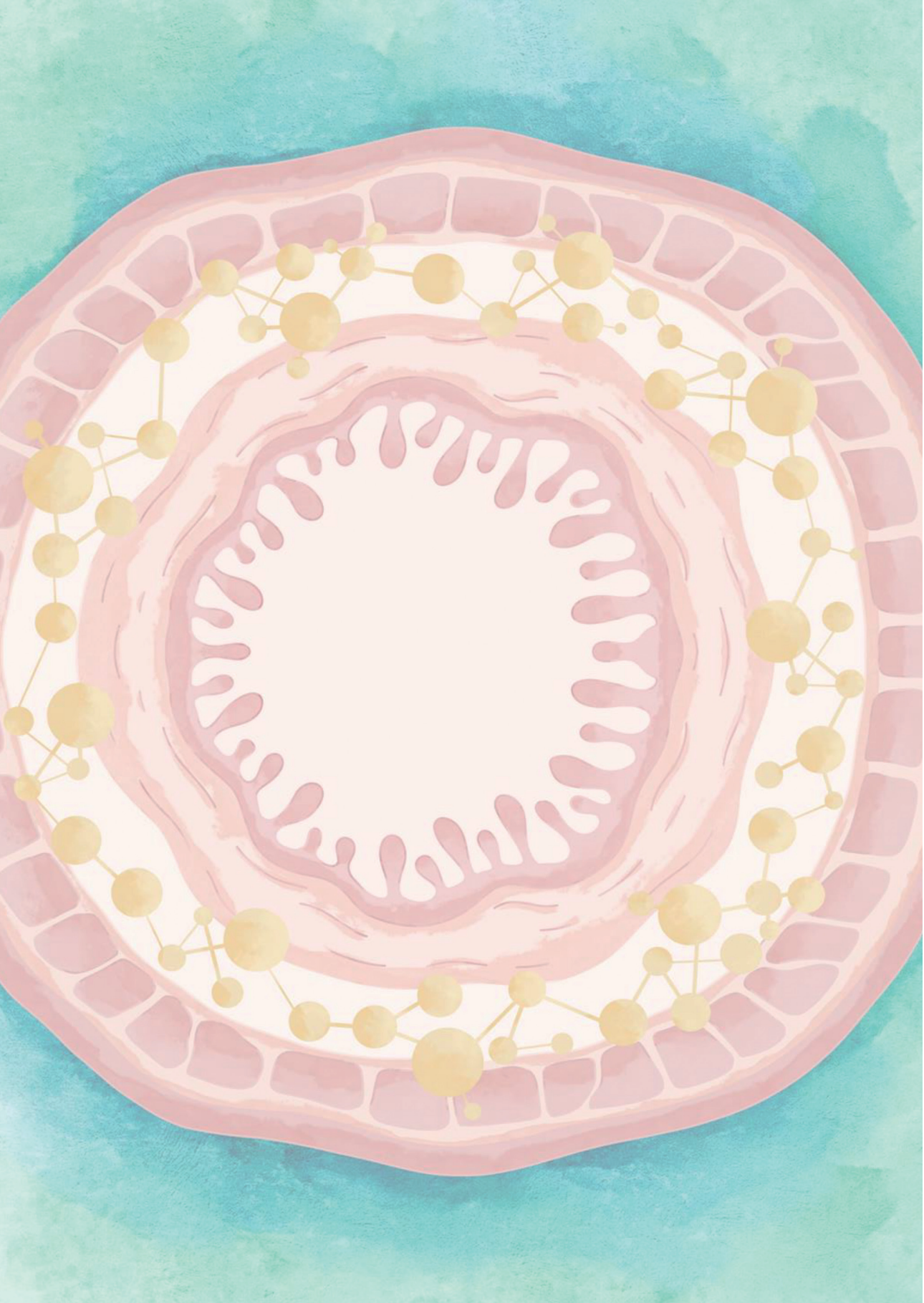

Chapter 6

General Discussion

Background

The gut microbiota is reported to play a significant role in the health of the host through active participation in a wide range of biochemical and metabolic activities (Gill et al., 2006; Human Microbiome Project, 2012). The isoflavone daidzein and the mycotoxin zearalenone (ZEN), exerting estrogenicity due to structural similarity to the naturally occurring hormone 17β-estradiol estradiol (E2) (Sun et al., 2016; Takemura et al., 2007), are known to be metabolized by the gut microbiota to form the more potent metabolites S-equol (Mayo et al., 2019) and α-zearalenol (α-ZEL) (Agahi et al., 2020), respectively. In spite of this, microbial metabolism has so far not been taken into account when defining physiologically based kinetic (PBK) models to be used in novel approach methodologies (NAMs) like quantitative in vitro to in vivo extrapolations (QIVIVE) in toxicological risk assessment. The aim of the present thesis was to develop such PBK models that include gut microbial metabolism and apply them for QIVIVE using daidzein and ZEN as the model compounds.

The main exposure route for daidzein and ZEN is from dietary intake, and the high exposure levels in some populations may actually raise concerns (Eisenbrand and Senate Commission on Food Safety of the German Research, 2007; Kowalska et al., 2016). For daidzein, though western populations have a relatively low dietary intake of isoflavones being generally lower than 2 mg/day (van Erp-Baart et al., 2003), in some Asian counties like China and Japan, dietary preferences for soybean and soy products may result in a daily consumption of isoflavones from 15-61 mg/day (Arai et al., 2000; Kim and Kwon, 2001; Wakai et al., 1999). This level can be as high as 120 mg/day if a person consumes soy supplements (Anderson et al., 2007; Eisenbrand and Senate Commission on Food Safety of the German Research, 2007; Merz-Demlow et al., 2000). Providers of these supplements often refer to beneficial health effects of the isoflavones, but the dose of the supplements is not controlled by any regulation, and raises concerns because of the potential risks related to the estrogenic activity (Eisenbrand and Senate Commission on Food Safety of the German Research, 2007). ZEN is a commonly found foodborne chemical contaminant, mainly present in corn and cereal crops at levels that increase upon bad storage conditions (Minervini et al., 2006). Since ZEN acts as an endocrine active compound, a tolerable daily intake (TDI) of 0.25 µg/kg bw was established by the European Food Safety Authority (EFSA) for ZEN (EFSA, 2011). To provide proofs of principle for studying the role of the gut microbiota on the ultimate effects of foodborne bioactive chemicals to the host using NAMs, the present thesis aimed to use in vitro and in silico methods to obtain a detailed insight into the microbial-mammalian co-metabolism of

daidzein and ZEN, and to translate this knowledge to an updated risk assessment using physiologically based kinetic (PBK) modeling, including PBK modeling integrated Monte Carlo simulation and PBK modeling based reverse dosimetry.

1. Overview of the results and main findings

In **Chapter 2,** a PBK model was developed for daidzein to describe its absorption, distribution, metabolism and excretion (ADME) within rats. The PBK model included a separate compartment to enable the description of the gut microbial transformation of daidzein. Being the most important estrogenic gut microbial metabolite, S-equol was included in the developed PBK model by creating a submodel, which was identical to the main model but could separately describe the kinetics of S-equol. To define the PBK model parameters for the gut microbial metabolism, rat feces were collected and incubated with the substrate daidzein under anaerobic conditions. Conditions for these anaerobic fecal incubation were optimized to achieve linear depletion of the substrate and linear formation of metabolites over time and concentration of feces. These optimized incubation conditions included the usage of PBS as the incubation solvent without any added external carbon sources, in order to remain closer to the intestinal conditions at the time of sampling. This allowed the definition of kinetic constants, including the apparent maximum velocity (V_{max}) and the apparent Michaelis–Menten constant (K_m), to describe the gut microbial conversion from daidzein to the metabolites dihydrodaidzein (DHD), S-equol and O-desmethylangolensin (O-DMA). The optimization of the incubation conditions for linearity over time and fecal concentration are essential to enable definition of kinetic constants for the PBK model. Similar anaerobic incubations can also be applied using fecal samples from other animal species and even from human in studies regarding their gut microbial metabolism of foodborne chemicals. Besides anaerobic fecal incubations, pooled liver S9 fractions were also incubated with S-equol to obtain kinetic parameters describing S-equol glucuronidation in the liver in the submodel. For validation of the developed PBK model, first a comparison was made between predictions obtained upon either including or excluding the gut microbiota compartment. This comparison revealed that S-equol was not present in the circulation when microbial metabolism was absent in the PBK model, while the prediction of plasma S-equol concentrations showed a typical pharmacokinetic curve once microbial activity was introduced into the model. Subsequently, to further evaluate the predictions made by the PBK model, the predicted maximum concentrations in plasma (C_{max}) of daidzein and S-equol upon oral administration of daidzein were compared with in vivo data reported in literature. This

showed an overall 1.22- and 1.07-fold difference for daidzein and S-equol, respectively. Since the model predicted outcomes are less than 2-fold from the observed in vivo value, the predictions were considered adequate (Sager et al., 2015).

To further evaluate the PBK model and assess which parameters influence the predicted C_{max} of daidzein and S-equol in a substantial way, a sensitivity analysis was performed. Results revealed that the normalized sensitivity coefficients (NSCs) for most of the PBK model parameters were dose-dependent. The sensitivity analysis indicated that the C_{max} of daidzein was largely affected by liver-related parameters, while parameters related to gut microbial activities had small effects on the C_{max} of daidzein, but considerably influenced the C_{max} of S-equol. The outcomes also indicated that the C_{max} of daidzein upon oral intake mainly depends on the amount of daidzein that is glucuronidated in the liver (Pritchett et al., 2008), while that of S-equol mainly relies on its formation in the large intestine (Legette et al., 2014). The linear sensitivity analysis performed presents a simple first tier approach to obtain initial information about which parameters influence the predicted C_{max} values most, while a more extended analysis of variability in the thus identified most influential parameters, for example via Monte Carlo modeling, as reported in **Chapter 5**, provided additional insight in the influence of intraspecies differences on the predicted C_{max} values.

Regarding the estrogenic potency, results from the estrogen receptor (ER) α-CALUX assay corroborated that the gut microbial metabolite S-equol is a more potent estrogen than its parent compound daidzein, having a 6.3- and 12.7- fold higher potency as derived from EC_{10} and EC_{50} values, respectively. Dietary exposure scenarios were subsequently translated to internal concentrations using the developed PBK model, in order to enable a comparison of these values to the EC_{10} values to obtain insight in the physiological relevance of the in vitro detected estrogenic activities for the in vivo situation. This comparison showed that for daidzein, predicted C_{max} values that would result from intake of daidzein at a level representing an Asian diet, a vegetarian diet and intake of food supplements, but not a Western diet, were predicted to be potentially higher than the EC_{10} values , while for S-equol, all the dietary intake levels resulted in predicted C_{max} values that were generally lower than the EC_{10} value of S-equol for ERα activation. Thus, it was concluded that daidzein plays the dominant role in ERα-mediated estrogenicity upon intake of this isoflavone, despite the higher estrogenic potency of its microbial metabolite S-equol.

To also characterize the role of the gut microbiota in humans, **Chapter 3** aimed to extend and apply the previously developed PBK model for rats to a PBK model for humans. This allowed predictions for the human situation and elucidated potential species differences between human and rats. To this end, human fecal samples were collected from 15 healthy donors, which were divided into two groups based on the capacity to convert daidzein to S-equol, resulting in a group of S-equol producers consisting of 6 donors and a group of S-equol nonproducers consisting of 9 donors. This result is in line with the reported ratio in the human population for the percentage of S-equol producers that varies from 30% to 50% (Arai et al., 2000). Consequently, two PBK models, one for S-equol producers and one for non-producers were developed using their respective kinetic parameters V_{max} and K_m for the formation of DHD, S-equol (only for producers), and O-DMA. In addition, kinetic parameters V_{max} and K_m for the formation of S-equol glucuronides and sulfates were derived from in vitro incubations with pooled human liver S9 fractions and were included in the human PBK model. Similarly to **Chapter 2**, the developed human PBK model for daidzein was validated by comparing model predictions with reported in vivo data. The model-based prediction for the C_{max} of daidzein was on average 1.62 times that of the reported in vivo C_{max}. The model validation for S-equol was performed by comparing the predicted versus the reported in vivo cumulative urinary excretion of conjugated S-equol, resulting in a value of 0.89 for the overall ratio. These validations revealed that the model adequately predicts the intrinsic level of daidzein and the formation of S-equol. To further characterize interspecies differences, **Chapter 3** also compared the gut microbial metabolism of daidzein in rats using kinetic date obtained from **Chapter 2** and in human using kinetic date obtained from **Chapter 3**. This comparison revealed that rat fecal samples showed much higher catalytic efficiencies (expressed in µL/h/g feces) than human fecal samples in the formation of all the metabolites DHD, S-equol and O-DMA, being 54-, 209- and 118-fold higher respectively (**Table 5** in **Chapter 3**). These substantial interspecies differences between rats and human were due to higher values for the apparent V_{max} and somewhat lower K_m values for the respective microbial conversions.

The results described provided a first proof-of-principle how microbial metabolism of daidzein in rats (**Chapter 2**) and in human (**Chapter 3**) can be included in PBK modeling. In order to apply this strategy to other foodborne chemicals as part of the development of NAMs, PBK models for rats and human, using ZEN as the model compound, were developed as described in **Chapter 4**. ZEN was selected as the model compound because it represents an important class of bioactive mycotoxins produced by *Fusarium* species, which, similar to

daidzein, shows estrogenic potential and can be metabolized by gut microbiota to a metabolite α-ZEL with higher estrogenicity than ZEN itself (Yazar and Omurtag, 2008). Thus, in **Chapter 4,** PBK models were built for rats and human for ZEN including a sub-model for α-ZEL. The PBK model for rats was evaluated by comparing the predicted C_{max} of ZEN to in vivo data, resulting in predictions that were only 1.3-fold higher than the in vivo data. The integration of the intestinal microbiota in both PBK models revealed that hepatic metabolism is dominant in the formation of α-ZEL despite of microbial metabolism. Additionally, the predicted C_{max} for ZEN and α-ZEL in human resulting from intake of ZEN at the level of the TDI were much lower than the in vitro EC_{10} values inducing ERα activation in the ERα-CALUX reporter gene assay. Despite the higher estrogenicity of α-ZEL, the results of this study suggest that at intake levels at or below the TDI, estrogenic effects are unlikely to occur. The PBK model corroborated that this can be ascribed to the efficient glucuronidation of ZEN and its metabolites, reducing the circulation of the biologically active aglycones (Zinedine et al., 2007). Also the study on ZEN provided a proof-of-principle for inclusion of intestinal microbial metabolism in PBK models for ZEN and its metabolite α-ZEL in the host and use of the resulting predictions to evaluate potential in vivo effects at realistic levels of exposure.

The application of the described in vitro−in silico strategy was successful for both daidzein and ZEN. However, in **Chapters 2-4**, the PBK models were defined using parameters reflecting average values, without considering interindividual differences in toxicokinetics that are likely to occur. Hence, **Chapter 5** aimed at investigating the interindividual differences in the predicted C_{max} of daidzein (expressed in daidzein equivalents) when taking interindividual differences in kinetics into account. To achieve this, individual kinetic parameters V_{max} and K_m for daidzein microbial conversion and hepatic glucuronidation were obtained in incubations of 24 individual fecal samples and 25 liver S9 fractions, respectively. Subsequently, a Monte Carlo simulation was performed taking into account these obtained kinetic variations, and also variations in 7 additional influential PBK model parameters. This allowed definition of chemical-specific adjustment factors (CSAFs) for daidzein, which indicated that the current default uncertainty factor for interindividual differences in kinetics of 3.16 is protective for the healthy adult population. In addition, the PBK model was used to extrapolate the ERα-CALUX assay derived in vitro concentration-response curve (**Chapter 2**) for daidzein to an in vivo dose-response curve for daidzein induced estrogenicity by PBK modeling-based reverse dosimetry taking the estrogenicity of S-equol into account. Subsequently, as the point of departure (PoD), the benchmark dose lower confidence limit for

10% effect ($BMDL_{10}$) was derived using a benchmark dose (BMD) analysis, allowing comparison of the $BMDL_{10}$ to the dietary exposure levels of daidzein. This comparison showed that an Asian diet and use of soy supplements may, in contrast to a Western diet, result in an estrogenic response in human in vivo, in line with the observations in **Chapter 2**. The results obtained illustrate the potential for use of this in vitro-in silico strategy, as part of the NAMs, in the safety and risk assessment of food-born chemicals.

2. General discussion

The present thesis developed PBK models for daidzein and ZEN both for rat and human, which included gut microbiota as a separate compartment to assess the role of gut microbial metabolism on their ultimate estrogenicity as well as interspecies differences between rat and human. In addition, human interindividual differences were also studied in this thesis by integrating PBK modeling with Monte Carlo simulation. Except for the overview of the results and main findings described above, the results of the present thesis will now be further discussed in a wider framework also considering future studies and future perspectives. Topics that are of interests to address in some more detail include:

- In vitro approaches to study the kinetics of microbial metabolism
- PBK model related considerations
- Scaling factors for in vitro to in vivo extrapolation
- Implications of human risk assessment

2.1 In vitro approaches to study the kinetics of gut microbial metabolism

The role of gut microbiota in the metabolism of drugs, environmental contaminants and foodborne chemicals has attracted substantial attention in recent years due to its high metabolic potential resulting from a large content of bioactive enzymes (Francino, 2015; Gill et al., 2006). There is an increasing trend to develop and boost in vitro and in silico techniques also in the field of gut microbial metabolism and its consequences for human health. Development of such in vitro and in silico based NAMs complies with the so-called 3Rs principle aiming at replacement, reduction and refinement of animal studies. Various available in vitro gut models try to mimic intestinal environments and cultivate core bacteria,

and aim to be representative for human gut microbiota and its interaction with chemicals of interest.

A main category of these models represent so-called dynamic fermentation models. These are multi-stage setups consisting of a series of connected glass reactors, such as the TNO in vitro model of the colon (TIM-2) (Aguirre et al., 2014; Kortman et al., 2015), the simulator of the human intestinal microbial ecosystem (SHIME) (de Wiele et al., 2004) and the Gastro-Intestinal SIMulator (SIMGI) (Tamargo et al., 2018). These systems are usually maintained by constant supply of N_2 and nutritional medium, and inoculated using human fecal suspensions to mimic the intestinal environment (Lacroix et al., 2015). However, this kind of time- and effort-consuming systems appear to have limited reproducibility due to fluctuations in the mock gut microbial community after a relatively long incubation time and experimental period (e.g 72 h), providing possibilities for dominant species to overcome others, causing loss of some important phylogenetic clades and accompanying metabolic functions (Nissen et al., 2020).

In addition to these dynamic fermentation models static incubations have been used to study gut microbial metabolism. For example, some in vitro studies isolated and incubated bacterial species responsible for daidzein and ZEN conversion in static anaerobic incubations (Hur et al., 2002; Matthies et al., 2009; Tamura et al., 2007), which provided insight in the role of single microbial species, but ignored the complex interaction network of gut microbiota as a "whole" community, thereby not reflecting the gut microbiota's overall metabolic activities. To overcome these drawbacks, in this thesis, fecal anaerobic incubations were performed with optimized conditions, using PBS and relatively short incubation times. To avoid changes in the microbial community during the incubations, the culture conditions in the studies of the present thesis were short, for example 0.5-1 hour, and PBS was used as culture medium to provide as little enrichment as possible, thereby being as close to the intestinal communities and conditions when sampled as possible. As a non-invasive approach, these cost-effective and fast fecal anaerobic incubations thus enabled to study human gut microbial metabolism and interindividual differences therein.

However, the in vitro approach based on fecal samples also has drawbacks, for example that not all bacteria may survive or maintain their in vivo appearance under the in vitro conditions and the fecal incubations do not explicitly include the microbiota from the upper part of the gastrointestinal tract. For the studies on daidzein and ZEN this latter item is not a substantial

issue since gut microbial metabolism in the upper gastrointestinal tract is reported not to dominate the metabolism of these substances (Clavel et al., 2017). A role for the microbiota in the upper gastrointestinal tract may have to be considered however for other compounds such as for example ethanol, which can be converted to acetaldehyde through metabolism by oral microbes and mucosal cells, accumulating in saliva and gastric juice due to inefficient local enzymatic detoxification (MAK, 2013).

Overall, in vitro approaches, compared to in vivo experiments, generally create a highly controlled experimental environment to study the microbial metabolism of xenobiotics, allowing testing levels that cannot be reached in an in vivo setup. Nevertheless, as described above, each in vitro approach has its own advantages and shortcomings to represent the complex mechanisms of gut microbial metabolism, and thus selection of appropriate strategies should be well considered based on the features of the model compound of interest and the scientific questions to be addressed.

2.2 PBK model related considerations

2.2.1 Kinetics for gut microbial metabolism of daidzein and ZEN

Previous in vitro fecal incubations have reported microbial metabolism of daidzein and ZEN to result in formation of S-equol and α-ZEL, respectively. However, from those studies kinetic parameters could not be derived since most of these studies focused on the isolation of bacterial strains capable of performing the conversions. The described in vitro anaerobic fecal incubations in the present thesis allowed the definition of kinetic parameters V_{max} and K_m, and the catalytic efficiency for the gut microbial conversion of daidzein and ZEN, which are essential input parameters for the PBK models.

For microbial conversion of daidzein, substantial interspecies differences were observed between rats and human, with rats showing 54- to 209-fold higher catalytic efficiency (expressed in mL/h/g feces) in the formation of DHD, S-equol and O-DMA (**Chapter 3**). Since rats have a lower body weight (on average 250 grams) compared to human (on average 70 kg), scaling the activity to a per kg bw basis, taking also into account that the fraction of rat feces is around 5% of the body weight, while in human the fraction is about 1.4% (Brown et al., 1997), an extra 3.6-fold would be added to the interspecies differences between rats and human. The interspecies difference in gut microbial conversion was somewhat less pronounced for ZEN, for which the catalytic efficiency (expressed in mL/h/g feces) for

microbial conversion appeared to be 36.4- and 100.2-fold higher in rats than in human for the formation of α-ZEL and β-ZEL, respectively (**Chapter 4**). The diversity of bacterial species was reported to be two or three times higher in rats than in human (Manichanh et al., 2010), but whether this differences in bacterial diversity contributes to the observed interspecies differences in the microbial conversion of daidzein and ZEN, and whether this will also be the case for other foodborne chemicals remains to be elucidated.

2.2.2 Kinetics for hepatic metabolism of daidzein and ZEN

As described in **Chapter 1**, after going through the microbial pathways in the large intestine, daidzein, ZEN and their respective metabolites are taken up and transported via the portal vein to the liver where they can undergo further metabolism (Drzymala et al., 2015; Yang et al., 2017). Results from the PBK models revealed that this metabolism by the liver largely affected their ultimate intrinsic levels both in rats and in human. The efficient conjugation observed in **Chapters 2-4** explains the low bioavailability of the free daidzein and ZEN both in in vivo studies and in the model predictions.

Distinct interspecies differences were observed between rats and human in daidzein and S-equol hepatic glucuronidation, with rats being generally more efficient than human, suggesting a species difference in the activities of enzymes responsible for hepatic glucuronidation reactions. For example, the main isoforms of uridine 5'-diphospho-glucuronosyltransferases (UGTs) responsible for isoflavone glucuronidation are UGT1A1 and UGT1A9 (Hanioka et al., 2018; Yang et al., 2017), and the activity of UGT1A1 in rat liver microsomes was reported to be 2-fold as high as that in human liver microsomes, which may contribute to the higher catalytic efficiency of liver glucuronidation in rats than in human. Less obvious interspecies differences were observed in ZEN and α-ZEL hepatic glucuronidation, with rats showing only slightly higher catalytic efficiencies than human, being 1.1-fold for both of ZEN and α-ZEL. These results are in line with literature reported activities for ZEN and α-ZEL glucuronidation by male rat and human liver microsomes (Pfeiffer et al., 2010).

Hepatic metabolism of ZEN also results in the formation of its reduced metabolites α-ZEL and β-ZEL. The pathway for ZEN reduction in liver showed a higher catalytic efficiency in human than in rats, being 445-fold and 2-fold higher for the formation of α-ZEL and β-ZEL, respectively. Together these species differences in ZEN metabolism result in a 76-times

higher PBK model-predicted liver concentration of α-ZEL in human than rats. Since α-ZEL acts as a more bioactive metabolite than the parent compound ZEN, this may indicate that the use of rats may not fully represent the human situation.

2.2.3 Scaling factors for in vitro to in vivo extrapolation

When developing PBK models, scaling factors are required to convert in vitro determined parameters values into parameters relevant for the organism as a whole that are included in the PBK model. In the present thesis, scaling factors were required mainly to convert kinetic data that describe in vitro gut microbial conversion, and small intestine tissue and liver S9 conjugation of daidzein and ZEN to the in vivo situation. While the scaling factors for converting metabolic rates obtained in in vitro incubations with S9 samples to the in vivo situation have been reported and shown to be adequate in previous studies (Chen et al., 2018; Ning et al., 2019; Punt et al., 2016), the scaling factor for converting the data from the anaerobic fecal incubations to the in vivo situation was not reported previously .

In the present thesis, rates for metabolic conversion by the gut microbiota obtained in fecal anaerobic incubations were scaled to the whole body using the average fecal fractions of body weight. This approach is based on the assumption that the fecal content in the body represents the part that contains the microbiota responsible for the metabolic activity. However, the fecal mass has individual variations and could also be affected by diet and the health conditions of the host, while there may also be an effect of the transit time, a parameter that describes the potential time available for interactions between the gut microbiota and the compound of interest. In the present thesis, the proofs of principle described and the adequate predictions from PBK modeling matching in vivo data provide support for use of this fecal fraction of body weight as a first tier approach for scaling of the in vitro kinetic parameters. Prerequisite is that the colonic metabolism is the major factor determining the intestinal microbial conversion and that contributions in for example the small intestine or mouth are negligible, which is the case for both of daidzein and ZEN.

Though the current thesis facilitated adequate predictions of in vivo data, the scaling factor for the kinetic constants obtained in the anaerobic fecal incubations may be refined to a further extent in future studies, for example by taking fecal transit time into account, which may help reduce uncertainties caused by their potential relevance (McCabe et al., 2015).

2.2.4 Implications for human risk assessment

The PBK models used in the present thesis were used for risk assessment. In a first approach (**Chapter 2**) the PBK models were used for so-called forward dosimetry translating the dose levels resulting from specific dietary intake scenario's to endogenous maximum levels that were subsequently compared to the active concentrations obtained in the in vitro ERα-CALUX bioassay to conclude on whether at these endogenous concentrations estrogenic responses would be indicated. In addition, PBK models were used for so-called reverse dosimetry. In **Chapter 5** of the present thesis, in vitro concentration-response curves obtained in the ERα-CALUX bioassay were translated to in vivo dose-response curves from which $BMDL_{10}$ values were derived which were subsequently compared to dose levels resulting from realistic exposure scenario's. Finally, combining the developed PBK models with Monte Carlo simulations to take interindividual differences into account provided a way to define a compound specific assessment factor (CSAF) for interindividual differences in kinetics that may provide a basis for a compound specific and more refined definition of a health-based guidance value that can be used in risk assessment. This is discussed to a further extent in the next section.

2.2.4.1 PBK modeling integrated Monte Carlo simulation and the derivation of CSAFs

In **Chapters 2-4**, PBK models were developed and validated using parameters with average values, without considering variations that may arise from the presence of interindividual differences in toxicokinetics. The combination of PBK modeling with Monte Carlo simulation provides an opportunity to evaluate the interindividual differences and to refine the default uncertainty factors to CSAFs. In **Chapter 5**, variations in microbial metabolism and hepatic glucuronidation of daidzein, as well as in 7 additional influential PBK model parameters were included in a Monte Carlo simulation, which resulted in the derivation of CSAFs that amounted to 1.97 covering the 95th percentile of the population and to 2.56 when considering the 99th percentile of the population. The obtained CSAFs, which are smaller than the default uncertainty factor of 3.16 describing the interindividual variation in toxicokinetics, indicate that the current uncertainty factor is protective for the heathy adult population. However, it should be noted that including sensitive subgroups in the population, such as children, pregnant women, menopausal women, and/or women with a history of breast cancer (Ogunro, 2014) in the Monte Carlo simulation, may widen the distribution of predicted C_{max} levels and thus increase the CSAF, in case they would show different toxicokinetics. As a result, the default uncertainty factor for differences in kinetics may turn out not to be sufficiently protective. However, it should be noted that the mode(s) of action underlying the potential

heightened susceptibility of these subgroups may perhaps more likely be related to toxicodynamic differences, which are covered by the default factor of 3.16 for interindividual differences in toxicodynamics. This remains an interesting topic for future research.

Furthermore, in the current thesis, in addition to the variability in PBK model kinetic parameters related to microbial metabolism and hepatic glucuronidation, which were shown to be influential in the sensitivity analysis, also the interindividual variability in 7 additional parameters that also have substantial impact on the predicted outcome, was included in the Monte Carlo simulations. The inclusion of the variability in as many additional influential parameters as possible would be welcomed in future studies, which may slightly increase the currently obtained CSAFs for variation in interindividual toxicokinetics.

2.2.4.2 Choice of the dose metric in PBK modeling-based evaluation and reverse dosimetry

To enable translating from in vitro concentration-response curves to in vivo dose-response curves, PBK model-based reverse dosimetry requires some extra considerations with respect to the selection of the proper dose metric. Four issues need to be considered when making this choice: 1) the choice between using C_{max} or the area under the blood concentration time curve (AUC); 2) the correction for protein binding between the in vitro and in vivo situations using the protein unbound fraction in these two situations; 3) the correction from blood to plasma concentrations; 4) the choice of intracellular or extracellular concentrations.

The choice between C_{max} and AUC mainly depends on the mode of action of the model compound. It has been suggested that for reversible toxic effects for which a threshold exists, C_{max} is the suitable dose metric for reverse dosimetry, while for accumulative and irreversible adverse effects such as tumor formation, the AUC is preferred due to the time-depend accumulation of the overall toxicity (Rietjens et al., 2019). Given that the estrogenicity of both daidzein and ZEN can be expected to be effects with a threshold, which act by a mode of action that requires a certain dose to exert a toxic effect and the estrogenic effect is likely to be dependent on the peak concentration in the relevant target tissues such as uterus, ovaries and mammary gland (Daston et al., 2010), in the present thesis, C_{max} was chosen for daidzein and ZEN in both PBK model validation (**Chapter 2-4**) and also as the dose metric in the subsequent reverse dosimetry for daidzein to translate in vitro concentrations to in vivo dose levels (**Chapter 5**).

However, when validating the model predictions for the microbial metabolites S-equol and α-ZEL, the dose metric selected was 24 h cumulative urinary excretion (**Chapter 3** and **Chapter 4**), due to the fact that adequate data on in vivo C_{max} values for the parent compounds or their metabolites upon oral administration were lacking. Moreover, considering the model evaluations by comparing of PBK model predictions to reported in vivo data, it should also be noted that the model predicts an average value while available literature data sometimes show wide variability. For example, C_{max} values reported for the test compound can vary substantially between different in vivo studies performed at similar oral dose levels (Gonthier et al., 2003; King and Bursill, 1998), which may due to fasting state of the animals but that often such information is not provided. Thus, the selection of the dose metric in model validation and reverse dosimetry needs upfront scientific considerations preferably taking the mode of action (MoA) of the model compound into account and also considering the quality of the available in vivo data.

The second issue being considered is the correction for protein binding. The unbound concentration is considered to be the best dose metric due to the fact that only the free fraction can bind to the estrogen receptor. The unbound fraction represents the fraction available for cellular interaction, while the total nominal concentration exhibits limited biological responses in target tissues (Csanady et al., 2002). Thus, the correction for protein binding is of importance. In PBK modeling reversed dosimetry, when extrapolating in vitro concentrations to the in vivo situation, the in vitro concentration-response curve obtained from the ERα-CALUX assay (**Chapter 2**) was translated to an in vivo dose-response curve, using the developed human PBK model to calculate the oral dose of daidzein resulting in each effective concentration from the in vitro curve. This extrapolation was based on the unbound in vitro cell exposure concentration which was set equal to the PBK model predicted unbound C_{max}. Thus, unbound fractions of 12.0% and 12.5% were used to correct the predicted C_{max} of daidzein and S-equol, respectively (Csanady et al., 2002). Since cell culture medium was prepared in albumin-free conditions, the unbound in vitro concentrations were not corrected for protein binding (fub=1.0), assuming that the protein binding in the serum free medium was negligible.

A third topic to consider is the correction from blood to plasma concentrations. A correction from blood to plasma concentration is necessary in addition to the correction for protein binding, since the PBK model predicts the blood concentration of model compounds while the cellular exposure usually refers to unbound plasma concentrations. It is reported that the

blood-to-plasma ratio depends on the ionization of compounds, as for neutral and basic compounds it is generally assumed to be 1 when experimental data are not available (Katyayan and Hui, 2019), so that the PBK model predicted blood C_{max} can be assumed to be equal to the plasma C_{max}, as was the case in the present thesis, while for some acidic compounds, it could be assumed to be 0.55 (Mamada et al., 2021) or obtained by experiments.

Except for the selection of C_{max}, the correction for the unbound fraction and the correction from blood to plasma concentrations, the forth issue is whether to use intracellular or extracellular concentrations. Theoretically, the most relevant and representative concentration exerting the biological effect would be the unbound intracellular concentration in the target tissue, which in the case of daidzein could be the uterus, mammary gland and/or ovary (Li et al., 2007). However, it is practically difficult to obtain these tissue samples especially from human, in order to enable quantification of tissue concentrations. Besides, material preparation and processing may lead to shifted pH and unstable intracellular components (Brunner and Langer, 2006), which makes it difficult to correct for intracellular protein binding. Taken all these factors into consideration, the extracellular unbound concentration was selected as the dose metric when performing PBK modeling-based reverse dosimetry, using in vitro unbound cell concentrations obtained from the ERα-CALUX assay set equal to the extracellular unbound plasma concentrations in the PBK model.

3. Future perspectives

The current thesis presents an in vitro-in silico approach to include the metabolic capacity of gut microbiota in the PBK models for rats and human describing the ADME of daidzein and ZEN. As described in the above sections, the developed PBK models based reverse dosimetry and Monte Carlo simulations, were able to predict the estrogenicity of daidzein for ERα activation, which provide promising NAMs in modern toxicology. Except for the issues already discussed above, some important aspects can be addressed in future studies regarding:

- In vitro model used
- Interactions between microbiota and xenobiotics
- PBK model refinement and extension
- Uncertainty factor for in vitro-in silico approaches

- Additive effects of foodborne chemicals

3.1 In vitro model used

The conditions of the in vitro fecal anaerobic incubation were optimized in this study, allowing derivation of kinetic parameters that were essential for PBK modeling. Use of feal samples was shown to result in adequate data and model predictions were confirmed to be sufficiently reflecting in vivo data. Hence, the utilization of fecal materials can be promoted and the in vitro fecal anaerobic incubations can be standardized, in order to apply the method to other chemicals subject to microbial conversions. More proofs of principle should be generated to support that feces could be representative for up to 65% of colonic genomes and also in functions (Lagkouvardos et al., 2017), and may provide a promising biological material in the future, playing a similar role to the well accepted liver S9 fractions, as a golden standard when studying metabolic capacity of gut microbiota. Further refinement of the scaling factor from in vitro feces to in vivo gut microbiota would be helpful to achieve this, for example by fitting the model predictions to actual in vivo data for a larger series of compounds for which the colon is the relevant site for their gut microbial metabolism.

Other developments in the field of in vitro models for intestine and gut microbiota activities, can also be considered for use in future studies, such as three-dimensional (3D) cell cultures (Fang and Eglen, 2017) and microdevices such as “organ-on-a-chip” (Zheng et al., 2016). These approaches usually apply co-cultures that not only include a single cell type but also other types of cells such as epithelium and immune cells, which create microenvironments mimicking tissue properties and cellular interactions (Zhang and Radisic, 2017). In the future, the development of these co-cultures may also enable the derivation of kinetic parameters to be used in PBK models.

3.2 Interactions between microbiota and xenobiotics

In recent years, evidence has been accumulating that the gut microbiota is actively involved in the metabolisms of xenobiotics through a wide range of biochemical activities and dysbiosis of the gut microbiota is considered to be associated with some diseases, such as non-alcoholic fatty liver disease, metabolic disorders and inflammatory bowel disease (Baumler and Sperandio, 2016; Scheperjans et al., 2015). However, except for the impact of microbial biotransformation on xenobiotics, xenobiotics in return, may also influence the community of microbiota in potential also leading to functional alterations (Francino, 2015; Maurice et al.,

2013). Behr et al. (Behr et al., 2017) reported that after treatment of rats with antibiotics, the diversity of the microbial community was drastically reduced and bile acid profiles markedly affected. This indicates the substantial influence that xenobiotics may have on gut microbiota in composition and function, and this may hold not only for antibiotics, but also turned out to be relevant for drugs such as the antidiabetic drug metformin and nonsteroidal anti-inflammatory drugs like ibuprofen and naproxen. (Rogers and Aronoff, 2016; Wu et al., 2017). There are a number of foodborne xenobiotics that are reported to affect the composition of the microbiota, meanwhile other factors can also affect microbial communities such as dietary changes, stress and temperature (Flandroy et al., 2018; Gill et al., 2006; Jovel et al., 2016), but whether that also leads to functional changes still needs to be elucidated. This complex bilateral interaction between xenobiotics and gut microbiota has so far not been taken into account to a significant extent when considering the role for microbiota in metabolism of the xenobiotics, and thus could be an interesting topic for further investigations, which could be considered and included in risk assessment of xenobiotics. Within this context it would also be of use to better define what changes in the microbial community can be considered adverse and which once are to be considered merely as adaptive.

3.3 PBK model refinement and extension

Despite the fact that the current developed PBK models made predictions that adequately matched available in vivo data, there are still some refinement and extensions that can be considered for future improvement when applying it to more chemicals.

First of all, the excretion routes for the elimination and clearance of the model compounds can be added to the PBK model by including the corresponding kinetics via urinary and fecal excretion (Schwen et al., 2012; Seow et al., 1998). In **Chapter 3** and **Chapter 4**, culminative urinary excretion of S-equol and α-ZEL was predicted, based on the assumption that all the conjugated metabolites would be excreted into urine, which gave accurate predictions compared with in vivo data. However, for compounds where for example active excretion plays a role in the kinetics and influences the blood concentrations, the excretion pathways can be considered and included.

Enterohepatic circulation is another aspect that can be seen as an extension for the PBK models developed in this thesis. It has been discussed in the previous sections that the low bioavailability of free daidzein and ZEN at target tissues is mainly caused by the highly

efficient conjugation in the liver. This glucuronidation in the liver leads to excretion, which can be followed by re-uptake and thus so-called “enterohepatic circulation”. This route begins with the absorption of daidzein and ZEN from the intestinal lumen, upon which it is transported to the liver via the portal vein. In the liver, extensive glucuronidation results in large proportions of conjugated daidzein and ZEN, which are partly secreted into the bile and pass the upper small intestine (Drzymala et al., 2015; Gardana et al., 2009) until encountering bacterial glucuronidases and sulfatases in the colon, resulting in unconjugated compounds that can be reabsorbed to start the cycle gain (Fujitani et al., 2019). This phenomenon can be captured in some in vivo studies presenting pharmacokinetic curves, resulting in a second peak a few hours after oral dosing upon a single administration of the substrate (Janning et al., 2000; Legette et al., 2014; Sepehr et al., 2007). The inclusion of this enterohepatic circulation may increase the accuracy for PBK model-based predictions especially at later time points.

3.4 Uncertainty factor for in vitro-in silico approaches

The methods and results of the present thesis contribute to the development and utilization of in vitro approaches, which fulfils the 3Rs principle. In addition, the advances of in vitro techniques enable the use of human models, which may provide a better basis for human risk assessment since compared to animal studies they are closer to the human situation and may reduce/eliminate the uncertainty factor of 10 describing interspecies differences. However, it should be noted that an additional safety factor may be needed when deriving health based guidance values based on BMDL10 values derived from in vitro-in silico predicted dose response curves. Such an extra uncertainty factor could for example account for the uncertainties connected to extrapolations from in vitro to in vivo data. Such uncertainties arise for example, from the required correction for protein binding in PBK modeling based reverse dosimetry which assumes the unbound extracellular concentration equal to the unbound concentration in the target organ, potential inaccuracies in the PBK model predictions reflected by (small) differences between predicted and in vivo available kinetic data, and/or suitability of the in vitro assay used to define the concentration response curve to mimic the critical in vivo effect. An extra uncertainty factor would cover these and other uncertainties connected to the establishment of PoDs using PBK model based reverse dosimetry and QIVIVE. Depending on expert judgement the additional assessment factor may be defined. For example, the PBK models developed and used in the present thesis for QIVIVE can be expected to introduce less uncertainty than a high throughput-in vitro in vivo extrapolation (HT-IVIVE) approach which uses simple kinetic equations and mostly ignores many of the

ADME characteristics of a compound (Wetmore, 2015). Overall, more examples and proofs-of-principles are need to introduce and define the additional uncertainty factor to be used when establishing health based guidance values using points of departure defined by in vitro-in silico approaches..

3.5 Additive effects of foodborne chemicals

Finally, in future risk assessment and risk management, consideration of additive effects caused upon combined exposure to different chemicals with the same toxicity, such as estrogenicity, should be considered. This is based on the fact that in real life scenarios, humans are mostly under exposure of mixtures composed of food components, drugs and environmental chemicals (Kortenkamp et al., 2007; Kumari and Kumar, 2020). **Chapter 5** could be presented as an example how to proceed when taking into account additive effects, which was done by expressing the overall C_{max} of daidzein and S-equol in daidzein equivalents. This is achieved by setting the potency of the parent compound as 1, and introducing a "relative potency factor (RPF)" for each of the metabolites or compounds with which combined exposure is expected, to enable definition of an overall concentration expressed in equivalents of the selected reference compound (Terry et al., 2015). In this approach the overall concentration in reference compound equivalents is calculated by summing up concentrations of the respective compounds multiplied by their RPF values. Clearly this approach only applies when there is evidence that the compounds act in an additive way. Although formally the RPF factors should be based on in vivo potencies, use of in vitro bioassays such as the ERα-CALUX assay in the present thesis, provides an alternative strategy to define the RPF values, provided the compounds tested are not subject to metabolic activation or detoxification, reactions generally not included in the in vitro bioassays. Obviously integrating the RPF approach with PBK modeling may solve these kind of issues as also shown in the present thesis in the combined evaluation of daidzein and S-equol. Consequently, standardizing and grouping chemicals into different categories on the basis of sharing similarity in toxicological mechanisms or toxic endpoint (Heys et al., 2016; Lambert and Lipscomb, 2007) would support the risk assessment of chemical co-exposures in the future.

4. Conclusion

In conclusion, the current thesis provides proofs-of-principle for inclusion of gut microbial metabolism in PBK modeling using in vitro fecal anaerobic incubations, which could successfully be applied to predict the intrinsic concentrations of the parent compounds and their corresponding microbial metabolites in the host. Furthermore, the integration of PBK modeling with Monte Carlo simulation, taking daidzein as an example, allowed assessment of interindividual differences, indicating a possibility in risk assessment to refine and/or evaluate the current default uncertainty factor for interindividual differences in toxicokinetics. Meanwhile, the application of PBK modeling-based reversed dosimetry enabled prediction of in vivo estrogenicity through ERα activation, while reverse and forward dosimetry provided ways to use the in vitro data combined with the PBK models in risk assessment. Altogether, the incorporation of gut microbial metabolism in the in vitro-in silico approach is an important step forward in the use of this NAM in risk assessment of foodborne chemicals and a relevant addition to current QIVIVE strategies which are a key elements of modern toxicity testing strategies.

References

Agahi, F., Juan, C., Font, G., and Juan-Garcia, A. (2020). In silico methods for metabolomic and toxicity prediction of zearalenone, alpha-zearalenone and beta-zearalenone. *Food Chem Toxicol* **146**, 111818.

Aguirre, M., Jonkers, D. M., Troost, F. J., Roeselers, G., and Venema, K. (2014). In vitro characterization of the impact of different substrates on metabolite production, energy extraction and composition of gut microbiota from lean and obese subjects. *PLoS One* **9**, e113864.

Anderson, J. W., Fuller, J., Patterson, K., Blair, R., and Tabor, A. (2007). Soy compared to casein meal replacement shakes with energy-restricted diets for obese women: randomized controlled trial. *Metabolism* **56**, 280-288.

Arai, Y., Watanabe, S., Kimira, M., Shimoi, K., Mochizuki, R., and Kinae, N. (2000). Dietary intakes of flavonols, flavones and isoflavones by Japanese women and the inverse correlation between quercetin intake and plasma LDL cholesterol concentration. *The Journal of nutrition* **130**, 2243-2250.

Behr, C., Kamp, H., Fabian, E., Krennrich, G., Mellert, W., Peter, E., Strauss, V., Walk, T., Rietjens, I., and van Ravenzwaay, B. (2017). Gut microbiome-related metabolic changes in plasma of antibiotic-treated rats. *Arch Toxicol* **91**, 3439-3454.

Brown, R. P., Delp, M. D., Lindstedt, S. L., Rhomberg, L. R., and Beliles, R. P. (1997). Physiological parameter values for physiologically based pharmacokinetic models. *Toxicology and industrial health* **13**, 407-484.

Brunner, M., and Langer, O. (2006). Microdialysis versus other techniques for the clinical assessment of in vivo tissue drug distribution. *The AAPS journal* **8**, E263-E271.

Chen, A., Zhou, X., Cheng, Y., Tang, S., Liu, M., and Wang, X. (2018). Design and optimization of the cocktail assay for rapid assessment of the activity of UGT enzymes in human and rat liver microsomes. *Toxicol Lett* **295**, 379-389.

Clavel, T., Lagkouvardos, I., and Stecher, B. (2017). From complex gut communities to minimal microbiomes via cultivation. *Curr Opin Microbiol* **38**, 148-155.

de Wiele, T. V., Boon, N., Possemiers, S., Jacobs, H., and Verstraete, W. (2004). Prebiotic effects of chicory inulin in the simulator of the human intestinal microbial ecosystem. *FEMS Microbiol Ecol* **51**, 143-53.

Drzymala, S. S., Binder, J., Brodehl, A., Penkert, M., Rosowski, M., Garbe, L. A., and Koch, M. (2015). Estrogenicity of novel phase I and phase II metabolites of zearalenone and cis-zearalenone. *Toxicon* **105**, 10-2.

EFSA (2011). Scientific Opinion on the risks for public health related to the presence of zearalenone in food. *EFSA Journal* **9**.

Eisenbrand, G., and Senate Commission on Food Safety of the German Research, F. (2007). Isoflavones as phytoestrogens in food supplements and dietary foods for special medical purposes. Opinion of the Senate Commission on Food Safety (SKLM) of the German Research Foundation (DFG)-(shortened version). *Mol Nutr Food Res* **51**, 1305-12.

Fang, Y., and Eglen, R. M. (2017). Three-Dimensional Cell Cultures in Drug Discovery and Development. *SLAS DISCOVERY: Advancing the Science of Drug Discovery* **22**, 456-472.

Francino, M. P. (2015). Antibiotics and the Human Gut Microbiome: Dysbioses and Accumulation of Resistances. *Front Microbiol* **6**, 1543.

Gill, S. R., Pop, M., DeBoy, R. T., Eckburg, P. B., Turnbaugh, P. J., Samuel, B. S., Gordon, J. I., Relman, D. A., Fraser-Liggett, C. M., and Nelson, K. E. (2006). Metagenomic analysis of the human distal gut microbiome. *science* **312**, 1355-1359.

Gonthier, M.-P., Donovan, J. L., Texier, O., Felgines, C., Remesy, C., and Scalbert, A. (2003). Metabolism of dietary procyanidins in rats. *Free Radical Biology and Medicine* **35**, 837-844.

Hanioka, N., Ohkawara, S., Isobe, T., Ochi, S., Tanaka-Kagawa, T., and Jinno, H. (2018). Regioselective glucuronidation of daidzein in liver and intestinal microsomes of humans, monkeys, rats, and mice. *Arch Toxicol* **92**, 2809-2817.

Heys, K. A., Shore, R. F., Pereira, M. G., Jones, K. C., and Martin, F. L. (2016). Risk assessment of environmental mixture effects. *RSC Advances* **6**, 47844-47857.

Human Microbiome Project, C. (2012). A framework for human microbiome research. *Nature* **486**, 215-21.

Hur, H. G., Beger, R. D., Heinze, T. M., Lay, J. O., Jr., Freeman, J. P., Dore, J., and Rafii, F. (2002). Isolation of an anaerobic intestinal bacterium capable of cleaving the C-ring of the isoflavonoid daidzein. *Arch Microbiol* **178**, 8-12.

Kim, J.-S., and Kwon, C.-S. (2001). Estimated dietary isoflavone intake of Korean population based on National Nutrition Survey. *Nutrition Research* **21**, 947-953.

King, R. A., and Bursill, D. B. (1998). Plasma and urinary kinetics of the isoflavones daidzein and genistein after a single soy meal in humans. *The American journal of clinical nutrition* **67**, 867-872.

Kortenkamp, A., Faust, M., Scholze, M., and Backhaus, T. (2007). Low-level exposure to multiple chemicals: reason for human health concerns? *Environ Health Perspect* **115 Suppl 1**, 106-14.

Kortman, G. A., Dutilh, B. E., Maathuis, A. J., Engelke, U. F., Boekhorst, J., Keegan, K. P., Nielsen, F. G., Betley, J., Weir, J. C., Kingsbury, Z., Kluijtmans, L. A., Swinkels, D. W., Venema, K., and Tjalsma, H. (2015). Microbial Metabolism Shifts Towards an Adverse Profile with Supplementary Iron in the TIM-2 In vitro Model of the Human Colon. *Front Microbiol* **6**, 1481.

Kowalska, K., Habrowska-Gorczynska, D. E., and Piastowska-Ciesielska, A. W. (2016). Zearalenone as an endocrine disruptor in humans. *Environ Toxicol Pharmacol* **48**, 141-149.

Kumari, M., and Kumar, A. (2020). Identification of component-based approach for prediction of joint chemical mixture toxicity risk assessment with respect to human health: A critical review. *Food Chem Toxicol* **143**, 111458.

Lacroix, C., de Wouters, T., and Chassard, C. (2015). Integrated multi-scale strategies to investigate nutritional compounds and their effect on the gut microbiota. *Curr Opin Biotechnol* **32**, 149-155.

Lagkouvardos, I., Overmann, J., and Clavel, T. (2017). Cultured microbes represent a substantial fraction of the human and mouse gut microbiota. *Gut Microbes* **8**, 493-503.

Lambert, J. C., and Lipscomb, J. C. (2007). Mode of action as a determining factor in additivity models for chemical mixture risk assessment. *Regul Toxicol Pharmacol* **49**, 183-94.

Legette, L. L., Prasain, J., King, J., Arabshahi, A., Barnes, S., and Weaver, C. M. (2014). Pharmacokinetics of equol, a soy isoflavone metabolite, changes with the form of equol (dietary versus intestinal production) in ovariectomized rats. *J Agric Food Chem* **62**, 1294-300.

Li, Y., He, W., Liu, H., Yao, X., and Hu, Z. (2007). Daidzein interaction with human serum albumin studied using optical spectroscopy and molecular modeling methods. *Journal of Molecular Structure* **831**, 144-150.

MAK (2013). Acetaldehyde. *MAK commission-Collection for Occupational Health and Safety* **2013b**.

Manichanh, C., Reeder, J., Gibert, P., Varela, E., Llopis, M., Antolin, M., Guigo, R., Knight, R., and Guarner, F. (2010). Reshaping the gut microbiome with bacterial transplantation and antibiotic intake. *Genome Res* **20**, 1411-9.

Matthies, A., Blaut, M., and Braune, A. (2009). Isolation of a human intestinal bacterium capable of daidzein and genistein conversion. *Appl Environ Microbiol* **75**, 1740-4.

Maurice, C. F., Haiser, H. J., and Turnbaugh, P. J. (2013). Xenobiotics shape the physiology and gene expression of the active human gut microbiome. *Cell* **152**, 39-50.

Mayo, B., Vazquez, L., and Florez, A. B. (2019). Equol: A Bacterial Metabolite from The Daidzein Isoflavone and Its Presumed Beneficial Health Effects. *Nutrients* **11**.

McCabe, M., Sane, R. S., Keith-Luzzi, M., Xu, J., King, I., Whitcher-Johnstone, A., Johnstone, N., Tweedie, D. J., and Li, Y. (2015). Defining the Role of Gut Bacteria in the Metabolism of Deleobuvir: In Vitro and In Vivo Studies. *Drug Metab Dispos* **43**, 1612-8.

Merz-Demlow, B. E., Duncan, A. M., Wangen, K. E., Xu, X., Carr, T. P., Phipps, W. R., and Kurzer, M. S. (2000). Soy isoflavones improve plasma lipids in normocholesterolemic, premenopausal women. *The American journal of clinical nutrition* **71**, 1462-1469.

Minervini, F., Giannoccaro, A., Fornelli, F., Dell'Aquila, M. E., Minoia, P., and Visconti, A. (2006). Influence of mycotoxin zearalenone and its derivatives (alpha and beta zearalenol) on apoptosis and proliferation of cultured granulosa cells from equine ovaries. *Reprod Biol Endocrinol* **4**, 62.

Ning, J., Rietjens, I., and Strikwold, M. (2019). Integrating physiologically based kinetic (PBK) and Monte Carlo modeling to predict inter-individual and inter-ethnic variation in bioactivation and liver toxicity of lasiocarpine. *Arch Toxicol* **93**, 2943-2960.

Nissen, L., Casciano, F., and Gianotti, A. (2020). Intestinal fermentation in vitro models to study food-induced gut microbiota shift: an updated review. *FEMS Microbiol Lett* **367**.

Ogunro, P. (2014). Antioxidant status and reproductive hormones in women during reproductive, perimenopausal and postmenopausal phase of life. *African journal of medicine and medical sciences* **43**, 49-57.

Pfeiffer, E., Hildebrand, A., Mikula, H., and Metzler, M. (2010). Glucuronidation of zearalenone, zeranol and four metabolites in vitro: formation of glucuronides by various microsomes and human UDP-glucuronosyltransferase isoforms. *Mol Nutr Food Res* **54**, 1468-76.

Pritchett, L. E., Atherton, K. M., Mutch, E., and Ford, D. (2008). Glucuronidation of the soyabean isoflavones genistein and daidzein by human liver is related to levels of UGT1A1 and UGT1A9 activity and alters isoflavone response in the MCF-7 human breast cancer cell line. *J Nutr Biochem* **19**, 739-45.

Punt, A., Paini, A., Spenkelink, A., Scholz, G., Schilter, B., van Bladeren, P. J., and Rietjens, I. M. (2016). Evaluation of Interindividual Human Variation in Bioactivation and DNA Adduct Formation of Estragole in Liver Predicted by Physiologically Based Kinetic/Dynamic and Monte Carlo Modeling. *Chem Res Toxicol* **29**, 659-68.

Rietjens, I., Ning, J., Chen, L., Wesseling, S., Strikwold, M., and Louisse, J. (2019). Selecting the dose metric in reverse dosimetry based QIVIVE : Reply to 'Comment on 'Use of an in vitro-in silico testing strategy to predict inter-species and inter-ethnic human differences in liver toxicity of the pyrrolizidine alkaloids lasiocarpine and riddelliine' by Ning et al., Arch Toxicol doi: https://doi.org/10.1007/s00204-019-02397-7', Arch Toxicol doi: https://doi.org/10.1007/s0020 4-019-02421-w. *Arch Toxicol* **93**, 1467-1469.

Rogers, M. A. M., and Aronoff, D. M. (2016). The influence of non-steroidal anti-inflammatory drugs on the gut microbiome. *Clin Microbiol Infect* **22**, 178 e1-178 e9.

Sager, J. E., Yu, J., Ragueneau-Majlessi, I., and Isoherranen, N. (2015). Physiologically Based Pharmacokinetic (PBPK) Modeling and Simulation Approaches: A Systematic Review of Published Models, Applications, and Model Verification. *Drug Metab Dispos* **43**, 1823-37.

Schwen, R. J., Nguyen, L., and Jackson, R. L. (2012). Elucidation of the metabolic pathway of S-equol in rat, monkey and man. *Food Chem Toxicol* **50**, 2074-83.

Seow, A., Shi, C.-Y., Franke, A. A., Hankin, J. H., Lee, H.-P., and Yu, M. C. (1998). Isoflavonoid levels in spot urine are associated with frequency of dietary soy intake in a population-based sample of middle-aged and older Chinese in Singapore. *Cancer Epidemiology and Prevention Biomarkers* **7**, 135-140.

Sun, M.-Y., Ye, Y., Xiao, L., Rahman, K., Xia, W., and Zhang, H. (2016). Daidzein: A review of pharmacological effects. *African Journal of Traditional, Complementary and Alternative Medicines* **13**.

Takemura, H., Shim, J. Y., Sayama, K., Tsubura, A., Zhu, B. T., and Shimoi, K. (2007). Characterization of the estrogenic activities of zearalenone and zeranol in vivo and in vitro. *J Steroid Biochem Mol Biol* **103**, 170-7.

Tamargo, A., Cueva, C., Laguna, L., Moreno-Arribas, M. V., and Muñoz, L. A. (2018). Understanding the impact of chia seed mucilage on human gut microbiota by using the dynamic gastrointestinal model simgi®. *Journal of Functional Foods* **50**, 104-111.

Tamura, M., Tsushida, T., and Shinohara, K. (2007). Isolation of an isoflavone-metabolizing, Clostridium-like bacterium, strain TM-40, from human faeces. *Anaerobe* **13**, 32-5.

Terry, C., Rasoulpour, R. J., Knowles, S., and Billington, R. (2015). Utilizing relative potency factors (RPF) and threshold of toxicological concern (TTC) concepts to assess hazard and human risk assessment profiles of environmental metabolites: a case study. *Regul Toxicol Pharmacol* **71**, 301-17.

van Erp-Baart, M.-A. J., Brants, H. A., Kiely, M., Mulligan, A., Turrini, A., Sermoneta, C., Kilkkinen, A., and Valsta, L. M. (2003). Isoflavone intake in four different European countries: the VENUS approach. *British Journal of Nutrition* **89**, S25-S30.

Wakai, K., Egami, I., Kato, K., Kawamura, T., Tamakoshi, A., Lin, Y., Nakayama, T., Wada, M., and Ohno, Y. (1999). Dietary intake and sources of isoflavones among Japanese. *Nutrition and cancer* **33**, 139-145.

Wetmore, B. A. (2015). Quantitative in vitro-to-in vivo extrapolation in a high-throughput environment. *Toxicology* **332**, 94-101.

Wu, H., Esteve, E., Tremaroli, V., Khan, M. T., Caesar, R., Manneras-Holm, L., Stahlman, M., Olsson, L. M., Serino, M., Planas-Felix, M., Xifra, G., Mercader, J. M., Torrents, D., Burcelin, R., Ricart, W., Perkins, R., Fernandez-Real, J. M., and Backhed, F. (2017). Metformin alters the gut microbiome of individuals with treatment-naive type 2 diabetes, contributing to the therapeutic effects of the drug. *Nat Med* **23**, 850-858.

Yang, N., Sun, R., Liao, X., Aa, J., and Wang, G. (2017). UDP-glucuronosyltransferases (UGTs) and their related metabolic cross-talk with internal homeostasis: A systematic review of UGT isoforms for precision medicine. *Pharmacol Res* **121**, 169-183.

Yazar, S., and Omurtag, G. Z. (2008). Fumonisins, trichothecenes and zearalenone in cereals. *Int J Mol Sci* **9**, 2062-90.

Zhang, B., and Radisic, M. (2017). Organ-on-a-chip devices advance to market. *Lab Chip* **17**, 2395-2420.

Zheng, F., Fu, F., Cheng, Y., Wang, C., Zhao, Y., and Gu, Z. (2016). Organ-on-a-Chip Systems: Microengineering to Biomimic Living Systems. *Small* **12**, 2253-82.

Zinedine, A., Soriano, J. M., Molto, J. C., and Manes, J. (2007). Review on the toxicity, occurrence, metabolism, detoxification, regulations and intake of zearalenone: an oestrogenic mycotoxin. *Food Chem Toxicol* **45**, 1-18.

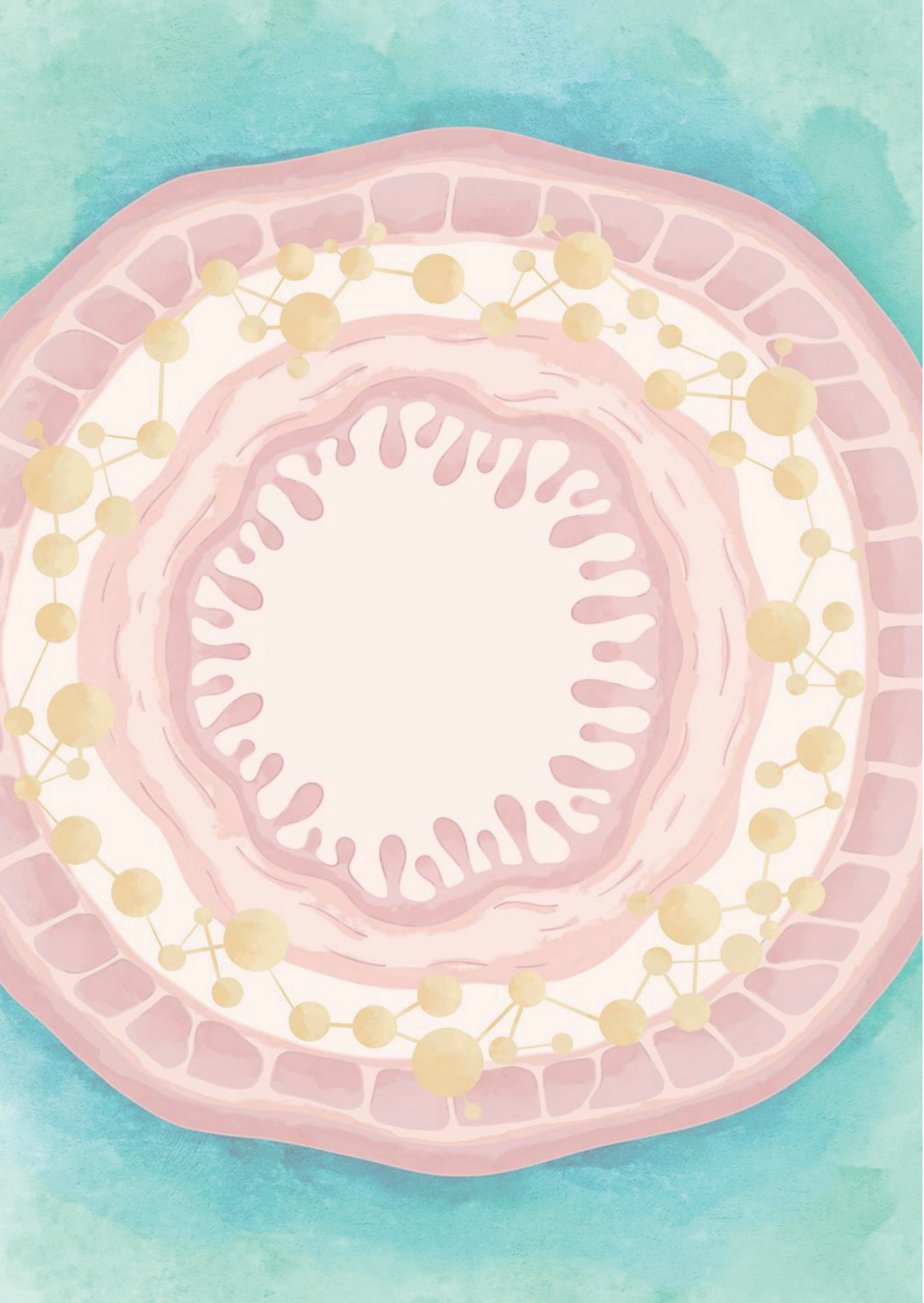

Chapter 7

Summary

The aim of the present thesis was to characterize the role of gut microbial metabolism in the toxicity of daidzein and zearalenone (ZEN) by including gut microbiota in physiologically based kinetic (PBK) models and applying these models for quantitative in vitro to in vivo extrapolations (QIVIVE). The results obtained provide proofs-of-principle for application of this novel approach methodology (NAM) for alternatives in animal testing, characterizing the consequences of the metabolism by the gut microbiota for toxicity of foodborne chemicals in the host without a need for in vivo studies in experimental animals or human intervention studies.

Chapter 1 introduced the gut microbiota and its metabolic capacity, which may affect the ultimate toxicity of a foodborne constituent through a wide range of biochemical activities. The soy isoflavone daidzein and the mycotoxin ZEN, selected as the two model compounds in this thesis, were introduced with their absorption, distribution, metabolism and excretion (ADME) characteristics and toxicity. The selection of these model compounds was based on the fact that daidzein and ZEN can be converted by gut microbiota to their more potent estrogenic metabolites S-equol and α-zearalenol (α-ZEL), respectively. In addition, background information on PBK modeling, Monte Carlo simulations and PBK modeling-based reverse dosimetry were also introduced in this chapter.

Chapter 2 developed a PBK model for daidzein in rats, which enabled the description of gut microbial activity by introducing a separate gut microbiota compartment. The model included a main model for daidzein and a submodel for its more bioactive microbial metabolite S-equol. By performing anaerobic incubations of rat fecal samples with daidzein, kinetic parameters for the formation of dihydrodaidzein (DHD), S-equol and O-desmethylangolensin (O-DMA) were obtained, scaled to the in vivo situation and included in the PBK model, which enabled prediction of plasma levels of daidzein and S-equol. The model was validated by comparison of predictions made for plasma levels (C_{max}) of daidzein and S-equol to levels reported in in vivo studies in literature. This comparison showed an overall 1.22- and 1.07-fold difference between predicted and observed daidzein and S-equol plasma levels, respectively. Additionally, the estrogen receptor (ER)α-CALUX assay was used to quantify the estrogenicity of daidzein and S-equol. S-equol showed a 12.7- fold higher potency than daidzein as derived from the EC_{50} values. Further comparison of dietary exposure scenarios indicated that an Asian diet, a vegetarian diet and intake of food supplements, but not a Western diet, were predicted to result in C_{max} values for daidzein that were higher than its EC_{10} for estrogenicity, while all predicted C_{max} values for S-equol were lower than the EC_{10}

for estrogenicity of S-equol, indicating that daidzein plays the dominant role in ERα-mediated estrogenicity despite of the higher estrogenic potential of its microbial metabolite S-equol.

Chapter 3 extended and applied the previously developed PBK model for rats to a PBK model for humans. To this end, human fecal samples were collected from 15 healthy donors, 6 of which were identified as S-equol producers while 9 were identified as S-equol nonproducers. Consequently, two PBK models were developed, one for S-equol producers and one for non-producers using their respective kinetic parameters V_{max} and K_m for the formation of DHD, S-equol (only for producers), and O-DMA. Model validation showed that model-based predictions for the C_{max} of daidzein were on average 1.62 times that of reported in vivo C_{max} values; model-based predictions for the cumulative urinary excretion of conjugated S-equol were on average 0.89 times that of the reported in vivo cumulative urinary excretion of conjugated S-equol, revealing the model predictions to be accurate. Additionally, Chapter 3 also characterized interspecies differences between rats and human in gut microbial metabolism of daidzein by comparing the kinetic data obtained in **Chapters 2 and 3**. This revealed that rat fecal samples showed much higher catalytic efficiencies than human fecal samples in the formation of all the metabolites DHD, S-equol and O-DMA, pointing at substantial interspecies differences.

In Chapter 4, ZEN and α-ZEL were chosen as model compounds in order to apply the above mentioned in vitro-in silico strategy to other foodborne chemicals as part of the development of NAMs. ZEN is an important bioactive mycotoxin. Similar to daidzein, ZEN shows estrogenic potential and can be metabolized by gut microbiota to a more potent metabolite, i.e. α-ZEL. Rat and human PBK models were developed for ZEN with a sub-model for α-ZEL, and included the intestinal microbial bioactivation of ZEN to α-ZEL. The PBK model for rats was evaluated by comparing the predicted C_{max} of ZEN to reported in vivo data, showing that the predictions were only 1.3-fold higher than reported in vivo data. Additionally, the predicted C_{max} for ZEN and α-ZEL in human upon exposure at the level of the so-called Tolerable Daily Intake (TDI) for ZEN of 0.25 mg/kg bw/day were much lower than the in vitro EC_{10} values in the ERα-CALUX reporter gene assay, suggesting that estrogenic effects are unlikely to occur at intake levels at or below the TDI .

In Chapter 5, the previously developed PBK model for daidzein in human was integrated with Monte Carlo simulations to study the interindividual differences in the predicted C_{max} of daidzein (expressed in daidzein equivalents) taking variations in gut microbial metabolism

and liver glucuronidation of daidzein, as well as in 7 additional influential parameters into account. Subsequently, chemical-specific adjustment factors (CSAFs) were derived at 95th and 99th percentiles of the Monte Carlo based predicted distribution for the C_{max} of daidzein. These CSAF values amounted to 1.97 and 2.54, respectively, indicating that the default uncertainty factor for interindividual differences in kinetics of 3.16 is protective for the healthy adult. Altogether, the application of PBK modeling integrated Monte Carlo simulation appeared a promising novel approach methodology (NAM) to assess interindividual variations in kinetics and to refine the human risk assessment of foodborne chemicals.

Chapter 6 summarized and discussed the main findings of the thesis. It presented the innovations and limitations of methods applied, and also provided future perspectives that can be addressed in the near future when studying the gut microbial metabolism of foodborne chemicals and its toxicological consequences. Altogether, the present thesis showed how to include the metabolism by gut microbiota in PBK modeling, and provided proofs-of-principle for use of this approach as alternative for animal testing in the risk assessment of foodborne constituents .

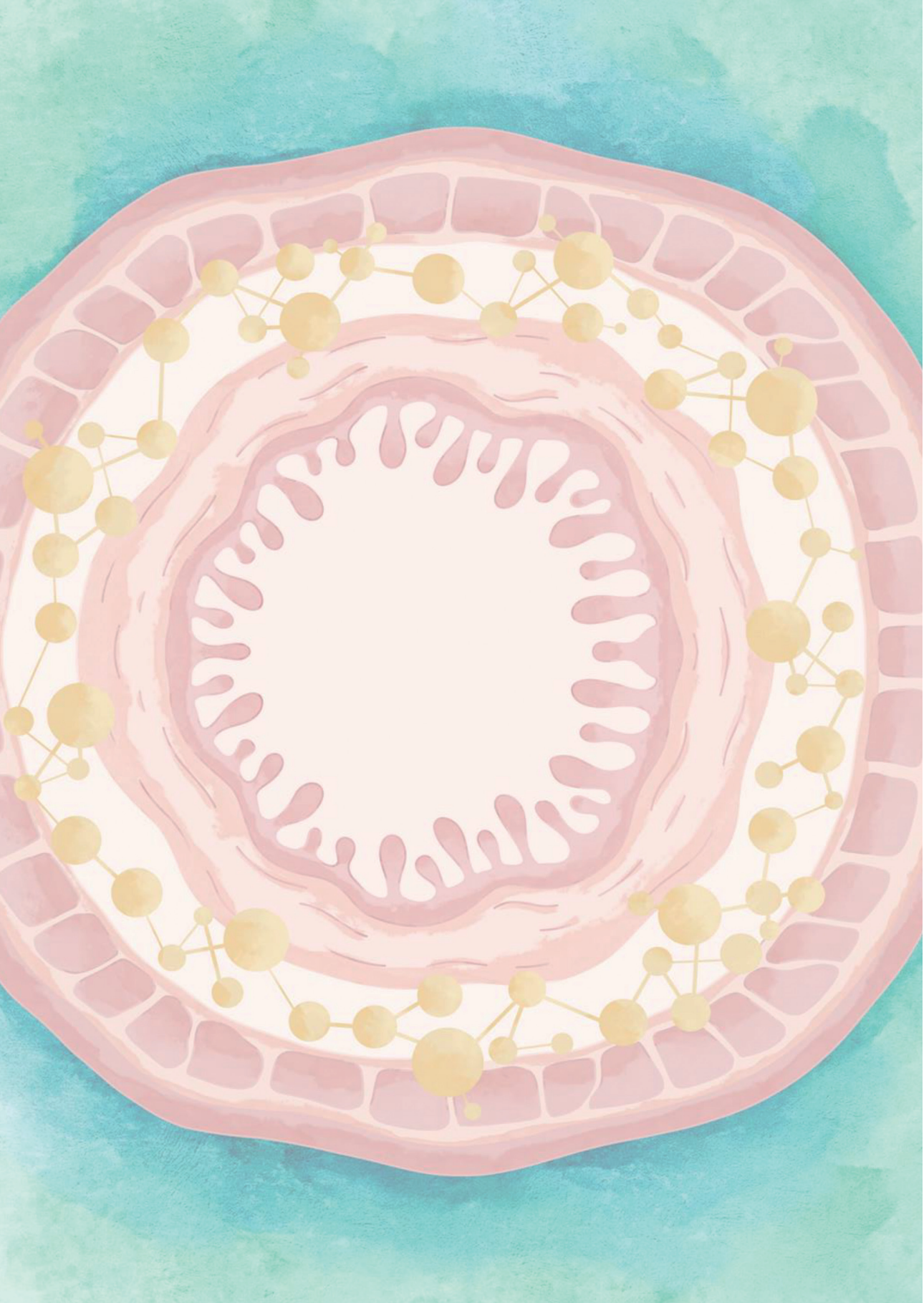

Appendix

Acknowledgements

About the author

List of publications

Overview of completed training activities

Acknowledgements

There have been many times when I was thinking how my thesis book would look like, and how I would pass this challenging yet delightful journey that turns me from a “PhD candidate” into a “Doctor”. Finally, it is time to wrap up this chapter in my life, and to thank the people that supported me through this five-year journey.

First of all, I would like to thank my highly appreciated promoter, Ivonne Rietjens, without whose support I probably never would have embarked on this adventure. Ivonne, thank you for giving me this precious opportunity to pursue my PhD in the Netherlands, a country brand new to me back then and I have deeply attached to in the last 5 years. You always asked the right questions, guided me in the right direction, and motivated me to make this project more compelling and relevant. I am deeply grateful for your patience, enthusiasm and unfailing support during my PhD studies. You were, are and will always be an inspiration and a role model to me.

Secondly, I would like express my sincerest appreciation to my co-promoter, Karsten Beekmann. We worked together for more than two years and were in close contact for the rest of my PhD studies. Karsten, you were a spark of inspiration to my dissertation. I really enjoyed our weekly talk when you were in TOX and also our “campus talk” when you moved to RIKILT, which did encourage me a lot in the final stage of my thesis writing. As an exceptional supervisor, you always listened to me with great patience and answered every question I had in great detail. You made me grow from a tyro into an independent researcher.

I would also like to thank Marije Strikwold, the last author of my last paper, whose readiness to jump into this project in the last stage is highly appreciated. I would like to thank you for your expertise which helped detect the blind spots in my project, and for your constructive comments that have been constant reassurances and points of reference in the chapter.

I am deeply indebted to our technicians and staff. Bert, our lovely “grandfather” in the lab, is the first person to introduce me to the lab and teach me UPLC, which I can always rely on when doing experiments. I feel so happy for you that after retirement, you can dedicate yourself to your beloved family and voluntary work. I am looking forward to seeing you again in my PhD defense. Sebas, thank you for your expertise in LC-MS which saved me many times from machine leakage. You are a “superman” in this lab. Laura, you are the “superwoman” in cell culture lab and thank you for introducing me to various techniques and for taking care of my students. Hans (van den Berg), Nacho and Wouter, thank you for your help in laboratory work as well as for helping order compounds. Nico, it was a great joy to attend your lectures on Environmental Toxicology, from which I learned a lot and got interested in animals. Hans (Bouwmeester), I really appreciate the encouragement you gave me in my first year. Nynke, I really enjoyed your Friday talk and thank you for sharing your academic experience with us. I am also grateful to our secretaries Lidy, Gerda and Carla, for their help with administrative issues.

In the TOX family, my colleagues were always an important source of support in my laboratory work as well as daily life. They were full of warmth and enthusiasm. Jiaqi and Akanksha, I would like to give special thanks to both of you for being my paranymphs. Jiaqi, you were always available without exception to assist me in the lab, and I enjoyed a lot our brainstorming of scientific arguments. Akanksha, we have spent so much time together in the office, gym, playground as well as Spain, and there were many exciting and joyful moments in my memory. We took many pictures and your cute smile is everywhere. I would also like to thank my lovely office mates Veronique, Yiming, Akanksha, Katja, Aafke and Germaine for being awesome companions. Peers of our "poep" group, Chen, Diana and Katja: I very much appreciated the hard but pleasant times we spent together in the small lab. Thanks to Rung for helping me build my PBK model. Thanks to Jia, who started as my colleague but now is a close friend. I am grateful to Biyao, Miaoying and Bohan, who offered me plenty of useful information in the last stage of my PhD. With my "foodie sisters": Qiuhui, Jing F, Danlei, Jingxuan and Xiyu, I had so many wonderful meals that warmed both my stomach and heart.

I would also like to thank my lovely (former) colleagues: Jing J, Suparmi, Shensheng, Shuo, Ixchel, Liang, Weijia, Lu, Marta, Annelies, Hugo, Merel, Yasser, Tessa, Frances, Ghaliya, Shivani Menno, Xukun, Nina, Katharina, Thijs, Edith, Felicia, Isaac, Wisse, and Alexandra. We had wonderful memories of PhD trip, lab trips, Christmas dinners and other celebrations. Meanwhile, I would like to thank my BSc and MSc students Ting, Quirine, Lucas and Geert for the nice experiences working with them.

My great gratitude goes to my closest friends. Without their valuable company and love, this would have been a lonely journey. Runcong, thank you for being my best friend as well as soul sister, and for your precious and unconditional friendship, which have been giving me healing power in many tough moments over the past 15 years. Hengxing, thank you for your warm and constant company since our adolescence. Ping, I would never forget the warm drinks in the winters. Shuai, I always appreciate your personality and great qualities. Rui, the kindness, sincerity and humor you brought in our friendship have benefited me greatly. Wenlong, thank you for your company and for helping me out in my difficult times.

I would also like to give my warmest thanks to my close friends, who have made this journey joyful and pleasant. Menglei, I'm so lucky to know you and I really appreciate all the happy moments we had together. Yuzhu, thank you for being my best chatting buddy in Wageningen. Du, knowing you in the last stage of our PhD really gave me relief in the tired moments. Sishi, thank you for being my great mentor and great friend. Hui and Yue, you made my vacation in China wonderful. Yanyan, thank you for your hospitality during my visit to Shanghai. Big thanks also go to my other important friends in China: Yarong, Bo, and Yuqi; and friends in the Netherlands: Lei L, Yaqi, Xinyuan, Jingjing, Caifang, Taojun, Ran, Sha, Tiantong and Weiwei.

Throughout this tough and emotional journey, my family has been my greatest and endless source of strength. My dearest Mom (Shuhua) and dad (Zengqi), thank you for your unwavering faith, trust and endless love, which encouraged and supported me all along this

journey, from Qingdao to Hong Kong, then to Shanghai and Wageningen. Finally, it's time to dedicate this dissertation to you. My warmest gratitude also goes to my beloved aunts, uncles and cousins, for their wholehearted support and love.

I will definitely miss the lake swans and the glorious sunsets of Wageningen a lot. In this small town, I have spent five of the most beautiful years of my youth. I appreciate the braveness of myself taking on the challenges of doing a PhD and made it.

About the author

Qianrui Wang was born on 24th January, 1993 in Shandong, China. She studied Food Science and Engineering at the Ocean University of China and obtained Bachelor of Engineering in 2015. Subsequently, Qianrui moved to Hong Kong to pursue her master's degree in Food Safety and Toxicology at the University of Hong Kong, and obtained Master of Science (with Distinction) in 2016. After spending 6 months doing an internship at Shimadzu Research Laboratory (Shanghai) Co. Ltd, Qianrui started her PhD in Toxicology at Wageningen University and Research under the supervision of Prof. Dr. Ivonne M. C. M. Rietjens. During her PhD studies, she followed the post-graduate education program in Toxicology as part of the training to be registered as European Registered Toxicologist.

List of publications

Wang, Q., Spenkelink, B., Boonpawa, R., Rietjens, I. M., & Beekmann, K. (2020). Use of Physiologically Based Kinetic Modeling to Predict Rat Gut Microbial Metabolism of the Isoflavone Daidzein to S-Equol and Its Consequences for ERα Activation. *Molecular nutrition & food research*, *64*(6), 1900912.

Wang, Q., Spenkelink, B., Boonpawa, R., & Rietjens, I. M. (2021). Use of Physiologically Based Pharmacokinetic Modeling to Predict Human Gut Microbial Conversion of Daidzein to S-Equol. *Journal of agricultural and food chemistry*, *70*(1), 343-352.

Mendez-Catala, D. M., **Wang, Q.**, & Rietjens, I. M. (2021). PBK Model-Based Prediction of Intestinal Microbial and Host Metabolism of Zearalenone and Consequences for its Estrogenicity. *Molecular nutrition & food research*, *65*(23), 2100443.

Wang, Q., Rietjens, I. M., Spenkelink, B., Wesseling S. & Strikwold M. Integrating physiologically based kinetic (PBK) and Monte Carlo modeling to predict the interindividual human variability in metabolism of daidzein. In preparation.

Overview of completed training activities

Discipline specific activities

Molecular toxicology	PET	2017
Cell Toxicology	PET	2017
Pathobiology	PET	2017
Laboratory of animal science	PET	2017
Organ Toxicology	PET	2018
Epidemiology	PET	2018
Immunotoxicology	PET	2018
Reproductive Toxicology	PET	2018

Conferences

40th Annual meeting of the Dutch Society of Toxicology (NVT), oral pitch, Ede, the Netherlands, 2019

55th Congress of the European Societies of Toxicology (EUROTOX), poster, Helsinki, Finland, 2019

59th Annual (virtual) meeting Society of Toxicology (SOT), poster, online, U.S., 2020
Award: Biological modeling specialty section (BMSS) best trainee abstract finalist

61st Annual meeting Society of Toxicology (SOT), poster, San Diego, U.S., 2022

General courses

VLAG PhD week	WUR	2017
Chemometrics	WUR	2018
Introduction to R	WUR	2018
Applied statistics	WUR	2018

Other activities

Preparation of research proposal	TOX-WUR	2017
PhD trip to Japan	TOX-WUR	2018
Scientific presentation at Division of Toxicology	TOX-WUR	2017-2022
Environmental toxicology	WUR	2017
General toxicology	WUR	2017
Food safety risk assessment	WUR	2017

Approved by the graduate school VLAG

The research described in this thesis was financially supported by China Scholarship Council (No. 201707720022 to Qianrui Wang), China

Financial support from Wageningen University for printing this thesis is gratefully acknowledged.

Cover design by Qianrui Wang & Rumin.
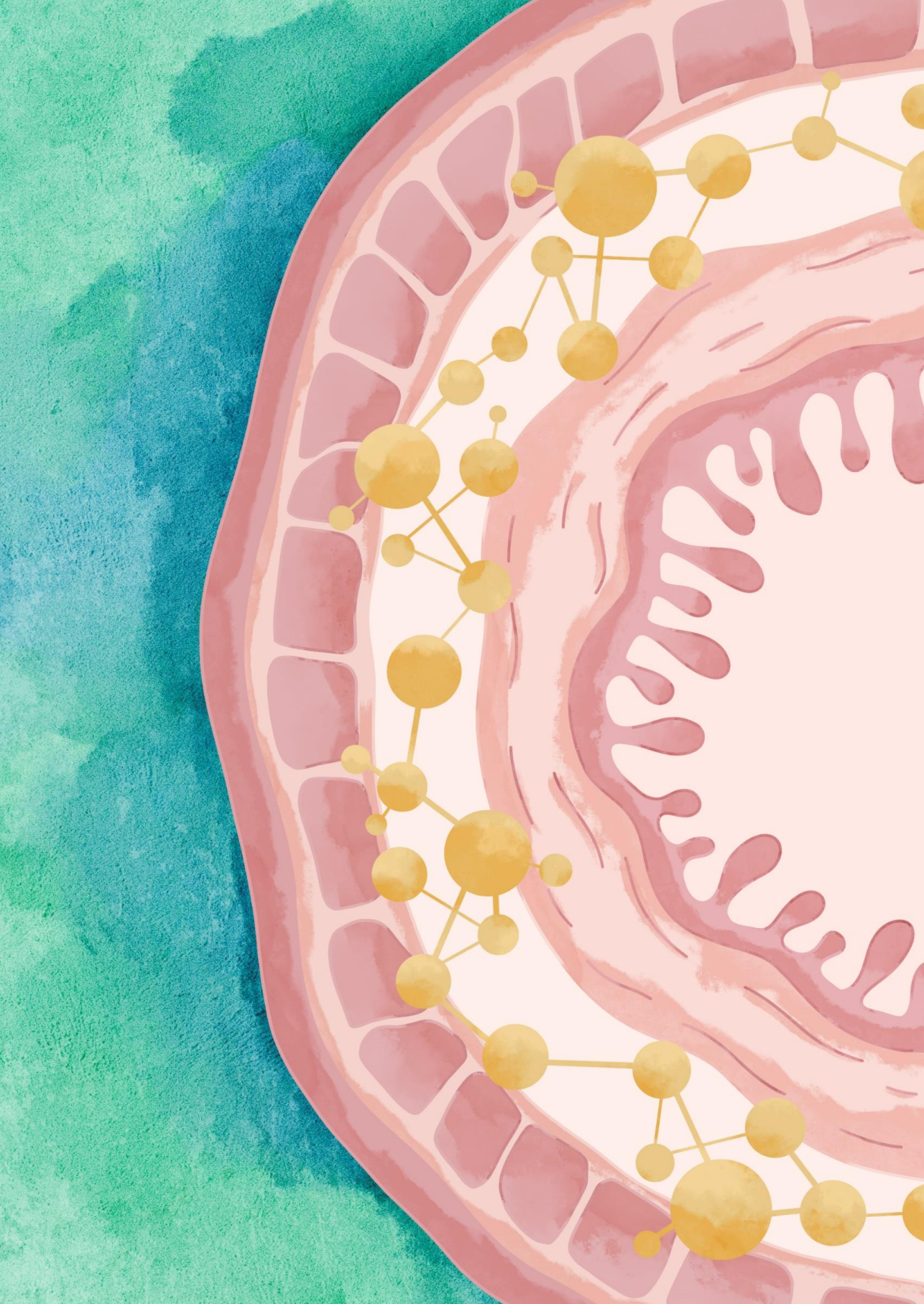
Printed by ProefschriftMaken || proefschriftmaken.nl